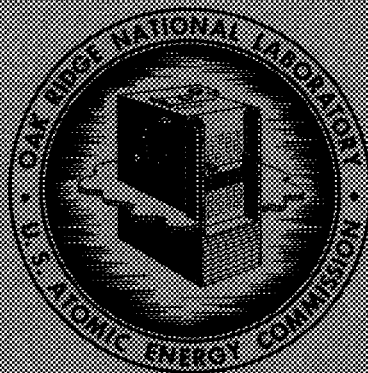


ORNL-3921  
UC-80 -- Reactor TechnologyAN EVALUATION OF HEAVY-WATER-MODERATED  
ORGANIC-COOLED REACTORS

P. R. Kasten

R. E. Adams	J. T. Roberts
R. S. Carlsmith	R. Salmon
R. H. Chapman	J. P. Sanders
E. P. Epler	R. S. Stone
E. H. Gift	D. R. Vondy
F. E. Harrington	C. S. Walker
M. L. Myers	T. N. Washburn
R. C. Olson	L. B. Yeatts

F. C. Zapp



OAK RIDGE NATIONAL LABORATORY

operated by

UNION CARBIDE CORPORATION

for the

U. S. ATOMIC ENERGY COMMISSION

CENTRAL RESEARCH LIBRARY  
DOCUMENT COLLECTION**LIBRARY LOAN COPY****DO NOT TRANSFER TO ANOTHER PERSON**If you wish someone else to see this  
document, send in name with document  
and the library will arrange a loan.

Printed in the United States of America. Available from Clearinghouse for Federal  
Scientific and Technical Information, National Bureau of Standards,  
U.S. Department of Commerce, Springfield, Virginia 22151  
Price: Printed Copy \$3.00; Microfiche \$0.65

#### LEGAL NOTICE

This report was prepared as an account of Government sponsored work. Neither the United States, nor the Commission, nor any person acting on behalf of the Commission:

- A. Makes any warranty or representation, expressed or implied, with respect to the accuracy, completeness, or usefulness of the information contained in this report, or that the use of any information, apparatus, method, or process disclosed in this report may not infringe privately owned rights; or
- B. Assumes any liabilities with respect to the use of, or for damages resulting from the use of any information, apparatus, method, or process disclosed in this report.

As used in the above, "person acting on behalf of the Commission" includes any employee or contractor of the Commission, or employee of such contractor, to the extent that such employee or contractor of the Commission, or employee of such contractor prepares, disseminates, or provides access to, any information pursuant to his employment or contract with the Commission, or his employment with such contractor.

Contract No. W-7405-eng-26

Reactor Division

AN EVALUATION OF HEAVY-WATER-MODERATED  
ORGANIC-COOLED REACTORS

P. R. Kasten

R. E. Adams	J. T. Roberts
R. S. Carlsmith	R. Salmon
R. H. Chapman	J. P. Sanders
E. P. Epler	R. S. Stone
E. H. Gift	D. R. Vondy
F. E. Harrington	C. S. Walker
M. L. Myers	T. N. Washburn
R. C. Olson	L. B. Yeatts
F. C. Zapp	

JANUARY 1967

OAK RIDGE NATIONAL LABORATORY  
Oak Ridge, Tennessee  
operated by  
UNION CARBIDE CORPORATION  
for the  
U.S. ATOMIC ENERGY COMMISSION

OAK RIDGE NATIONAL LABORATORY LIBRARIES



3 4456 0548219 9



## FOREWARD

This report presents ORNL evaluations of heavy water moderated organic cooled (HWOCR) reactor power plants based on designs submitted late in 1965 to the U. S. Atomic Energy Commission by the Atomics International-Combustion Engineering joint group (AI-CE) and by the Babcock and Wilcox Company (B&W). During 1966, both AI-CE and B&W developed revised HWOCR designs having improved performance characteristics. These revised designs have also been evaluated by ORNL, the results of which are being reviewed by the design sponsors, by the staff of the U. S. Atomic Energy Commission, and by others. Report ORNL-3921, Supplement summarizing these results will be issued following the reviews. Comments of reviewers on ORNL's evaluation of both the original and revised designs will be contained in ORNL-3921, Supplement.



## CONTENTS

	<u>Page</u>
FOREWORD .....	iii
ABSTRACT .....	xi
1. INTRODUCTION .....	1
1.1 Bases for Evaluation .....	1
1.2 Reactor Systems Studied .....	2
1.3 Procedures Followed .....	3
1.4 Limitations of the Study .....	4
1.5 Evaluation Areas and Personnel .....	5
1.6 Acknowledgments .....	5
References .....	7
2. GROUND RULES AND COST BASES .....	8
2.1 Power Cost Components .....	8
2.1.1 Fuel-Cycle Cost .....	8
2.1.2 Reactor Plant Capital Cost .....	8
2.1.3 Reactor Plant Operating Cost .....	9
2.2 Financing Conventions .....	9
2.3 Value of Materials .....	10
2.4 Reactor Plant .....	10
2.5 Fuel Fabrication Plant.....	11
2.6 Fuel Reprocessing Plant .....	11
2.7 Fuel Preparation .....	12
2.8 Fuel Shipping .....	12
Reference .....	13
3. DESCRIPTION OF REACTORS .....	14
3.1 Plant Design .....	14
3.2 Core Design .....	17
3.2.1 AI-CE Uranium-Fueled Core .....	17
3.2.2 B&W Thorium-Uranium-Fueled Core .....	19
References .....	20

4.	PHYSICS ANALYSIS OF HWO CR SYSTEMS .....	21
4.1	Zero-Dimensional Depletion Calculations .....	21
4.2	Calculation of Spectra and Cross Sections .....	22
4.3	Calculation of Reactivity Coefficients .....	23
4.4	Optimization of the Fuel Cycles .....	24
4.5	Calculation of Power-Peaking Factors .....	25
4.6	Physics of the Uranium-Fueled HWO CR .....	26
4.6.1	Multidimensional Reactor Calculations .....	26
4.6.2	Reactivity Coefficients .....	34
4.6.3	Reactor Depletion Calculations .....	35
4.6.4	Comparison of ORNL and AI-CE Depletion Results Obtained by the Same Method .....	39
4.6.5	Comparison of Zero- and One-Dimensional Depletion Results .....	40
4.7	Physics of the Thorium-Cycle HWO CR .....	41
4.7.1	Multidimensional Reactor Calculations .....	41
4.7.2	Reactivity Coefficients .....	48
4.7.3	Reactor Depletion Calculations .....	49
4.7.4	Comparison of ORNL and B&W Depletion Results Using the Same Method .....	49
	References .....	56
5.	ENGINEERING EVALUATION OF REACTOR CORES .....	58
5.1	Fluid Flow and Heat Transfer Analyses .....	62
5.1.1	Evaluation of the Computer Codes .....	63
5.1.2	Evaluation of Correlations Used in the Codes ...	66
5.1.3	Formulation of Input Data for the Codes .....	71
5.1.4	Analysis of the Output of the Codes .....	81
5.1.5	Discussion and Evaluation of the Reactor Cores .....	86
5.1.6	Conclusions .....	90
5.2	Fuel Element Performance Evaluation .....	94
5.2.1	AI-CE Fuel Element .....	94
5.2.2	B&W Nested Cylinders .....	99
5.2.3	B&W Pin-Cluster Fuel Assembly .....	102

5.3	Core Material Compatibility Evaluation .....	104
5.3.1	Coolant-Cladding Compatibility .....	105
5.3.2	Coolant-Fuel Compatibility .....	106
5.3.3	Cladding-Fuel Compatibility .....	108
5.3.4	Conclusions .....	111
5.4	Core Design Criteria Evaluation .....	112
5.4.1	Mechanical Properties of SAP .....	112
5.4.2	Radiation Effects on SAP .....	115
5.4.3	SAP Process Tube Design .....	115
5.4.4	SAP Fuel-Cladding Design .....	115
5.4.5	Zircaloy Calandria Tube Design .....	116
5.4.6	Zircaloy Process Tubes .....	116
5.4.7	Conclusions .....	117
5.5	Organic Coolant Evaluation .....	118
5.5.1	Physical Properties .....	119
5.5.2	Thermal and Radiolytic Stability .....	121
5.5.3	Corrosion and Fouling .....	125
5.5.4	Other Properties .....	128
5.5.5	Conclusions .....	128
5.6	Reactor Controls and Safety Evaluation .....	129
5.6.1	Control and Safety Aspects of the Plant .....	129
5.6.2	Reactor Startup .....	132
5.6.3	Restart After a Scram .....	135
5.6.4	Safety System Requirements .....	136
5.6.5	Reactor Control System Requirements .....	140
5.6.6	Reactor Shutdown Margin .....	150
5.6.7	Conclusions .....	151
	References .....	153
6.	ENGINEERING REVIEW OF PLANT DESIGN .....	160
6.1	Reactor Vessels and Internal Structures .....	161
6.1.1	Calandria and Shield .....	161
6.1.2	Fuel Channel Assemblies .....	163
6.2	Refueling and Fuel Handling .....	170
6.2.1	Refueling Operations .....	170
6.2.2	Fuel Handling .....	175

6.3	Plant Availability .....	176
6.4	Control Rod Systems .....	179
6.4.1	Shutdown Rods .....	179
6.4.2	Control of Spatial Power Distribution and Power Level .....	180
6.5	Primary Heat Transfer Systems .....	181
6.6	Heavy-Water Systems .....	185
6.7	Organic Coolant Decomposition, Recovery, and Makeup .....	187
6.8	Instrumentation and Controls .....	189
6.8.1	Plant Controls .....	189
6.8.2	Nuclear Instrumentation .....	190
6.9	Containment Structure .....	195
6.10	Turbine-Generator System .....	197
6.11	Electrical Systems .....	204
6.12	Service Systems .....	204
6.13	Site and Structures .....	205
6.14	Plant Safeguards .....	205
	References .....	206
7.	CAPITAL COSTS .....	209
7.1	Capital Cost Breakdown for AI-CE Reference Design Conditions .....	209
7.2	Capital Cost Normalization of B&W Concepts .....	215
7.3	Moderator and Coolant Investment .....	217
7.4	Cost Uncertainties .....	218
7.5	Effect of Recommended Design Changes on Estimates of Capital Costs .....	219
	References .....	221
8.	OPERATION AND MAINTENANCE COSTS .....	222
	References .....	223
9.	FUEL PREPARATION COST .....	224
9.1	Estimating Method .....	224
9.2	UF <sub>6</sub> -to-UO <sub>2</sub> Conversion for AI-CE Fuel .....	225
9.3	Preparation of Thorium Fuels for B&W Designs .....	227
9.4	Summary .....	228
	References .....	230

10.	FUEL FABRICATION COSTS .....	231
10.1	General Procedure for Cost Estimating .....	231
10.2	Fabrication Costs for AI-CE Fuel.....	231
10.3	Fabrication Costs for B&W Fuels .....	233
10.4	Summary .....	238
	References .....	241
11.	SPENT-FUEL PROCESSING COSTS .....	243
11.1	Cost Bases and Assumptions .....	243
11.1.1	Capital Investment .....	246
11.1.2	Annual Operating Costs .....	247
11.1.3	Radioactive Waste Disposal Costs .....	248
11.1.4	Plant Sizing .....	250
11.2	Cost Estimates .....	250
11.2.1	Throw-Away Fuel Cycle .....	252
11.2.2	Comparison with B&W and AI-CE Estimates .....	252
11.2.3	Comparison with NPS Processing Charges .....	253
11.3	Summary and Conclusions .....	253
	References .....	254
12.	FUEL SHIPPING COSTS .....	256
12.1	Spent-Fuel Shipping Costs .....	256
12.1.1	Description of Cask .....	259
12.1.2	Method of Calculation .....	260
12.1.3	Optimization Procedures .....	262
12.2	Recycled Fresh-Fuel Shipping Costs .....	263
12.3	Nonrecycled Fresh-Fuel Shipping Costs .....	264
12.4	Discussion of Results .....	264
	References .....	265
13.	FUEL-CYCLE COSTS .....	267
13.1	Calculation of Average Lifetime Fuel-Cycle Costs .....	267
13.2	Calculation of Equilibrium Fuel-Cycle Cost .....	269
13.3	Special Aspects of HWOGR Fuel-Cycle Economics .....	269
13.4	AI-CE Design Fuel-Cycle Costs .....	270
13.5	B&W Design Fuel-Cycle Costs .....	272
13.6	Summary of Effects of Variations in Ground Rules .....	276
	References .....	279

14. REACTOR PERFORMANCE .....	280
Reference .....	287
15. SUMMARY AND CONCLUSIONS .....	288
15.1 Reactor Systems Studied .....	288
15.2 Evaluation of Core Designs .....	289
15.2.1 Fluid Flow and Heat Transfer Analyses .....	290
15.2.2 Power-Peaking Factors .....	292
15.2.3 Organic-Coolant Behavior .....	293
15.2.4 Temperature Conditions .....	294
15.2.5 Materials Evaluations .....	297
15.2.6 Safety and Control Considerations .....	299
15.2.7 Fuel-Cycle Conditions .....	300
15.3 Evaluation of Plant Designs .....	301
15.4 Performance Evaluation .....	304
15.5 Engineering Development Requirements .....	306
15.5.1 Process-Tube and Cladding Material .....	306
15.5.2 Organic Coolant .....	307
15.5.3 Control and Safety .....	308
15.5.4 Thermal and Hydraulic Studies .....	308
15.5.5 Fuel-Element Performance .....	308
15.5.6 Components .....	309
APPENDIX A. BASIS FOR FIXED CHARGES ON NUCLEAR PLANTS .....	313
APPENDIX B. COMPUTER CODES USED IN HWO CR EVALUATION .....	315
APPENDIX C. REVIEW OF ORGANIC COOLANT HEAT TRANSFER CORRELATIONS AND PHYSICAL PROPERTIES .....	326
APPENDIX D. REVIEW OF CRITICAL HEAT FLUX CORRELATIONS .....	339
APPENDIX E. REVIEW OF ENGINEERING HOT-CHANNEL FACTORS .....	347
APPENDIX F. ANALOG COMPUTER STUDY OF HWO CR CONTROL DYNAMICS ...	349
APPENDIX G. COMPARISON OF ADVANCED CONVERTER FUEL- PROCESSING COSTS ON DIFFERENT BASES .....	365

Abstract

A technical evaluation of heavy-water-moderated organic-cooled power reactors (HWOCR) was performed based on 1000-Mw(e) design concepts supplied by Atomics International and Combustion Engineering (AI-CE) jointly and by Babcock & Wilcox (B&W). The AI-CE plant was designed for the uranium fuel cycle (carbide fuel), while the B&W core designs were based on use of the thorium fuel cycle (oxide and also metal fuels). The power-production costs associated with the designs were obtained from estimates of capital, operating and maintenance, and fuel-cycle costs. For the technological evaluation it was considered that the reactor design must be feasible but may involve engineering development. Required developments were identified, and the design and predicted plant engineering performance were subjected to review and evaluation.

The HWOCR-U reactor plant showed promise of producing power at a cost of about 3.5 mills/kwhr(e) in investor-owned plants of 1000-Mw(e) capacity, and the associated average conversion ratio was about 0.7. The HWOCR-Th reactor design conditions showed lower fuel burnup costs than those for the HWOCR-U system, with the average conversion ratio being about 0.8; at the same time, power costs under the reference ground rules for the designs submitted were about 0.4 mill/kwhr(e) higher than those for the uranium-fueled reactor. Changing the design could improve the performance of the thorium reactors, but the associated power cost would apparently still be higher than that of the uranium-fueled reactor.

Evaluations of the thermal and hydraulic performance of the reactor cores led to the conclusion that the coolant outlet temperature would not be above about 700°F for the designs submitted. Film formation on the SAP cladding, with an accompanying increase in sheath temperature and associated changes in thermal and hydraulic performance, cannot be neglected. Also, heat transfer coefficients need to be based on the fuel assembly conditions, and experimental measurements of these coefficients are needed. Additional testing of the uranium and thorium fuel materials is required to demonstrate that the specified maximum burnup can be

achieved under HWOCR operating conditions; tests of organic coolant and its film-forming action under HWOCR conditions need further investigation.

Use of SAP for process tubes and fuel cladding involves a material having low ductility and one for which specifications and information on permissible design stresses have not been completely developed. Experimental measurements and long-term tests are required to verify the practicality of SAP for HWOCR use. Also, the positive coolant temperature coefficient of the HWOCR imposes stringent demands on the operation of the safety and control systems.

## 1. INTRODUCTION

Heavy-water-moderated organic-cooled reactor systems are believed to be capable of producing low-cost power in plants having large capacities. Such reactors represent advanced converters in the sense that they have higher conversion ratios and lower specific fissile inventories than the light-water reactors presently being built. Thus it is hoped that such systems, in conjunction with providing low-cost power, will give improved fuel utilization.

Early in 1965 the Oak Ridge National Laboratory (ORNL) was requested by the USAEC to perform an evaluation of heavy-water organic-cooled power reactors (HWO CR). This study was to involve technical evaluation of the design concepts and was to include a comparative evaluation with the results of the advanced converter reactor study reported previously.<sup>1</sup> The reactor plant design was to be based on a 1000-Mw(e) reactor system. The design of a system utilizing the uranium fuel cycle was to be provided by Atomics International-Combustion Engineering (AI-CE). The AI-CE design concept is presented in a report<sup>2</sup> submitted to ORNL on October 1, 1965. In addition, Babcock & Wilcox (B&W) was to develop core designs based on the use of thorium and recycle fuel. The associated core design study<sup>3</sup> results were presented to ORNL in early October 1965; subsequently, revised core designs were summarized in a report<sup>4</sup> presented on November 15, 1965.

### 1.1 Bases for Evaluation

The status of HWO CR development is such that application of HWO CR power plants is foreseen in the early 1970's. If breeder reactor construction dominates in about 25 years, the period of particular interest for HWO CR's is the two decades following 1970. This study is therefore directed toward evaluating HWO CR's constructed during that time period.

The evaluation factor that encompasses all others in commercial application of reactors is power production cost, and this is the primary consideration in determining the incentive for developing HWO CR's. Considerations such as fuel utilization and conservation of fuel resources

are important factors in determining plant economics, but they should be consistent with yielding minimum power costs over a given period of time. Of course, in evaluating economics, future conditions must be properly weighed, and attitudes of governmental agencies, as reflected in tax provisions and in the regulation of financing and rates, must be taken into consideration.

Based on the above, this study was directed toward estimating the cost of power from HWO CR's built in the period following 1970. The power cost was obtained from estimates of capital, operating, and fuel cycle costs. The technological evaluation was on the basis that the reactor design must be feasible today; this implies that although engineering development might be required to make the design practicable, application of the design should not depend on a technological breakthrough. Required developments were identified, and the design and predicted engineering performance of the reactor plants were subjected to review and evaluation; because of the nature of the problems and time limitations, engineering judgments concerning achievable performance were often involved.

## 1.2 Reactor Systems Studied

HWO CR's have lattice-type cores in which the organic coolant is separate from the heavy-water moderator. Based on design conditions, the coolant consists primarily of a mixture of ortho- and metaterphenyls, and it leaves the reactor at 750°F. Steam is produced at 725°F and 900 psig in the steam cycle; the resulting overall system thermal efficiency is about 35%. The nominal plant power rating is 1000 Mw(e).

The AI-CE study considered the entire power plant design, including the reactor, heat exchange, and steam systems. The plant designs for both the uranium and thorium fuel cycles were essentially based on the AI-CE study; however, the AI-CE core design utilized the uranium fuel cycle, while the B&W core designs considered the thorium cycle. For both fuels, on-power refueling with bidirectional movement of fuel in adjacent channels was considered.

The AI-CE core design is based on the use of uranium carbide fuel made from slightly enriched uranium. Also, the fuel feed material is

always slightly enriched uranium; the plutonium obtained at the end of each fuel-exposure cycle is sold. Bidirectional fueling of adjacent fuel channels in the core is accomplished with two fueling machines, one at each end of the core. Coolant flow is always in the direction of fuel movement. The fuel is clad with a sintered aluminum product (SAP or XAP, consisting of aluminum oxide dispersed in a matrix of aluminum) and is located in 492 fuel channels.

Two basic fuel elements are considered for the B&W core designs. One design utilizes an annular metallic fuel element clad with Zircaloy-4; the other considers clusters of pins of oxide fuel clad with XAP. The initial fuel consists of thorium with  $^{235}\text{U}$  added as the fissile material. In subsequent cycles, the bred  $^{233}\text{U}$  is recycled, and makeup  $^{235}\text{U}$  is added as needed. Bidirectional fueling in adjacent channels is accomplished with one refueling machine operating from one end of the reactor. Coolant flow through the reactor core is unidirectional, however. With the metallic fuel assembly, 299 process tubes are used; with the oxide fuel assembly, 335 process channels are used.

Additional details of the plant and reactor core designs obtained from the AI-CE and B&W studies are summarized in Chapter 3.

### 1.3 Procedures Followed

At the initiation of this study, the time period and economic context associated with the reactor evaluation were defined and a set of ground rules was formulated. The major provisions of the ground rules are given below, and Chapter 2 lists them in detail.

1. The technology to be used in the reactor plant is generally restricted to that which would be feasible for a smaller prototype reactor to be built for startup in 1970.

2. Economic parameters are to represent the average conditions existing during the life of reactors built in the period 1970-1990. Private ownership of reactor fuel fabrication and processing plants is assumed for the reference conditions.

3. The total electrical capacity of a reactor plant is 1000 Mw(e); however, the fuel fabrication and processing industry is based on

servicing plants with a total capacity of 15,000 Mw(e) associated with a given reactor core design. Consequently, the fuel fabrication and processing industry size varies with the fuel burnup.

4. The fuel-cycle cost is based on present-value accounting in which the system behavior is averaged over a 30-year period.

5. The uranium from the thorium-uranium-fueled cores is recycled throughout the reactor lifetime, but for the uranium-fueled cores the sale of plutonium with no recycle is assumed.

In presenting the results in this report, separate chapters are devoted to the major subdivisions of the study. The engineering appraisals of the core and of the plant are presented in different sections, as are the capital, operating, fuel preparation, fuel fabrication, shipping, and fuel processing cost estimates. Reactor physics analyses are discussed separately. A chapter on fuel-cycle costs combines the results of the physics and unit cost studies, and the optimum fuel cycle costs are in turn added to the operating and capital costs in the chapter on power costs. The major results of this study and the most important conclusions are summarized in the final chapter.

#### 1.4 Limitations of the Study

The objectives of this study were to evaluate the proposed reactor designs, compare them with each other, and evaluate the HWOCR in relation to the results from the advanced converter reactor study.<sup>1</sup> In so doing the specific designs provided by AI-CE and B&W were employed. The designs presented at this time may not necessarily represent the optimum designs that will be developed for the two fuel cycles. In our evaluation of the proposed design, changes that needed to be incorporated in the specifications were pointed out and their effects indicated.

The power costs for these reactors were obtained on the basis of a specified economic context. While some economic factors were varied in the evaluation, this was done in a gross manner and not on the basis of reoptimizing the core design for different economic conditions. In general, the reactor concepts were optimized for the production of power at the lowest cost on the basis of the reference ground rules.

In estimating costs, successful development of components required by the design was postulated. The most common example is the specification of equipment that is larger than any now being built, although there are some component features that have not been demonstrated even in smaller size. Development needs are identified in the engineering evaluation chapters and the extent to which they represent extrapolations of technology is noted. In addition, there are other areas where not enough information has been obtained at this time. Key areas which were difficult to judge on an absolute basis and which to a large extent involved engineering judgment included materials compatibility, design criteria evaluation, relationship between refueling ability and operation and maintenance costs, and reactor control and safety.

The performance of the HWOCR plants can be compared with the advanced-converter-reactor performance reported previously.<sup>1</sup> However, care must be taken in making such comparisons because the design specifications associated with the pertinent concepts have changed since the original study; also, the HWOCR evaluation was based on slightly different ground rules relative to plutonium price and fuel preparation, fabrication, and processing costs. Thus, only gross comparisons can be made, but these are still meaningful when recognition is given to the different bases employed.

### 1.5 Evaluation Areas and Personnel

The study was organized by function, with different groups responsible for the physics and fuel cost analyses, control studies, engineering and design evaluations, and the cost estimates associated with capital investment and fuel preparation, fabrication, shipping, and processing. The areas and personnel involved are given in Table 1.1.

### 1.6 Acknowledgments

As noted previously, design and cost information was supplied by AI-CE and B&W with regard to their design concepts. In all cases these firms were very cooperative in providing information required in the evaluation.

Table 1.1. HWO CR Evaluation Areas and Associated Personnel

---

Study Coordination

Paul R. Kasten

Reactor Physics

R. S. Carlsmith, E. H. Gift, R. E. Hoskins (TVA),  
 L. Jung, D. R. Vondy, D. B. Wehmeyer (consultant),  
 F. G. Welfare

Engineering Evaluation of Reactor Cores

Core Thermal Performance

R. C. Olson, R. H. Chapman, J. P. SandersFuel Performance, Material Compatibility, and  
Design Criteria

R. E. Adams, R. C. Olson

Organic Coolant

L. B. Yeatts

Reactor Controls and Safety

E. P. Epler, R. S. Stone, C. S. WalkerPlant Design and Cost Evaluation

R. C. Olson, E. P. Epler, R. D. Frey, H. A. McLain,  
 M. L. Myers, R. C. Robertson, R. Salmon, C. S. Walker,  
 L. V. Wilson, F. C. Zapp

Fuel-Cycle Cost Estimates

Fuel Preparation

F. E. Harrington

Fuel Fabrication

T. N. Washburn, A. L. Lotts

Fuel Processing

J. T. Roberts, F. E. Harrington, J. O. Blomeke,  
 R. Salmon

Fuel Shipping

R. Salmon

Total Fuel Cycle Costs

R. S. Carlsmith, E. H. Gift, D. R. Vondy

---

The authors wish to acknowledge the valuable guidance and assistance of M. W. Rosenthal, who organized the study initially. Also, valuable advice and assistance was provided by D. A. Douglas concerning materials problems.

We also gratefully acknowledge the editorial assistance of Ann W. Savolainen and her staff in preparing this report for publication.

#### References

1. M. W. Rosenthal et al., A Comparative Evaluation of Advanced Converters, USAEC Report ORNL-3686, Oak Ridge National Laboratory, January 1965.
2. Combustion Engineering, Inc., and Atomics International, Heavy Water Organic Cooled Reactor - 1000 Mwe Nuclear Power Plant Preliminary Conceptual Design, USAEC Report AI-CE-Memo-6, Vols. I and II, Oct. 1, 1965.
3. Babcock & Wilcox Company, Thorium Fuel Cycle for Heavy Water Moderated Organic Cooled Reactors, Quarterly Technical Report No. 2, April-June 1965, USAEC Report BAW-393-2, October 1965.
4. Babcock & Wilcox Company, 1000 MWe Thorium HWOCR - Preliminary Conceptual Design Data for ORNL Evaluation, USAEC Report (unnumbered), Nov. 15, 1965.

## 2. GROUND RULES AND COST BASES

The technology used in the reactor power plant design was in general that which would be feasible for smaller prototype reactors to be built for startup in 1970. The reactors evaluated were presumed to begin operating with unirradiated fuel, and the plant lifetime was taken to be 30 years. Fuel-cycle costs were based on the integral number of fueling cycles that came closest to 30 years. In the thorium systems, bred fuel was recycled throughout the reactor lifetime; in the uranium fuel cycle, the sale of plutonium without recycle was assumed.

### 2.1 Power Cost Components

#### 2.1.1 Fuel-Cycle Cost

The fuel-cycle cost was resolved into the following components: (1) burnup cost, (2) fuel preparation cost, (3) fabrication cost, (4) processing cost, including ultimate waste disposal cost, (5) shipping cost, (6) fixed charges on fissile and fertile inventories, and (7) interest charges on operating capital invested in fabrication, processing, and shipping facilities and in inventories of special materials. The fixed charges and interest were computed by the "present-worth" formula. A value was assigned to fuel discharged from the reactor at the end of plant life (~30 years) that included linearly prorated credits for fabrication and debits for processing of partially irradiated fuel. In computing the present worth of the power produced, the price of power and the plant factor were assumed not to change with time.

#### 2.1.2 Reactor Plant Capital Cost

Capital costs were estimated for each reactor plant. It was assumed that the plant was one of a number of the same type to be built and that the equipment and system for the plant had been fully developed. However, discount credits for quantity orders of equipment were not assumed.

Capital cost breakdowns were arranged in accordance with the system of accounts given in Volume 1 of the AEC Handbook "Guide to Nuclear Power Cost Evaluation."<sup>1</sup> Estimates of indirect costs appropriate to the reactor

size were also based on the breakdown used in Ref. 1. However, new estimates were made of percentages applied for each indirect cost item to reflect recent experience. Fixed charges on the reactor plant were taken as constant over the plant life, with a reference value of 12% per year for investor-owned utilities and with an alternate value of 7% per year to represent public ownership. The components of these fixed charge rates are given in Appendix A.

### 2.1.3 Reactor Plant Operating Cost

Operating and maintenance costs were estimated for each reactor plant.

## 2.2 Financing Conventions

Private ownership of fuel and of fabrication and reprocessing plants was assumed for the base cases. Because of uncertainty as to their values, various fixed charge rates, interest rates, and values of materials were used, as indicated in the following paragraphs. Single values of each quantity were specified, however, for use in selecting reference designs.

Ownership of fissile and fertile materials during fabrication and processing, as well as when on site at the reactor, was considered to be vested in the reactor plant. Inventory charges on fissile and fertile inventories were computed with a reference value of 10% per year; values were also computed at 5% per year to represent public ownership. For determining the inventory charges, changes from initial to final values were assumed to occur linearly with time during irradiation.

Interest charges on the fabrication cost of fuel elements were computed in the same way as the fixed charges on fuel. For this purpose, the fuel elements were assumed to depreciate linearly with time over the period of irradiation. The reference discount factor for computing present worth was 6% per annum; however, 4% was used with the lower fixed charges and interest rates that represented public ownership. Interest payments and collection of revenue were assumed to be made twice a year.

Heavy water was treated as a nondepreciating asset, and the inventory cost was computed with 10% per year as the reference value; an alternate value of 5% per year was associated with public ownership.

### 2.3 Value of Materials

1. Natural uranium: reference value of \$8.00/lb of  $U_3O_8$ , alternate value of \$16/lb of  $U_3O_8$ .
2. Unirradiated thorium: \$5.00/lb of  $ThO_2$ .
3. Unirradiated enriched uranium: the value was based on a separate work cost of \$30/kg.
4. Depleted uranium of low enrichment: the value corresponded to its enrichment in  $^{235}U$  based on total uranium present, with no additional penalty for  $^{236}U$  content.
5. Highly enriched uranium containing  $^{233}U$ : the value of the fuel mixture was computed from its isotopic composition by assigning the  $^{235}U$  the same value per gram it has in 90% enriched uranium (reference value of \$12/g), assigning the contained  $^{233}U$  one and one-half times the value of the  $^{235}U$ , and assigning a negative value to the  $^{236}U$  equal to that of the  $^{235}U$ .
6. Plutonium: the fissile content was valued at five-sixths of the value of the  $^{235}U$  in uranium of 90% enrichment.
7.  $D_2O$ : a value of \$20/lb was assigned to  $D_2O$  of 99.86% purity.
8. Conversion of  $U_3O_8$  to  $UF_6$ : \$2.70 per kilogram of uranium.

### 2.4 Reactor Plant

The electric station was assumed to have a net capability of 1000 Mw(e), with one reactor per station. The condenser pressure was assumed to be 1.5 in. Hg abs. A reactor plant availability factor of 0.9 was required to achieve an average plant factor of 0.8 over the plant life.

The uranium-cycle reactor was assumed to be loaded initially with unirradiated uranium and to be refueled with unirradiated uranium throughout its life. The thorium-cycle reactor was assumed to be fueled initially with either plutonium or unirradiated enriched uranium and thorium, and plutonium or unirradiated enriched uranium was to be used as required for initial refuelings. After a suitable delay for processing and refabrication, however, recycle fuel of the same composition and amount as that

discharged (after subtracting processing losses) was assumed to be available for use with makeup  $^{235}\text{U}$  or plutonium.

Fuel was considered to be received at the reactor site 60 days before loading. The cooling time before shipment of irradiated fuel was established for each concept.

The loss rate of heavy water used in the evaluation was that estimated by the reactor designer.

### 2.5 Fuel Fabrication Plant

The fabrication plant was considered to be centrally located at the same site as the processing plant. The plant was assumed to be designed for fabricating a single type of fuel element and to be capable of serving an electrical industry of 15,000-Mw(e) capacity of the concept being studied.

A reference value of 22% per year was used for the fixed charge rate on depreciating capital, and costs were also estimated for an alternate value of 15% per year. The unit fuel fabricating cost was assumed to remain the same throughout the 30-year plant life. The design of the fuel elements was specified in detail by the proponents. Holdup time was established for each concept. Losses of plutonium, uranium, and thorium were assumed to be 0.2% per pass.

### 2.6 Fuel Reprocessing Plant

The reprocessing plant was assumed to be centrally located at the same site as the fabrication plant. The plant was assumed to be designed for processing a single type of fuel element and to be capable of serving an electrical industry of 15,000-Mw(e) capacity of the concept being studied.

A reference value of 22% per year was used for the fixed charge rate on depreciating capital, and costs were also estimated for an alternate value of 15% per year. The price for reprocessing was assumed to remain the same during the life of the reactor. Losses were assumed to be 1% per pass for thorium, uranium, and plutonium. Protactinium losses were

based on a 180-day decay time from the time of discharge from the reactor. Holdup time was established for each concept.

## 2.7 Fuel Preparation

Fuel preparation was defined to include the preparation of ceramic-grade oxide powder, arc-fused oxide fragments, sol-gel oxide fragments, or thorium metal powder or sponge, as appropriate. Enriched uranium obtained as  $UO_6$  and plutonium obtained as nitrate were assumed to be converted to the proper form for inclusion in the fuel as part of the fuel preparation steps. The facilities required for fuel preparation were assumed to be associated with those for reprocessing or fabrication as suitable, and cost estimates were based on the financing conventions applied to the other plants.

## 2.8 Fuel Shipping

Shipping costs for fresh and spent fuels were estimated for each reactor concept. It was assumed that fabrication and reprocessing were to be performed at the same site, located 1000 miles from the reactor. For spent fuels, casks were assumed to be purchased at a cost of \$1.00 per pound of cask weight; casks were shared among 15 identical reactors; the upper weight limit for casks was 110 tons loaded; the cask life was 30 years; handling cost was \$500 per round trip; rail freight rates were \$0.0193 per pound for loaded casks and \$0.0181 per pound for empty casks; and property insurance cost was 0.05% of the value of the shipment, including cask and contents. Casks used for shipping recycled fresh fuel (thorium cycle) were assumed to be the same type as those used for spent fuels. Fresh fuels having essentially no gamma activity were assumed to be shipped in nonshielded containers. The cost of liability insurance was included in the charges against the reactor, processing, and fabrication plants.

Reference

1. Guide to Nuclear Power Cost Evaluation, USAEC Report TID-7025, Vol. 1, Mar. 15, 1962.

### 3. DESCRIPTION OF REACTORS

Brief descriptions are given here of the power plant and reactor core designs as presented by the design sponsors. More detailed information is given in Chapters 5 and 6. Additional information is given in the reports<sup>1-3</sup> of the design sponsors. The basic plant design was obtained from the AI-CE study; the core designs considered were the uranium fuel cycle (AI-CE study) and the thorium fuel cycle (B&W study).

#### 3.1 Plant Design

The HWOOR power plant uses a 3093-Mw(t) heavy-water-moderated organic-cooled reactor as the heat source to produce superheated steam that is delivered to the turbine at 900 psig and 725°F. Operating on a nuclear reheat steam cycle, the system generates 1076 Mw(e) net. The plant features a process-tube reactor with on-power refueling, carbon steel primary loops, recovery facilities for decomposed organic coolant, primary heat transfer system components located outside the containment building, and efficient energy utilization that yields a net plant efficiency of 34.8%. A simplified flow diagram obtained from the AI-CE study is shown in Fig. 3.1.

Santowax OM coolant (primarily a mixture of ortho- and metaterphenyls) is used to transfer heat from the reactor to the primary heat exchangers. Coolant at 750°F, which is collected in the outlet mixing tank, separates into three parallel loops and is pumped by 90,000-gpm turbine-driven pumps to the superheaters, reheaters, and steam generators. Superheated steam is generated in the evaporator and superheater and is delivered to the turbine-generator. After passing through the steam generator, the 595°F (560°F in B&W design) coolant flows back to the reactor through an inlet mixing tank. Since the pumps and heat exchangers of the primary heat transfer system loops are located in a separate building from the reactor, two motor-operated isolation valves are provided in the inlet and outlet lines of each loop to prevent fission products from being circulated with the coolant if released by fuel-element rupture.

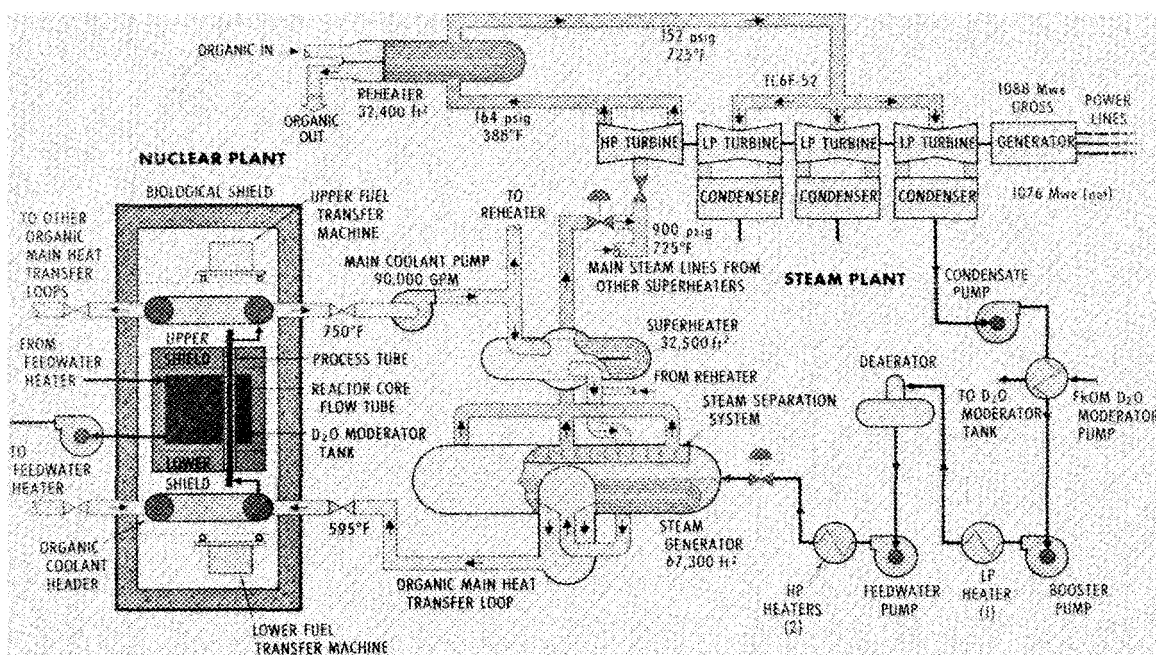


Fig. 3.1. Simplified Schematic Flow Diagram of 1000-Mw(e) HWOCR. (From Ref. 1.)

During reactor operation, the organic coolant undergoes radiolytic and pyrolytic decomposition at the rate of about 1450 lb/hr. The decomposition products, which consist of low boilers, intermediate boilers, high boilers, and decomposition gases, as well as corrosion products, are continuously removed from the coolant stream in order to maintain the coolant at an acceptable purity level. Decomposition gases are removed in degasifiers; corrosion products and particulate matter are removed by passing a fraction of the stream through an activated clay adsorbent and filters. High boilers are removed by distillation and are converted to usable coolant by catalytic hydrocracking. This high-boiler recovery system reduces the coolant loss (due to decomposition) to about 150 lb/hr.

The turbine-generator plant has a single tandem-compound, six-flow, 1800-rpm, steam turbine; the unit has 52-in. last-stage buckets and internal moisture removal features. Steam enters the turbine at 900 psig and 725°F and is reheated before being returned to the three double-flow low-pressure casings, where it expands to the condenser pressure of 1.5 psig. A portion of the hot reheat steam is used to drive the primary pump

and feedwater pump turbines. Extraction steam from the turbine, along with energy deposited in the moderator, is used for feedwater heating.

The basic AI-CE plant design is generally applicable to the three reactor concepts under consideration. However, there are differences in detail between the AI-CE uranium-fueled concept and the two B&W thorium-fueled concepts. Plant and core characteristics for the three designs are compared and summarized in Table 3.1.

Table 3.1. Summary of Reactor Characteristics  
(Supplied by design sponsors)

	AI-CE UC-Fueled Design	B&W (Th-U)O <sub>2</sub> Fueled Design	B&W Th-U Metal- Fueled Design
<b>Reactor power</b>			
Total fission power, Mw	3093	3082	3082
Net electrical power, Mw	1076	1076	1076
Net thermodynamic efficiency, %	34.8	34.9	34.9
<b>Coolant</b>			
Composition	Santowax OM + 10% high boilers	Santowax OM + 10% high boilers	Santowax OM + 10% high boilers
Reactor pressure drop, header to header, psi	184	222	218
Flow rate, lb/hr	110 × 10 <sup>6</sup>	89.9 × 10 <sup>6</sup>	89.9 × 10 <sup>6</sup>
Core inlet temperature, °F	595	560	560
Mean core outlet temperature, °F	750	750	750
Number of coolant loops	3	3	3
<b>Core thermal performance</b>			
Average heat flux, Btu/hr·ft <sup>2</sup>	134,100	135,000	148,900
Maximum heat flux, Btu/hr·ft <sup>2</sup>	356,000	349,000	360,000
Maximum fuel surface temperature, °F	850	850	850
Average core power density, kw/liter	15.2	14.1	14.9
Average specific power, kw/kg of fertile material	25.1	53.0	33.0
<b>Description of core and fuel</b>			
Moderator material	D <sub>2</sub> O	D <sub>2</sub> O	D <sub>2</sub> O
Reflector material	D <sub>2</sub> O	D <sub>2</sub> O	D <sub>2</sub> O
D <sub>2</sub> O inventory, lb	654,000	633,000	621,000
Fuel material	UC	(Th-U)O <sub>2</sub>	Th-U
Equivalent diameter of core, ft	21.9	20.1	19.0
Active height of core, ft	18	23	24.3
Number of channels	492	335	299
Number of assemblies per channel	5	6	6
Fuel element type	37-pin cluster	66-pin cluster	5 nested cylinders
Lattice pitch, in. (square)	10.5	11.67	11.67
Process tube material	SAP-895	SAP	SAP
Process tube inside diameter, in.	4.32	5.00	5.00
Process tube thickness, in.	0.116	0.093	0.093
Calandria tube material	Zircaloy-2	Zircaloy-2	Zircaloy-2
Calandria tube inside diameter, in.	5.094	5.366	5.366
Calandria tube thickness, in.	0.052	0.072	0.072
Cladding material	SAP	XAP-004	Zircaloy-4
Cladding outside diameter, in.	0.521	0.356	
Cladding thickness, in.	0.020	0.020	0.025
Fuel thickness or diameter, in.	0.476	0.316	0.100

Table 3.1 (continued)

	AI-CE UC-Fueled Design	B&W (Th-U) <sub>2</sub> Fueled Design	B&W Th-U Metal- Fueled Design
Description of fuel cycle			
Fuel management scheme	Continuous, on line, bidirec- tional	Continuous, on line, bidirec- tional	Continuous, on line, bidirec- tional
In-core residence time at 0.8 load factor, years	2.0	1.3	2.1
Core average fuel exposure, Mwd/MT	15,000	20,000	20,000
Control system			
Method of shim control	Soluble poison and poison rods	Soluble poison and poison rods	Soluble poison and poison rods
Number of shim rods	60	60	60
Rod material	Borated stainless steel	Borated stainless steel	Borated stainless steel
Total rod worth, % $\delta k$	0.5	0.5	0.5
Method of safety control	Poison rods	Poison rods	Poison rods
Number of safety rods	84	84	84
Rod material	Stainless steel-- B <sub>4</sub> C	Stainless steel-- B <sub>4</sub> C	Stainless steel-- B <sub>4</sub> C
Total rod worth, \$ $\delta k$	4	4	4
Reactor vessel			
Type	Calandria	Calandria	Calandria
Material	Stainless steel	Stainless steel	Stainless steel
Outside diameter	25 ft	22 ft 3 in.	21 ft 5 in.
Turbine plant			
Throttle steam pressure, psig	900	900	900
Throttle steam temperature, °F	725	725	725
Type of steam cycle	Superheat, nu- clear reheat	Superheat, nu- clear reheat	Superheat, nu- clear reheat
Feedwater return temperature, °F	420	420	420
Arrangement of turbine-generators	Tandem compound, six flow	Tandem compound, six flow	Tandem compound, six flow

### 3.2 Core Design

A summary of the core design features is included in Table 3.1. Because of the similarity in core concepts, the following descriptions are given primarily in terms of the AI-CE design, with those B&W core features cited that emphasize the differences in the designs for the two fuel cycles.

#### 3.2.1 AI-CE Uranium-Fueled Core

The core consists of 492 fuel channels, with each containing a stack of five SAP-clad slightly enriched uranium carbide fuel assemblies. The fuel feed material is always slightly enriched uranium, and the plutonium

obtained at the end of each fuel-exposure cycle is sold. The fuel channels are arranged vertically in a calandria vessel that contains the heavy-water moderator. Each channel is defined by a 4.32-in.-ID, 0.116-in.-thick SAP process tube, containing the coolant, which is surrounded by a 5.09-in.-ID, 0.052-in.-thick Zircaloy-2 calandria tube in contact with the moderator. There is an insulating gap of  $\text{CO}_2$  between the process tube and the calandria tube that also serves as a leak-detection volume. Carbon steel extensions of the SAP tubes terminate at horizontal planes approximately 12 ft above and below the 3-ft-thick reactor end shields. The reactor end shields and circumferential thermal shields are joined to provide a  $\text{CO}_2$ -filled cavity around the reactor. The reactor vessel is a stainless steel calandria tank in the form of a cylinder 25 ft in diameter and 20 ft high. The  $\text{D}_2\text{O}$  moderator fills the space between the calandria tubes, while Santowax OM coolant is circulated through the process tubes.

Each fuel assembly consists of 37 uranium carbide fuel rods clad in SAP tubes. Thirty-one rods of 0.521-in. diameter and six rods of 0.324-in. diameter are used to form a fuel assembly of 4.260-in. diameter. The rods are spaced by means of spiral fins. Each fuel assembly has an overall length of 44 in., and five such assemblies are stacked in a process tube. The average power output per process tube is about 5.9 Mw(t), and the average fuel specific power is about 25 kw per kilogram of fertile material. The fuel assemblies are on a 10.5-in.-square lattice pitch.

Bidirectional on-line refueling is used for shim control; two machines operate together from above and below the reactor to effectively move fuel in opposite directions in adjacent process tubes. The coolant flow is also bidirectional and in the same direction as the fuel feed within each tube. The coolant joins the inlet and outlet headers through individual pigtailed connections connected to the carbon steel extensions; it enters the reactor at  $595^\circ\text{F}$  and undergoes a pressure drop of about 185 psi in passing through the reactor (one pass).

Reactivity shutdown control is provided by 84 horizontal rods of boron-carbide and stainless steel; these rods are held out of the core region by  $\text{D}_2\text{O}$  hydraulic pressure during reactor operation and are inserted by springs for shutdown. Xenon oscillation and power level control are provided by 60 vertically adjustable absorber rods supported by steel

tapes; these tapes are stored on motor-driven drums located at the top of the reactor between process tubes. Control during startup and also backup shutdown control are provided by dissolving boron in the moderator.

### 3.2.2 B&W Thorium-Uranium-Fueled Core

The basic arrangement of the B&W core is similar to that of the AI-CE core described above. However, there are significant differences. The initial fuel for the B&W core consists of thorium with  $^{235}\text{U}$  added as the fissile material; in subsequent cycles the bred  $^{233}\text{U}$  is recycled with makeup  $^{235}\text{U}$  added as needed. The B&W designs consider two basic fuel assemblies; one utilizes annular metallic fuel elements, and the other has pin-type clusters containing oxide fuel.

The metallic assembly consists of five 0.10-in.-wall thorium-uranium metal cylinders clad in Zircaloy-4 and arranged concentrically in the process tube with a Santowax region in the center. The coolant channels between cylinders are of varying thicknesses that decrease toward the center. The fuel cylinders, together with the cladding, are made by a coextrusion process. Six assemblies are stacked in a channel, and there are 299 channels in the core. The average power generation per channel is 9.75 Mw(t), and the specific power is 33 w per kilogram of fertile material.

The oxide pin assembly consists of a 66-pin cluster of  $\text{ThO}_2\text{-UO}_2$  clad in XAF-004. The fuel pins are 0.356 in. in outside diameter and are arranged in a hexagonal array between a hexagonal can and the process tube to approximate an annular region. The space inside the hexagonal can is filled with Santowax and orificed relative to coolant flow so that the Santowax outlet temperature is the same as that of the main coolant. Six fuel assemblies make up the loading for one channel. The core has 335 channels, and the average power generation is 8.7 Mw(t) per channel. The average specific power is 53 kw per kilogram of fertile material.

B&W employs a larger process tube, 5.00-in. ID rather than 4.32 in., and a larger calandria tube, 5.37-in. ID rather than 5.09 in. The B&W lattice pitch is 11.67 in. compared with 10.5 in. for the AI-CE design.

Coolant flow is downward through the core in all channels in the B&W design rather than being bidirectional. B&W uses bidirectional fuel management, but the handling is all accomplished by one refueling machine at

the top. The design thus requires that a channel be completely unloaded when one of the six assemblies is replaced. The organic coolant enters the reactor at 560°F and undergoes a pressure drop of about 220 psi in passing through the reactor.

The B&W reactor vessels are of stainless steel construction but have integral stainless steel end shields instead of the separate carbon steel end shields used in the AI-CE design. The heights of the moderator tank inside the 3-ft-deep end shields are 25 ft 2 in. for the pin-type fuel elements and 26 ft 5 in. for the cylinder design. The diameters of the vessels are 22 ft 3 in. and 21 ft 5 in. for the pin and cylinder designs, respectively.

#### References

1. Combustion Engineering, Inc., and Atomics International, Heavy Water Organic Cooled Reactor - 1000 Mw(e) Nuclear Power Plant Preliminary Conceptual Design, USAEC Report AI-CE-Memo-6, Vols. I and II, Oct. 1, 1965.
2. Babcock & Wilcox Company, Thorium Fuel Cycle for Heavy Water Moderated Organic Cooled Reactors, Quarterly Technical Report No. 2, April-June, 1965, USAEC Report BAW-393-2, October 1965.
3. Babcock & Wilcox Company, 1000 MWe Thorium HWOCR - Preliminary Conceptual Design Data for ORNL Evaluation, USAEC Report (unnumbered), Nov. 15, 1965.

#### 4. PHYSICS ANALYSIS OF HWOCR SYSTEMS

The reactor physics analysis computations for the three reactor cores evaluated were made in a manner analogous to that used in the comparative evaluation of advanced converters.<sup>1</sup> In both evaluations the primary emphasis was placed on determining the economic performance of the systems when operated with appropriate fuel-management schemes. Thus an important goal was the calculation of fuel feed requirements and discharge fuel composition as a function of fuel feed burnup.

Since the three heavy-water-moderated organic-cooled reactors involved in this study are very similar, the calculational procedures employed were for the most part the same. The major differences required in procedure were brought about by the different placement of fuel within the pressure tube and the different fuel materials. Careful attention was given to details of the cell and spectrum calculation to provide the best choice of computational techniques.

##### 4.1 Zero-Dimensional Depletion Calculations

The zero-dimensional multigroup code TONG<sup>2</sup> was used almost exclusively for the depletion calculations in this study. The point depletion model was chosen primarily to hold the computer time requirements to a reasonable level. The model appears to be adequate for use in large reflected cores in which the power distribution is relatively uniform in space. In order to include the effects of neutron leakage, the critical group-dependent bucklings were computed for the reactors zoned both radially and axially following the indicated loadings of the respective reactor sponsor. This calculation was done by ASSAULT<sup>3</sup> in two-dimensional r-z geometry.

In the TONG calculation the core may be reloaded by a multibatch technique by identifying the individual batches of fuel separately. The code will currently handle 15 separate batches of fuel. The cycle sequence for removing fuel batches can be specified, as well as the replacement fuel composition. After a suitable delay for reprocessing (a specified number of refueling intervals) the recovered fuel may be returned

to the core along with a specified makeup fuel. Control can be maintained by various options of poison control, moderator composition changes, or fuel composition changes. Thus a complete history of the operating life of a reactor can be established with one continuous computer calculation.

#### 4.2 Calculation of Spectra and Cross Sections

The TONG program uses modified versions of GAM-I<sup>4</sup> and THERMOS<sup>5</sup> to calculate fast and thermal group cross sections for use in the depletion studies. The basic cross sections<sup>6</sup> used in this study were essentially those used in the comparative evaluation of advanced converters.<sup>1</sup> The only changes were for <sup>233</sup>Pa and <sup>232</sup>Th.

For <sup>233</sup>Pa we used the more recently measured resolved resonance parameters<sup>7</sup> but did not change the total resonance integral. For thorium we used a negative energy resonance to give the known non-1/v energy dependence and recalculated the cross section in the thermal energy range. The new cross section is the same as the old one at 2200 m/s, and the overall effect of the change should be unimportant.

We used only the <sup>233</sup>U cross-section set that yields the lower (0.17) average alpha above 0.4 ev rather than the cross-section set which yields the higher (0.23) average alpha. Recent experimental measurements<sup>8,9</sup> lend further support to this choice, although the matter cannot yet be regarded as completely settled.

In the epithermal energy range, resonance parameters were used to determine shielded cross sections for the fertile isotopes (including <sup>234</sup>U and <sup>240</sup>Pu) and for <sup>233</sup>Pa, <sup>236</sup>U, and <sup>242</sup>Pu. Shielded cross sections for zirconium were also obtained from the resonance parameters. Unshielded group cross-section data were used for all other nuclides, including the fissile nuclides.

In order to allow for spectrum changes with time, all depletion calculations were made with five fast groups (above 1.86 ev) and four thermal groups. These nine group cross-section sets were computed specifically for each reactor design.

To treat the enhanced fast fission and absorption caused by heterogeneity of fuel and moderator, neither of which are included in the basic

GAM-I calculations, we developed a procedure for computing group advantage factors. These factors were incorporated in the GAM-I fast spectrum and multigroup cross-section calculations. This procedure was found to improve significantly the agreement between the results of TONG calculations and corresponding results from critical and exponential facility experiments.<sup>10</sup>

The THERMOS code was modified to obtain the individual fuel pin disadvantage factors in the thermal range and subsequently to obtain group-averaged cross sections appropriate to the entire unit cell of fuel pin cluster, pressure tube, and associated D<sub>2</sub>O moderator. In this procedure two successive THERMOS cases are required. The first, or pin-cell, calculation modifies the basic 30-group cross sections by applying flux factors to all materials within the average pin cell. The second THERMOS calculation treats the pressure tube and its accompanying moderator as a unit cell and uses the adjusted 30-group set of cross sections for the final spectrum and cross-section averaging.

#### 4.3 Calculation of Reactivity Coefficients

Reactors of the type considered in this evaluation tend to be over-moderated, since the minimum pressure-tube spacing is dictated by mechanical considerations. As a result, the moderator temperature coefficients can be positive. The use of an organic as the coolant with its attendant high neutron losses to hydrogen makes the coolant temperature and coolant void coefficients positive also. The fuel Doppler coefficient is negative but not large. The combination of the reactivity coefficients can produce a condition in which an increase in power causes the reactivity to increase.

To determine the magnitudes of the reactivity coefficients a large number of GAM-I and THERMOS calculations were made. The following quantities were investigated:

1. fuel temperature from 68 to 1200°F,
2. coolant temperature from 190 to 675°F,
3. moderator temperature from 68 to 190°F,

4. coolant void from zero to 100%,
5. moderator purity from 99.75 to 97.0 mole % D<sub>2</sub>O.

Thermal scattering kernels for hydrogen, oxygen, deuterium, and carbon were computed specifically for each temperature. Since hydrogen is in the cell as a coolant and as a part of the moderator and carbon is in the cell as part of the coolant and as diluent in the fuel, it was presumed necessary to provide scattering kernels for each of these materials at more than one temperature.

Very few applicable experiments have been run that provide data for evaluating the method used in computing the various reactivity coefficients. Comparison with two Zed-2 experiments<sup>10</sup> shows our calculations to have been within 50% of the experimental coolant void coefficient.

#### 4.4 Optimization of the Fuel Cycles

In the short time available, it was not possible to investigate in detail the behavior of each reactor concept. At the same time, it was desirable that the fuel cycle be optimized with respect to the specified economic parameters. This required defining an approach to equilibrium-cycle operation and optimizing the equilibrium cycle. An optimization of the startup cycle was not attempted, but efforts were made to prevent penalizing either concept by choice of a poor approach to equilibrium.

In order to optimize cycles for low fuel costs, the cycle times were varied around that chosen by the sponsors. This was done by adding fuel or subtracting fuel at the beginning of each cycle.

In general the procedure followed was to specify a small excess reactivity value at the start of each depletion time step. Each cycle was then divided into an appropriate number of time steps; at the beginning of each intermediate time step the reactor was brought back to the specified value of reactivity by the addition of fuel. Depletion over a small time step was done without additional poison, and the time steps were chosen so that the change in reactivity over a time step was generally about 1%. In this manner the continuous refueling assumed for these reactors should be approximated quite well.

A basic difference in the initiation of the first fuel cycles was considered for the AI-CE and the B&W designs. For the AI-CE reactor depletion calculation an axially zoned enrichment was assumed, as indicated in the proposal.<sup>10</sup> The fuel management for the first cycle in this reactor was assumed to be no different from that for the other cycles. The lowest enrichment fuel was withdrawn quite soon after startup. For the B&W reactors the axial loading was assumed to be uniform. In order that the fuel elements would not be removed prematurely, it was assumed that the reactor would be loaded initially with sufficient reactivity such that no fuel would be withdrawn before it had an accumulated lifetime of about one-fourth the average for later batches. Succeeding cycles were treated as in the AI-CE design, except that discharge uranium was recycled in the B&W design, whereas no fuel recycle occurred in the AI-CE design.

#### 4.5 Calculation of Power-Peaking Factors

Power-peaking factors were investigated in some detail for all three reactors. A more complete study was made for the AI-CE reactor, with investigation of the effects of depletion.

In general the procedure involved investigation of the effects discussed below:

1. Gross radial and axial power distributions were obtained from two-dimensional r-z calculations. In these calculations the regions containing the end fittings were specifically identified. The compositions in each region were assumed to be averages of those of two adjacent fuel channels.

2. The channel interaction between fresh and depleted fuel was obtained by mocking up two adjacent fuel channels as slabs in a two-dimensional x-y geometry calculation for which the axial region concentrations could be explicitly described.

3. The local radial power distribution was obtained from THERMOS calculations in which the volume within the process tube was subdivided into at least three different fuel regions. This calculation was performed for all reactors at beginning of life. For the AI-CE reactor the

effect of radial changes in fuel composition on local power density as a function of depletion was also investigated.

#### 4.6 Physics of the Uranium-Fueled HWO CR

Our reactor physics analysis of the uranium-fueled HWO CR was divided into three parts:

1. Multidimensional calculations of the core and reflector were made to determine the critical core bucklings and the power density distribution throughout the core. The reactivity computed for these cases served as a check on the reactivity of the zero-dimensional calculations.

2. Fuel, coolant, and moderator reactivity coefficients were computed.

3. Reactor depletion calculations were made for fuel-cycle and long-term-behavior analysis of the reactor.

##### 4.6.1 Multidimensional Reactor Calculations

The basic multidimensional calculations consisted of an r-z calculation of the entire core, as described in the AI-CE report,<sup>10</sup> an x-y calculation of two adjacent channels, and a radial calculation to obtain the local power distribution within the pressure tube. The two-dimensional r-z calculations were done for startup conditions and for the equilibrium fuel composition predicted from the TONG zero-dimensional calculation. Critical group-dependent bucklings were computed from the startup case and used in all subsequent depletion cases. The computed bucklings are given in Table 4.1. The corresponding geometric buckling based on 1.0-ft reflector savings was  $0.000070 \text{ cm}^{-2}$ . Thus the critical buckling for the radially and axially zoned core was substantially greater than the geometric buckling. This is especially evident for the higher energy groups. Table 4.2 shows a comparison of the two-dimensional calculation with several point calculations made with different buckling approximations. This table indicates that the use of bucklings derived from a two-dimensional calculation of an axially and radially zoned core will improve the accuracy of the zero-dimensional method for at least the effective criticality and the conversion ratio.

Table 4.1. Group-Dependent Bucklings  
for the Uranium-Fueled HWOCR

Group	Upper Energy (ev)	Buckling ( $\text{cm}^{-2}$ )
1	$1.0 \times 10^7$	
2	$8.21 \times 10^5$	0.00061
3	$3.18 \times 10^4$	0.00038
4	1230.0	0.00025
5	47.9	0.00012
6	1.86	0.00015
7	0.65	0.00015
8	0.18	0.00011
9	0.06	0.00002

Table 4.2. Comparison of Point and Dimensional  
Calculations

Average fuel enrichment: 0.800 wt %

Method	Buckling	$k_{\text{eff}}$
Two dimensional		1.0370
Zero dimensional	0.00007	1.0448
Zero dimensional	From two-dimensional calculation	1.0377

Gross power distributions were computed from the two-dimensional r-z calculations at both startup and equilibrium concentrations as predicted by the zero-dimensional depletion calculation. These results are presented in Tables 4.3 and 4.4 as a power density map of the core. The tables show a gross maximum-to-average power ratio of 1.653 at startup and 1.595 for the equilibrium core. Since the power distributions for both cases are relatively alike, it appears that AI-CE made good choices for the initial concentrations. Figure 4.1 shows the relative radial power density along the horizontal section containing the gross maximum power. Our calculated maximum-to-average power ratio is 1.39 compared with the 1.17

Table 4.3. AI-CE 1000-Mw(e) HWOCR Gross Power Density Distribution for the Initial Core Loading

Axial Zone	Distance from Axial Mid-Plane (cm)	Gross Power Density <sup>a</sup>									
		Inner Radial Zone					Outer Radial Zone				
		8.8 cm <sup>b</sup>	26.3 cm	113.8 cm	166.3 cm	236.4 cm	236.4 cm	275.6 cm	314.7 cm	329.4 cm	334.3 cm
Outer	270.5	0.523	0.514	0.490	0.449	0.367	0.380	0.301	0.195	0.157	0.147
	262.7	0.625	0.614	0.585	0.537	0.439	0.454	0.360	0.234	0.189	0.179
	227.6	1.140	1.119	1.067	0.982	0.807	0.835	0.666	0.432	0.351	0.334
	196.3	1.462	1.437	1.372	1.266	1.052	1.089	0.875	0.570	0.464	0.441
	165.1	1.653	1.625	1.554	1.442	1.219	1.262	1.026	0.674	0.548	0.519
Nonfueled											
Intermediate	161.6	1.555	1.530	1.464	1.358	1.151	1.237	1.007	0.662	0.539	0.510
	126.5	1.563	1.537	1.474	1.374	1.189	1.277	1.054	0.699	0.572	0.544
	91.3	1.543	1.520	1.460	1.368	1.198	1.287	1.070	0.714	0.585	0.557
	56.2	1.509	1.487	1.431	1.346	1.187	1.276	1.066	0.714	0.584	0.555
Nonfueled											
Central	52.8	1.448	1.426	1.373	1.291	1.139	1.228	1.026	0.687	0.563	0.534
	37.7	1.397	1.376	1.325	1.248	1.103	1.188	0.994	0.667	0.549	0.522
	22.6	1.376	1.356	1.306	1.230	1.089	1.174	0.983	0.660	0.544	0.518
	7.6	1.368	1.348	1.299	1.224	1.085	1.168	0.979	0.658	0.542	0.516

<sup>a</sup>Data normalized to an average power density of 1.0 in fueled regions.

<sup>b</sup>Core radius.

Table 4.4. AI-CE 1000-Mw(e) HWCCR Gross Power Density Distribution for the Equilibrium Core Loading

Axial Zone	Distance from Axial Mid-Plane (cm)	Gross Power Density <sup>a</sup>									
		Inner Radial Zone					Outer Radial Zone				
		8.8 cm <sup>b</sup>	26.3 cm	113.8 cm	166.3 cm	236.4 cm	236.4 cm	275.6 cm	314.7 cm	329.4 cm	334.3 cm
Outer	270.5	0.353	0.349	0.340	0.326	0.300	0.305	0.261	0.178	0.146	0.139
	262.7	0.406	0.402	0.392	0.375	0.346	0.352	0.302	0.206	0.172	0.167
	227.6	0.763	0.755	0.735	0.704	0.650	0.660	0.568	0.387	0.324	0.316
	196.3	1.065	1.054	1.026	0.982	0.900	0.915	0.784	0.532	0.446	0.435
	165.1	1.380	1.366	1.331	1.273	1.152	1.171	0.992	0.672	0.560	0.542
Nonfueled											
Intermediate	161.6	1.405	1.391	1.355	1.297	1.171	1.209	1.023	0.692	0.576	0.558
	126.5	1.541	1.527	1.490	1.429	1.287	1.327	1.119	0.759	0.637	0.622
	91.3	1.595	1.581	1.546	1.490	1.362	1.405	1.194	0.815	0.685	0.669
	56.2	1.548	1.553	1.523	1.479	1.399	1.444	1.258	0.867	0.726	0.704
Nonfueled											
Central	52.8	1.540	1.528	1.499	1.456	1.385	1.435	1.255	0.866	0.725	0.703
	37.7	1.424	1.413	1.388	1.353	1.313	1.360	1.207	0.838	0.707	0.690
	22.6	1.374	1.364	1.340	1.309	1.289	1.335	1.197	0.833	0.704	0.689
	7.6	1.352	1.342	1.319	1.291	1.280	1.325	1.193	0.833	0.723	0.689

<sup>a</sup>Data normalized to an average power density of 1.0 in fueled regions.

<sup>b</sup>Core radius.

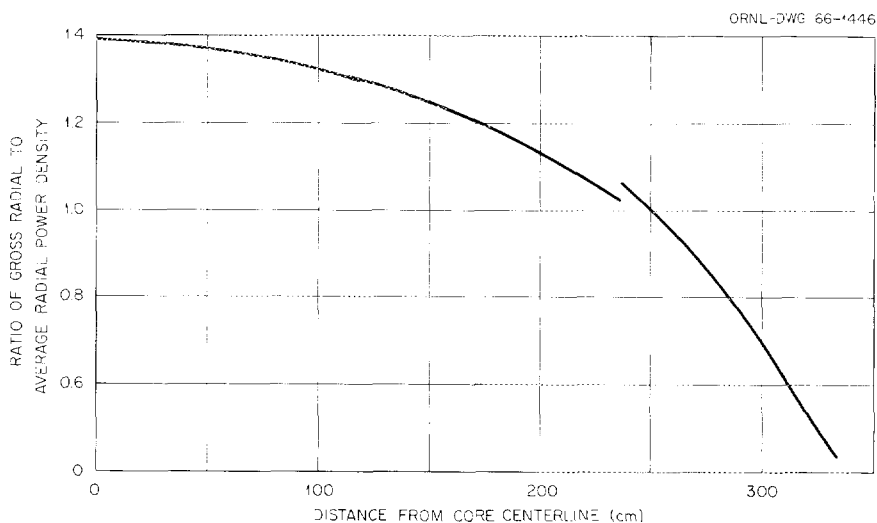


Fig. 4.1. Gross Radial Power Distribution for AI-CE HWOCR Design Conditions.

reported by AI-CE.<sup>11</sup> Thus, for the startup fuel concentrations, as chosen by AI-CE, the ORNL calculations do not show the high degree of power flattening reported by AI-CE.<sup>11</sup> Because of this, a series of one-dimensional radial calculations were done to investigate the amount of change in average fuel concentration required to further flatten the radial power distribution. The base concentrations chosen were those associated with the midplane of the equilibrium core. These concentrations were representative of those fuel feed rates which would yield final exposures of about 16,800 Mwd/MT in the inner zone and 12,600 Mwd/MT in the outer zone. Nominal  $\pm 5$  and  $\pm 10\%$  changes in each of these concentrations were made in successive calculations. The results indicate that changing the fuel concentrations by about 5% should permit achievement of the maximum-to-average power ratio given in the AI-CE design report. Fuel-concentration changes of this amount would have only a minor effect on the economic performance of the reactor. A 10% change in fuel concentration is equivalent to a final reactivity lifetime of approximately 18,500 Mwd/MT in the inner zone and 11,600 Mwd/MT in the outer zone. Thus, small changes in fuel concentration and neutron leakage have relatively large effects on radial power distribution, which emphasizes the need for careful spatial reactivity

control in order to limit power-peaking factors throughout reactor operations.

The x-y calculation of two adjacent channels yields information on the effects of the significantly different fuel concentrations on the local power density. These calculations were made for the startup core compositions specified by AI-CE and for the equilibrium distribution computed by TONG. These results are presented in Table 4.5 as an axial power density traverse. Figure 4.2 shows the axial power density distribution along a fuel channel for the startup core and the equilibrium core. The maximum-to-average power density ratio for these two channels is 1.609 for the startup core and 1.516 for the equilibrium core. The combination of the fine axial and channel interaction effects on the power density was found to be 1.250 for the startup core.

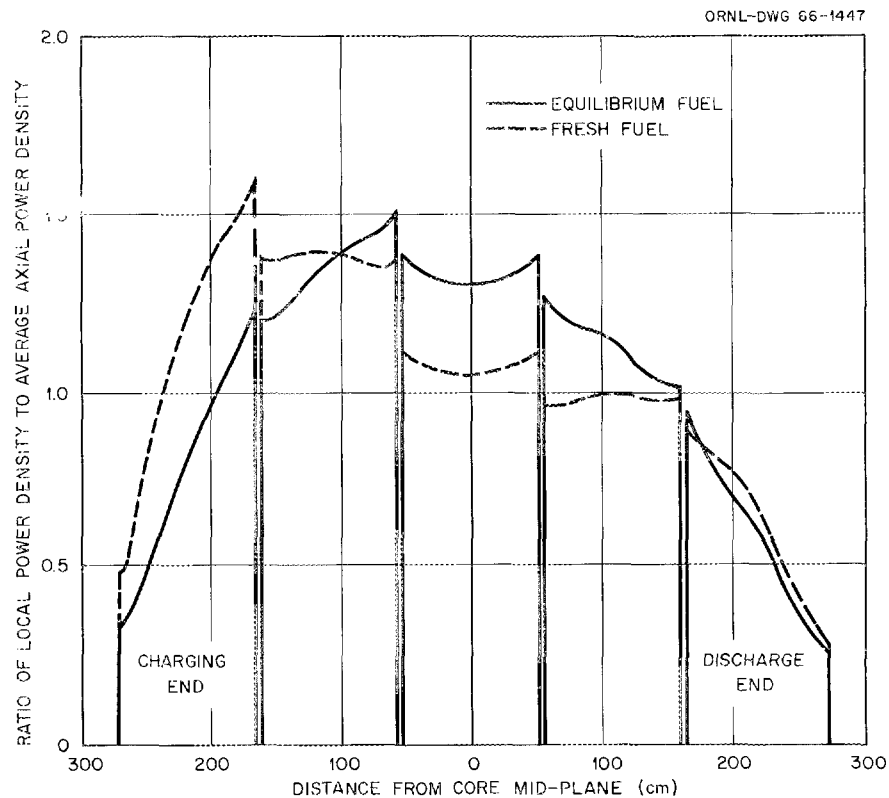


Fig. 4.2. AI-CE 1000-Mw(e) HWO CR Axial Power Distribution for a Two-Dimensional Biaxial Refueling Cell Model.

Table 4.5. AI-CE 1000-Mw(e) HWOCR Axial Power Distribution<sup>a</sup>

Axial Zone	Distance from Reactor Mid-Plane (cm)	Ratio of Local Fuel Power Density to the Average Axial Fuel Power Density			
		Initial Core Loading		Equilibrium Core Loading	
		Charging End	Discharge End	Charging End	Discharge End
Outer	270.5	0.504	0.277	0.337	0.249
	267.0	0.543	0.302	0.358	0.263
	260.0	0.633	0.354	0.413	0.302
	235.4	0.985	0.551	0.651	0.475
	217.8	1.200	0.671	0.822	0.595
	200.2	1.368	0.765	0.964	0.703
	175.6	1.529	0.856	1.154	0.848
	168.6	1.581	0.881	1.220	0.901
	165.1	1.609	0.891	1.255	0.932
Nonfueled					
Intermediate	161.6	1.386	0.971	1.216	1.005
	158.1	1.382	0.971	1.213	1.005
	151.1	1.376	0.968	1.219	1.013
	126.5	1.389	0.979	1.308	1.090
	108.9	1.392	0.981	1.367	1.139
	91.3	1.381	0.973	1.411	1.175
	66.7	1.357	0.958	1.462	1.224
	59.7	1.367	0.961	1.494	1.257
	56.2	1.373	0.962	1.516	1.281
	Nonfueled				
Central	52.7	1.121	1.120	1.399	1.382
	49.2	1.109	1.108	1.375	1.363
	42.2	1.087	1.085	1.343	1.337
	17.6	1.058	1.058	1.324	1.323

<sup>a</sup>Calculated for a two-dimensional bidirectional refueling cell model.

The fine radial power density was investigated by THERMOS calculations. Depletion effects were included by doing the calculations for fuel mixtures corresponding to reactivity lifetimes predicted by the zero-dimensional depletion cases and assuming a spatial dependence of the nuclides within the fuel region in accordance with a previous one-dimensional depletion calculation.<sup>12</sup> The results are given in Table 4.6 as a function

Table 4.6. Radial Power Density Distribution in Fuel Element Cell as a Function of Irradiation for AI-CE Core

	Inner Ring Plus Central Pin	Second Ring	Outer Ring
Number of fuel pins	7	12	18
Fuel volume fraction	0.1898	0.3260	0.4842
Relative power density			
For 1,000 Mwd/T irradiation	0.629	0.817	1.269
For 3,000 Mwd/T irradiation	0.645	0.834	1.251
For 7,000 Mwd/T irradiation	0.658	0.842	1.241
For 15,000 Mwd/T irradiation	0.697	0.860	1.213

of burnup and relative position within the pressure tube. These results are quite similar to those reported by AI-CE in Fig. II-16 of Ref. 11.

Our power distribution results at startup may be summarized in comparison with those reported by AI-CE as follows:

	<u>ORNL</u>	<u>AI-CE</u>
Gross radial power ratio	1.39 (1.17)*	1.17
Gross axial power ratio	1.20	1.33
Fine radial power ratio	1.27	1.30
Fine axial power ratio	1.25	1.175

We made no check on the AI-CE estimate of 1.05 for the local flux tilt due to xenon oscillation. It appears to be a reasonable estimate.

---

\*The 1.39 value was obtained for the specific AI-CE design conditions; however, the gross radial power ratio is very sensitive to fuel concentrations and neutron leakage, and we concur that a 1.17 value can be obtained without significant economic penalty.

#### 4.6.2 Reactivity Coefficients

Calculations were made with GAM-I and THERMOS to determine the reactivity coefficients associated with fuel, coolant, and moderator temperature change, coolant void, and moderator purity. The results are presented and compared with those of similar computations performed by AI-CE in Table 4.7. There are considerable uncertainties in the quantitative results for the reactivity coefficient calculations, as indicated by the variation between ORNL and AI-CE results for the same cores. However, the same general effects are observed from both sets of data. Based on these results, the HWOCR will have

1. significant, positive coolant and moderator temperature coefficients for the equilibrium core;
2. strong, positive coolant void coefficients;
3. a negative fuel temperature coefficient both with fresh and equilibrium fuel mixtures.

Table 4.7. Summary of Reactivity Coefficients for AI-CE HWOCR

	Reactivity Coefficients		
	Equilibrium Concentrations		ORNL <sup>b</sup> Startup Concentrations
	AI-CE <sup>a</sup>	ORNL <sup>a</sup>	
Fuel temperature, $\Delta k_e / \Delta T (^{\circ}\text{F})$	$-0.4755 \times 10^{-5}$	$-0.5586 \times 10^{-5}$	$-0.5245 \times 10^{-5}$
Coolant temperature, $\Delta k_e / \Delta T (^{\circ}\text{F})$	$+0.5299 \times 10^{-4}$	$+0.4054 \times 10^{-4}$	$+0.2077 \times 10^{-5}$
Moderator temperature, $\Delta k_e / \Delta T (^{\circ}\text{F})$	$+0.4401 \times 10^{-5}$	$+0.8205 \times 10^{-6}$	$-0.1129 \times 10^{-4}$
Moderator purity, $\Delta k_e / (\Delta\% \text{H}_2\text{O})$ 0.9975 to 0.99 mole fraction D <sub>2</sub> O	-0.015913	-0.01956	-0.02704
Coolant void, $\Delta k_e / (\Delta\% \text{void})$			
At 33 1/3% void	$+0.1110 \times 10^{-3}$	$+0.5793 \times 10^{-4}$	$+0.4008 \times 10^{-3}$
At 66 2/3% void	$+0.1046 \times 10^{-3}$	$+0.4995 \times 10^{-4}$	$+0.4220 \times 10^{-3}$
At 100% void	$+0.1097 \times 10^{-3}$	$+0.3967 \times 10^{-4}$	$+0.4696 \times 10^{-3}$

<sup>a</sup>Calculated for the nearly critical condition,  $k_{\text{eff}} \sim 1.005$ .

<sup>b</sup>Calculated for the supercritical condition,  $k_{\text{eff}} \sim 1.16$ .

#### 4.6.3 Reactor Depletion Calculations

The primary reactor depletion calculations were made with the TONG code. The core materials, dimensions, and physical temperatures employed in these calculations were those specified in the AI-CE report.<sup>10</sup> The initial core loading specified by AI-CE was to be zoned into two radial and ten axial zones. Equilibrium feed enrichment to each equal-volume radial zone was to be the same with the outer zone feed rate greater than that of the inner zone. This was to result in the outer radial zone having an average reactivity lifetime of 13,300 Mwd/MT and the inner zone having a lifetime of 16,700 Mwd/MT. Thus the core as a whole had an average reactivity lifetime of 15,000 Mwd/MT. Fueling of the reactor was to be countercurrent in adjacent channels with five fuel assemblies per channel. Initial axial enrichments were specified in each zone.

The TONG calculation with five fast- and four thermal-neutron groups was used to estimate the concentration behavior in the AI-CE reactor. To approximate closely the operation of continuous refueling, 15 zones (the maximum allowed by the code) were chosen for the calculation. At startup these 15 zones were loaded with five different concentrations representing the average fuel concentrations along a channel in the inner and outer radial zones. In the depletion calculation described here a cycle is defined as the time between refuelings of each of the 15 zones. Thus 15 cycles are required to replace the core completely, and with the exception of the initial core loading, each zone remains in the core for 15 cycles. Critical group-dependent bucklings from two-dimensional calculations were employed for all depletion calculations. As reported earlier, comparison of zero- and two-dimensional calculations showed good agreement at startup.

At each depletion time step within a cycle the reactor was maintained with the excess reactivity between 0.004 and 0.000. Thus the average excess reactivity was approximately 0.002, corresponding to insertion of one-half of the available shim rod worth. For fuel cost calculations, all fuel added during a cycle was assumed to be added at the beginning of the cycle. At the end of each cycle the fuel in the zone having the greatest exposure was removed for reprocessing, and sufficient fresh fuel was added to maintain reactivity. The depletion calculations were made

for three reactivity lifetimes. The summary of the results for these three cases is given in Table 4.8 as cases Q-1, Q-2, and Q-3. Representative core neutron balances as a function of time are given in Table 4.9. The final neutron balance is representative of the equilibrium core. The conversion ratio as a function of time is given in Fig. 4.3. Lifetime mass balances of the heavy metals are given in Table 4.10.

For case Q-2 with an average reactivity lifetime of 15,000 Mwd/MT, AI-CE predicts an initial enrichment of 1.16 wt %  $^{235}\text{U}$ . Our results give a required enrichment of 1.17 wt %  $^{235}\text{U}$ . For the equilibrium core AI-CE predicts an average of 3.16 g of fissile plutonium per kilogram of uranium at discharge, while our results predict 3.20. The agreement of these two quantities is excellent.

We also estimated the effect on the fuel cycle of the reduced neutron economy if it should be necessary to increase the neutron absorptions in shim control rods. For our base calculations we assumed this amount to be approximately 0.2%, on the average. Table 4.11 shows the effect that small, additional amounts of such control poison will have on the equilibrium feed enrichment and on the equilibrium fuel-cycle cost.

Table 4.8. Summary of Cycle Performance for AI-CE Design

	Cases		
	Q-1	Q-2	Q-3
First cycle			
Initial reactivity (no rods)	1.004	1.004	1.004
Initial enrichment, wt % $^{235}\text{U}$	0.786	0.784	0.782
Equilibrium cycle			
Initial reactivity (no rods)	1.004	1.004	1.004
Cycle time, full-power days	510	600	675
Discharge exposure, Mwd/MT of U	12,869	14,842	16,801
Feed enrichment, wt % $^{235}\text{U}$	1.088	1.168	1.251
Discharge enrichment, wt % $^{235}\text{U}$	0.234	0.210	0.189
Discharge Pu, g/kg of U feed	4.83	5.1	5.33
Pu composition, wt %			
$^{239}\text{Pu}$	54.9	52.8	51.1
$^{240}\text{Pu}$	28.6	28.8	28.7
$^{241}\text{Pu}$	11.9	12.7	13.3
$^{242}\text{Pu}$	4.6	5.7	6.9

Table 4.9. Neutron Balance for AI-CE Core  
at 15,000 Mwd/MT, Case Q-2

Cycle number	1, start	6, end	12, end	18, end	36, end
Time, years	0	0.6533	1.3065	1.9598	3.9196
Absorptions					
H in coolant	0.0395	0.0275	0.0252	0.0250	0.0251
H + D in D <sub>2</sub> O	0.0135	0.0101	0.0094	0.0094	0.0094
<sup>235</sup> U	0.4638	0.2307	0.2175	0.2179	0.2171
<sup>236</sup> U		0.0018	0.0025	0.0027	0.0026
<sup>238</sup> U	0.4006	0.3202	0.3038	0.3024	0.3033
<sup>239</sup> Pu		0.2310	0.2293	0.2286	0.2294
<sup>240</sup> Pu		0.0366	0.0481	0.0481	0.0481
<sup>241</sup> Pu		0.0185	0.0320	0.0323	0.0322
<sup>242</sup> Pu		0.0002	0.0009	0.0009	0.0009
O in D <sub>2</sub> O	0.0028	0.0025	0.0025	0.0025	0.0025
Al	0.0417	0.0291	0.0266	0.0264	0.0265
Zr	0.0106	0.0077	0.0072	0.0071	0.0072
<sup>135</sup> Xe		0.0222	0.0219	0.0219	0.0219
<sup>149-152</sup> Sm		0.0105	0.0122	0.0124	0.0123
Fission products		0.0241	0.0343	0.0357	0.0348
Leakage	0.0275	0.0273	0.0266	0.0267	0.0267
Total	1.0000	1.0000	1.0000	1.0000	1.0000
Conversion ratio	0.8197	0.7010	0.6928	0.6901	0.6919

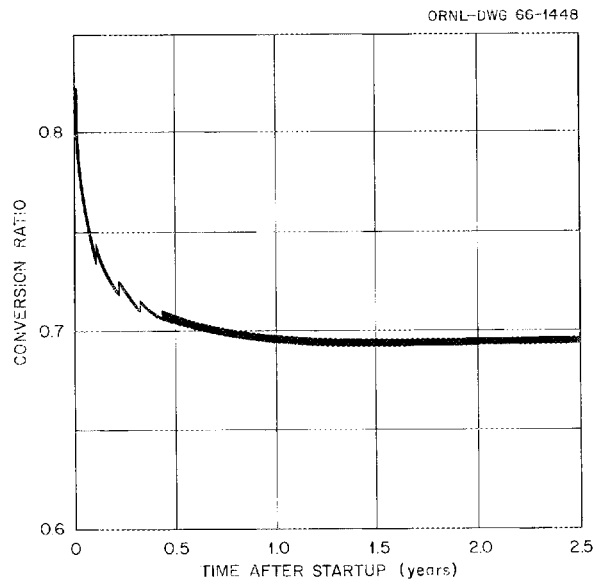


Fig. 4.3. Conversion Ratio for AI-CE HWOCR at 15,000 Mwd/MT.

Table 4.10. Cumulative Mass Balance for Total Reactor History of AI-CE Design

	Cases		
	Q-1	Q-2	Q-3
Reactivity lifetime, Mwd/MT	13,000	15,000	17,000
History time, years, at 0.8 plant factor	5.0	5.75	6.5
Equilibrium fuel residence time, days, at 0.8 plant factor	645	750	840
Initial loading, kg			
<sup>235</sup> U	975.76	972.77	970.74
Total U	124,158	124,155	124,153
Total purchased material, kg			
<sup>235</sup> U	4,643	4,934	5,240
Total U	463,639	463,543	464,236
Final core loading (at discharge), kg			
<sup>235</sup> U	660.18	662.35	667.18
Total U	122,855	122,768	122,686
Fissile Pu	298.72	315.66	330.40
Total discharge (including final core), kg			
<sup>234</sup> U	0	0	0
<sup>235</sup> U	1,518	1,432	1,363
<sup>236</sup> U	505.32	563.55	619.94
<sup>238</sup> U	454,863	454,298	453,746
Fissile Pu	1,298	1,353	1,407

Table 4.11. Effect of Increased Control Poison on AI-CE HWOCR

Average Control Poison (%)	Reactivity Lifetime (Mwd/MT)	Equilibrium Fuel Cost (mills/kwhr)	Feed Enrichment (wt % <sup>235</sup> U)
0.2	14,830	0.852	1.169
0.7	14,827	0.868	1.187
1.0	14,824	0.884	1.204

#### 4.6.4 Comparison of ORNL and AI-CE Depletion Results Obtained by the Same Method

In order to compare our reactivity calculations and basic nuclear data with those of AI-CE we made one depletion calculation with essentially the AI-CE depletion method. This scheme may be described as the depletion of the reactor at a given initial enrichment with cross sections based on supercritical conditions for some specified depletion time.

An AI-CE calculation of this type was available for a depletion time of approximately 7200 hr and an initial  $^{235}\text{U}$  enrichment of 1.16 wt %.<sup>12</sup> A comparison of our results with those of AI-CE is shown in Table 4.12. The group-dependent bucklings previously described were used in the leakage computation. The data show a consistent difference of only 1% in  $k_{\text{eff}}$ . Absorption rates in the important nuclides, hydrogen, zirconium, aluminum,

Table 4.12. Comparison of AI-CE and ORNL Data for AI-CE HWOCR Neutron Balance

Depletion time, hr	0		180		7,239	
	AI-CE	ORNL	AI-CE	ORNL	AI-CE	ORNL
$k_{\text{eff}}$	1.193	1.185	1.151	1.140	1.008	0.994
Computation	AI-CE	ORNL	AI-CE	ORNL	AI-CE	ORNL
Absorptions						
Hydrogen	0.0380	0.0350	0.0362	0.0337	0.0320	0.0296
Oxygen	0.0069	0.0026	0.0068	0.0026	0.0065	0.0025
Zirconium	0.0081	0.0083	0.0078	0.0080	0.0070	0.0072
Carbon	0.0007	0.0008	0.0006	0.0007	0.0006	0.0006
Aluminum	0.0343	0.0314	0.0328	0.0302	0.0291	0.0266
Deuterium	0.0033	0.0055	0.0031	0.0054	0.0027	0.0050
$^{235}\text{U}$	0.5519	0.5553	0.5161	0.5246	0.1984	0.2095
$^{238}\text{U}$	0.3337	0.3353	0.3241	0.3281	0.2940	0.3034
$^{239}\text{Pu}$			0.0176	0.0098	0.2494	0.2438
$^{240}\text{Pu}$			0.0001	0	0.0586	0.0443
$^{241}\text{Pu}$			0	0	0.0358	0.0236
$^{149}\text{Sm}$			0.0051	0.0039	0.0053	0.0080
$^{135}\text{Xe}$			0.0261	0.0255	0.0215	0.0229
Fission products			0.0011	0.0017	0.0387	0.0476
Leakage	0.0231	0.0258	0.0224	0.0257	0.0205	0.0254
Total	0.9999	1.0000	0.9999	0.9999	1.0001	1.0000

$^{235}\text{U}$ , and  $^{239}\text{Pu}$ , are in substantial agreement. Early differences in  $^{239}\text{Pu}$  absorption are probably a result of specific treatment of  $^{239}\text{Np}$  in the ORNL computation.

#### 4.6.5. Comparison of Zero- and One-Dimensional Depletion Results

The zero-dimensional depletion model used to represent bidirectional, continuous refueling is a simplified one. A somewhat more complex and potentially more exact depletion model uses an explicit axial representation of the core in one dimension. In this model the axial traverse is subdivided into many layers. The bidirectional refueling requires that the fuel composition layers of the axial sandwich be alternately those corresponding to two adjacent fuel regions. For example, if we designate "1" as fresh fuel and numbers 2, 3, and 4 as fuel of progressively higher fuel depletion (with 4 being the discharge fuel), the sandwich is as follows: 4, 1, 3, 2, 2, 3, 1, 4. The symmetry of the core is such that only one-half of this sandwich need be actually included in the calculation; that is, layers 4, 1, 3, 2. Region sizes were chosen to give approximately the same center-to-center spacing as the distance between adjacent channels in order to obtain approximately the correct flux distribution. However, we found in exploratory calculations that the fluxes, but not the power, in adjacent channels are very nearly the same.

In our calculations we start with an initial fuel distribution. The core is depleted, while being kept critical with changes in poisoning, until the excess reactivity is gone. Material in each of the numbered regions is then interchanged with the next higher numbered region; that is, 1 becomes 2, 2 becomes 3, 3 becomes 4, and 4 is discharged from the core. Fresh fuel of a predetermined enrichment is added in region 1. A criticality search for the new control poison requirement is then made, and the depletion for the next cycle is begun. This cycle of refueling and depletion is continued for the desired number of times.

We did this calculation for the AJ-CE core with the code ASSAULT. Fifteen axial regions were used instead of the four regions assumed in the above illustrations of the method. The depletion results of this

one-dimensional calculation are compared with those of the point depletion calculation, Q-2, in Table 4.13. The data show that the one-dimensional calculation leads to slightly more favorable results than the point calculation. Nevertheless, the agreement between the two calculations is very close and gives confidence in the results obtained from the point calculational model.

Table 4.13. Comparison of One- and Zero-Dimensional Depletion Calculations

	Case R-1, One-Dimensional Depletion	Case Q-2, Zero-Dimensional Depletion
Startup enrichment, wt % $^{235}\text{U}$	0.820	0.784
Equilibrium		
Feed enrichment, wt % $^{235}\text{U}$	1.159	1.168
Discharge enrichment, wt % $^{235}\text{U}$	0.197	0.210
Discharge fissile Pu, g/kg of U	3.34	3.34
Core conversion ratio	0.694	0.694
Reactivity lifetime, Mwd/MT	16,009	14,842
Average excess reactivity	0.008	0.002

#### 4.7 Physics of the Thorium-Cycle HWO CR

The reactor physics analysis of the thorium-cycle HWO CR also consisted of the computation of critical bucklings and power densities by multidimensional calculations, the computation of reactivity coefficients, and the reactor depletion calculations for fuel-cycle and long-term reactor behavior. In this case, since B&W submitted two fuel element designs consisting of (1) a nested cylinder with thorium-uranium metal fuel and (2) a cluster of pins with  $\text{ThO}_2\text{-UO}_2$  fuel, both designs were evaluated.

##### 4.7.1 Multidimensional Reactor Calculations

The basic multidimensional calculations performed were an r-z calculation of the entire core approximately as described in the B&W conceptual

design report.<sup>13</sup> The core was represented as having three equal-volume radial zones and a uniform axial loading. Fuel concentrations approximately equal to those in Fig. 3.2 of the B&W report<sup>13</sup> were used.

The critical group-dependent bucklings obtained from these calculations are reported in Table 4.14. For comparison the corresponding geometric bucklings based on a 1.0-ft reflector saving are 0.000072 and 0.000061 for the nested-cylinder and the pin-cluster designs, respectively. Thus as in the AI-CE design the critical buckling for the radially zoned reactor is substantially greater than the geometric buckling, especially for the higher energy groups.

Gross power distributions were computed from the two-dimensional r-z calculations for the assumed startup conditions. These results are presented in Tables 4.15 and 4.16 for the nested-cylinder and pin-cluster cores, respectively. These tables show a gross maximum-to-average power ratio, which occurs on the horizontal plane through the center of the reactor, of 1.67 for the nested-cylinder design and 1.86 for the pin-cluster design. Figure 4.4 shows the relative radial power density along the same horizontal section. The maximum-to-average radial power distribution of 1.14 shown in Fig. 4.4 may be compared with the value of 1.17 reported for the B&W design. The degree of power flattening achieved by the three radial fuel regions is quite high.

Table 4.14. Group-Dependent Bucklings  
for the Thorium-Cycle HWOCR

Group	Upper Energy (ev)	Buckling ( $\text{cm}^{-2}$ )	
		Nested Cylinder	Pin Cluster
1	$1.0 \times 10^7$		
2	$8.21 \times 10^5$	0.00072	0.00050
3	$3.18 \times 10^4$	0.00040	0.00031
4	1230.0	0.00026	0.00022
5	47.9	0.00020	0.00018
6	1.86	0.00017	0.00016
7	0.65	0.00011	0.00010
8	0.18	0.00012	0.00013
9	0.06	-0.000005	0.000026

Table 4.15. B&W Nested-Cylinder Fuel Element Gross Power Density Distribution for the Initial Core Loading

Axial Zone	Distance from Axial Mid-Plane (cm)	Gross Power Density <sup>a</sup>											
		Central Fuel Region				Intermediate Fuel Region				Outer Radial Zone			
		6.6 cm <sup>b</sup>	118.8 cm	150.9 cm	167.0 cm	167.0 cm	201.5 cm	224.6 cm	236.1 cm	236.1 cm	258.9 cm	274.0 cm	289.2 cm
Outer	370.7	0.233	0.228	0.225	0.223	0.229	0.217	0.201	0.190	0.214	0.176	0.142	0.112
	364.6	0.254	0.249	0.246	0.243	0.250	0.236	0.220	0.207	0.233	0.192	0.155	0.127
	350.3	0.337	0.331	0.326	0.323	0.332	0.315	0.293	0.278	0.311	0.257	0.208	0.172
	330.0	0.470	0.462	0.456	0.452	0.464	0.441	0.411	0.388	0.437	0.361	0.292	0.242
	289.2	0.726	0.713	0.705	0.698	0.717	0.681	0.636	0.601	0.675	0.558	0.451	0.374
	248.5	0.973	0.957	0.946	0.936	0.962	0.914	0.853	0.806	0.906	0.748	0.606	0.499
Nonfueled													
Intermediate	246.8	0.982	0.965	0.954	0.945	0.971	0.922	0.861	0.813	0.914	0.755	0.611	0.504
	226.5	1.071	1.053	1.041	1.031	1.060	1.007	0.940	0.888	0.999	0.825	0.668	0.553
	185.8	1.254	1.233	1.219	1.207	1.241	1.180	1.101	1.040	1.170	0.967	0.782	0.648
	145.1	1.401	1.377	1.361	1.348	1.385	1.317	1.229	1.160	1.305	1.078	0.872	0.722
	124.7	1.481	1.456	1.440	1.426	1.465	1.392	1.298	1.226	1.379	1.139	0.923	0.760
Nonfueled													
Central	123.0	1.486	1.461	1.444	1.430	1.470	1.396	1.303	1.230	1.383	1.143	0.925	0.762
	102.7	1.521	1.495	1.478	1.464	1.504	1.430	1.335	1.260	1.417	1.171	0.948	0.784
	62.0	1.603	1.575	1.558	1.542	1.585	1.507	1.408	1.330	1.495	1.235	1.000	0.828
	21.2	1.640	1.612	1.594	1.578	1.622	1.542	1.439	1.359	1.529	1.262	1.022	0.846
	0.8	1.667	1.638	1.619	1.603	1.648	1.566	1.462	1.380	1.552	1.282	1.038	0.855
Nonfueled													

<sup>a</sup>Data normalized to an average power density of 1.0 in fueled regions.

<sup>b</sup>Core radius.

Table 4.16. B&W Pin-Clustered Fuel Element Gross Power Density Distribution for the Initial Core Loading

Axial Zone	Distance from Axial Mid-Plane (cm)	Gross Power Density <sup>a</sup>											
		Central Fuel Region				Intermediate Fuel Region				Outer Fuel Region			
		10.4 cm <sup>b</sup>	52.0 cm	114.4 cm	176.7 cm	176.7 cm	195.0 cm	222.5 cm	249.9 cm	249.9 cm	268.4 cm	286.9 cm	306.1 cm
Outer	350.0	0.255	0.253	0.247	0.232	0.240	0.231	0.214	0.186	0.209	0.179	0.140	0.099
	340.0	0.306	0.304	0.296	0.279	0.287	0.278	0.257	0.224	0.251	0.214	0.167	0.124
	294.0	0.638	0.633	0.615	0.581	0.599	0.580	0.537	0.470	0.527	0.450	0.352	0.261
	256.8	0.889	0.883	0.857	0.810	0.835	0.808	0.748	0.654	0.732	0.626	0.489	0.362
	238.2	1.055	1.047	1.017	0.961	0.990	0.959	0.888	0.775	0.869	0.743	0.580	0.423
Nonfueled													
Intermediate	232.3	1.090	1.082	1.050	0.992	1.023	0.990	0.917	0.801	0.897	0.767	0.600	0.437
	213.7	1.153	1.145	1.112	1.051	1.084	1.049	0.972	0.849	0.951	0.813	0.636	0.471
	176.5	1.351	1.341	1.303	1.232	1.271	1.230	1.140	0.998	1.117	0.956	0.747	0.554
	139.2	1.510	1.498	1.455	1.376	1.419	1.373	1.272	1.111	1.245	1.064	0.832	0.616
	120.6	1.649	1.637	1.589	1.502	1.549	1.499	1.388	1.213	1.359	1.162	0.908	0.662
Nonfueled													
Central	114.7	1.667	1.655	1.607	1.519	1.567	1.516	1.404	1.227	1.374	1.175	0.919	0.669
	96.1	1.652	1.640	1.593	1.506	1.553	1.503	1.393	1.218	1.363	1.166	0.911	0.675
	58.8	1.738	1.726	1.676	1.586	1.635	1.583	1.468	1.284	1.438	1.231	0.962	0.713
	21.6	1.776	1.763	1.712	1.620	1.670	1.616	1.498	1.309	1.466	1.253	0.980	0.726
	2.94	1.862	1.849	1.795	1.697	1.750	1.694	1.569	1.371	1.536	1.313	1.027	0.748
Nonfueled													

<sup>a</sup>Data normalized to an average power density of 1.0 in the fueled regions.

<sup>b</sup>Core radius.

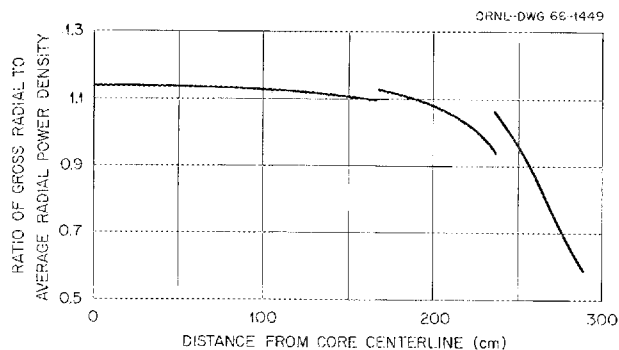


Fig. 4.4. Gross Radial Power Distribution for B&W Nested-Cylinder Design.

For the oxide-fueled case a two-dimensional x-y calculation was made using the equilibrium axial fuel distribution obtained from the TONG depletion calculation. This calculation included explicitly both the axial variation in fuel in two adjacent channels and the coolant density change along the channels. The effect of the coolant density change is significant, since flow is downward in all channels in the B&W designs. The results are presented in Table 4.17 and in Fig. 4.5 as an axial power density traverse. The maximum-to-average power ratio computed was 1.74 in

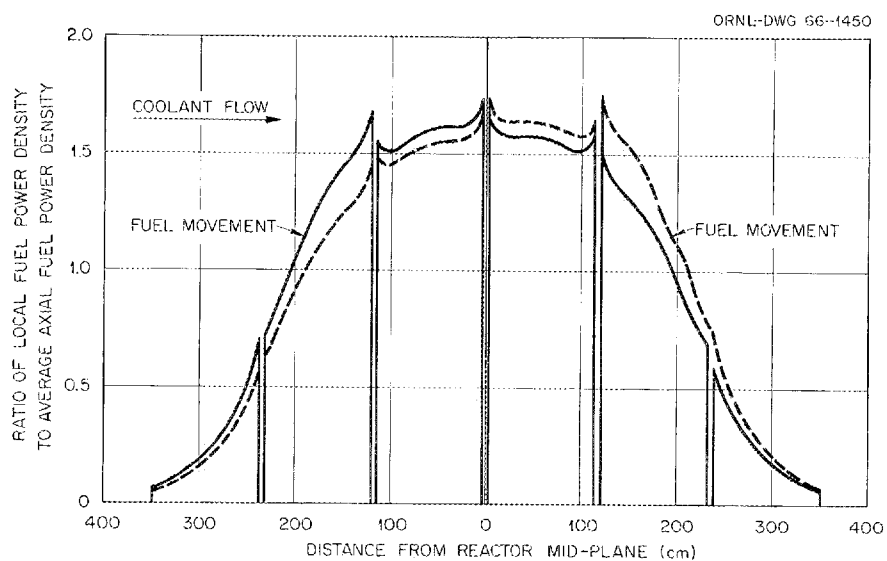


Fig. 4.5. B&W 1000-Mw(e) HWOCR Thorium-Uranium Oxide Concept Axial Power Distribution from Two-Dimensional Bidirectional Refueling Model.

Table 4.17. B&W 1000-Mw(e) ThO<sub>2</sub>-UO<sub>2</sub>-Fueled HWOCR Axial Power Distribution

Axial Zone	Distance from Reactor Mid-Plane (cm)	Ratio of Local Fuel Power Density to the Average Axial Fuel Power Density <sup>a</sup>			
		Coolant Inlet End		Coolant Outlet End	
		Cold End Fuel Charge	Hot End Fuel Charge	Cold End Fuel Charge	Hot End Fuel Charge
Outer	350.0	0.064	0.052	0.059	0.073
	344.4	0.070	0.058	0.066	0.079
	333.2	0.092	0.077	0.087	0.104
	316.4	0.136	0.114	0.128	0.153
	294.1	0.215	0.181	0.202	0.240
	271.7	0.331	0.278	0.307	0.366
	255.0	0.458	0.383	0.420	0.503
	243.8	0.590	0.484	0.529	0.645
	238.2	0.697	0.555	0.605	0.760
Nonfueled					
Intermediate	232.3	0.719	0.627	0.683	0.782
	226.7	0.762	0.659	0.717	0.828
	215.6	0.877	0.754	0.818	0.950
	198.8	1.055	0.906	0.979	1.138
	176.4	1.259	1.081	1.161	1.351
	154.1	1.415	1.217	1.296	1.508
	137.3	1.503	1.292	1.369	1.592
	126.1	1.583	1.361	1.437	1.670
	120.6	1.667	1.431	1.508	1.756
Nonfueled					
Central	114.7	1.561	1.496	1.574	1.641
	109.1	1.516	1.455	1.528	1.592
	97.9	1.510	1.450	1.516	1.579
	81.2	1.547	1.486	1.543	1.606
	58.8	1.589	1.527	1.571	1.634
	36.5	1.613	1.550	1.579	1.642
	19.7	1.626	1.564	1.579	1.642
	8.5	1.670	1.606	1.612	1.675
	2.9	1.738	1.672	1.674	1.740
Nonfueled					

<sup>a</sup>Calculated with a two-dimensional bidirectional refueling cell model.

the channel for which the fuel movement was opposite to coolant flow. The power ratio from fine axial and channel interaction effects was computed to be 1.156.

The fine radial power density distribution was also investigated for startup conditions. These results are given in Table 4.18 as a function of radial position for both B&W designs. The maximum-to-average local radial power ratio was found to be 1.451 for the nested-cylinder design and 1.265 for the pin-cluster design.

Table 4.18. Fine Radial Power Density Distribution for B&W Designs

Pin-Cluster Design			Nested-Cylinder Design			
Fuel Region No.	Outer Radius (cm)	Ratio of Region Average Power to Cell Average Power	Fuel Region No.	Inner Radius (cm)	Outer Radius (cm)	Ratio of Region Average Power to Cell Average Power
0	2.589		1	3.056	3.310	0.668
1	3.843	0.737	2	3.703	3.957	0.731
2	5.096	0.858	3	4.366	4.620	0.828
3	6.350	1.268	4	5.050	5.304	1.038
			5	5.778	6.032	1.451

The overall results may be compared with those reported by B&W as follows:

	Nested Cylinder		Pin Cluster	
	ORNL	B&W	ORNL	B&W
Gross radial power ratio	1.142	1.17	1.237	1.17
Gross axial power ratio	1.460	1.33	1.505	1.33
Fine radial power ratio	1.451	1.29	1.265	1.20
Fine axial power ratio	1.130	1.05	1.156	1.17

#### 4.7.2 Reactivity Coefficients

Reactivity coefficient calculations similar to those made for the AI-CE design were made for the two B&W designs, but only for startup conditions. These results are presented in Table 4.19 for both B&W core designs. Since B&W did not make a similar set of calculations, our results may not be compared. The general effects apparent from this study are similar to those of the AI-CE study; thus the B&W cores will have

1. significant positive coolant temperature coefficients,
2. strong, positive, coolant void coefficients,
3. a negative fuel coefficient,
4. a negative time-zero moderator coefficient.

A comparison of these results with those computed for the AI-CE uranium-fueled HWOCR indicates that the thorium-fueled reactor has a more positive coolant temperature coefficient of reactivity initially.

Table 4.19. Summary of Reactivity Coefficient Calculations for B&W Designs

	Reactivity Coefficients	
	Nested-Cylinder Core	Pin-Cluster Core
Fuel temperature, $\Delta k_e / \Delta T (^{\circ}F)$	$-0.8016 \times 10^{-5}$	$-0.5170 \times 10^{-5}$
Coolant temperature, $\Delta k_e / \Delta T (^{\circ}F)$	$+0.1550 \times 10^{-4}$	$+0.6758 \times 10^{-5}$
Moderator temperature, $\Delta k_e / \Delta T (^{\circ}F)$	$-0.2427 \times 10^{-4}$	$-0.1630 \times 10^{-4}$
Moderator purity, $\Delta k_e / (\Delta \% H_2O)$		
0.9975 to 0.99 mole fraction $D_2O$	-0.01828	-0.01866
0.9975 to 0.98 mole fraction $D_2O$	-0.01853	-0.02019
0.9975 to 0.97 mole fraction $D_2O$	-0.01870	-0.02078
Coolant void, $\Delta k_e / (\Delta \% \text{ void})$		
At 33 1/3% void	$+0.2957 \times 10^{-3}$	$+0.3089 \times 10^{-3}$
At 66 2/3% void	$+0.3039 \times 10^{-3}$	$+0.3026 \times 10^{-3}$
At 100% void	$+0.3359 \times 10^{-3}$	$+0.3322 \times 10^{-3}$

#### 4.7.3 Reactor Depletion Calculations

The primary reactor depletion calculations were zero-dimensional and were made with the TONG code. The core materials, dimensions, and temperatures were taken from the B&W design report<sup>14</sup> insofar as possible. B&W gave no method for the approach to the assumed continuous refueling of the reactor cores. Since the calculation of 30-year fuel-cycle costs required that some assumption be made about the reactor startup, it was assumed that the initial core loading would be sufficient to give a burnup of 3000 to 5000 Mwd/MT in the first fuel to be removed for reprocessing. During this period of time the reactor was assumed to be kept critical by poison control. All succeeding cycles were then computed by the continuous refueling method described previously for the AI-CE uranium-fueled HWOCR. For the B&W reactors 12 zones of uniform fuel concentration were chosen for the calculation. The group-dependent bucklings described in Section 4.7.1 (Table 4.14) of this Chapter were used for the depletion calculations.

Reactor lifetime results are summarized in Tables 4.20 and 4.21 as cases X-1, X-2, X-3, and W-1, W-2, W-3 for the nested-cylinder and pin-cluster designs, respectively. For each design fuel exposures of 17,000, 20,000, and 23,000 Mwd/MT were computed to allow some degree of cost optimization. Representative neutron balances as a function of time for the two designs are given in Tables 4.22 and 4.23. The final neutron balance of these tables is representative of the equilibrium cores. Lifetime mass balances of the heavy metals are given in Tables 4.24 and 4.25 for the nested-cylinder and pin-cluster designs, respectively.

#### 4.7.4 Comparison of ORNL and B&W Depletion Results Using the Same Method

In order to compare our reactivity calculations and basic nuclear data with those of B&W, one depletion calculation was made using the B&W depletion method. This scheme may be described as the depletion of the reactor at a given initial enrichment from supercritical until the reactivity just equals 1.0. The depletion is then continued for an additional equal depletion time with the reactor in the subcritical state.

Table 4.20. Summary of Cycle Performance for  
B&W Nested-Cylinder Design

	Cases		
	X-1	X-2	X-3
First cycle			
Initial reactivity (no rods)	1.1	1.1	1.1
Initial enrichment, wt % $^{235}\text{U}$	2.044	2.044	2.044
Final cycle			
Initial reactivity (no rods)	1.004	1.004	1.004
Cycle time, full-power days	515	606	697
Exposure, Mwd/T of U + Th	16,888	19,840	22,768
$^{235}\text{U}$ makeup enrichment, wt %	0.392	0.474	0.570
$^{235}\text{U}$ recycle enrichment, wt %	0.287	0.288	0.289
$^{233}\text{U}$ recycle enrichment, wt %	1.347	1.349	1.348
Total fissile feed enrichment, wt %	2.026	2.111	2.207

Table 4.21. Summary of Cycle Performance for  
B&W Pin-Cluster Design

	Cases		
	W-1	W-2	W-3
First cycle			
Initial reactivity (no rods)	1.1	1.1	1.1
Initial enrichment, wt % $^{235}\text{U}$	2.213	2.213	2.213
Final cycle			
Initial reactivity (no rods)	1.004	1.004	1.004
Cycle time, full-power days	276	378	432
Exposure, Mwd/T of U + Th	14,747	19,845	22,805
$^{235}\text{U}$ makeup enrichment, wt %	0.486	0.672	0.775
$^{235}\text{U}$ recycle enrichment, wt %	0.391	0.365	0.354
$^{233}\text{U}$ recycle enrichment, wt %	1.405	1.425	1.424
Total fissile feed enrichment, wt %	2.282	2.462	2.553

Table 4.22. Neutron Balance for B&W Nested-Cylinder Core, Case X-2,  
Calculated for 20,000 Mwd/MT, 12 Zones, and Critical Buckling

Cycle number	1, start	7, end	15, end	45, end	60, end	74, end
Time, years	0	1.090	2.198	6.352	8.429	10.367
Nuclide						
Hydrogen	0.0332	0.0366	0.0366	0.0359	0.0353	0.0349
Deuterium	0.0048	0.0050	0.0051	0.0050	0.0050	0.0050
Boron	0.0788					
Carbon	0.0005	0.0005	0.0005	0.0005	0.0005	0.0005
Oxygen	0.0024	0.0024	0.0024	0.0024	0.0024	0.0024
Aluminum	0.0087	0.0095	0.0096	0.0094	0.0092	0.0091
Zirconium	0.0172	0.0184	0.0184	0.0181	0.0180	0.0179
<sup>232</sup> Th	0.3340	0.3551	0.3560	0.3506	0.3461	0.3427
<sup>233</sup> Pa		0.0077	0.0077	0.0075	0.0074	0.0073
<sup>233</sup> U		0.1546	0.2489	0.3292	0.3295	0.3275
<sup>234</sup> U		0.0028	0.0071	0.0231	0.0281	0.0313
<sup>235</sup> U	0.4925	0.3138	0.2079	0.1178	0.1173	0.1195
<sup>236</sup> U		0.0033	0.0052	0.0083	0.0092	0.0100
<sup>238</sup> U	0.0022	0.0023	0.0025	0.0030	0.0032	0.0034
<sup>239</sup> Pu		0.0017	0.0019	0.0023	0.0025	0.0026
<sup>135</sup> Xe		0.0214	0.0209	0.0204	0.0204	0.0204
<sup>149</sup> Sm		0.0067	0.0065	0.0060	0.0059	0.0059
Fission products		0.0326	0.0372	0.0348	0.0345	0.0343
Leakage	0.0257	0.0255	0.0255	0.0257	0.0255	0.0253
Total	1.0000	1.0000	1.0000	1.0000	1.0000	1.0000
Conversion ratio	0.6690	0.7403	0.7704	0.8116	0.8134	0.8132

Table 4.23. Neutron Balance for B&W Pin-Cluster Design, Case W-2,  
Calculated for 20,000 Mwd/T, 12 Zones, and Critical Buckling

Cycle number	1, start	7, end	15, end	45, end	60, end	74, end	100, end
Time, years	0	0.648	1.337	3.922	5.215	6.507	8.661
Nuclide							
Hydrogen	0.0523	0.0573	0.0577	0.0571	0.0564	0.0557	0.0549
Deuterium	0.0062	0.0066	0.0066	0.0066	0.0065	0.0065	0.0064
Boron	0.0800						
Carbon	0.0007	0.0008	0.0008	0.0008	0.0008	0.0008	0.0008
Oxygen	0.0034	0.0035	0.0035	0.0035	0.0035	0.0035	0.0034
Aluminum	0.0278	0.0304	0.0306	0.0304	0.0300	0.0296	0.0292
Zirconium	0.0081	0.0087	0.0088	0.0087	0.0086	0.0085	0.0084
<sup>232</sup> Th	0.3023	0.3230	0.3239	0.3217	0.3181	0.3150	0.3111
<sup>233</sup> Pa		0.0076	0.0076	0.0075	0.0074	0.0073	0.0071
<sup>233</sup> U		0.1174	0.2066	0.2995	0.3028	0.3018	0.2988
<sup>234</sup> U		0.0017	0.0045	0.0172	0.0217	0.0250	0.0289
<sup>235</sup> U	0.4909	0.3556	0.2560	0.1522	0.1485	0.1495	0.1527
<sup>236</sup> U		0.0021	0.0035	0.0064	0.0074	0.0082	0.0095
<sup>238</sup> U	0.0015	0.0017	0.0018	0.0025	0.0027	0.0030	0.0033
<sup>239</sup> Pu		0.0012	0.0014	0.0019	0.0021	0.0022	0.0025
<sup>135</sup> Xe		0.0227	0.0223	0.0218	0.0217	0.0217	0.0217
<sup>149</sup> Sm		0.0064	0.0064	0.0058	0.0058	0.0058	0.0057
Fission products		0.0264	0.0313	0.0296	0.0293	0.0291	0.0288
Leakage	0.0268	0.0269	0.0267	0.0268	0.0267	0.0268	0.0266
Total	1.0000	1.0000	1.0000	1.0000	1.0000	1.0000	1.0000
Conversion ratio	0.6125	0.6692	0.6922	0.7328	0.7363	0.7374	0.7375

Table 4.24. Cumulative Mass Balances for the Reactor History of the B&W Nested-Cylinder Design

Case number	X-1	X-2	X-3
Plant factor	0.8	0.8	0.8
Reactivity lifetime, Mwd/MT	17,000	20,000	23,000
History time, years	11.0	12.9	14.8
Last cycle time, days, at 0.8 load factor	648	756	876
Initial loading, kg			
<sup>235</sup> U	1,905	1,906	1,905
Total U	2,038	2,050	2,038
<sup>232</sup> Th	91,159	91,159	91,159
Total purchased material, kg			
<sup>235</sup> U	4,810	5,329	5,887
Total U	5,144	5,730	6,296
<sup>232</sup> Th	134,768	136,011	137,219
Final core loading (at discharge), kg			
<sup>233</sup> U	1,279	1,282	1,284
<sup>235</sup> U	417.31	443.01	473.71
Total U	2,748	2,890	2,995
Total discharge (including final core), kg			
<sup>233</sup> U	8,045	8,209	8,326
<sup>234</sup> U	1,723	1,929	2,103
<sup>235</sup> U	3,063	2,877	2,758
<sup>236</sup> U	2,537	2,753	2,971
<sup>238</sup> U	1,149	1,307	1,268
<sup>232</sup> Th	636,356	634,901	633,487
Total material recycled (after losses), kg			
<sup>233</sup> U	6,274	6,433	6,547
<sup>234</sup> U	1,198	1,359	1,498
<sup>235</sup> U	2,530	2,319	2,170
<sup>236</sup> U	1,896	2,049	2,202
<sup>238</sup> U	881.72	994.74	958.19
<sup>232</sup> Th	510,941	509,698	508,491

Tables 4.26 and 4.27 compare neutron balances for the pin-cluster and nested-cylinder designs as computed by ORNL and B&W. The ORNL results in Table 4.26 also consider use of geometric or critical bucklings. At startup all the pin-cluster cases compare well with respect to initial reactivity and conversion ratio. At end of life the computed conversion ratios still agree quite well, but the agreement in reactivity is poorer. This indicates that for the same final reactivity the B&W cases would show

Table 4.25. Cumulative Mass Balances for the Reactor History of the B&amp;W Pin-Cluster Design

Case number	W-1	W-2	W-3
Plant factor	0.8	0.8	0.8
Reactivity lifetime, Mwd/MT	15,000	20,000	23,000
History time, years	6.0	8.0	9.2
Last cycle time, days, at 0.8 load factor	348	468	540
Initial loading, kg			
<sup>235</sup> U	1,277	1,277	1,277
Total	1,370	1,370	1,370
<sup>232</sup> Th	56,328	56,328	56,328
Total purchased material, kg			
<sup>235</sup> U	3,453	4,151	4,565
Total U	3,705	4,453	4,898
<sup>232</sup> Th	82,291	83,545	84,242
Final core loading (at discharge), kg			
<sup>233</sup> U	829.22	839.21	841.13
<sup>235</sup> U	345.02	365.35	377.88
Total U	1,888	2,067	2,159
Total discharge (including final core), kg			
<sup>233</sup> U	5,010	5,278	5,374
<sup>234</sup> U	886	1,149	1,275
<sup>235</sup> U	2,647	2,297	2,155
<sup>236</sup> U	1,728	2,055	2,234
<sup>238</sup> U	915	1,017	1,076
<sup>232</sup> Th	394,355	392,886	392,070
Total material recycled (after losses), kg			
<sup>233</sup> U	3,864	4,116	4,209
<sup>234</sup> U	597.28	793.11	890.08
<sup>235</sup> U	2,203	1,840	1,690
<sup>236</sup> U	1,268	1,500	1,625
<sup>238</sup> U	692.40	758.34	796.03
<sup>232</sup> Th	316,699	315,446	314,749

a higher conversion ratio than the ORNL cases. The nearly 3% difference in final reactivity is worth approximately 0.05 in conversion ratio. Also, the ORNL results in Table 4.26 indicate that use of the geometric buckling rather than the critical buckling has the effect of increasing the conversion ratio by approximately 0.02; neutron losses to leakage are decreased by 25 to 20% throughout the reactivity lifetime if geometric rather than critical bucklings are employed.

Table 4.26. Neutron Balances for B&amp;W Pin-Cluster Design Based on Depletion from Supercritical

Time-zero element	ORNL Results				B&W Results	
	For Geometric Buckling		For Critical Buckling		Absorptions	Productions
	Absorptions	Productions	Absorptions	Productions		
Hydrogen	0.0531		0.0528		0.0563	
Deuterium <sup>a</sup>	0.0063	0.0065	0.0063	0.0062	0.0035	
Carbon	0.0007		0.0007		0.0007	
Oxygen	0.0034		0.0034		0.0051	
Aluminum	0.0282		0.0280		0.0268	
Zirconium	0.0082		0.0081		0.0080	
Thorium	0.3068	0.0038	0.3044	0.0038	0.3144	0.0041
<sup>235</sup> U	0.5717	1.1571	0.5678	1.1496	0.5694	1.1625
<sup>238</sup> U	0.0017	0.0000	0.0017	0.0000	0.0016	0.0000
Leakage	0.0199		0.0268		0.0142	
Total	1.0000	1.1674	1.0000	1.1596	1.0000	1.1666
Conversion ratio	0.5369		0.5369		0.5478	
End of life	379 days		379 days		400 days	
Hydrogen	0.0625		0.0623		0.0656	
Deuterium <sup>a</sup>	0.0070	0.0067	0.0070	0.0067	0.0038	
Carbon	0.0009		0.0009		0.0008	
Oxygen	0.0037		0.0037		0.0051	
Aluminum	0.0332		0.0331		0.0311	
Zirconium	0.0095		0.0094		0.0089	
<sup>232</sup> Th	0.3473	0.0039	0.3453	0.0039	0.3562	0.0041
<sup>233</sup> Pa	0.0094	0.0000	0.0092	0.0000	0.0084	0.0001
<sup>233</sup> U	0.2254	0.5083	0.2240	0.5053	0.2306	0.5307
<sup>234</sup> U	0.0053	0.0000	0.0052	0.0000	0.0046	0.0001
<sup>235</sup> U	0.1890	0.3834	0.1880	0.3815	0.1906	0.3899
<sup>236</sup> U	0.0037	0.0000	0.0036	0.0000	0.0032	0.0001
<sup>238</sup> U	0.0017	0.0000	0.0017	0.0000	0.0015	0.0000
<sup>239</sup> Pu	0.0016	0.0031	0.0016	0.0031	0.0023	0.0036
<sup>135</sup> Xe	0.0225		0.0224		0.0235	
<sup>149</sup> Sm	0.0067		0.0066		0.0053	
Fission products	0.0490		0.0489		0.0436	
Leakage	0.0216		0.0271		0.0149	
Total	1.0000	0.0954	1.0000	0.9005	1.0000	0.9286
Conversion ratio	0.8472		0.8254		0.8317	

<sup>a</sup>The ORNL results include the n,2n reactions in the deuterium absorptions.

Table 4.27 shows that for the nested-cylinder design the agreement in initial reactivity is good, but the computed conversion ratios are significantly different. This difference seems to be caused primarily by the neutron losses from leakage. The difference of approximately 0.05 in conversion ratio is again evident at the end of life condition. As in the pin-cluster case the agreement in final reactivity is poorer than at

Table 4.27. Neutron Balances for B&amp;W Nested-Cylinder Design Based on Depletion from Supercritical.

	ORNL Results for Critical Buckling		B&W Results	
	Absorptions	Productions	Absorptions	Productions
Time-zero element				
Hydrogen	0.0346		0.0324	
Deuterium <sup>a</sup>	0.0049	0.0049	0.0026	
Carbon	0.0005		0.0004	
Oxygen	0.0024		0.0043	
Aluminum	0.0090		0.0090	
Zirconium	0.0177		0.0184	
Thorium	0.3433	0.0111	0.3582	0.0060
<sup>235</sup> U	0.5607	1.1260	0.5572	1.1309
<sup>238</sup> U	0.0020	0.0001	0.0022	0.0001
Leakage	0.0248		0.0153	
Total	1.0000	1.1420	1.0000	1.1370
Conversion ratio	0.6077		0.6426	
End of life	600 days		600 days	
Hydrogen	0.0389		0.0356	
Deuterium <sup>a</sup>	0.0053	0.0050	0.0027	
Carbon	0.0005		0.0004	
Oxygen	0.0025		0.0043	
Aluminum	0.0102		0.0098	
Zirconium	0.0194		0.0196	
Thorium	0.3704	0.0110	0.3832	0.0059
<sup>233</sup> Pa	0.0089	0.0002	0.0079	0.0001
<sup>233</sup> U	0.2620	0.5882	0.2651	0.6074
<sup>234</sup> U	0.0076	0.0002	0.0064	0.0001
<sup>235</sup> U	0.1590	0.3202	0.1654	0.3363
<sup>236</sup> U	0.0052	0.0002	0.0043	0.0002
<sup>238</sup> U	0.0019	0.0001	0.0020	0.0001
<sup>239</sup> Pu	0.0019	0.0035	0.0031	0.0046
<sup>135</sup> Xe	0.0205		0.0221	
<sup>149</sup> Sm	0.0064		0.0049	
Fission products	0.0549		0.0476	
Leakage	0.0246		0.0156	
Total	1.0000	0.9283	1.0000	0.9547
Conversion ratio	0.8671		0.9156	

<sup>a</sup>The ORNL results include the n,2n reactions in the deuterium absorptions.

startup. The comments with respect to the relationship between reactivity and conversion ratio mentioned for the pin-cluster cases also apply here. Thus for nonrecycled fuel and exposures of about 20,000 Mwd/MT, our calculations give a conversion ratio about 5% lower than that obtained by B&W.

#### References

1. M. W. Rosenthal et al., A Comparative Evaluation of Advanced Converters, USAEC Report ORNL-3686, Oak Ridge National Laboratory, January 1965.
2. D. R. Vondy and T. B. Fowler, Computer Code TONG for Zero-Dimensional Reactor Depletion Calculations, USAEC report to be issued.
3. D. R. Vondy, T. B. Fowler, and M. L. Tobias, Reactor Depletion Code ASSAULT, USAEC report to be issued.
4. G. D. Joanou et al., GAM-I -- A Consistent P-1 Multigroup Code for the Calculation of Fast Neutron Spectra and Multigroup Constants, USAEC Report GA-1850, General Atomic, June 28, 1961.
5. H. Honeck, THERMOS -- A Thermalization Transport Theory Code for Reactor Lattice Calculations, USAEC Report BNL-5826, Brookhaven National Laboratory, September 1961.
6. Communication from E. H. Gift, Oak Ridge National Laboratory to M. W. Rosenthal, August 15, 1964, GAM-I and THERMOS Cross Section Libraries for Use in ORNL Evaluation Studies.
7. A. B. Smith, Reports to the AEC Nuclear Cross Sections Advisory Group Meeting at Columbia University, June 4-5, 1964, USAEC Report WASH-1048, pp. 83-85.
8. Knolls Atomic Power Laboratory, Report of the Advanced Development Activity -- Progress Report for Period August 6 to November 5, 1965, USAEC Report KAPL-2600-10, Nov. 18, 1965.
9. Bettis Atomic Power Laboratory, Reactor Physics, Engineering, and Mathematics Progress Report for Period April 1 to July 1, 1965, USAEC Report WAPD-MRJ-30, Aug. 9, 1965.

10. F. G. Welfare, Comparison of TONG Calculations with Critical Experiments, Internal Memorandum, Oak Ridge National Laboratory, Aug. 6, 1965.
11. Combustion Engineering, Inc., and Atomics International, Heavy Water Organic Cooled Reactor - 1000 Mwe Nuclear Power Plant Preliminary Conceptual Design, USAEC Report AI-CE-Memo-6, Oct. 1, 1965.
12. D. B. Wehmeyer, Comparison of Power Distribution and Fuel Depletion Calculations for the HWOCR, Internal Memorandum, Oak Ridge National Laboratory, Sept. 24, 1965.
13. Personal Communication R. S. Harding to E. H. Gift, Oak Ridge National Laboratory, Oct. 27, 1965.
14. Babcock & Wilcox Company, 1000 MWe Thorium HWOCR - Preliminary Conceptual Design Data for ORNL Evaluation, USAEC Report (unnumbered), Nov. 15, 1965.

## 5. ENGINEERING EVALUATION OF REACTOR CORES

Some major engineering characteristics of the three core designs are summarized in Table 5.1. Important bases for the design specifications selected by AI-CE are

1. a maximum cladding surface temperature of 850°F,
2. a minimum DNB\* ratio of 2.0,
3. no subcooled nucleate boiling in the core,
4. a maximum average coolant velocity of 30 fps at the coolant average density,
5. a maximum carbide fuel center-line temperature of 2400°F or less and no strain of the cladding as a result of fuel growth,
6. no fouling film on fuel element surface.

The B&W design was based on the same limiting conditions, except that the average coolant velocity was not limited to 30 fps. Also, the maximum fuel temperatures were different because oxide and metal fuels were considered.

The maximum permissible temperature of the SAP cladding and the maximum permissible temperature of the organic coolant must be considered in the selection of the maximum permissible fuel surface temperature. In their reference design report<sup>1</sup> (pages II-3 and II-4), AI-CE indicates that the major considerations are the strength, creep, and elongation properties of the SAP cladding and that 850°F appears to be a maximum permissible temperature, although higher temperatures could be sustained for limited periods of time. We agree with this specification but wish to emphasize that the SAP strength properties employed are based on values inferred by extrapolation of experimental data; thus 850°F should be considered the maximum permissible fuel surface temperature until further experimental results are obtained.

The cladding surface temperature criterion is also related to the maximum temperature that the coolant can sustain, since coolant contacts the fuel element surface. The limitation on coolant temperature is determined by the relationship between coolant radiation damage, pyrolytic

---

\*DNB = departure from nucleate boiling.

Table 5.1. Engineering Characteristics of the HWOOR Cores as Supplied by the Sponsors

	AI-CE Design	B&W Nested-Cylinder Design	B&W Pin-Cluster Design
Net power transferred to coolant, Mw(t)	2921	2921	2921
Total coolant flow, lb/hr	$110 \times 10^6$	$89.9 \times 10^6$	$89.9 \times 10^6$
Coolant inlet temperature, °F	595	560	560
Coolant outlet temperature, °F	750	750	750
Maximum average coolant velocity, fps	30	37	32
Pressure drop over fuel, psi	142 <sup>a,b</sup>	158 <sup>b,c</sup>	169 <sup>c,d</sup>
Pressure at reactor discharge header, psia	100	100	100
Maximum power per pressure tube, Mw(t)	7.30	12.36	10.2
Number of pressure tubes	492	299	335
Pressure tube inside diameter, in.	4.320	5.000	5.000
Total active fuel length, ft	17.3	24.0	22.0
Total length of assemblies, ft	18.0	24.375	23.41
Number of assemblies per pressure tube	5	6	6
Fuel material			
Fuel	Hyperstoichiometric UC	Th-U alloy	(Th-U)O <sub>2</sub>
Fabrication method	Casting	Coextrusion	Vibratory compaction
Cladding material	SAP	Zircaloy-4	SAP
Fuel element design			
Fuel outside diameter, in.	0.476	4.800-2.656	0.316
Fuel thickness, in.		0.100	
Cladding thickness, in.	0.020	0.025	0.020
Fuel-cladding gap, in.	0.0025		
Fission-gas plenum, in.	0.60		1.81
Fuel length, in.	41.7	48	44
Fuel operating conditions at rated power			
Average burnup in element, Mwd/T	16,700	20,000	20,000
Maximum burnup in rod, Mwd/T	20,500		
Maximum heat rating, kw/ft	26.7		11.85
Maximum cladding temperature, °F	850	850	850
Maximum fuel temperature (hot spot), °F	2400	945	4750
Power-peaking factors			
Basic radial	1.17	1.17	1.17
Local radial (maximum)	1.31	1.29	1.21
Basic axial	1.33	1.33	1.33
Local axial (maximum)	1.17	1.05	1.17
Gross axial	1.45 <sup>e</sup>	1.40	1.56
Flux tilt	1.05	1.05	1.05
Mixing factor, %	64	0	64
Engineering factors			
Coolant temperature change	1.09	1.17 (hot) <sup>f</sup>	1.09
Temperature drop across the film	1.21		1.21
Heat flux	1.12		1.12

<sup>a</sup>Includes 25-psi drop (total) for the four assembly junctions.

<sup>b</sup>Includes 1.5-velocity-head entrance and exit loss to pressure tube.

<sup>c</sup>Corrected for static head.

<sup>d</sup>Does not include entrance and exit loss to the pressure tube.

<sup>e</sup>Interpreted from Fig. II-9 of Ref. 1; value used by AI-CE is 1.48.

<sup>f</sup>For the two high-power channels; factor is 1.32 for outer channel.

damage, and fouling of the fuel element surface as a function of operating conditions. Due to mixing of the fluid adjacent to the surface with the bulk coolant, only a small portion of the coolant will remain at the fuel element surface temperature for short periods of time. However, it is known that under irradiation, the damage to the coolant increases markedly with increasing temperature; also, the kinetics of the damage and the film formation processes have not been established. It appears that with a limiting cladding surface temperature of 850°F, the limiting coolant temperature is determined by surface fouling. The available experimental data indicate that the temperature drop across the surface-fouling film at maximum HWOCR heat fluxes may be 25--50°F. Thus, we do not believe that specification 6 corresponds to a feasible condition based on present information. The influence of fouling on core thermal performance and the heat transfer and fluid flow factors are discussed in Section 5.1. Fuel element surface fouling is discussed in Section 5.5.

It is not possible to predict accurately the critical heat flux under HWOCR conditions because of lack of pertinent heat flux data and uncertainties in predicting the vapor pressure of the cracked and recycled organic coolant. It appears that a minimum DNB ratio of 2 is too low as a reasonable design basis at this time and that a value of 4 should be used.

The criterion of "no subcooled nucleate boiling in the core" is desirable, but insufficient information is presently available about conditions that will assure no subcooled nucleate boiling and not limit the amount of diphenyl. From the standpoint of feasibility, it was considered that the DNB ratio was the governing criterion, with no additional restrictions on subcooled nucleate boiling as such.

The maximum average coolant velocity of 30 fps appears to be reasonable, but there will be variations from this value. Since the maximum average coolant velocity is specified at the average coolant density, there will be velocities in some subchannels that will be greater than the average and, for sections of the pressure tube where the temperature of the coolant is above its average, the average velocity will be greater than 30 fps. We understand that the velocity limitation was specified

on the basis of vibrational considerations. We have not attempted to make a vibrational analysis of the fuel assembly in the coolant stream since, if vibrational problems do develop at specified velocities, these will be evaluated in required fluid-flow mockup studies. There are several methods by which such vibrational problems can be eliminated.

The selection of the maximum coolant velocity is also dependent upon consideration of the pumping power requirements and the associated heat transfer characteristics as a function of coolant flow rate. Pressure losses are dependent upon the velocity to the 1.8 power, and heat transfer rates are dependent on the velocity to the 0.8 power. Our calculations indicate that considerable flexibility exists in specifying even the average coolant velocity, with reasonable values being in the 25 to 40 fps range.

The limitation on fuel center-line temperature is influenced by fuel growth as a function of temperature and exposure, which in turn is related to the behavior of fission-product gases under reactor conditions. Based on present information, we judge that the specified maximum value of 2400°F for carbide fuel is too high for the fuel element design under consideration and that 2200°F is the maximum feasible temperature. This value may change as more experimental data become available and may be lower than 2200°F. At the same time, for the specified AI-CE design conditions, we did not find that the maximum center-line temperature exceeded the 2200°F value. We concur that fuel growth should not strain the SAP cladding.

The stipulation that no fouling film should exist on the fuel element surfaces, while it is desirable, cannot be justified on the basis of present operating experience. As discussed in Section 5.5, we feel that allowance should be made in the present design for the presence of a film, and we believe that the film will be of such a magnitude that a minimum temperature difference of 25 to 50°F will exist across it at the maximum surface temperature. If 850°F is considered to be the maximum temperature for the SAP cladding, as previously stated, the limitation must be imposed that the maximum temperature of the coolant in contact

with the film be about 800 to 825°F based on the fouling-film temperature drop of 25 to 50°F.

In addition to the considerations discussed above, attention must be given to materials compatibility and to mechanical and physical properties of the materials as functions of design conditions and reactor control characteristics. These factors are discussed in the sections that follow.

### 5.1 Fluid Flow and Heat Transfer Analyses

In the evaluation of the hydraulic and thermal performance of the proposed core designs, the basic criteria were examined along with the values selected for the design parameters. In doing this, it was necessary, for the most part, to use initially the flux distribution information furnished by the designers. As information formulated by ORNL became available, it was included in this evaluation. Disagreements with the design parameters and dependent variables are discussed below and their influences on operating conditions are indicated.

A prominent design feature of the pin-type elements proposed by both AI-CE and by B&W is that advantage is taken of the mixing between the fluid flowing in the various subchannels between the elements to reduce the temperature rise of both the coolant and the cladding at the hottest subchannel. Careful analysis of the effect of mixing is a rather involved process and has been handled for previous reactor designs only in a general manner. To facilitate the analysis of this effect of mixing, copies of two computer codes were obtained from Combustion Engineering and adapted for our IBM-7090 computer. For reference purposes, these codes are called U-3 and THEME 1, and they are discussed in more detail in Appendix B of this report.

The evaluation of the thermal and hydraulic performance of the proposed cores was resolved into three tasks: (1) evaluation of the codes, (2) formulation of the input data, and (3) analysis of the output of the codes.

### 5.1.1 Evaluation of the Computer Codes

The two codes differ in two principal features: (1) purpose and (2) treatment of the mixing concept. U-3 considers each subchannel of the pressure tube (or at least a symmetrical segment of it); THEME 1 considers the hot subchannel as an individual channel but represents the remainder of the flow channel in terms of its hydraulic and thermal equivalent. Consequently, U-3 can be used to study a reactor design in detail, and THEME 1 is useful in making engineering parameter studies.

U-3 treats mixing by entering a proportionality constant which, when multiplied by the average linear velocity in the pressure tube, produces the crossflow rate between subchannels. It is possible, then, to write an energy balance over an incremental segment of length and to produce the temperature change with intersubchannel flow. THEME 1, on the other hand, uses the mixing factor defined on page II-8 of Ref. 1 to determine the temperature rise in the hot subchannel with mixing over a given increment of length. In addition, it is possible to enter the engineering factors directly into THEME 1. They can be entered only in an oblique manner in U-3.

U-3 Code. U-3 appears to be an adequate representation of the conditions existing in the pressure tube provided, particularly for the case of mixing, the proper input values can be obtained. Although the hydraulic correlation does not appear to be conservative, its application in this case leads to a conservative value (overestimation) of the pressure loss due to friction. The hydraulic calculations are not completely satisfactory, since they are made before and independently of the thermal calculations. For the hydraulic calculations, all physical properties are evaluated at an average fluid temperature, which is in turn based on an inlet temperature and an estimated temperature rise in the hot pressure tube (both input values). The flow distribution obtained from these calculations is then used throughout the thermal calculations.

The thermal calculations are also dependent upon the empirical correlations entered in the code; these correlations are discussed later in this section and in Appendices C and D. The energy balances are also

dependent on the proper representation of the power input for the increment over which the balance is made.

The spatial distribution of the power is considered by using several input factors. The easiest to incorporate are the basic radial and the flux tilt factors. The most difficult spatial effect to represent is the local radial factor in the process tube since, with increasing burnup (associated with movement of the fuel assembly through the reactor), fuel is preferentially burned from the outer fuel elements. This causes a change in the local radial power distribution with position. The code does not permit a representation of this variation, and it is necessary to incorporate a judicious average that is a good representation of both the total heat added to the coolant and the heat flux at the "hot spot." It would be possible to alter the code to represent the rod radial factor as a function of axial position in the pressure tube, but the problem is not quite that simple, since fuel is not exposed to the same flux over the exposure period. Therefore, the rod radial factor is not, in general, adequately represented by one number.

A second problem in the energy balance calculations is associated with the use of predetermined length increments (an input value). In addition, the gross axial (product of basic and local axial) flux is substituted at selected positions over the height of the reactor, and linear interpolations are made between these points. If the perturbations in the axial flux are smaller than the predetermined increments (such as they would be with the application of a local axial factor over a short length), the perturbation is never seen in the heat input calculation. In the U-3 code, however, the axial flux is entered both as a normalized point flux and a normalized integral flux so that the perturbations are represented in the flux integral. Again, the code could be altered to eliminate this difficulty.

The most dubious concept used in the code is the model representing fluid mixing. This concept is based on the hypothesis that the cross-flow rate between subchannels is proportional to the average linear velocity in the pressure tube. The applicability of this model was based on comparisons of calculated temperatures with experimental measurements

for wire-wrapped elements. In wire-wrapped elements there is a much better direction of flow between subchannels, and the physical situation appears to be much more predictable. The applicability of this model to spirally finned elements where opposing flows are created is yet to be proven. In addition, an estimate must be made as to the relative effectiveness of each interconnecting path for effecting crossflow. It is difficult to know the proper crossflow value when the spirally finned elements are adjacent to walls or when straight-finned elements are present.

THEME 1 Code. The same hydraulic correlations as those used in U-3 are used in THEME 1. The estimate of the pressure drop is even more conservative (overestimate), however, because the entire pressure tube is represented as one equivalent flow channel.

The heat transfer coefficient correlation is the same as the one used in U-3. The basic radial flux and the flux tilt factors are entered in this code and applied in the same manner as for U-3. The local radial factors must be entered only for those elements bordering on the hot subchannel, but the same problem as in U-3 exists in representing their axial variation. The gross normalized axial flux values are entered at selected axial positions, and temperature calculations are made only at these positions.

In this code the calculation of the effect of mixing is exact because it depends upon the definition of the mixing factor. The validity of the results of this calculation depends directly upon the accuracy with which the mixing factor can be determined.

As was previously mentioned, the engineering factors can be entered directly into THEME 1. There is a factor, however, of 1.04 that is built into the code to account for the maldistribution of flow between pressure tubes. If this factor is included in the engineering factor (as it is in the factors given in Ref. 1), the builtin factor must be factored out. It may be worthwhile at this point to mention that flow redistribution (that is, nonuniform flow in the subchannels) is incorporated in the calculation by both U-3 and THEME 1 and that this factor (which also has a value of approximately 1.04 according to AI-CE) should be multiplied by

the factors given in Ref. 1 if another mode of calculation is used (such as assuming uniform flow distribution between flow subchannels).

### 5.1.2 Evaluation of Correlations Used in the Codes

As mentioned above, both U-3 and THEME 1 employ the same pressure loss and heat transfer coefficient correlations. In addition, THEME 1 has an empirical correlation that predicts the critical heat flux from which the critical heat flux ratio is calculated.

Pressure Loss Correlation. The pressure loss correlation used in the codes is one expressed by Colebrook<sup>2</sup> in 1939. This expression extended the correlation for flow in a so-called "transition" region, which is used here as that region between smooth pipe flow and flow for which the friction factor is constant. (This transition region should not be confused with the transition region from laminar to turbulent flow, which occurs between Reynolds numbers of 2100 and 4000.) Moody,<sup>3</sup> in 1944, presented the Colebrook function in the well-known Moody diagram and also gave an approximate equation that agrees with the Moody diagram within  $\pm 5\%$  for values of the Reynolds number between 4000 and  $10^7$ . He recommended a tolerance of  $\pm 10\%$  for the Moody-diagram friction factors for other than the smooth-pipe data.

For flow in noncircular channels, a review by Waggener<sup>4</sup> recommends the use of the equivalent hydraulic diameter (which is equal to four times the cross-sectional flow area divided by the wetted perimeter). The article noted that for flow in triangular channels the data fell about 3% under the Moody smooth line, and for flow in square channels the data fell about 10% under the Moody line for Reynolds numbers between  $10^4$  and  $2 \times 10^5$ . Since the calculations in the codes are for smooth pipe and for irregular shapes that will have small equivalent diameters, the Reynolds numbers will be small and therefore the estimated friction factors should be large.

The conclusion is that, while the pressure drop correlation used in the codes may not be conservative, its application to this type of flow channel will result in a conservative calculation (that is, an over-estimation) of the pressure drop. The Colebrook equation is not the most

convenient relation for use in the code, since it cannot be solved explicitly for the friction factor. The sensitivity of this relationship was such, however, that it did not require excessive machine time. Use of the Moody approximation, however, would have resulted in a faster calculation, and the result would have been as meaningful.

Heat Transfer Coefficient Correlation. The heat transfer correlation used in both U-3 and THEME 1 codes to predict the heat transfer coefficient at the surface of the cladding is the one used by Oldaker,<sup>5</sup> who stated that it agrees very closely with the correlation of Rogers of Canadian General Electric Company. The correlation used is

$$\text{Nu} = 0.0243 \text{Re}^{0.8} \text{Pr}^{0.4}, \quad (1)$$

where Nu is the Nusselt number, Re is the Reynolds number, and Pr is the Prandtl number. Members of the AI-CE study team claimed that this correlation, with the present physical property data, predicted heat transfer coefficients that were below all experimental values.

Our analysis of the present heat transfer data based on the best values for the physical properties currently available does not confirm the above conclusion. This analysis is discussed in more detail in Appendix C to this report. For smooth tubes and annuli, the heat transfer correlation obtained by MIT<sup>6</sup> for organic coolant appears to be best. This relation is

$$\text{Nu} = 0.023 \text{Re}^{0.8} \text{Pr}^{0.4}, \quad (2)$$

where the symbols have the same significance as in the previous equation. Reevaluation of other current data, superimposed on correlations recommended in the ORGEL program, are presented together with the values indicated by these two equations in Fig. 5.1 (Refs. 7-9). The MIT data<sup>6</sup> are given in Fig. 5.2, along with the MIT and ORGEL correlations.

The presence of the closely spaced fins in the pin-cluster design requires a reduction in the coefficient of Eq. (2). Experimental data have shown that even allowing for fin efficiency, the presence of closely spaced fins creates a restricted flow area between the fins which leads to lower coefficients than predicted for widely spaced fins or bare surfaces. We estimate that the coefficients computed from correlations

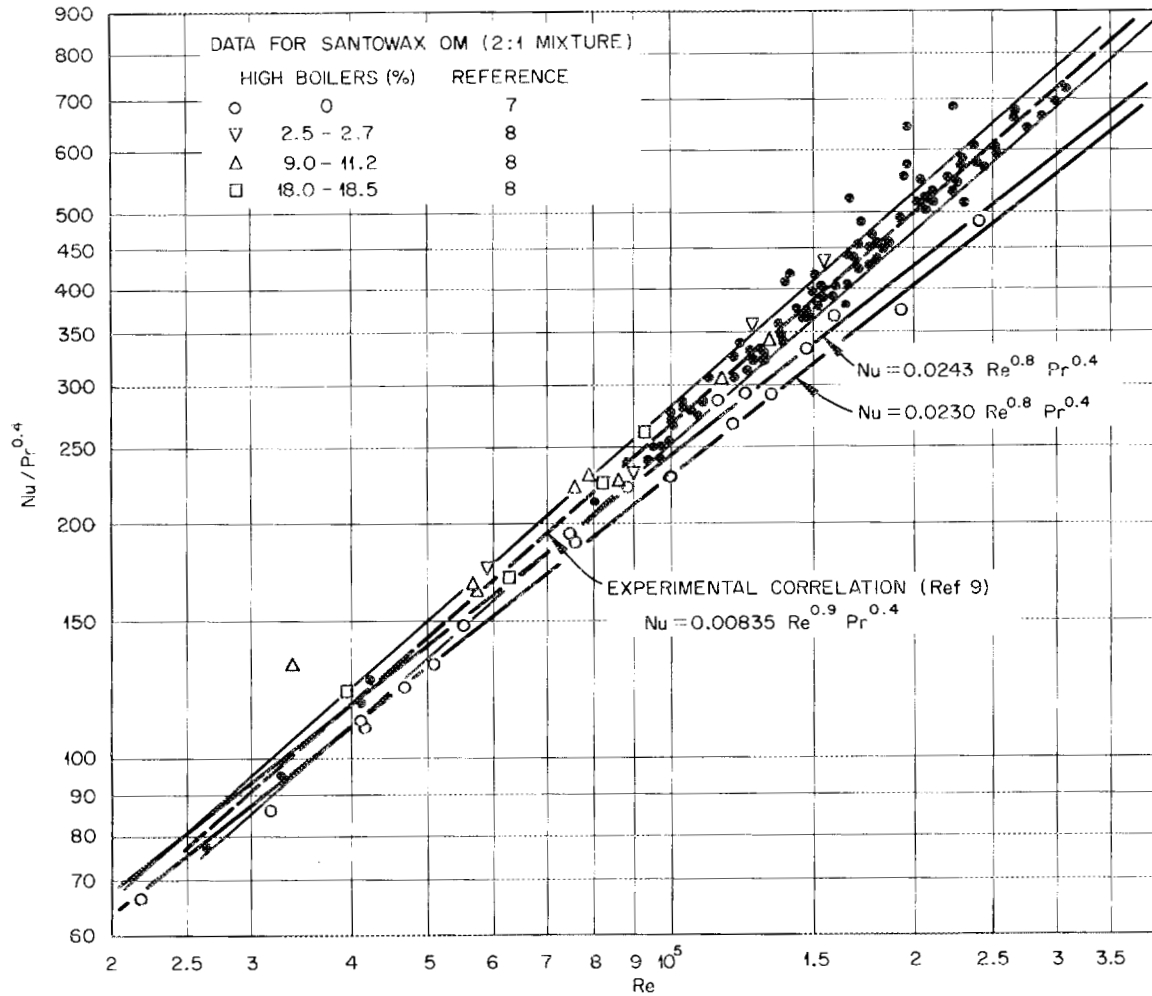


Fig. 5.1. Comparison of Heat Transfer Correlations.

based on smooth-tube and annuli data should be reduced by about 10% to account for the effects of noncircular geometry and of decreased velocity between the fuel pin fins. The resulting heat transfer relation is then

$$Nu = 0.021 Re^{0.8} Pr^{0.4} \quad (3)$$

The net effect of using Eq. (3) is to reduce the heat transfer coefficient 15% below that used by AI-CE in their code calculations. The calculations made by B&W were based on the same correlation as that used by AI-CE.

Critical Heat Flux Correlation. The critical heat flux correlation used to calculate the DNB ratios, which was cited on page II-13 of Ref. 1,

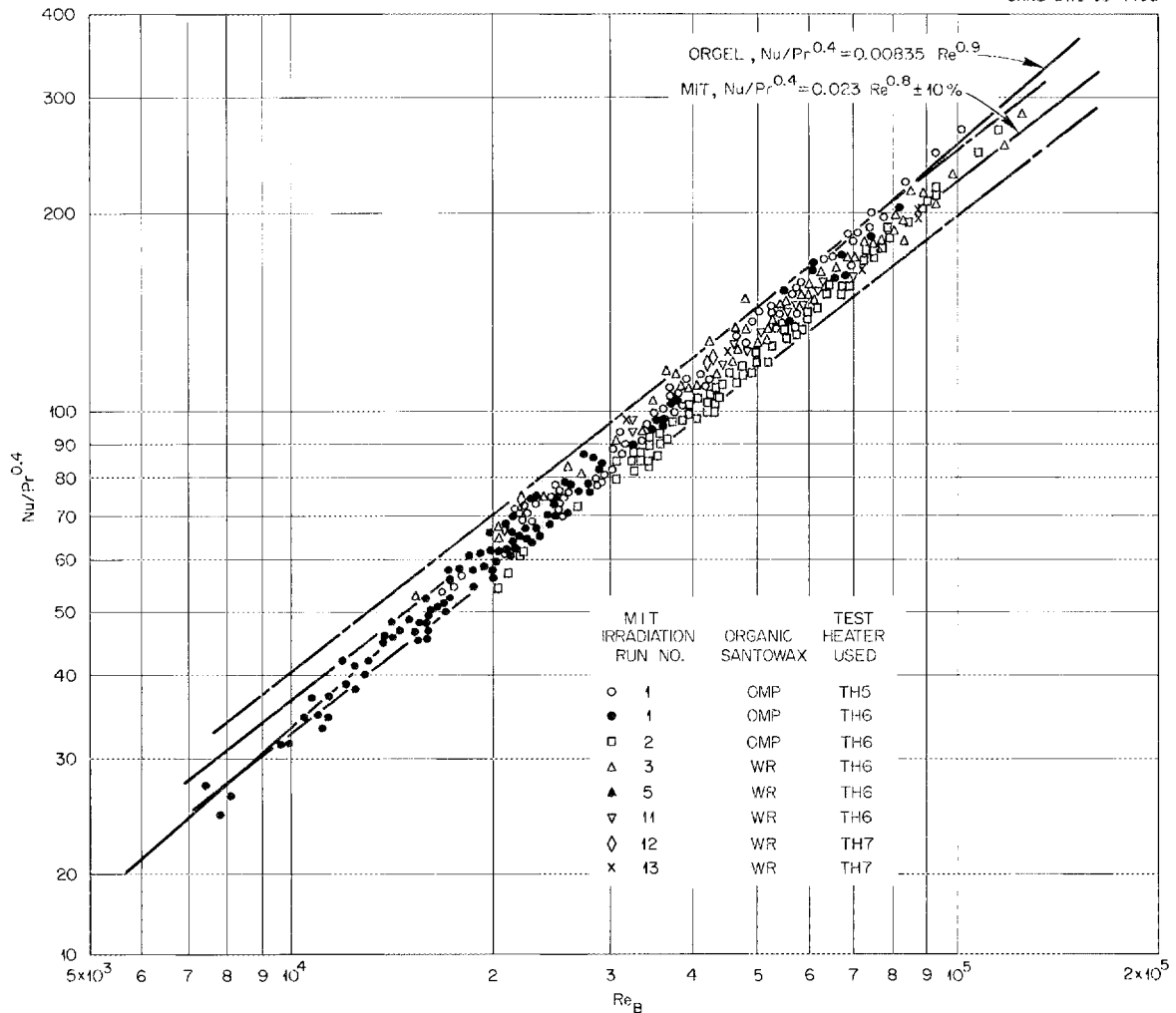


Fig. 5.2. Heat Transfer Data for MIT-Irradiated Organic Coolant.

was not the same as the correlation employed in THEME 1 for this purpose. The correlation cited by AI-CE, which is recommended in the "Organic Heat Transfer Manual,"<sup>10</sup> is the same as that given by Lurie and Robinson.<sup>11</sup> It is

$$\left(\frac{Q}{A}\right)_c = 129,000 + 11 \Delta T_{\text{sub}} G^{0.8}, \quad (4)$$

where  $(Q/A)_c$  is the critical heat flux in Btu/hr·ft<sup>2</sup>,  $\Delta T_{\text{sub}}$  is the sub-cooling in °F, and  $G$  is the mass velocity in lb/sec·ft<sup>2</sup>. The correlation used in THEME 1 is that developed by Core and Sato,<sup>12</sup> which is of

the form

$$(Q/A)_c = 100,000 + 407 \Delta T_{\text{sub}} V^{2/3} , \quad (5)$$

where the similar terms have the same significance as above and  $V$  is the linear velocity in fps. Lurie and Robinson<sup>11</sup> investigated ORME-II coolant and Santowax R with various additives and were able to correlate their results and previous data (including those of Core and Sato<sup>12</sup>) with their expression. Since the two correlations represent the same data, we conclude that approximately the same DNB heat flux will result from either correlation. B&W also used Eq. (5) to estimate the DNB heat flux in their reference reactor design.

Boxall and his co-workers<sup>13</sup> in the Canadian organic coolant program reported a more recent "asymptotic" heat flux correlation for Santowax OM plus 30% OMRE high boilers. Their results, when converted to the system of units used above, are given by

$$(Q/A)_c = 311,700 + 577 \Delta T_{\text{sub}} V^{2/3} . \quad (6)$$

Our conclusion, based on a limited review, which is discussed in more detail in Appendix D, is that this correlation derived from the Canadian organic coolant program is the most reliable and convenient to use. From the short discussion reported by Boxall and his co-workers<sup>13</sup> it appears that this study is more recent and takes advantage of earlier work. It is more extensive in that length effects have been investigated, and it is more applicable since the coolant, Santowax OM with 30% OMRE high boilers, is probably more representative of the coolant proposed for the reference reactor designs than the other coolants tested.

As is indicated in Appendix D, all the previously discussed correlations were derived from experiments with heated tubes or annuli. Rogers and Barns<sup>14</sup> point out that it is meaningless to apply these equations to predict DNB failure heat fluxes for a multirod fuel bundle design, even when subchannel conditions are used to evaluate the parameters. Also, Rogers<sup>15</sup> points out that use of a DNB correlation from annuli or tubes to establish the maximum permissible heat fluxes for organic-cooled fuel bundles may lead to unsafe designs. However, since no correlations exist

for multirod bundles, we believe it reasonable to use Eq. (6), which is not directly applicable, together with a reasonable safety factor applied in the form of a DNB ratio. The AI-CE design bases specified a minimum DNB ratio of 2, based on use of Eq. (5); we judge that the DNB ratio should be no less than 4 and that this value should be used in conjunction with Eq. (6). The relatively high DNB ratio is due to the uncertainties associated with the coolant composition and with application of a correlation based on data not directly applicable to multielement fuel bundles.

Since Eqs. (5) and (6) are of the same form, it is readily seen that Eq. (5) predicts lower values for the critical heat flux than does Eq. (6). Thus, for a given design heat flux, the DNB ratio associated with Eq. (6) will be higher than the ratio associated with Eq. (5). For the HWOCR-U conditions, a DNB ratio of 4 applied to Eq. (6) corresponds to a DNB ratio of 2.5 applied to Eq. (5).

### 5.1.3 Formulation of Input Data for the Codes

As previously stated, the applicability of the codes depends in many ways on the accuracy with which the input data can be formulated. Important factors about which the uncertainty exists are discussed in the following sections. They are: (1) the mixing factor, (2) the flux-peaking factors, and (3) the engineering factors.

Mixing Factor. For the U-3 code, the mixing factor is a constant which, when multiplied by the average velocity in the pressure tube, gives the crossflow rate between subchannels. In the THEME 1 code the mixing factor is defined in terms of temperature rises as given on page II-8 of Ref. 1. It is

$$M = \frac{\Delta T_{HC} - \Delta T_{HC}^M}{\Delta T_{HC} - \Delta T_A}, \quad (7)$$

where  $M$  is the mixing factor,  $\Delta T_{HC}$  is the temperature rise in the hot subchannel without mixing,  $\Delta T_{HC}^M$  is the temperature rise in the hot subchannel with mixing, and  $\Delta T_A$  is the overall temperature rise in the pressure tube. After the flow rates and heat input have been established,

the temperature rise in the hot subchannel without mixing and the temperature rise in the pressure tube can be calculated. Then from the value of the mixing factor, the temperature rise in the hot subchannel with mixing can be calculated.

The basis for a selection of a value for these mixing constants began with a recommended value for the crossflow rate between subchannels of 0.175 lb/ft·sec, which was cited on page 23 of Ref. 16. This value was for a wire-wrapped pin with a smaller pitch than employed in the AI-CE design. Extrapolation of the crossflow rate to a lower value to adjust for the longer pitch (4 ft) of the spiral fins and extrapolation back to a higher value to account for the effect of multiple fins rather than a single wire led Combustion Engineering to a value of 0.038 lb/ft·sec, which they believe is a conservative estimate. They would estimate that the most probable range for this crossflow rate is between 0.04 and 0.1 lb/ft·sec, and therefore their selected value is below the lower limit of their estimate.

The above procedure represents extreme extrapolation of existing experimental data; experimental study of the proposed AI-CE assembly is required to verify the procedure. There is one redeeming feature, however, in that a "little mixing goes a long way" in affecting the temperature rise in the hot subchannel. To demonstrate this and also to establish a relationship between mixing and the maximum surface temperature, a series of identical cases were run with both U-3 and THEME 1 for the AI-CE design in which only the amount of mixing was varied. For U-3, crossflow rates varying from 0.01 to 0.15 lb/ft·sec were used. The corresponding mixing rate constants (in the units of the code) ranged from 0.0001628 to 0.002441 g/cm<sup>2</sup> for an average velocity of 30 fps. A plot of the corresponding maximum surface temperatures in channel 8 (the hot channel is indicated by AI-CE, see Fig. II-2 of Ref. 1) as a function of crossflow rate is shown in Fig. 5.3.

The same case calculated with THEME 1 employed mixing factors [as previously defined in Eq. (7)] from 0.05 to 0.80. The results are shown in Fig. 5.4. By comparing the maximum surface temperatures obtained in the "hot channel," it is possible to relate the crossflow rate with the

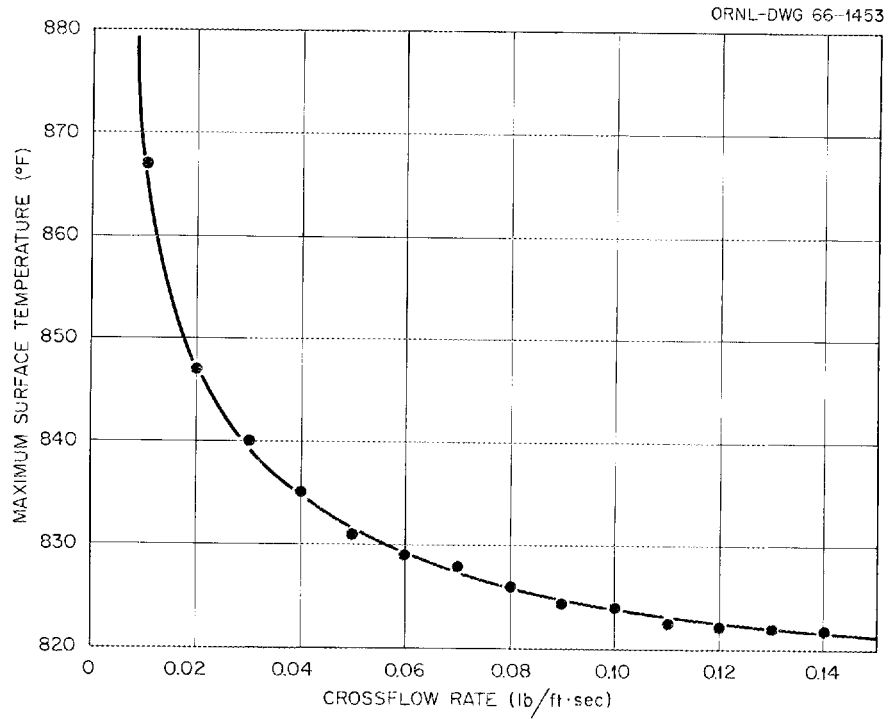


Fig. 5.3. Effect of Crossflow Rate on Maximum Surface Temperature.

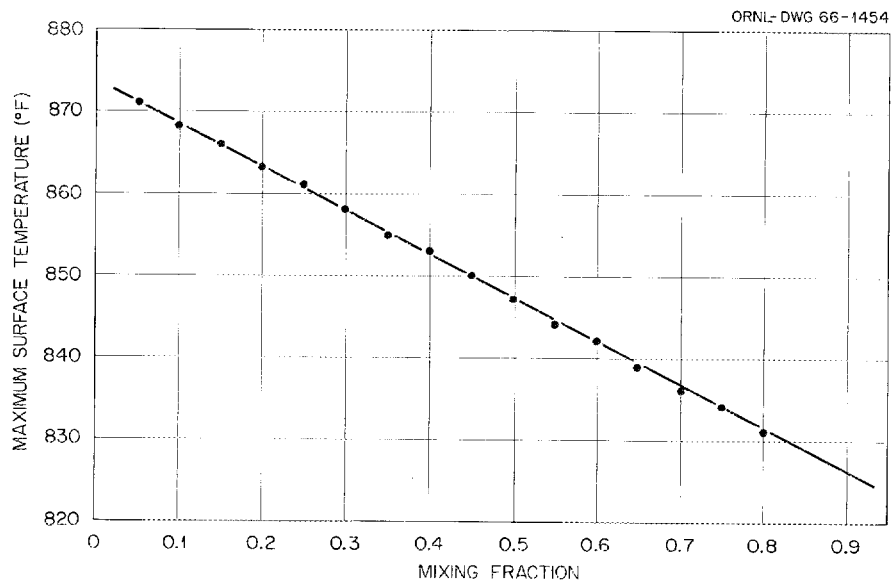


Fig. 5.4. Effect of Mixing Fraction on Maximum Surface Temperature.

temperature rise mixing factor. This relationship is shown in Fig. 5.5. A similar relationship obtained by AI-CE is presented in this plot, and it is from this plot that a mixing factor of 64% was predicted based on the extrapolated crossflow rate of 0.038 lb/ft·sec.

Several important features can be noted in the relationship presented in Fig. 5.5. First, the relationship is quite steep over the most probable range of values; that is, a large change in the crossflow rate produces only a small change in the temperature rise mixing factor. Therefore there can be a considerable error in the prediction of the crossflow rate without making a major error in the mixing factor.

Second, there is a difference between the curves produced by AI-CE and by our calculations. Several factors account for this variation. For our comparison, we defined similar cases as those having similar maximum cladding temperatures, and these similarities were based on comparing the output of THEME 1, which included the engineering factors, with the output of U-3, which had been corrected to include the engineering factors. AI-CE, on the other hand, simply used the output from the U-3 code to evaluate the mixing factor as defined in Eq. (7). Therefore, in effect, AI-CE was defining similar cases as those with the same outlet

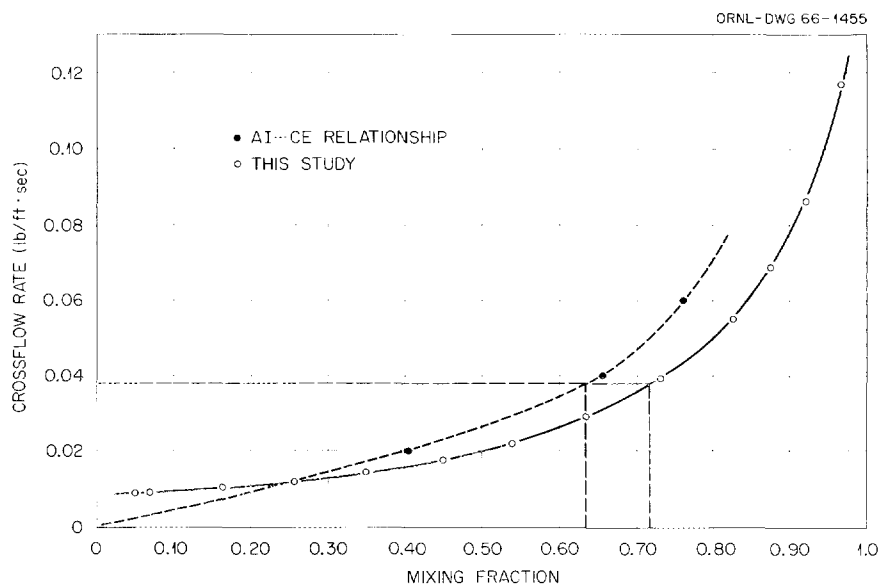


Fig. 5.5. Relationship Between Mixing Fraction and Crossflow Rate.

temperature from the hot subchannel. Since this is not the limiting condition in the design of these reactors, we believe that our choice for the basis of similarity is more meaningful for this comparison. In addition, the effects of the engineering factors were not included in the comparison developed by AI-CE, while they were included in the construction of our curve.

The major conclusion that can be drawn from the comparison of these two curves is that the differences are relatively small, and our calculations show that the AI-CE relationship is conservative. The differences in the two curves may account for the differences we obtained in the maximum surface temperatures based on THEME 1 and U-3 as compared later in this section. This would indicate that if the criterion that similar maximum surface temperatures be developed is used to compare the two representations of mixing, the mixing factor should be something like 72% rather than 64%.

It should be emphasized that the relation indicated in Fig. 5.5 was calculated only for the AI-CE design and cannot be applied with confidence to any other design without further study. It was, in effect, applied to the B&W pin design, however, when the assumption was made that the AI-CE mixing factor applied to the B&W design. Another notable point is that it would be expected that the relationship shown in Fig. 5.5 would pass through the point (0,0); that is, zero crossflow should produce zero mixing. AI-CE drew their curve through this point, but our calculations did not indicate that the curve passes through point (0,0). This result indicates that the representations of the effect of mixing in the two programs are not completely consistent, particularly at very low mixing rates.

Flux-Peaking Factors. The problem of accurately representing the variation of the local flux-peaking factor for a rod as a function of axial position in both the U-3 and THEME 1 codes was discussed above. Not only does this factor influence the total heat input to the coolant and the maximum cladding surface temperature, but it also influences the designation of the "hot subchannel."

Fig. 5.6 indicates the dependence on the local radial factors on burnup for the AI-CE design. Data for the outer ring of fuel and the second ring of fuel were obtained from Fig. II-16 of Ref. 1. Also shown on Fig. 5.6 are similar values calculated by ORNL, as well as the values recommended as "judicious" choices to represent the entire length, as given by AI-CE. For the inner ring and center pin, ORNL calculations indicated local rod radial factors of 0.63, 0.64, and 0.70 at 1000, 3000, and 15,000 Mwd/MT of uranium, respectively. The recommended choices by AI-CE were 0.66 for the inner ring and 0.56 for the center pin. Good agreement is indicated between the ORNL calculations and the AI-CE values for the outer ring. The lower values for the second ring calculated by ORNL indicate that the AI-CE numbers should give a conservative estimation of the performance of the "hot subchannel," which lies between the outer and second ring.

Local radial flux factors were furnished by B&W for each pin in their  $\text{ThO}_2$  design. No dependence upon axial position was indicated, and in this case, where the conversion ratio is higher, the variation should be smaller than for the AI-CE design.

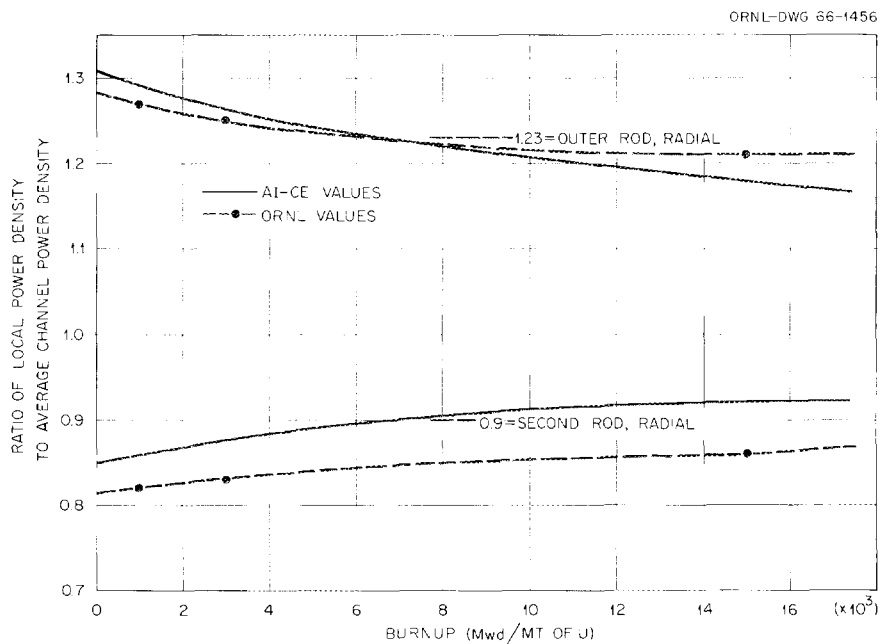


Fig. 5.6. Local Rod Radial Flux Factors as a Function of Burnup.

The gross axial flux factors, which are the product of the basic axial flux factor and the local axial flux factor, are entered in the code at selected axial locations. In the U-3 code the normalized local flux and the normalized integral flux up to that position are entered in the code. In THEME 1, only the normalized local flux is entered, and the integration is performed within the code. In both cases, a linear interpolation is made to estimate the flux between the selected points.

For the AI-CE design, the axial flux distribution was obtained from Fig. II-9 of Ref. 1. Values were read from this plot for substitution in the code. The maximum was read as 1.45, but we were later informed by AI-CE that it was 1.48. However, since all the points were normalized to this value, no effort was made to alter our input. We have recently obtained results from our own calculations, and both the ORNL values and the AI-CE values are shown in Fig. 5.7.

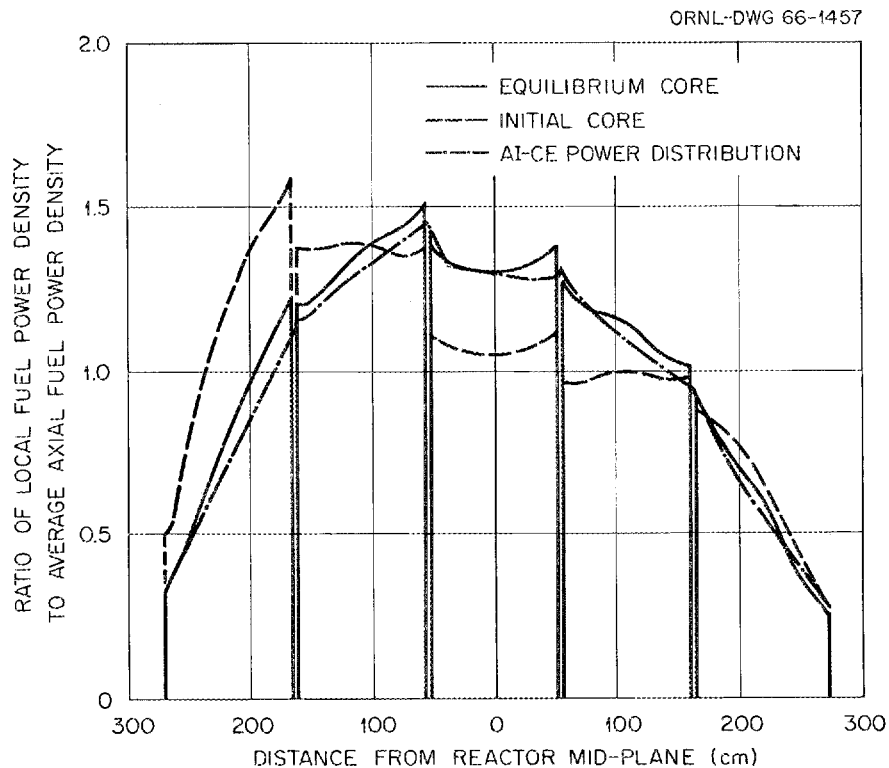


Fig. 5.7. AI-CE 1000-Mw(e) HWOCR Axial Power Distribution from Two-Dimensional Bidirectional Fueling Model.

For the B&W cores, the axial flux distribution was constructed based on the statement that it was represented by a chopped cosine with a peak-to-average ratio of 1.33. This was assumed valid; in addition, a local radial factor of 1.17 for the pin assembly and 1.05 for the nested-cylinder element was imposed upon the 1.33 factor. We recently completed our calculations of the axial flux distribution for these two designs, and these results together with our assumed values are shown in Figs. 5.8 and 5.9.

In Chapter 4 of this report, ORNL calculations for the basic radial flux distribution are given for both the B&W designs and the AI-CE design. The value given by both organizations for this factor was 1.17 and, in the case of the B&W designs, the values calculated by ORNL differed only slightly. For the AI-CE design conditions, a value of 1.39 was found, which is a significant change from the value of 1.17. However, by small changes in fuel exposure or fuel enrichment conditions, a value of 1.17 can be obtained. In addition, it has been found that the maximum developed surface temperature is not very sensitive to variations in the basic radial factor if fluid-flow orificing matches flow to the basic radial

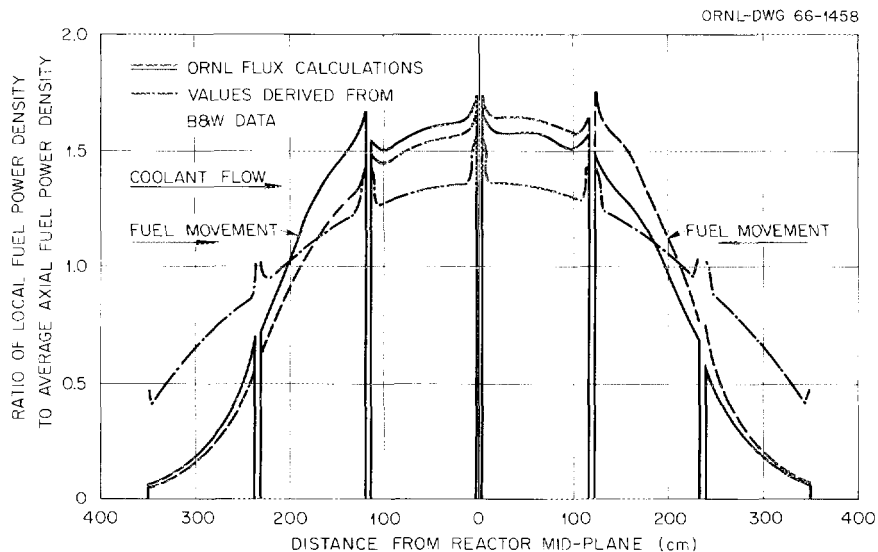


Fig. 5.8. B&W 1000-Mw(e) HWOCR Thorium-Uranium Oxide Concept Axial Power Distribution from Two-Dimensional Bidirectional Refueling Model.

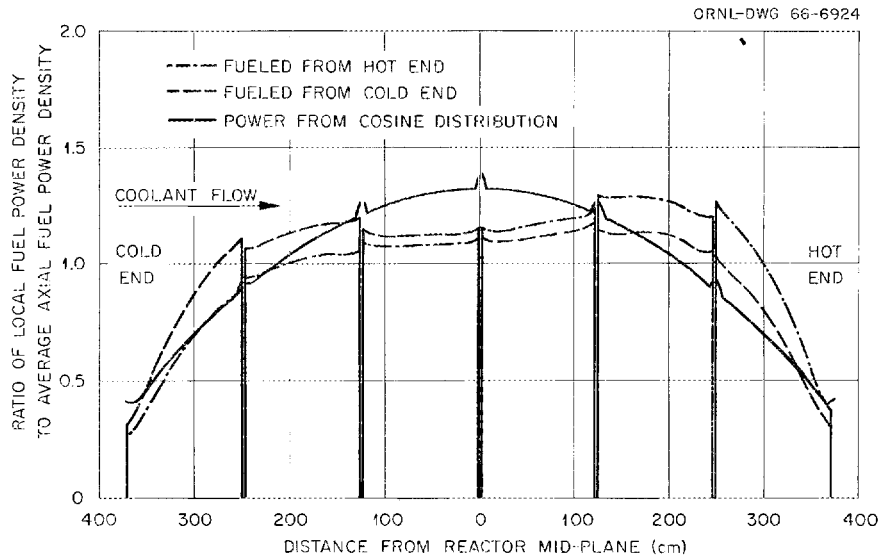


Fig. 5.9. Axial Power Distribution for B&W Nested-Cylinder HWOCR from Two-Dimensional Axial Bidirectional Fueling Cell Model.

power distribution. Under the latter circumstances, if the hot pressure tube (at the center of the reactor) is considered, the heat generation rate increases proportionately with the increase in the basic radial flux factor. If the coolant flow rate is also increased proportionately, the bulk temperature of the coolant is the same at relative axial positions in either case (except for small changes in heat capacity with temperature). The surface temperature is the sum of the bulk coolant temperature plus the temperature drop across the film. The temperature drop across the film is directly proportional to the heat flux and inversely proportional to the heat transfer coefficient. The heat flux is directly proportional to the basic radial flux factor, and the heat transfer coefficient is directly proportional to the velocity to the 0.8 power, which in turn is proportional to the basic radial flux factor to the 0.8 power, if orificing is to follow the basic radial flux factor. The net result is that

$$\Delta T_f = \frac{BR}{(BR)^{0.8}} \cong (BR)^{0.2}, \quad (8)$$

where BR is the basic radial flux factor. Equation (8) states that the

temperature drop across the film is proportional to the basic radial flux factor to the 0.2 power, if orificing corresponds to the basic radial flux factor.

For the specific case of the AI-CE reactor, increasing the basic radial flux factor from 1.17 to 1.39 represents an increase in 18.8%, but  $(1.188)^{0.2}$  is equal to 1.035, so the increase in the temperature drop across the film is only 3.5% when flow is properly orificed. At the "hot spot" of the hot subchannel in this design the temperature drop across the film is 75.6°F and the corresponding increase is 2.6°F. Even when this increase is multiplied by the engineering factor for the film temperature drop of 1.21, the increase is only 3.2°F. At the same time, increasing the basic radial flux factor from 1.17 to 1.39 (and also the orificing factor) increases the pressure loss due to friction through the hot pressure tube from 117 to 161 psi.

Engineering Factors. In order to evaluate the engineering factors as given by AI-CE in Table II-1 of Ref. 1 and as adopted by B&W, it was necessary to know their component parts. It was also necessary to know the exact definitions of these engineering factors, since they differed from similar factors used in other reactor designs and in the literature. A breakdown of these factors is given in Table 5.2.

A discussion of the factors is given in Appendix E. On the whole, the values used appear to be conservative, particularly the factor of

Table 5.2. Components of the Engineering Factors<sup>a</sup>

Component	F(Q/A)	F( $\Delta T_F$ )	F( $\Delta T_C$ )
Flow maldistribution between process tubes	1.0	1.03	1.04
Local coefficient uncertainty	1.0	1.05	1.00
Mechanical: pellet diameter, density, eccentricity, enrichment, etc.	1.10	1.10	1.02
Rod and bundle location and bowing	1.02	1.02	1.03
Total factor (product of components)	1.12	1.21	1.09

<sup>a</sup>For definition of these factors see p. II-8 of Ref. 1.

1.10 for mechanical effects in  $F(Q/A)$  and  $F(\Delta T_f)$ ; however, we question the factor of 1.02 for mechanical effects in  $F(\Delta T_c)$ . It appears from a review of similar factors by Chelemer and Tong<sup>17</sup> that a factor of 1.04 might be more appropriate. This would make  $F(\Delta T_c)$  equal to 1.11.

It should be remembered, as discussed earlier, that these factors do not include a factor for flow redistribution, which is handled by the codes. In comparing these engineering factors with similar factors where this redistribution is not included in the calculation, an additional factor (multiplier) of 1.04 should be included.

As discussed in Appendix E, the factor of 1.04 for flow maldistribution appears optimistic, and a factor of 1.05 is more realistic. Since the 1.04 factor is built into the calculations of THEME 1, however, and since the suggested change is small, no attempt was made to assess the associated change in the final calculated values.

#### 5.1.4 Analysis of the Output of the Codes

AI-CE Design. As would be expected, using the design parameters in the manner in which they applied them to their codes, the AI-CE design fell within their design specifications. From THEME 1, for velocities approaching 30 fps, the pressure drop per pressure tube was 110 psi. This compared well with the predicted value of 117 psi given by AI-CE. The maximum surface temperature under these conditions was 849.5°F. This figure did not allow, however, any uncertainty in the prediction of the film heat transfer coefficient. If we lower the calculated film heat transfer coefficient by 15% (see Appendix C), we raise the maximum surface temperature by about 19.5°F. In addition, if we assign a value of 1.11 to  $F(\Delta T_c)$  instead of 1.09, the maximum surface temperature increases another 2.5°F to a maximum value of about 872°F.

From calculations with the U-3 code, the average velocity in the pressure tube having maximum flow is 30.0 fps, and the predicted pressure drop is 116.8 psi; this pressure drop agrees closely with the value of 117 given by AI-CE. The maximum surface temperature given by this calculation is 835°F, and it occurs in channel 4 rather than channel 8 (see Fig. II-2 of Ref. 1). No allowance was made in this calculation for flow

maldistribution, so it appears that the engineering factors can be applied directly to the result. By applying a factor of 1.11 to the coolant temperature rise and 1.21 to the film temperature difference and using a heat transfer coefficient value which overall is 15% lower than that used by AI-CE, a maximum surface temperature of 876°F is obtained. This should be compared with the value of 872°F obtained from the THEME 1 calculation. The difference can be attributed to the difference in the equivalence of the mixing factor and crossflow rate, as shown in Fig. 5.5, and illustrates the difficulty in determining the maximum surface temperature precisely. These differences probably lie within the range of uncertainty in the prediction of the flux factors and the engineering factors.

Based on results of ORNL calculations of power-peaking factors (see Fig. 5.7), we find a corresponding maximum surface temperature of 878°F in channel 8 as calculated by THEME 1; the maximum value obtained from U-3 (now for channel 4) was 878°F. All these values were obtained for a basic radial power factor of 1.17, which appears achievable.

In calculating the DNB ratio, the amount of subcooling needs to be evaluated, and this requires knowing the boiling temperature of the coolant at the pressure existing at the "hot spot" in the reactor. If a plot is made for the vapor pressure of the coolant as a function of temperature, as given in Table III-2, page III-3, of Ref. 1, and an interpolation is made for 10% high boilers, a boiling temperature of 900°F is found to correspond to a pressure of 100 psia, which is the outlet pressure from the reactor. For this pressure, the DNB ratio calculated by THEME 1 is 2.44. However, a more realistic pressure estimate for the "hot spot" location would be about 190 psia, which corresponds to a boiling temperature of 1000°F based on these same data. Substituting the value of 1000°F for the value of 900 used in the code results in a DNB ratio of 3.61. The corresponding AI-CE value is 4, as given in Fig. II-5 of Ref. 1; since the DNB ratio is very sensitive to the estimated values of boiling temperature and pressure at the "hot spot," there appears to be good agreement between our value and the AI-CE value for the conditions cited.

In addition to the above, evaluation of the vapor pressure must also take into consideration the effect of increased biphenyl content, as discussed in Section 5.5. The data for coolant containing 12% biphenyl led us to a "best guess" for the equilibrium coolant vapor pressure-temperature relationship that indicated a boiling temperature of 910°F at 190 psia. Based on this value the DNB ratio is 2.56 at the "hot spot" location.

As discussed previously, we estimate that the lowest feasible DNB ratio based on present information is about 2.5 if the heat-flux correlation incorporated in THEME 1 is employed [the correlation used in the code appears conservative, so a DNB ratio of 2.5 based on that correlation actually corresponds to a DNB ratio of 4 based on Eq. (6)]. Thus, we consider the AI-CE design conditions to be feasible relative to permissible heat flux and DNB ratio.

A criterion specified by AI-CE but which was not actually considered was that no subcooled nucleate boiling should occur in the core. We do not know whether the criterion is required and have assumed that it is not necessary. Only further data on fuel element performance and reactor kinetic performance as a function of DNB ratio can determine this. If the criterion of no subcooled nucleate boiling is required, the permissible heat flux could be below specified values and would be dependent on the biphenyl concentration of the coolant.

B&W Pin-Cluster Design. From the results of THEME 1, the pressure drop predicted for the B&W pin design is 177 psi, which is the same as the value reported by B&W (corrected for static head). The only difference is that, according to information from B&W, their value does not include entrance and exit losses to the assemblies, while the value from THEME 1 allows 1.5 velocity heads for the losses. The maximum surface temperature predicted by THEME 1 is 832°F based on B&W's designation of the hot channel and B&W's power distribution factors. This value is based on the heat transfer coefficient relation used by AI-CE. Lowering the coefficient by 15% increases the maximum surface temperature to about 850°F. Again, if the engineering factor,  $F(\Delta T_c)$ , is changed to 1.11, the maximum surface temperature is increased by an additional 3°F to a value of 853°F.

Code U-3 predicts a pressure drop through the pressure tube of 179.9 psi, which agrees well with the calculations from THEME 1. The maximum surface temperature occurs in one of the channels adjacent to the flow blocker (not the same as the one designated by B&W); however, it differs by less than 2°F from the more normal channel. Applying the values of the engineering factors to these results [a value of 1.11 is used for  $F(\Delta T_c)$ ] and using the heat transfer coefficient obtained from Eq. (3) results in a maximum surface temperature of about 858°F, again using the specification of the axial power distribution as given by B&W.

The value of 858°F predicted by U-3 should compare with the value of 853°F predicted by THEME 1. No precise explanation for the variation can be made at this time. The most probable explanation, at present, appears to be that the relationship between the crossflow rate and the mixing factor for the two designs, as shown in Fig. 5.5, does not hold for the B&W design. Since the U-3 code had to be modified considerably to describe mixing in the B&W design, it is possible that the effectiveness of crossflow in limiting the hot channel temperature rise was different than in the AI-CE design.

These calculations were repeated for the ORNL axial power distribution shown in Fig. 5.8 and the local radial power factors determined by ORNL. The results of these calculations are summarized in Table 5.3 for the channel designated as the hot subchannel by B&W. This channel was a triangular channel just inside and touching the two outer pins nearest the corner of the hexagonal array. Actually U-3 calculations indicated that higher surface temperatures were developed in the subchannel adjacent to the circular flow blocker, but this situation could easily be remedied by reducing the size of the flow blocker and permitting more flow.

The B&W pin-cluster design had significantly higher axial peaking factors than the AI-CE core design, which accounts for the high surface temperatures. We initially thought these factors could be reduced by shortening the B&W core length, but recent calculations indicated that reducing the B&W core length to that of the AI-CE reactor did not lower the axial peaking factors. It is probable that these factors can be lowered by use of a different fuel-shuffling scheme; placing the more

Table 5.3. Maximum Surface Temperatures in the  
B&W Pin Design for the Heat Transfer  
Coefficient Based on Eq. (3)

(ORNL-based power peaking factors)

Fuel Insertion Position	$F(\Delta T_c)$	Code	Maximum Temperature (°F)
Top	1.09	THEME 1	880
Top	1.11	THEME 1	882
Bottom	1.09	THEME 1	892
Bottom	1.11	THEME 1	893
Top	1.09	U-3	882
Top	1.11	U-3	886
Bottom	1.09	U-3	888
Bottom	1.11	U-3	891

highly burned fuel at the center of the reactor could reduce the maximum value significantly. Changing the fueling scheme also changes the required fuel enrichment and can influence a number of other design features. Since such a study would essentially require a detailed design-parameter investigation, it was considered outside the scope of this evaluation.

B&W Nested-Cylinder Design. Only the U-3 code was useful in evaluating the B&W nested-cylinder design. A major difference was found in the calculation of the pressure loss due to friction through the assemblies. A value of 191 psi was predicted by U-3, while the value listed by B&W, corrected for static head, was 166 psi. This figure was supposed to include 1.5 velocity heads for losses at entrance and exit from the restricted flow area, according to B&W.

In calculating the maximum sheath temperatures, B&W did not apply the engineering factors to their design as such, but they made recalculations with their TANC code and allowed the maximum possible deviations in geometry and concentrations. These calculations were discussed with the B&W personnel, and their approach appears to be realistic if the correct dependence on the neutron flux variations was entered. For the present study it was felt that applying the same engineering factors as

those used for the pin-cluster design would be reasonable; because of the good flow geometry, Eq. (2) was used in obtaining the heat transfer coefficient. For these conditions, a maximum surface temperature of 847°F was found when  $F(\Delta T_c)$  was equal to 1.09; 850°F was calculated when  $F(\Delta T_c)$  was 1.11. These results are based on the B&W power-peaking factors.

For the gross axial power distribution calculated by ORNL (and shown in Fig. 5.9) the maximum surface temperature was encountered on the outer wall of the outer cylinder. The coolant issuing from the outer channel was not the hottest coolant, so decreases in temperature could probably be better obtained by decreasing the amount of fuel in the outer cylinder than by increasing the flow of coolant in the outer channel. Applying the engineering factors that were used in the case of the pins, we found surface temperatures of 860°F for  $F(\Delta T_c)$  equal to 1.09 or 864°F for  $F(\Delta T_c)$  equal to 1.11 for fuel entering at the top of the reactor. For fuel entering the bottom of the coolant channel (that is, new fuel encountering hot coolant), the maximum temperatures are slightly higher. The maximum surface temperature, at the same location as before and corresponding to the 864°F value above, was found to be 879°F.

Based on recent calculations at ORNL, decreasing the length of the fuel channel to that in the AI-CE design did not lower the axial power peaking factor of the nested-cylinder design. An improvement would probably be obtained by changing the fuel-shuffling scheme to one which positioned the most highly exposed fuel in the center part of the reactor. Such a scheme would also decrease the axial power peaking factor in the AI-CE reactor but is not needed as much as in the B&W concept. Because optimization of the refueling scheme involves a number of design considerations other than minimization of the axial power peaking factor, parameter studies concerning the refueling scheme were considered outside the scope of our evaluation and were not performed.

#### 5.1.5 Discussion and Evaluation of the Reactor Cores

Based on the ORNL evaluation and use of the engineering and heat transfer factors, and using the ORNL power-peaking factors, it appears that the AI-CE core design gives a maximum surface temperature of about

878°F, which exceeds the specified maximum value of 850°F. The B&W pin-cluster design has a maximum fuel-surface temperature of about 884°F for fuel elements that move in the same direction as the coolant flow, while the maximum temperature is about 892°F for elements whose fuel movement is opposite to that of coolant flow. Thus, by using the same coolant flow arrangement as proposed by AI-CE, the maximum fuel surface temperature for the pin-cluster element would be about 884°F. We consider the AI-CE arrangement feasible, economical, and applicable to the B&W design.

The B&W annular-cylinder design has a maximum fuel-surface temperature of about 864°F for fuel entering the reactor in the same direction as coolant flow, and about 879°F for fuel entering the reactor in a direction opposite to that of coolant flow. Again, we consider the AI-CE coolant-flow arrangement to be feasible for the B&W concept, and if utilized for the annular cylindrical elements, the maximum fuel-surface temperature would be about 864°F.

If the axial peaking factors can be significantly reduced by changes in the fuel management scheme or by design changes, the maximum fuel surface temperatures can be reduced considerably for both the AI-CE and B&W concepts, with more potential reduction possible in the B&W concept.

In reporting all the foregoing maximum surface temperatures, no allowance was made for the effect of a fouling film on the heat transfer surface. The possibility of the presence of such a film has already been mentioned and will be discussed in more detail in Section 5.5. The effect of such a film would be to increase the maximum surface temperature by 25 to 50°F, according to our estimates. The result would be to increase the surface temperatures, which are already above the allowable value of 850°F based on our estimates of the flux-peaking factors and the correlations used for the heat transfer coefficient.

Remedies for these overtemperatures have already been suggested. Increasing the coolant velocity would improve heat transfer, and at the same time increase pumping requirements; as pointed out previously, it appears feasible to increase the core pressure drop. An obvious remedy for the overtemperature due to the fouling film is to decrease the inlet and outlet temperature and thereby maintain the same total power generation

but reduce the surface temperature.\* Unfortunately, a decrease in the bulk coolant temperature of 50°F does not produce a corresponding reduction in the fuel element surface temperature. The reason for this is that the heat transfer coefficient is dependent upon the coolant physical properties, and a decrease in temperature produces a decrease in the heat transfer coefficient, and also changes the location of the peak surface temperature. Of these two effects, the latter is the more significant one, based on U-3 calculations in which the reactor inlet coolant temperature was decreased below the design value. The heat transfer coefficient was varied in accordance with the variation in coolant physical properties with temperature; a constant mass flow rate was assumed. Reducing the inlet coolant temperature by 50°F in the AI-CE reactor led to a reduction in maximum fuel surface temperature of about 38°F; these results were obtained with the heat transfer coefficient and engineering factors ORNL specified previously. Thus, the coolant temperature has to be reduced about 65°F to compensate for a 50°F drop across the fouling film, based on an 850°F maximum fuel surface temperature.

There are several additional factors that require investigation and which have a major bearing on the final reactor design. These investigations should include (1) the exact determination of the effect of mixing on the hot-channel temperature rise, (2) a study of the possibility of subcooled nucleate boiling in the coolant, (3) an analysis of the effect of off-centered assemblies in the pressure tube on maximum surface temperatures, and (4) an examination of the end-plate design and its effect on pressure loss and flow redistribution in the AI-CE assembly.

Effect of Mixing. As was discussed previously in this section, the determination of the crossflow rate was the result of extreme extrapolation from data for essentially a different type of assembly. Relating

---

\*The maximum surface temperature can be reduced by other methods. One would be to reduce the power output per process tube by increasing the number of tubes in the reactor. This has been done in the Demonstration Plant design and the surface temperature has been reduced to below 860°F at design conditions (maximum power output), with no allowance for film deposit.

this crossflow rate to a factor expressing the temperature rise in the hot subchannel was dependent upon an assumed and unproven model. The effect of mixing must be experimentally determined for the particular design, and additional work is necessary before extending this to even similar designs. There is no substitute here for additional experimental investigations.

Effect of Off-Centered Assemblies. In making these calculations for both the AI-CE and B&W pin designs, it was assumed that a 30-mil clearance existed on each side of the assembly. During the course of the calculations, it became apparent that very small changes in flow areas (almost below the limits of the engineering tolerances) could make significant differences in the redistribution of flow in the assembly. These differences would, in turn, affect the maximum temperatures developed in the assembly. It is certain that the positioning of an assembly so that zero clearance existed on one side and 60 mils clearance on the other would have a profound effect on the flow distribution and resultant temperatures. Although this effect could be estimated through a series of recalculations, this study was not made. To be truly meaningful, the recalculations should be coupled with a reevaluation of the rod radial flux factors. The factor of 1.02 included in the engineering factors to account for this effect does not appear adequate to account for the deviation that might result.

Effect of End-Plate Misalignment. A point that has not been examined in detail in the AI-CE design is the pressure loss allowed for the end plates between assemblies. At present, approximately 6 psi is allowed for each of the four junctions; this is only a little over one velocity head for the average velocity in the assembly. It is assumed that the end-plate design has not been thoroughly established but that it will afford at least as much flow area as in the pin section. However, misalignment of the end plates could present a considerably more restricted flow passage and consequently a considerably higher pressure loss. Even more important, the misalignment of the end plates could cause an unfavorable redistribution of flow and "starve" (at least temporarily) the hot subchannel. Since power peaking occurs at the ends of the fuel

assemblies, "flow starving" at these points in high flux regions would be particularly unfortunate.

It is strongly recommended that much more attention be given to the study of the end-plate design and that some consideration be given to the orientation of adjacent assemblies so that excess pressure losses and possible channel starving can be avoided.

#### 5.1.6 Conclusions

Evaluation of the thermal and hydraulic characteristics of HWOCR reactor cores consisted of an evaluation of certain computer codes, formulation and evaluation of the input data, and analysis of the output of the codes. Application of the codes appears to be satisfactory, with the reservations that the mixing model, which proved adequate to correlate intersubchannel flow in wire-wrapped bundles, might not prove as accurate for spirally finned elements, and application of this mixing model to the present design represents a large extrapolation.

According to recent heat transfer data, the correlation for the heat transfer coefficient used in the codes, and by AI-CE and B&W, appears high by about 5%. In addition, to account for the geometry and flow conditions that exist with pin-cluster elements, the coefficient should be decreased by an additional 10% for axial flow in fuel bundles. The correlation for the critical heat flux used in the codes is not directly applicable to rod bundles, and a DNB ratio of at least 3 appears advisable. In addition, the biphenyl concentration in the equilibrium coolant appears higher than indicated by AI-CE, which results in lower DNB ratios than would otherwise be the case.

In formulating the input data for the codes considerable deviation was found between the power peaking factors as specified in the designs and those calculated by ORNL. In the AI-CE design, the major difference was in the basic radial flux pattern; however, this difference could be adjusted by varying the enrichment or feed rate. In the B&W design, the major difference was in the axial flux pattern. Our calculations indicate that the thorium-fueled reactor tends to have higher axial power peaking factors than does the uranium-fueled system. The engineering

factors supplied by the sponsors appeared to be slightly low, and minor adjustments were made in these.

Based on the AI-CE design conditions with no fuel-surface fouling, we estimate a maximum cladding surface temperature of 878°F, as compared with a maximum allowable surface temperature of 850°F. Under the same conditions, temperatures in the range of 884 to 892°F were calculated for the B&W pin-cluster design, depending upon the direction of flow of coolant with respect to the fuel movement. For the B&W nested-cylinder design, the maximum surface temperatures were 864 and 879°F, again depending upon the direction of coolant flow. The maximum temperatures for the B&W reactors can be reduced if the axial power-peaking factors can be lowered to AI-CE values.

Inclusion of a fouling film on the heat transfer surface will tend to increase maximum surface temperatures. It is estimated that such a film will exist and have a 25 to 50°F temperature drop across it. Lowering the coolant temperature by 50°F would not produce a corresponding reduction in the surface temperature, since the effect of temperature on the coolant properties would decrease the heat transfer coefficient; the corresponding reduction in surface temperature would only be 38°F for the AI-CE design conditions. Lowering the bulk coolant temperature by 50°F would, however, have the effect of increasing the DNB ratio to 3.15 based on Eq. (5) and to about 4.9 based on Eq. (6).

The pressure drop across the fuel assemblies may be affected by film buildup, but it is expected that any increase can be accommodated in the design with little or no penalty. We estimate that the maximum film buildup for the temperature drop assumed, that is, 50°F drop across the film, would not exceed 1 mil in thickness. If a film of this thickness deposited uniformly on the surfaces of the fuel elements (AI-CE design), the cross-sectional flow area would be reduced about 1.8%. For the same flow rate through the core, the frictional pressure loss in the core would be increased by approximately 3.3% or about 3.8 psi. The total system pressure loss, however, would increase only about 1.3%. The actual effect would be that flow would decrease a small amount depending upon the characteristic curve of the pump. At most the drop in flow is estimated to be 1.3 gpm (for a pressure drop of 3.8 psi) or about 0.5%.

The above analysis does not take into account the effect of any change in surface roughness. Canadian data indicate that a smooth film forms if the deposition rate is slow, as it is assumed to be for the HWOCR design. That being the case, the effect of change in surface roughness is expected to be negligible.

In the AI-CE design, 24 psi has been allowed for the pressure loss at the four junctions between the five assemblies in each pressure tube. This value of 6 psi loss per junction represents only a rough estimate at the present time and may vary over a considerable range depending upon the degree of alignment of the flow channels in adjacent assemblies. This loss could be significantly reduced and rendered more predictable by alignment of the assemblies as discussed in this report. The variable nature of the pressure loss at this interassembly junction makes a consideration of the pressure loss due to film formation insignificant at this time.

In order to achieve a maximum surface temperature not in excess of 850°F for the AI-CE design conditions with a 25°F temperature drop across the coolant fouling film at the position of peak surface temperature, the coolant outlet temperature would have to be lowered about 70°F to 680°F. The corresponding decrease in outlet coolant temperature for a 50°F temperature drop across the fouling film would be about 100°F, or an outlet temperature of 650°F. At the same time, it is possible to alter the reactor design conditions so that the outlet coolant temperature can be increased at less economic penalty than that associated with operating the present design at an outlet temperature in the 650 to 680°F range. For example, it is possible to lower the fuel surface temperature by increasing the coolant velocity or by decreasing the fuel power density. In particular, since the fuel inventory charge has a low value, the reactor could be redesigned with advantage taken of this situation. However, such a change would involve some penalties in capital costs and in fuel inventory costs that would need to be evaluated. Alternatively, the thickness of the fuel element cladding could be increased, so that a higher surface temperature would be permissible without leading to excessive stresses in the SAP cladding. Such a change would increase the required fuel

element enrichment and would lead to an increase in the diameter of the SAP process tube, and could not be incorporated into the design without some penalty in fuel-cycle performance and power-production cost. Nonetheless, such design changes undoubtedly would introduce less penalties than would the direct application of the lower coolant temperatures discussed above. To investigate the above matter thoroughly would require extensive design optimization studies, and these were outside the scope of our evaluation. At the same time, in evaluating HWOCR performance, consideration should be given to the above alternatives. To account for reoptimization of design conditions, it is estimated that the equivalent outlet coolant temperature to be associated with the present AI-CE design is 675 to 700°F for a fouling film temperature drop of 25 to 50°F at the position of maximum fuel surface temperature. The above outlet coolant temperature range is used in evaluating the AI-CE concept. Such a condition can be considered equivalent to increasing the fuel cladding thickness so that a maximum SAP surface temperature of about 870°F is permissible, with the decrease in nuclear performance associated with such a design change accounted for by decreasing the outlet coolant temperature about 7°F.

The B&W thorium design conditions resulted in higher maximum fuel temperatures than those of the AI-CE core design, and for these circumstances the effective outlet coolant temperature would need to be reduced in accordance with the above discussion to values in the 660 to 690°F range. However, if bidirectional coolant flow were employed, rather than the unidirectional flow specified, the nested-cylinder case would improve significantly and lead to effective outlet coolant temperatures in the 675 to 700°F range. Thus in evaluating the B&W core designs the effective outlet coolant temperature for the pin design is considered to be 660 to 690°F; the corresponding range for the nested-cylinder design is 675 to 700°F.

Redesign of the thorium cores probably could lead to a significant decrease in the axial power peaking factors, since these were much larger than the corresponding values in the AI-CE design. The high peaking factors were due to the spaces between fuel assemblies and the high absorption cross section associated with the fuel. These power peaks could be reduced by using only fertile material at the ends of the assemblies.

However, there would be associated changes in fuel fabrication costs and in nuclear performance to be considered. Such studies were not performed here, but they should be included in any redesign studies of the thorium-fueled cores. If axial power peaking can be significantly decreased, the outlet coolant temperature could increase to values above 700°F.

There are several additional factors that require further investigation. These are (1) experimental measurement of fluid mixing in flow channels containing spirally finned elements, (2) the conditions associated with subcooled nucleate boiling, (3) the effect of off-centered assemblies in the pressure tube on fluid flow conditions, and (4) the effect of fuel assembly and plate placements on pressure loss and flow distribution in the AI-CE design. To investigate these areas, full-scale mockups representing HWOCR design conditions are required, with detailed measurements made of variables such as flow, temperature, and fluid mixing under HWOCR operating conditions. Also, studies of the effect of changes in parameter values on variable behavior would assist in design optimization.

## 5.2. Fuel Element Performance Evaluation

Fuel element performance characteristics were examined for each reactor to identify areas that might limit the life of the fuel element. Of principal concern were fission-gas release and fuel swelling and the ability of the fuel cladding to maintain its integrity. Many other factors can contribute to fuel element damage, and it is the improbable concurrence of a combination of factors that often causes fuel element failure. Since the probability of a failure increases with severity of the operating conditions, extensive testing is required to determine performance under HWOCR conditions.

Fuel element characteristics of the three reactor fuel assemblies are listed above in Table 5.1.

### 5.2.1 AI-CE Fuel Element

The AI-CE fuel element has 37 SAP-clad tubes containing cast hyperstoichiometric UC. The free-standing cladding is 0.020 in. thick and has 12 extruded fins that spiral at 90° per foot. The fuel rods are

44 in. long and are nested into Zircaloy-4 end plates. Dimensions are such that fins of adjacent elements touch and support each other. Five fuel elements are stacked vertically in the reactor. The 12 outer fuel rods are attached to both end plates and support the weight and hydraulic forces exerted on the fuel elements above. These rods operate at the highest power level and sustain maximum burnup in the channel. The fuel assembly has a radial clearance of 0.030 in. between it and the 4.320-in. ID of the SAP pressure tube.

The approximately 3-in.-long UC fuel slugs are cast and formed to give a 0.0025-in. radial clearance in the cladding. The fuel element life is about 700 days, and maximum burnup in any rod is 20,500 Mwd/T. The coolant inlet temperature is 595°F. Cladding temperature and heat rating increase as the fuel element moves through the reactor. The maximum rated cladding temperature and the heat rating of any rod are 850°F and 26.6 kw/ft, respectively.

Irradiation tests of SAP-clad UC fuel elements were made in the X-7 loop of the Canadian NRX reactor at heat ratings up to 14 kw/ft. Several elements were examined after a peak burnup of 8000 Mwd/T, and some were reinserted and operated to a calculated burnup of 11,500 Mwd/T.<sup>18</sup> Detailed information on postirradiation examination is not yet available. Additional irradiation tests have been carried out by Atomics International in the U-305 experiment, and the detailed results should be available soon.

The AI-CE fuel element was analyzed with respect to its expected performance at the higher heat ratings, power levels, and burnups projected for the HWOCR conditions. From the viewpoint of fuel element performance, a principal concern is that fuel rod design and operating conditions be such that fuel swelling and fission-gas release will not cause cladding failure.

Uranium carbide is a proven fuel material and has been tested extensively during the past several years.<sup>19-21</sup> Although many tests have been made with hypostoichiometric UC or with (U-Pu)C fuels, hyperstoichiometric UC (fuel employed in HWOCR) is usually considered superior to either. Fission-gas release is temperature dependent, and data have been obtained at burnups of 40,000 Mwd/T that show less than 1% gas release

at temperatures of 2000°F or below.<sup>19-20</sup> An analysis<sup>20</sup> of the data by Atomics International is shown in Fig. 5.10. More recent data have confirmed these results.<sup>22</sup> Swelling of UC during irradiation increases about linearly with burnup to well beyond expected MWOCR exposures. Swelling

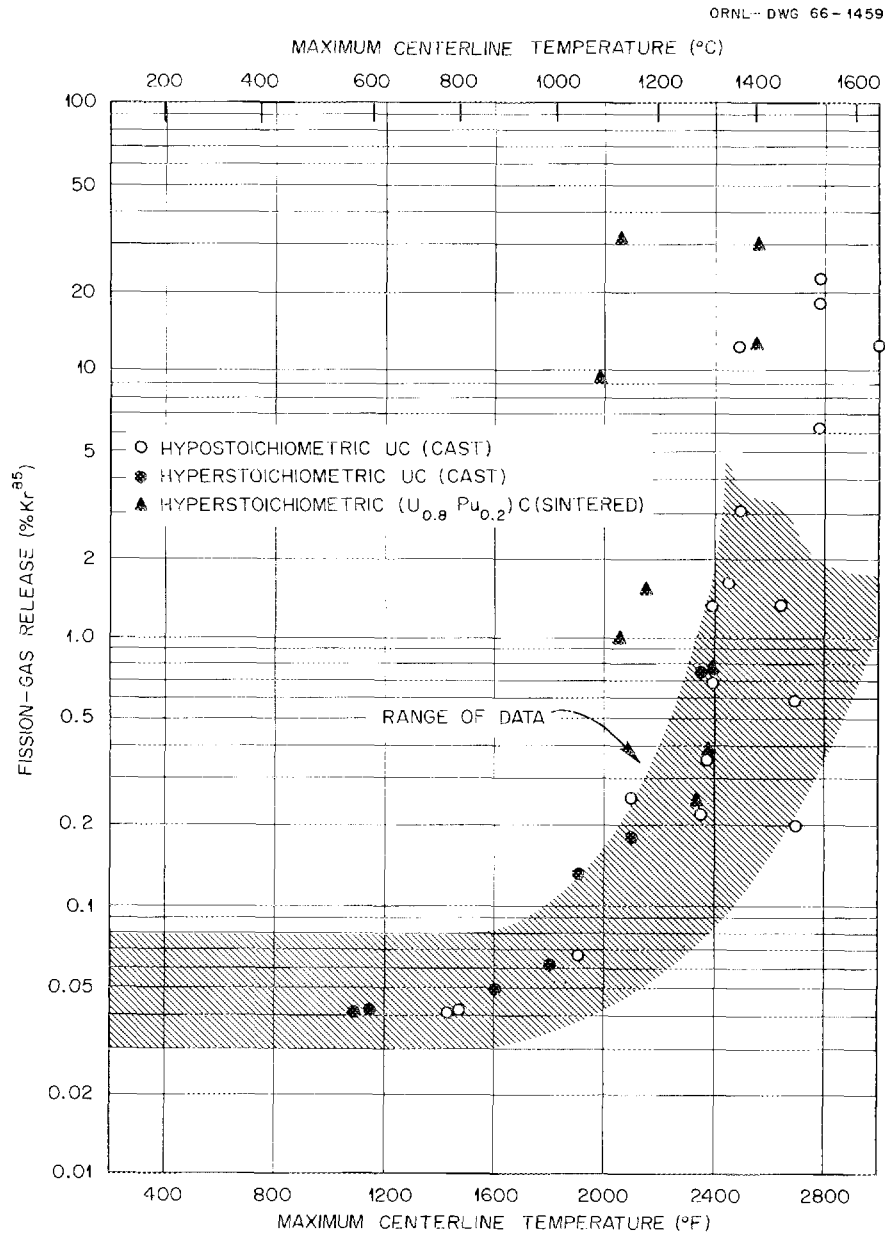


Fig. 5.10. Uranium Carbide and Uranium-Plutonium Carbide Fission-Gas Release. (From Ref. 19)

is also temperature dependent, as shown in Fig. 5.11. These data also have been confirmed by more recent results.<sup>22</sup>

The maximum temperature of the AI-CE fuel is critically dependent on heat transfer across the gap at the interface between the fuel and the cladding. The heat transfer across the radial gap, initially 0.0025 in. thick and containing helium gas, changes as the fuel swells to reduce gap thickness and as the gas conductivity is reduced by dilution with released fission gases. Heat-generation rates of local portions of the fuel change as the fuel element progresses through the reactor. Atomics International has examined these factors in detail and concluded that the maximum fuel temperature will be about 2000°F.<sup>18</sup> Our calculations, based on AI-CE estimates of cladding temperature and power peaking factors, indicate temperatures of about 2100°F at the ends of the outer fuel rods

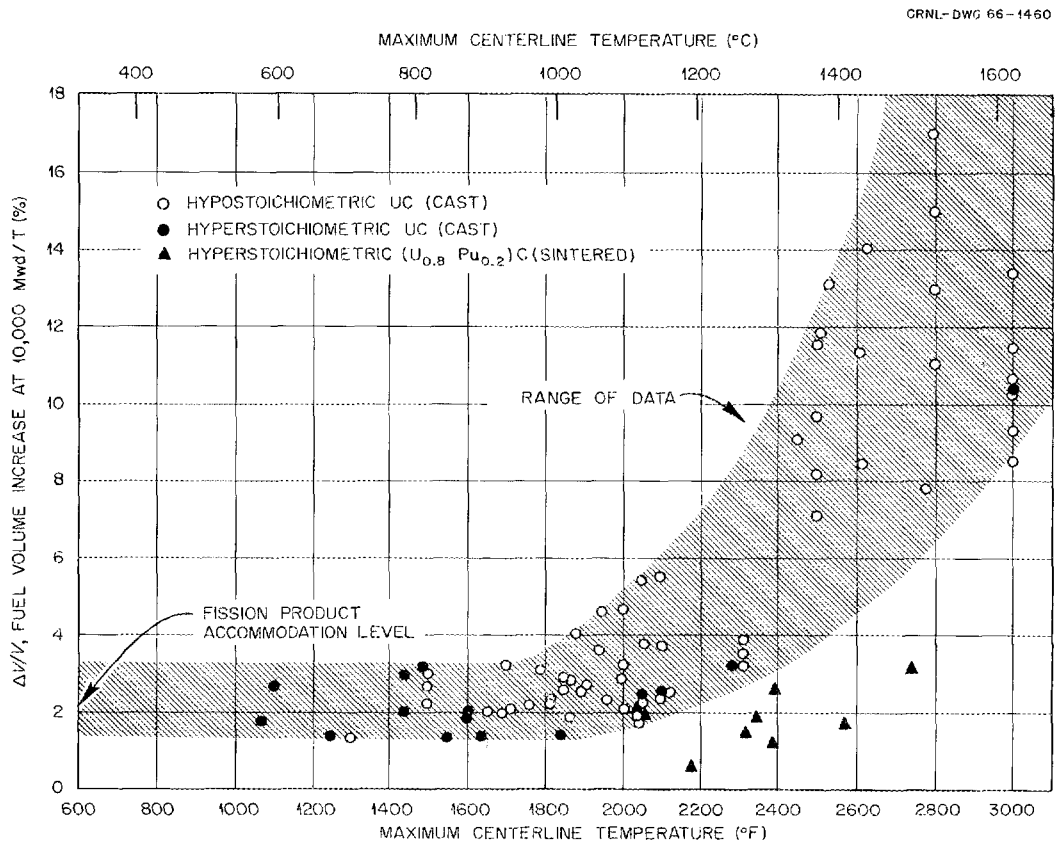


Fig. 5.11. Uranium Carbide and Uranium-Plutonium Carbide Fuel Volume Increase. (From Ref. 19)

during residence in the first two positions with conduction through helium gas in the fuel-cladding gap. Temperatures at succeeding positions will be lower, as will temperatures of other rods that have lower radial power peaking factors. We consider the above conditions to be feasible. Estimates of maximum fuel temperatures are subject to considerable inaccuracies, however, because heat transfer across the fuel-cladding interface is a function of many variables. Contact between tiny projections may reduce thermal resistance at the interface, and dimensional variations from fabrication tolerances preclude accurate calculations.

From the available data, Atomics International concludes that fission-gas release from the most highly rated element will be about 0.31% and calculates that internal pressure will not exceed about 300 psi with a fission-gas plenum 0.60 in. long. We concur with these data if fuel swelling does not exceed 2% per 10,000-Mwd/T exposure.

The AI-CE fuel element is designed on the basis of 2% fuel swelling per  $10^4$  Mwd/T, from which it is concluded that the cladding strain would be 0.5% at a maximum fuel exposure of 24,000 Mwd/T. The data of Fig. 5.11 indicate that 3% swelling is a distinct possibility. Based on the 0.005-in. diametral clearance, an isotropic 3% volume increase would exceed the expected limit of 0.5% strain for SAP cladding at regions where local burnup reaches about 16,000 Mwd/T. Thus, although we agree that the 2% volumetric expansion per 10,000-Mwd/T exposure is a feasible value, a larger rate may be applicable. Additional information on fuel swelling must be obtained before successful operation of the HWOCR at the proposed burnup can be predicted.\*

---

\*The reference fuel element described in AI-CE-Memo-25 (Ref. 23) is similar to the element considered above, but radial clearance between fuel and cladding is increased from 0.0025 to 0.0035 in. and the length of the fission gas plenum is increased from 0.60 to 1.0 in. This will accommodate greater swelling and fission-gas release. Based on heat ratings for the 750-Mw(e) design, the maximum fuel temperature will be increased by about 200°F above the AI-CE-Memo 6 design value,<sup>1</sup> a condition we consider to be excessive. At the lower heat ratings associated with 500-Mw(e) operation the element described in AI-CE-Memo-25 (Ref. 23) will have a maximum temperature of about 1900°F, which is much more conservative. Testing will of course be required to establish performance in the radiation environment.

In addition to the above factors, several other problem areas for the AI-CE fuel element will require investigation. Data indicate that hyperstoichiometric UC is more subject to cracking than is UC of lower carbon content.<sup>22</sup> The effects of vibration and thermal cycling may cause chipping of cracked fuel. If particles become trapped at the fuel-cladding interface, these could cause excessive local stresses in a low-ductility material like SAP. Also, the fuel cladding fins will bear against the inner wall of the SAP pressure tubes, and the action of aluminum against aluminum could lead to wear or galling of the inner surface of the pressure tubes. Such phenomena may also influence the forces required to remove fuel elements from the reactor. The performance of the fuel element in organic coolant with respect to fuel tube bowing and behavior after cladding failure as a function of fabrication tolerances must also be determined.

Conclusions. The UC fuel element appears to be properly designed and suited for HWOCR application based on present information and feasibility conditions. It should be capable of operating at proposed heat ratings and temperatures. Available data are not yet sufficient to establish fuel element life. Achievement of the desired burnup will be critically dependent on the fuel swelling at operating conditions; increases in radial gap thickness to accommodate greater swelling will cause significant increases in maximum temperature. The strict limitations on gap thickness imply rigid control of dimensional variations of both the UC fuel and the inside diameter of the SAP cladding. Additional irradiation testing is also required to demonstrate that reactor operating conditions do not lead to other difficulties that will limit the life of the fuel elements.

#### 5.2.2 B&W Nested Cylinders

The B&W reactor has five concentric fuel tubes fabricated of coextruded Zircaloy-4-clad thorium-uranium metal. All fuel tubes have 0.025-in.-thick Zircaloy-4 cladding; the fuel thickness is 0.100 in., and it consists of thorium containing approximately 2% enriched uranium. Tube outer diameters range from 4.800 to 2.656 in. The coolant channel

spacings, which range from 0.078 to 0.137 in., are maintained by three spiral spacers (1/8 in. thick) attached by welding to the outer fuel cladding surface; these spacers normally have bearing surfaces only at the ends of the fuel tubes. Fuel tubes are welded into the lower end plates and are free to expand axially. The fuel elements are 48 in. long, and six elements are stacked vertically within the SAP process tube. A central moderator can of Zircaloy-2 supports the weight of the fuel elements. Fuel elements spend one-sixth of their life in each vertical position. The inlet coolant temperature is 560°F, and the outlet temperature is 750°F. In all fuel channels, the outer tube operates at the highest temperature and power level and achieves the highest burnup. The average burnup in the fuel is projected at 20,000 Mwd/T.

Techniques for fabrication of Zircaloy-clad tubes of thorium-uranium alloy fuel have been developed for tubes 1.75 in. OD by 1.05 in. ID,<sup>24</sup> and 8-in.-long specimens of such tubes are being tested at the Pacific Northwest Laboratory in high-pressure water-cooled loops. The fuel cladding temperature is about 400°F, and the maximum fuel temperature has varied between about 1080 and 860°F. The fuel volume increase has been determined by density measurements; at approximately 11,000 Mwd/T exposure, it was about 1.5% for the most highly rated specimen.<sup>25</sup> The Savannah River Laboratory has tested a 10-ft-long tube, 2.5 in. OD and 1.85 in. ID, in the HWCTR to an exposure of 3600 Mwd/T. The time-weighted average cladding surface temperature and the maximum metal temperature at the point of maximum burnup were 482 and 880°F, respectively. The fuel volume increase was about 0.8% at the region of maximum exposure and produced a 0.005-in. increase in the outside diameter and about a 0.001-in. decrease in the inside diameter.<sup>26</sup> Capsule irradiation tests<sup>27</sup> of unclad thorium-uranium alloys at Argonne National Laboratory indicate swelling of approximately 2% per atom percent burnup at temperatures below about 1000°F for burnups up to 4 at. % (approximately 40,000 Mwd/T). High fissile enrichment and short exposure times for the latter tests, however, prevent direct application of the data to HWOCR conditions.

Zircaloy-4 claddings have been found suitable for operation in organic-cooled reactors if strict control of coolant composition is maintained. Data on hydride absorption are discussed in Section 5.3.

Areas of Concern. The metal-fueled reactor represents a significant extrapolation beyond present technology, as is recognized. Nested-cylinder fuel elements have been considered for several reactor systems; however, tests of this type of fuel element have been limited to single, relatively small-diameter tubes. Problems of coolant flow control, effects of vibration on fuel cylinders, distortion as a result of nonuniform temperatures, or fuel swelling can be significant with multiple nested fuel elements. Additional research is necessary to establish that the fuel elements will operate as proposed.

Comparison of projected HWOGR operating conditions with actual fuel test conditions shows that the projected fuel burnup and the cladding surface temperatures are higher than values associated with test conditions; also, coolant pressures during test operations have been higher than proposed HWOGR pressures. However, the proposed fuel assemblies have a favorable geometry because of the relatively thin (0.100-in.) fuel thickness. Thus, proposed maximum fuel temperatures are well within the values existing during tests. Also, fuel swelling based on 3% volume change per atom percent burnup will cause less than 0.5% strain in the outer cladding of the smallest fuel element and less than 0.25% strain in the largest fuel tube.

The practicality of operating Zircaloy-4 clad tubes in organic coolant is yet to be established. Compatibility problems and hydriding rates are discussed in Section 5.3. Hydrides in zirconium reduce the ductility, but the magnitude of the effect is a function of many variables. These include the composition, orientation, and fabrication history of the alloy and the stress conditions and temperature environment. Significant factors are the orientation of the hydride platelets relative to the principal stress and the relation between platelet size and metal thickness. Thus permissible hydride concentrations cannot be specified with certainty. Early work suggests a permissible limit of 250 ppm hydrogen.

Severe embrittlement has been detected at significantly lower concentrations, but claddings with up to 400 ppm hydrogen have been found in fuel elements that operated without failure to 10,500 Mwd/T.<sup>28</sup>

Two additional factors complicate the problem of predicting permissible hydrogen concentrations for the cladding of the nested-cylinder fuel element. The texture developed in coextruded tubing is such that hydride platelets precipitate with maximum dimensions perpendicular to the stress direction<sup>29</sup> and will therefore have maximum detrimental effect. The possibility exists that more favorable textures may be developed by special fabrication procedures.<sup>30</sup> On the other hand, the fuel element geometry (thin fuel layer and large tube diameters) is such that fuel swelling is expected to cause little cladding strain, so little ductility may be required of this type of fuel element.

Conclusions. The nested-cylinder fuel element appears to be well designed, and it should be operable at the heat ratings and temperature limits proposed. It represents a reasonable extrapolation of present technology, but additional testing is required to demonstrate that projected life and burnup can be achieved under reactor operating conditions. It must be shown that fuel element distortions resulting from thermal gradients or fuel swelling do not adversely affect operation of large, closely spaced nested tubes, and also that the many factors affecting hydrogen pickup and hydride embrittlement can be controlled to insure satisfactory life for fuel elements of this geometry.

### 5.2.3 B&W Pin-Cluster Fuel Assembly

The pin-cluster fuel assembly has 66 fuel pins (0.356 in. OD, 0.020-in. wall) arranged around a hexagonal moderator can. The fuel cladding is extruded SAP 004 and has six cooling fins 0.030 in. thick and 0.065 in. high that spiral with a 1 1/2-in. pitch. Fuel rods are attached to the SAP lower base plate and are bound as a bundle around the central moderator can with circular straps of Zircaloy-2 to reduce vibration of fuel rods. Six fuel assemblies are stacked vertically in the reactor, and their weight is carried by the central moderator cans.

The fuel is Vipac (vibration-compacted) sol-gel (Th-U) $O_2$  of 88% theoretical density. A 1.81-in.-long fission-gas plenum is provided at the top of each fuel pin.

The performance of pelletized  $UO_2$  fuels in Zircaloy or stainless steel cladding in pressurized water systems has been demonstrated at heat ratings and burnups which exceed those proposed for the HWOCR. Vibratory compaction is a satisfactory method for fabricating oxide fuels into stainless steel or Zircaloy tubes, as has been demonstrated by research at several laboratories.<sup>31-34</sup> Early failures with such fuels were traced to impurities and adsorbed gases in the fuel and have been largely avoided by improvements in fabrication techniques. There is considerable experience with water-cooled fuel elements to indicate that water-logging or fuel washout from defective or failed vibration-compacted fuel elements does not cause substantial fuel losses. Fuel has been tested in the PRTR, and  $UO_2$ - $PuO_2$  at a heat rating of 15 kw/ft has achieved exposures of 10,000 Mwd/T; tests are being started in the Saxton Reactor using similar fuels with heat ratings and exposures equivalent to those proposed for the oxide-fueled HWOCR.<sup>34</sup>

The feasibility of operating  $UO_2$  fuel elements with SAP cladding has been demonstrated up to 12,000 Mwd/T in the OMRE. Four fuel elements, each 3 ft in length and containing 25 fuel rods loaded with pellets of 95% theoretical density, were operated at cladding temperatures up to 850°F. No failure occurred and postirradiation examination disclosed no bowing, deformation, or other adverse effects. Heat ratings were significantly lower (maximum central temperature of 2270°F) than proposed for the B&W fuel elements.<sup>35</sup>

SAP-clad  $UO_2$  pellet fuels have been tested at heat ratings in excess of those proposed. Some failures have occurred in long test rods at burnups of only 2400 Mwd/T. Evidence was found of sheath strain even though adequate diametral clearance was provided; some evidence of surface reaction between the SAP and the  $UO_2$  was also found at sheath temperatures in excess of 430°C.<sup>36</sup>

ORNL experience with (Th-U) $O_2$  fuels has indicated that physical changes which develop during irradiation will occur at heat ratings at

least 10% higher than with  $UO_2$  under similar conditions. Vibration-compacted (Th-U) $O_2$  rods have been operated to 20,000 Mwd/T at heat ratings of up to 26 kw/ft with no evidence of swelling and with less than 30% fission-gas release.<sup>37</sup>

Areas of Concern. The principal area of concern is that the fuel element has not yet been tested under operating conditions. The combination of SAP cladding and vibration-compacted fuel has not been tested under proposed conditions. Calculations indicate that the fission-gas pressure will not cause excessive cladding stresses if fission-gas release is no more than 15%, which appears to be a reasonable estimate. Additional data are needed to demonstrate that fuel cracking does not strain the SAP cladding excessively. It is also possible that SAP cladding cannot withstand the vibrational energy required to attain the fuel density proposed.

Conclusions. The SAP-clad vibration-compacted element shows promise for HWO CR application; however, additional data and testing are required to show that the fuel element will operate satisfactorily under the proposed conditions. Particularly, experiments must be performed to demonstrate that the effect of burnup in SAP-clad vibration-compacted fuel is not detrimental to the cladding. Also, it must be shown experimentally that SAP cladding is not adversely affected by the vibratory compaction operation.

### 5.3 Core Material Compatibility Evaluation

Satisfactory performance of a reactor depends on the ability of the core materials to retain their integrity over the operating life. It is therefore essential that the reactor materials be compatible with their environment. For this study, a brief survey was made to define the compatibility relations among the coolant, cladding, pressure tube, and fuel materials under conditions normally to be encountered in operation. Behavior of the materials under grossly abnormal conditions, such as failure of pressure or calandria tubes, is not discussed here.

### 5.3.1 Coolant-Cladding Compatibility

Compatibility between the coolant and the fuel-element cladding in its operating environment is of major importance. The maximum cladding temperature for all the reactors is specified as 850°F, although a given fuel element will experience this maximum temperature only a fraction of its core residence time. Residence times of the fuel elements are about 700 days for the AI-CE SAP-clad UC fuel, 600 days for the B&W metal fuel, and about 400 days for the B&W oxide fuel.

Coolant-SAP Compatibility. SAP is the cladding material for the AI-CE fuel and for the B&W oxide fuel; it is also proposed as the process tube material for both reactors. Considerable data from capsule tests and from reactor and loop experiments have established that aluminum claddings operate satisfactorily with organic coolants at temperatures up to which pyrolysis of the coolant becomes excessive.<sup>13,35,38-40</sup> ORGEL (Euratom organic-cooled reactor) investigators have shown that corrosion effects are negligible (order of mg/dm<sup>2</sup> per 2000 hr, where 1 mg/dm<sup>2</sup> is equivalent to  $1.5 \times 10^{-6}$  in.) when water concentrations are less than approximately 1000 ppm. Water vapor contents of several thousand ppm can cause severe intergranular attack, but such high water concentrations should not be encountered.<sup>39</sup>

Coolant-Zircaloy Compatibility. Zircaloy-4 is proposed as cladding for the B&W thorium-uranium metal fuel. The performance of zirconium alloys in organic coolants has been under investigation in Canada since early 1961, and the basic compatibility of the materials has been established. Of concern is the rate of hydrogen pickup by the zirconium and the effect of the absorbed hydrides on the physical properties and life of the cladding.

Available Canadian data on hydriding rates have been summarized by Sawatzky and others.<sup>13,41,42</sup> Hydriding rates are quite sensitive to several variables, in particular the coolant composition and the condition of the metal surface. Several important effects are listed below.

1. Hydriding is inhibited by a thin oxide film on the metal surface, such as that formed by air oxidation or steam autoclaving. It is most

effective if formed at temperatures near coolant operating temperatures. Finger prints or scratches destroy the effectiveness of the film.

2. Chlorides as a coolant impurity have a marked detrimental effect and increase the hydriding rate.

3. Water vapor in the coolant at levels of approximately 60 to 200 ppm appears to reduce the hydriding rate, particularly if excessive chloride is present in the coolant.

4. The hydriding rate seems to be enhanced by neutron irradiation.<sup>41</sup> Based on scanty data, the enhancement factor appears to be under a value of 2 for a thermal-neutron flux of  $4 \times 10^{13}$  neutrons/cm<sup>2</sup>.sec.

5. Based on a 5000-hr test, hydriding rates of Zircaloy-4 in organic coolant at about 716°F are only slightly greater than those obtained with water coolant at 680°F. The data suggest a hydriding rate of about  $5 \times 10^{-3}$  μg/cm<sup>2</sup>.hr in organic coolant at 716°F; at 608°F the rate is reduced to about one-tenth<sup>41</sup> of the above value. Within the scatter band, presumably caused by variations in coolant purity, the hydrogen pickup by Zircaloy-4 is approximately linear with exposure time.

6. Hydriding rates of Zr-2.5% Nb are about one-fourth those for Zircaloy-4, which are about one-half those for Zircaloy-2.<sup>41</sup>

The possibility of using fins as hydride sinks to which absorbed hydrogen will diffuse because of their lower operating temperature is also suggested by the Canadian data.<sup>13,42</sup> Hydrogen contents of Zircaloy-2 wire wrap ranged up to 9000 ppm with adjacent Zircaloy-2 cladding hydrogen contents in the range of 200 to 550 ppm.

Canadian investigators conclude that zirconium alloys show definite promise for use as cladding or hot process tubes in organic-cooled systems but that further research is necessary to define operational limits that will assure satisfactory life of reactor components.<sup>42</sup>

### 5.3.2 Coolant-Fuel Compatibility

It is to be expected that an occasional fuel element failure will occur in the operating reactor. The effects of such failures will be less serious with respect to reactor operation if good compatibility exists between the fuel and the coolant. If significant reactions occur,

entrance of coolant through tiny cladding flaws can cause cladding deformations that will rapidly increase the size of the hole. Similarly, if reactions are negligible, longer operation of failed fuel elements can be permitted before it is necessary to discharge them.

Coolant-UC Compatibility. The stability of UC in organics has been demonstrated in experiments investigating reactions of unclad uranium metal with organics.<sup>38</sup> In these tests, reactions at 750°F were limited to slight surface attack (<3 mg/cm<sup>2</sup> per month, <6 × 10<sup>-2</sup> mils per month) for 4500-hr tests. Much more rapid corrosion can occur with hydrogen overpressure. The threshold hydrogen pressure for the metal-organic reaction is temperature dependent; it is near 1 atm at 572°F and about 15 atm at 752°F. UC forms as the reaction product at high hydrogen pressures. The data obtained suggest that UH<sub>3</sub> forms by reaction of U with the H<sub>2</sub> and that the UH<sub>3</sub> then reacts with the organic to form UC. Thus, stability of UC in the organic coolant seems assured and reaction between UC and coolant will be negligible.

Coolant-ThO<sub>2</sub>-UO<sub>2</sub> Compatibility. No data were found on the compatibility between organic coolants and (Th-U)O<sub>2</sub> fuels. Little reaction is expected, since neither ThO<sub>2</sub> nor UO<sub>2</sub> is reduced by organic decomposition products. The excellent compatibility of UO<sub>2</sub> fuel with organic coolant is indicated by results of experiments described by Parkins of Atomics International.<sup>43</sup> In these tests, defected SAP-clad UO<sub>2</sub> elements were tested by temperature cycling to force coolant through the defected SAP. No evidence of chemical reaction was found. A three-week test in a reactor caused the release of some gaseous fission products, but no fuel particles escaped into the coolant. Thus, no compatibility problems appear evident between coolant and oxide fuels.

Coolant-Thorium Metal Compatibility. Limited data are available which indicate that thorium metal has good compatibility with organic coolants.<sup>40</sup> However, some reactions can occur from oxide or chloride impurities, and significant hydrogen overpressures can lead to hydriding. Static tests gave weight changes equivalent to less than 1 mil of metal consumed per month at 900°F and appreciably less corrosion than that at 800°F. Comparative data indicate thorium to be slightly less resistant

to attack than uranium metal, for which there are considerable data to indicate excellent compatibility with organic coolants. Experiments with defected aluminum-clad uranium slugs (1/16-in. hole through the cladding) showed no attack until significant hydrogen pressures were developed. Parkins<sup>43</sup> described a failure of a U-3.5% Mo fuel element in the OMRE in which coolant flow restriction led to overheating and subsequent melting of some of the fuel elements. Examination disclosed no formation of UC, and there was no evidence of chemical reaction between the organic coolant and the melted uranium metal. Only volatile fission products were detected in the coolant.

Compatibility of Coolant with Cladding Failures. Occurrence of a cladding failure permits coolant to enter a region of essentially zero coolant flow. Decomposition of the stagnant organic coolant within the defect and in any adjacent clearance space yields a porous mass that can be penetrated by additional coolant. Continuation of the process can yield a slowly growing solidified mass that leads to interference with coolant flow. This growth process should not occur with metallic fuel elements that have bonded claddings. However, with the nonbonded fuel pins, coolant leakage into the element combined with thermal and radiation damage to the stagnant coolant should be avoided. If pin cladding defects occur during operation, the defective fuel elements should be removed from the reactor immediately. In water-cooled reactors operation with defective elements can be tolerated. Experiments with defective elements in organic-cooled loops will be required to evaluate the magnitude of this problem.

### 5.3.3 Cladding-Fuel Compatibility

It is necessary for satisfactory fuel element operation that reactions between cladding and fuel not destroy cladding integrity during the life of the fuel element. Chemical reactivities of the cladding-fuel combinations are considered in the following sections. Mechanical effects were considered in Section 5.2.

SAP-UC. Data on compatibility between UC and SAP indicate that this combination is more reactive than UO<sub>2</sub> and aluminum. Early work by ORNL

established that in powder compacts, UC reacted with aluminum in 10 hr at a temperature of 1148°F and that UC<sub>2</sub> was much less reactive than UC.<sup>44</sup> Danish investigators<sup>45</sup> found slight reaction between UC and SAP in 7300 hr at 842°F and marked reaction for the same time at 977°F. They found that the reaction could be prevented by anodizing the SAP prior to the test; with anodized specimens there was no reaction after 9200 hr at 1112°F. Atomics International found no reaction after 12,000 hr at 850°F and only slight reaction after 12,000 hr at 950°F.<sup>23</sup>

Irradiation test results from the X-721 loop experiments showed little or no reaction between SAP and UC operated for 3500 hr at a 740 to 840°F cladding temperature.<sup>18</sup>

The fuel material is specified to be hyperstoichiometric uranium carbide. It is desirable that the carbon content of the fuel not drop below the stoichiometric composition in order to avoid formation of uranium metal at the grain boundaries of the UC. Elemental uranium diffuses rapidly into aluminum at temperatures above approximately 572°F, and cladding penetration leads to rapid failure in oxidizing coolants. Although no reaction would occur between uranium and the organic coolant, the defective element might lead to operating problems, as discussed above in Section 5.3.2.

On the basis of the compatibility data, it appears that SAP and hyperstoichiometric UC will be suitable for use in the HWOCR environment. Since the oxide surface on aluminum inhibits the reaction between UC and SAP, potential destruction of the oxide film under dynamic conditions of HWOCR operation must be considered. Irradiation tests of prototype fuel rods will be required to demonstrate that fuel chipping and abrasion do not accelerate reactions and limit fuel element life.

SAP-ThO<sub>2</sub>. The proposed B&W oxide fuel consists of vibration-compacted (Th-U)O<sub>2</sub> fuel in SAP cladding. No data on compatibility between SAP or aluminum and ThO<sub>2</sub> have been found, but thermodynamic considerations suggest that the chemical reactivity will be less than with UO<sub>2</sub>.

A study at ORNL of pressed compacts of UO<sub>2</sub> and aluminum powder (-100 +325 mesh) showed extensive reaction at 1112°F and some reaction at 932°F.<sup>46</sup> The reaction is favored by intimate contact and very fine

particle size of the  $UO_2$ , and the data suggest that the formation of reaction products inhibits the reaction.

An investigation at Atomics International with pellets of  $UO_2$  placed between SAP and aluminum pellets showed no reaction in 5000 hr at  $1000^\circ F$ .<sup>35</sup> Danish investigators found no reaction between  $UO_2$  and SAP in 14,300 hr at  $850^\circ F$  or in 8500 hr at  $977^\circ F$ . They found no reaction after 1000 hr at  $1100^\circ F$  but marked reaction after 8000 hr.

These data may be compared with those from experiments with  $UO_2$  and zirconium in which uranium penetrated about 3 mils into zirconium cladding in 9500 hr at  $1100^\circ F$ . With Zr- $UO_2$ , reaction rates were extremely slow at 750 and  $950^\circ F$ .<sup>47</sup> In a more recent study of the Zr- $UO_2$  system, it was concluded that the combination would be limited to  $1290^\circ F$  for a two-year life.

Irradiation tests on  $UO_2$  with SAP or aluminum cladding have been made by several investigators. Atomics International obtained satisfactory performance at exposures up to 12,000 Mwd/T of uranium in fuel elements tested in OMRE with peak cladding surface temperatures of  $850^\circ F$ .<sup>18</sup> Canadian investigators studied SAP-clad  $UO_2$  fuels and found some reactions at temperatures above  $806^\circ F$ .<sup>13</sup> Satisfactory performance to low burnup was reported for elements operating at a maximum sheath temperature of  $932^\circ F$ , and SAP-clad  $UO_2$  fuel is specified as the initial fuel for the WR-1 organic-cooled reactor.

Zircaloy-4-Thorium Metal. Limited data are available on the compatibility of the Zircaloy-4 cladding and thorium metal fuel tubes specified for the B&W nested-cylinder concept. The zirconium cladding is metallurgically bonded to the thorium metal, and some metal diffusion occurs. Short-time heat treating experiments at Hanford<sup>24</sup> indicated the major portion of the bond to be 70.6 wt % zirconium. Bond thicknesses as a function of heat treatment, based on Hanford and ORNL data,<sup>48</sup> are indicated in Table 5.4.

Valid extrapolations to the much longer times and lower temperatures of interest for the B&W reactor cannot be made for these data. However, it seems likely that satisfactory performance will be obtained, particularly in view of the low reactivity between the thorium metal and the

Table 5.4. Bond Thickness Between Zircaloy-4  
and Thorium Metal as a Function of  
Heat-Treating Temperature

Treating Temperature (°F)	Diffusion Zone Thickness (mils) for Indicated Heat Treatment Time			
	1/2 hr	1 hr	3 hr	4 hr
1652	2.0			
1472	0.6	1.0	1.6	
1382		0.6	1.1	
1292			0.15	0.2 <sup>a</sup>
1202				(b)
1112				(c)

<sup>a</sup>Data from Ref. 48.

<sup>b</sup>Irregular diffusion layer.

<sup>c</sup>No apparent diffusion.

coolant. However, additional data on the performance of such fuel elements are required to establish that significant changes in volume or cladding ductility do not develop. Data from recent Hanford irradiation tests may be enlightening when they become available, but the maximum operating temperatures are about 180°F less than proposed for the B&W reactor.

#### 5.3.4 Conclusions

It appears that the only coolant compatibility problem for these reactor systems is that of hydriding of the Zircaloy-4 cladding in the reactor with thorium-uranium metal fuel. Even for that core, use of Zircaloy-4 appears feasible; however, additional development work is necessary. Although reactions can occur between the various fuel and cladding components it does not appear that such reactions will proceed to the point where serious cladding failures result. If cladding failures occur in the unbonded (pin type) fuel elements, the defective elements should be removed from the reactor. Additional test data under reactor operating conditions will, of course, be required to verify this evaluation of present information.

## 5.4 Core Design Criteria Evaluation

The ability to build and operate the reactor as proposed will depend largely on the extent to which the reactor operating conditions do not lead to failure of the materials used. Of particular concern are the mechanical properties of SAP, since SAP is a relatively new material for which specifications and design stresses have not yet been developed.

### 5.4.1 Mechanical Properties of SAP

The term SAP is a general designation for alloys of aluminum metal and aluminum oxide in which the oxide content ranges between about 6 and 14%. The strength of the alloy increases with oxide content while the ductility decreases. Mechanical properties have been reported by many investigators,<sup>13,45,49-51</sup> and much of the information has been compiled into a draft of a SAP Materials Handbook edited by Harlow.<sup>52</sup>

SAP has good nuclear properties and good mechanical strength at high temperatures. Its limitations are that (1) statistical uncertainties in SAP property data are considerable, (2) it has low ductility at high temperatures and low strain rates, particularly under creep conditions, and (3) it is an anisotropic material, with strength and ductility in the transverse or circumferential direction of tubes being significantly less (about 30% less for stress-rupture data) than in the axial direction. Furthermore, results of a few notched-specimen stress-rupture tests indicate that notches seriously reduce rupture strength.

The use of SAP in organic-cooled reactors is being currently investigated by research at ORNL and AI. A principal objective at ORNL is to investigate and develop technology to produce material with consistent properties. Data have indicated three main reasons for reported scatter in property data. First, differences in fabrication techniques can affect properties, and in the past suppliers have improved their processes without changing final product designation. Second, SAP properties are particularly sensitive to variables in testing techniques. Both high-temperature strength and elongation are affected by strain rate. Inconstant test temperature and mechanical alignment during testing are also more

critical with SAP than with usual engineering material. Finally, unrecognized flaws in the test material can cause significant variations in measured properties. Surface scratches and oxide stringers or inclusions can increase stress at local regions. Anisotropy effects may also be significant in comparing mechanical property data obtained on the same material fabricated in different shapes.

It is probable that strict attention to fabrication and test variables will reduce the variations in property data for SAP.

Ductility of SAP. The low ductility of SAP at low strain rates is a serious limitation. Work at ORNL has shown that fracture ductility is an important function of strain rate, but strain rates in the range of 1% per hour or less are sufficient to limit total elongation to 1% or less. The ORNL SAP development program is not directed toward improving the ductility of SAP, and it is probable that SAP components in the HWOCR must be designed on the basis of a maximum of about 0.5% creep strain.

It should be pointed out that the low ductility and notch sensitivity of SAP are not indications of brittleness. SAP actually fractures in a ductile manner. However, because the metal has low capacity for work hardening at high temperatures, most of the deformation is confined to the local area of initial yielding, so low values of elongation are obtained. Because of its greater ductility at higher strain rates, SAP would exhibit greater deformation under transient conditions than in steady-state creep. The effects of transient stresses on material exposed to long-time creep must be determined before the effect of low ductility on performance of SAP components in organic-cooled reactors can be evaluated.

Strength of SAP. AI-CE design stresses for SAP pressure tubes were taken from plots based on the Larson-Miller correlation of stress-rupture data; values of 6100 psi at the 595°F inlet temperature and 4500 psi at the 750°F outlet temperature were derived. However, the Larson-Miller correlation has been shown to have serious limitations.<sup>53</sup> A simple plot of available hoop stress-rupture data based on tests of 100 hr or more is shown in Fig. 5.12. Because so few data were available, they were supplemented by values of 70% of the axial stress-rupture data obtained in long-time tests. Based on the ASTM code criterion of either 60% of

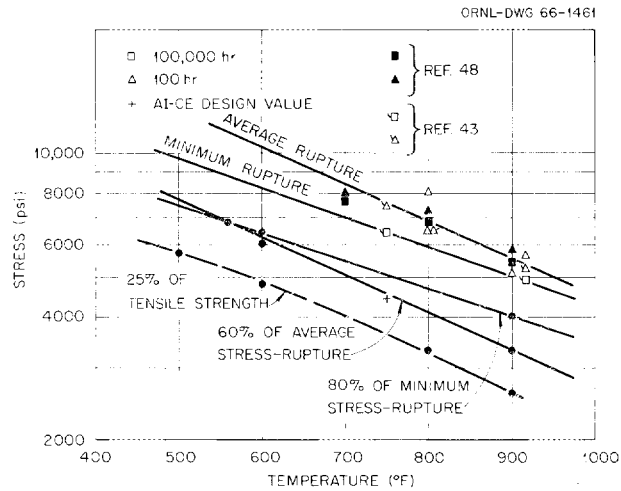


Fig. 5.12. Design Stress for SAP 895; Transverse Rupture Strength.

the average values or 80% of the minimum values and the stress-rupture data given in Fig. 5.12, the AI-CE design strength values appear to be reasonable.

The ASME Code for Unfired Pressure Vessels (Section 5) specifies that the design stresses should not exceed one-fourth of the tensile strength at the operating temperatures. Values of one-fourth the tensile strength from longitudinal and transverse directions of extruded bars, as reported by Boxall and Fleming,<sup>49</sup> are also plotted on Fig. 5.12. These values are significantly below the design stress determined from stress-rupture data and suggest limiting design values of about 4900 psi at 595°F and 3500 psi at 750°F if one-fourth of the tensile strength is to be the criterion.

The ASME nuclear code (Section 3) specifies design stresses of one-third the tensile strength, but this applies to ferrous materials. Similar code specifications have been written for isolated nonferrous materials, but these have physical properties much different than those of SAP. To date there are no ASME nuclear code design criteria for the use of SAP materials, since there is insufficient information and experience.

We do not know what design criteria should apply relative to use of SAP. Those specified by AI-CE may indeed be satisfactory and are considered to be feasible. For pressure tubes, creep-stress data are most important; the additional restriction imposed by limiting stresses to

one-fourth the tensile strength at the operating temperature may not be justified for materials with the low creep rate of SAP. On the other hand, the limited experience with SAP does not appear to justify any relaxation of established criteria. Much additional material and component testing is required before design criteria can be satisfactorily established.

#### 5.4.2 Radiation Effects on SAP

Effects of neutron irradiation on the strength and tensile ductility of SAP alloys were investigated to a limited extent by Danish workers.<sup>45</sup> Test specimens exposed to an integrated neutron flux of  $4.5 \times 10^{20}$  neutrons/cm<sup>2</sup> ( $E > 2.9$  Mev) showed reduced ductility and increased strength when irradiated at 104°F and tested at room temperature. Specimens similarly tested after irradiation at 527°F showed no effects from irradiation. Apparently irradiation damage effects are annealed at 527°F, but additional information at higher exposure and temperatures is needed.

#### 5.4.3 SAP Process Tube Design

The maximum AI-CE process tube stresses are the hoop stress of 6020 psi at the 595°F inlet temperature and the 3890-psi axial stress at the 750°F outlet temperature. These stresses are within the design specifications determined by the stress-rupture criterion or by values based on one-third the ultimate strength, but they are above those determined by one-fourth the tensile strength.

The B&W reactor has 5.0-in.-ID 0.093-in.-wall process tubes. Hoop stresses at the 560°F inlet temperature are about 8170 psi and 7700 psi for the nested-cylinder and pin-cluster designs, respectively. The stresses at the 750°F outlet coolant temperature are correspondingly about 3580 and 3500 psi. The stresses at the inlet end are too high, and it appears that the process tube thickness will have to be increased by about 25% to reduce stresses to values consistent with AI-CE values.

#### 5.4.4 SAP Fuel-Cladding Design

SAP cladding is used for the AI-CE fuel and for the B&W vibration-compacted-oxide pin-cluster fuel element. The AI-CE fuel cladding is

subjected to fluid pressure and hydraulic forces and the weight of the fuel elements above it. An analysis of the stresses developed agrees essentially with that of the proponents, and it is concluded that the strength of SAP is adequate for this application.

SAP cladding for the B&W reactor fuel does not support the fuel weight. Stresses are thus determined by coolant or fission-gas pressure. The strength of SAP appears to be adequate in this application. The feasibility of using vibratory compaction with the brittle SAP sheaths has been demonstrated for 4-ft-long elements; however, longer elements have failed during loading.

#### 5.4.5 Zircaloy Calandria Tube Design

Zircaloy calandria tubes are used in these reactor concepts. Ordinarily these tubes are subjected to slight loads from the static head of the moderator, but axial stresses from weight loads and thermal stresses are also involved. Calculations cited by AI-CE for a similar reactor suggest that stresses will be well within the design limit of 13,000 psi for Zircaloy-2.

Zircaloy pressure tubes are used in the NPD, CVTR, and CANDU reactors, and successful performance has been established in pressurized-water reactors. The CANDU tubes are based on a design stress of 15,900 psi at 570°F and the CVTR tubes on 18,000 psi at 250°F.<sup>54</sup>

Rupture of a process tube would allow the hot coolant to contact the calandria tube and subject it to the coolant pressure and to additional thermal stresses. Calculations indicate that if coolant flow through a failed process tube is sufficient to maintain the initial temperature differential across the calandria tube wall, the thermal stress will be approximately 13,000 psi and the hoop stress will be an additional 5000 psi. The possibility that a SAP pressure tube might rupture with sufficient violence to cause failure of the Zircaloy calandria tube appears remote.

#### 5.4.6 Zircaloy Process Tubes

The feasibility of using Zircaloy process tubes in organic-cooled reactors is being considered in Canada,<sup>36,49,50</sup> and some Zircaloy-4

process tubes are to be used in the WR-1 reactor. Of principal concern are the hydrogen-absorption rate and the effect of hydrogen on the ductility of the metal. These factors were discussed with respect to the Zircaloy-clad thorium-metal fuel tubes in Sections 5.3.1 and 5.2.2.

In Canadian experiments Zircaloy-4 process tubes were used in an organic-cooled loop. No excessive hydriding occurred in 5000 hr of irradiation at temperatures which ranged from 626 to 752°F. There is considerable experimental evidence to show that control of coolant composition is a major factor affecting hydriding rates. For instance, chloride impurities accelerate the adsorption rate, while the presence of small amounts of water decreases hydriding, apparently because it assists in maintenance of a  $ZrO_2$  barrier layer. Further reductions in hydriding rates are considered feasible either by applying a metal barrier to the surface of the Zircaloy or by developing an improved zirconium-base alloy. Aluminum coatings have been found to be an effective hydrogen barrier, probably due to the presence of a thin  $Al_2O_3$  surface layer.<sup>41</sup> Initial tests indicated that aluminum-clad Zircaloy surfaces were damaged by thermal cycling, but thinner cladding may be more stable. A considerable development effort would be needed to achieve a successful structure of this type. Zirconium-2.5% niobium has been found to hydride at about one-fourth the rate for Zircaloy-4 and therefore offers an attractive alternate material. Current work to control textures of Zircaloy alloys so that hydride platelets form parallel to direction of stress may relax the necessity for low hydriding rates.<sup>13</sup> Thus, although the practical use of Zircaloy process tubes for organic-cooled reactors is yet to be established, several potential methods appear available for improving the performance of Zircaloy tubes under HWOCR conditions.

#### 5.4.7 Conclusions

On the basis of the limited data available, it is concluded that the use of SAP for process tubes as proposed in the AI-CE reactor is feasible; the B&W reactor will require thicker process tubes than specified. The use of SAP fuel claddings appears feasible for both designs. However, additional information will be required before the effect of low SAP ductility on design criteria can be adequately evaluated.

The process tube is a very important part of the reactor core, since it separates the organic coolant from the Zircaloy-2 calandria tube. Although the process tube can be replaced, it would be necessary to shut down the reactor during replacement. Thus, it is most important for the process tube to have a long life. Although the present designs appear feasible, it is not certain that a material having the low ductility of SAP will have sufficient life under the rigors of reactor operation. Thus, it appears advisable that, in addition to the SAP development program, an extensive backup program be carried out relative to the development of satisfactory zirconium-alloy process tubes.

The use of Zircaloy for the calandria tube appears to be feasible. Also, as discussed in Section 5.3, the use of Zircaloy as cladding for the metal fuel elements appears feasible. However, much more information on the effects and control of hydriding is needed.

### 5.5 Organic Coolant Evaluation

Of the many types of organic compounds examined in the past as potential organic coolants, the aromatic hydrocarbons are the most stable toward heat and radiation. The choice of reactor coolant from this general class of compounds was made on the basis of economic considerations in conjunction with desirable physical and chemical properties. The terphenyl isomers have low vapor pressures compared with water and can operate at relatively high temperatures; they are also practically inert or noncorrosive toward standard construction materials and various types of reactor fuels. Thus, it is possible to use carbon steel for pipes, valves, and other coolant system components. The organic fluid is known to acquire little induced activity from reactor irradiation;<sup>55</sup> therefore, little or no shielding is required for the primary coolant system, and maintenance can be accomplished directly.

A commercially available mixture of the terphenyl isomers, Santowax OM,\* is charged to the coolant system initially. However, under the effects of reactor heat and radiation, high-boiling products (HB) are

---

\*Monsanto Chemical Company trade name.

formed. Through purification, an equilibrium concentration of HB's is maintained. AI-CE has estimated that a value of 10 wt % HB provides the best compromise between associated physical and heat transfer properties, rate of HB formation, and cost of purification; we concur that this is a reasonable value.

### 5.5.1 Physical Properties

Compositions of the reactor coolant at equilibrium and of the HB are characterized in Table 5.5, as presented by AI-CE.<sup>23</sup> Estimated values for the physical properties of the coolant are given in Table 5.6 that

Table 5.5. Approximate Composition of Organic Coolant and High-Boiler Product

	Content (%)
Santowax OM + 10% HB	
Low boilers	<0.03
Biphenyl	2
Terphenyls	77
Intermediate boilers	11
High boilers	10
High-boiler product composition by molecular weight range	
226-268	6
269-344	6
345-420	10
421-496	73
497-572	1
573-648	<1
>648	3
High-boiler product composition by compound distribution	
Polyphenyls	75
Triphenylene	15
Phenanthrenes	2
Olefins	3
Other types	5

Table 5.6. Properties of Organic Coolant Based on Data for Santowax OMP

Property	Value of Property at Indicated Temperature <sup>a</sup>			
	500°F	600°F	700°F	800°F
Density, g/cm <sup>3</sup>				
With no HB	0.917	0.870	0.824	0.776
With 10% HB	0.930	0.885	0.839	0.794
With 20% HB	0.944	0.900	0.855	0.810
With 30% HB	0.958	0.915	0.871	0.829
Viscosity, cp				
With no HB	0.54	0.37	0.26	0.20
With 10% HB	0.66	0.43	0.30	0.23
With 20% HB	0.79	0.51	0.35	0.26
With 30% HB	0.98	0.63	0.43	0.31
Specific heat with 0 to 30% HB, <sup>b</sup> Btu/lb.°F	0.534	0.566	0.599	0.631
Thermal conductivity, Btu/hr.ft.°F				
With no HB	0.069	0.066	0.062	0.059
With 10% HB	0.071	0.068	0.065	0.061
With 20% HB	0.073	0.070	0.067	0.064
With 30% HB	0.075	0.072	0.069	0.067
Vapor pressure, psia				
With no HB	2	6	16	40
With 14% HB <sup>c</sup>		7	20	50
With 37% HB <sup>c</sup>		17	39	89

<sup>a</sup>Melting point of organic with 10% HB is 178°F.

<sup>b</sup>Decrease at 30% HB is <2.0%.

<sup>c</sup>Estimated from OMRE coolant data.

are based on data for a similar coolant, Santowax OMP, which has had considerable study. Additional physical property data are given in Appendix C; as indicated there the coolant physical property values measured and used by various groups have led to nearly the same heat transfer coefficients for high-boiler concentrations of 10%.

At present no organic-cooled reactor has operated with a catalytic hydrocracker for recovery of coolant from the HB; also, the products fed to the coolant system from the hydrocracking units could have a marked influence on the equilibrium composition of the reactor coolant and the HB composition. It is this equilibrium composition that will establish the properties of the coolant. Experimental results reported by Gardner<sup>56</sup> indicate that the equilibrium concentration of biphenyl in the coolant will be about 12%, which is significantly above the 2% estimate by AI-CE when a hydrocracker unit is utilized (see Chapt. 6, Sect. 6.7 this report). Under these circumstances the vapor pressure will be greater than would be the case with lower biphenyl content and results in a calculated DNB ratio of about 2.5, based on Eq. (5). Lowering the maximum coolant temperature to 800°F (which decreases the outlet coolant temperature to about 700°F or lower) results in a calculated DNB ratio of 3.15.

The presence of biphenyl and alkyl biphenyls in the reactor coolant at the expected levels (about 12% biphenyls and 5% alkyl biphenyls) will decrease the density of the coolant about 2% and the viscosity about 8.5%, while the thermal conductivity and specific heat will remain essentially the same; the heat transfer coefficient will increase about 2%. Thus, the presence of the biphenyls will tend to improve heat transfer characteristics.

#### 5.5.2 Thermal and Radiolytic Stability

The pyrolytic damage to terphenyl mixtures is minor at a temperature of 750°F, being about 0.5 wt % per day.<sup>57</sup> However, Gardner<sup>56</sup> found that the rate of HB formation in reclaimed coolant increased more than four-fold upon going from 750 to 825°F; about 7 wt % HB formed at 750°F after two days, while 31 wt % HB formed at 825°F in the same time interval. Also, early work on pyrolysis and radiolysis indicates that the combination of radiation and temperature at temperatures above some "threshold" value leads to a marked increase in radiation damage.<sup>58</sup> This threshold temperature is usually below that associated with significant damage due to pyrolysis alone. More recent information is given by MIT results<sup>59</sup> obtained from irradiations of Santowax WR in the central fuel position

of the MIT research reactor. Figure 5.13 gives values for terphenyl disappearance as a function of irradiation temperature and coolant composition and shows the marked increase in the rate of degradation at temperatures above 700°F; the results indicate also that temperatures above 800°F in combination with high radiation levels lead to very high coolant-degradation rates. Since the HWOCR design conditions permit fuel element surface temperatures as high as 850°F, there will be significant destruction of the coolant in contact with such surfaces. Although little information is available concerning the influence of coolant damage rate on coolant fouling-film formation, it appears reasonable that surface fouling tends to increase with increasing fuel element surface temperature, with the degree of fouling influenced by the coolant purity and flow rate. Also, coolant damage will influence the coolant makeup rate.

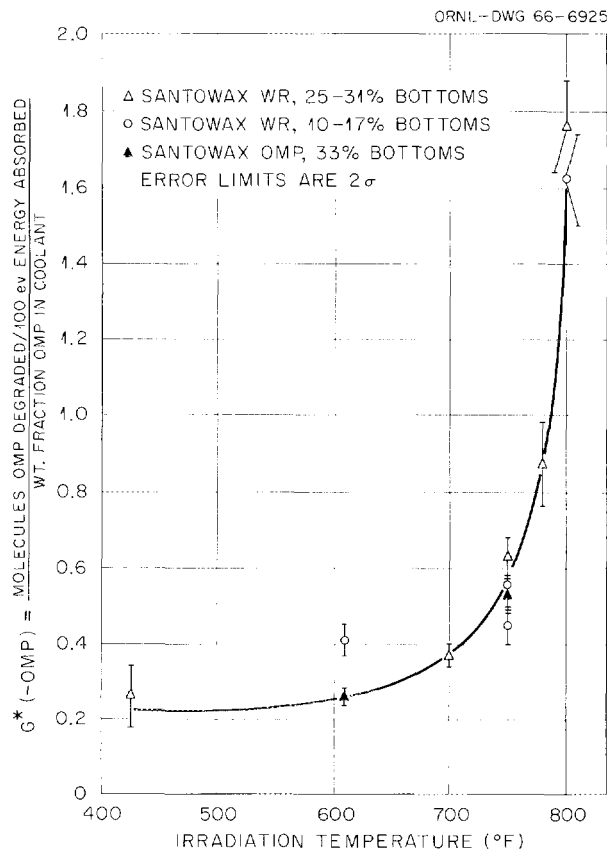


Fig. 5.13. Effect of Temperature on Degradation of Terphenyl Coolants in MIT Loop Irradiations (Taken from Ref. 59).

Coolant damage, as calculated by AI-CE, was based on

$$G = f_n G_n + f_\gamma G_\gamma,$$

where

$G$  = molecules of terphenyl decomposed per 100 ev of energy absorbed from the total radiation field,

$f_n = 0.77 = 77\%$  absorption of radiation energy due to neutrons,

$f_\gamma = 0.23 = 23\%$  absorption of radiation energy due to gammas,

$G_\gamma$  = molecules of terphenyl decomposed per 100 ev of energy absorbed from gammas,

$G_n$  = molecules of terphenyl decomposed per 100 ev of energy absorbed from fast neutrons.

The literature<sup>60-62</sup> shows general agreement on the value of  $0.20 \pm 0.01$  for the  $G_\gamma$  of unirradiated Santowax at temperatures between 600 and 700°F. The ratio  $G_n/G_\gamma$  at these temperatures is no more than 4 to 5, so the value of  $G_n$  is approximately 0.9 around 700°F. As the HB concentration builds up, the rate of terphenyl degradation decreases because of the decreased terphenyl concentration. There is some evidence that second-order kinetics are associated with the radiolysis degradation of terphenyl;<sup>59</sup> on this basis, the  $G$  values for terphenyl degradation would decrease with increasing HB content, as indicated in Table 5.7. To date, however, there

Table 5.7. Calculated  $G$  Values for HWOCR Coolant<sup>a</sup>

Terphenyl Content (%)	Average Core Temperature								
	600°F			650°F			700°F		
	$G_\gamma$	$G_n$	$G$	$G_\gamma$	$G_n$	$G$	$G_\gamma$	$G_n$	$G$
100	0.19	0.83	0.68	0.19	0.86	0.71	0.20	0.90	0.74
90	0.15	0.68	0.56	0.16	0.70	0.58	0.16	0.73	0.60
80	0.12	0.53	0.44	0.12	0.55	0.45	0.13	0.58	0.48
70	0.091	0.41	0.34	0.094	0.42	0.35	0.098	0.44	0.36

<sup>a</sup>AI-CE values based on second-order kinetics for radiolysis.

is no conclusive evidence that these calculated G values can be applied directly to HWOCR conditions.

In-pile irradiations<sup>63, 64</sup> of biphenyl and the terphenyls indicate that G for biphenyl is 1.5 to times the same quantity for Santowax R or the terphenyls; however, the rate of HB formation from diphenyl degradation on a weight basis would be about the same as for the terphenyls. Also, the degradation associated with the coolant at temperatures above about 800°F will be disproportionately high, but the volume of such coolant is low.

Based on 100% load factor, the AI-CE calculations indicated that about 10 Mw of thermal energy was absorbed in the coolant due to fast-neutron slowing down, while the corresponding value for gamma energy absorption was about 3 Mw(th). The results of our calculations agreed with the energy absorption due to neutron slowing down [10 Mw(th) at full power], but we estimate that about 6 Mw(th) of gamma energy is absorbed by the coolant. Because of the complex geometry involved, it is difficult to perform an exact calculation for the energy deposition in the coolant. We believe the above sets of values are in reasonable agreement, particularly since the influence of gamma absorption is relatively small and the economic difference associated with the two sets of values is insignificant. In what follows we will consider that 10 Mw(th) is deposited in the coolant due to neutron slowing down and that 4.5 Mw(th) of gamma energy is absorbed in the coolant when the reactor is operating at full power.

Based on their reactor conditions, AI-CE calculated a full-power coolant decomposition rate of 1450 lb/hr and a pyrolytic decomposition rate of about 30 lb/hr. For the same conditions, we estimate the terphenyl radiolytic decomposition rate to be about 1600 lb/hr and the pyrolytic decomposition rate to be about 250 lb/hr, based on an outlet coolant temperature of 750°F. However, considering fouling effects and fuel surface temperature limitations, we estimate that the maximum coolant outlet temperature will be about 700°F. For this outlet temperature and the energy deposition rates given previously, we estimate that the terphenyl radiolytic decomposition rate will be about 1430 lb/hr, and

that the pyrolytic decomposition rate will be about 70 lb/hr. These latter values are the ones used in our evaluation.

Accurate measurements of radiation damage to coolant have been performed primarily in loops having no internal fuel elements; thus, the neutron energy spectrum in these tests did not necessarily represent the spectrum that would exist in an HWO CR fuel channel. Also, temperature and flow distributions need to be representative of reactor values. Experimental measurements of coolant degradation rates need to be performed under HWO CR conditions before the accuracy of the above values can be determined.

### 5.5.3 Corrosion and Fouling

The low-corrosion characteristics of terphenyls in contact with a number of structural materials have been demonstrated repeatedly. No corrosion or mass transfer<sup>65</sup> was found in tilting-furnace capsules in which specimens of type 304 stainless steel, mild steel, carbon steel, 2S aluminum, aluminum-288, and SAP were exposed to o- and p-terphenyl up to 1000 hr at temperatures as high as 770°F. An ORGEL investigator<sup>66</sup> reports that different types of SAP, carbon steel, and stainless steel tested statically between 750 and 845°F showed good resistance to pure terphenyl mixtures during exposure times of 24 to 2000 hr. In-pile tests<sup>67</sup> with a number of different types of steels and aluminum showed that they were all essentially inert or unreactive to the virgin organic coolants. The presence of water at the 400 ppm level in the coolant seemed to have no corrosive effect<sup>68</sup> on any of these materials, except aluminum alloys; polyphenyls with 0.1 to 0.2% (1000 to 2000 ppm) water corroded aluminum seriously. The presence of oxygen in irradiated coolant produced a more pronounced corrosive action than did water. However, 18-8 stainless steel continued to show good corrosion resistance regardless of the water and oxygen content in the environment. In no cases did irradiation appear to influence the corrosion rate. However, the presence of chlorine-containing compounds in the organic coolant enhanced the attack on all steels. Additional information on basic compatibility is given in Sections 5.3 and 5.4.6.

The situation with regard to fuel element fouling under proposed HWOCR conditions does not appear as favorable as above. In one experiment,<sup>69</sup> fuel bundles of UO<sub>2</sub> clad with SAP were irradiated for about four months in the NRX reactor; the organic coolant temperature was approximately 590°F, and the maximum sheath temperature was 860°F. Surface heat fluxes were roughly 100 w/cm<sup>2</sup>. A film about 80-μ thick covered the sheath over the fueled sections after irradiation. The film, 40 wt % polymerized organic and 60 wt % Fe<sub>3</sub>O<sub>4</sub>, increased the sheath temperature by 108°F. At the same time, negligible film formation occurred on nonfuel surfaces. Also, film buildup on fuel surfaces appeared to be greatest during periods of erratic reactor or loop operation. Although these results were not too encouraging, the Epilogue in Ref. 69 indicated that fouling problems could be eliminated by improved operation of the clay absorption columns associated with coolant purity control. However, later results<sup>70, 71</sup> have not entirely substantiated the Epilogue statement.

Test results reported in Ref. 70 were based on low-fouling-rate systems. The lowest deposition rates were observed in unfueled sections of the loop, and these were sometimes used to characterize the results. The lowest deposition rate reported for a fueled section was 0.14 μg/cm<sup>2</sup>.hr. Recent experimental results were obtained during operation of the U-305 loop. The results indicate some fouling of the fuel surface, although there have been periods of operation when fouling did not appear to increase with increasing exposure, based on temperature measurements. In general, it appeared<sup>71</sup> that the fouling rate was higher than that obtained in the X-7 loop<sup>70</sup> and that a fouling rate of about 0.2 μg/cm<sup>2</sup>.hr is a realistic minimum rate to expect at a heat flux of 100 w/cm<sup>2</sup> and HWOCR operating conditions. This is equivalent to a rise in fuel surface temperature of 45°F at a heat flux of 100 w/cm<sup>2</sup> for one year based on measurements of the thermal resistance of deposits generated at low deposition rates.<sup>70</sup> Since the peak heat flux in the proposed HWOCR systems exceeds 100 w/cm<sup>2</sup>, the peak fuel element temperature is 850°F, and the fuel would generally remain within the core about two years, it is estimated that a fouling film cannot be neglected. The actual temperature drop through this film cannot be accurately specified at this time; based

on present information, a value of 25 to 50°F under peak temperature conditions is judged to be feasible and to correspond to film-formation rates under HWOCR conditions.

Any impurity in the coolant that reacts with mild steel to place iron in solution will increase the rate of film formation and, finally, fouling of the fuel elements; this can lead to cladding failure due to overheating. Also, there is experimental evidence<sup>55</sup> that oxygen reacts rapidly with irradiated coolants to form compounds that corrode mild steel systems and lead to fouling. A Canadian report<sup>72</sup> presents evidence that chlorine in combined form causes a fouling problem when it is present in the coolant at a concentration greater than about 5 ppm. Inorganic particulate matter, such as rust, welding slag, and metal filings from piping and containment vessels, will also contribute to the plugging of coolant channels.

Based on present information, the best way to minimize film formation and fouling of the fuel elements is to exclude contaminants from the coolant. AI-CE has specified procedures, coolant purity, and purification systems to approach this objective.<sup>73</sup> They specify purging the coolant system with dry nitrogen before filling it with Santowax, circulating the Santowax with the distillation system operating prior to startup, and maintaining a nitrogen atmosphere over the coolant during operation to prevent contact with air. The proposed refueling operation appears to require minimal contact between coolant and air. Particulate matter is removed as the coolant passes through glass spool filters located at several different places in the lines. In addition, distillation removes about 70% of the oxygen-containing compounds and all inorganic particulates, if they reach this point in the system.

As long as the role of contaminants is recognized and the proper precautions are exercised to exclude and remove them, there is no reason to expect the construction materials recommended by AI-CE for the coolant system to undergo significant corrosion or massive fouling under the proposed environmental conditions.

#### 5.5.4 Other Properties

The explosive characteristics, temperature limits of flammability, and minimum spontaneous ignition temperatures for related materials, i.e., biphenyl, Santowax R, and irradiated OMRE coolant, were determined by the Bureau of Mines, Division of Explosives Technology.<sup>74</sup> Canadian tests<sup>75</sup> established that with favorable geometry for air access and heat retention, Santowax OM is susceptible to spontaneous combustion at 735°F and probably at a temperature as low as 660°F. No flame was evident but red hot areas were visible inside the insulation.

The available information<sup>76</sup> on the irritating effects of polyphenyl coolants on the eyes, pulmonary passages, and skin, as well as their ability to sensitize individuals, indicates that care and precautions are required to handle them safely. However, no difficulty is expected if good industrial hygiene practices are followed and respirators and protective clothing are used. The estimated lethal dose<sup>77</sup> of Santowax R for a 180-lb man is nearly 1/2 lb ingested. Furthermore, the coolant components are much too involatile at room temperature for one to inhale a serious dose.

#### 5.5.5 Conclusions

The use of Santowax OM as the coolant in these HWOCR systems appears satisfactory. We estimate that the degradation rate of the coolant will be about 1500 lb/hr under design power conditions, with an average outlet coolant temperature of 700°F. Use of a hydrocracker unit to recover about 90% of the degraded coolant will result in biphenyl concentrations in the coolant which will influence the DNB ratio, but present design conditions appear feasible relative to permissible DNB ratio. Corrosion in HWOCR systems does not appear to be a problem; however, the formation of a fouling film cannot be neglected. It is estimated that the temperature drop across the fouling film on the fuel surface in these HWOCR systems will be 25 to 50°F under favorable conditions at peak fuel surface temperature positions.

## 5.6 Reactor Controls and Safety Evaluation

Control of the HWOCR is dependent on the regulation of all the variables that affect reactivity. Reactivity is affected by the movement of neutron-absorbing control rods, the variation of boron concentration in the D<sub>2</sub>O moderator, and the variation of temperatures in the fuel, the moderator, and the organic coolant. While control rods and boron concentration can be controlled directly, the temperatures that affect reactivity are determined by numerous interdependent variables. These variables include all factors that affect heat transfer coefficients in the reactor core, as well as the relationships between reactor power, coolant flow, and temperature of the coolant entering the reactor. It is the behavior of these interdependent variables that characterizes the control and safety problems of this reactor.

### 5.6.1 Control and Safety Aspects of the Plant

The temperature coefficients of reactivity of both the organic coolant and the D<sub>2</sub>O moderator are positive, and the void coefficient of the coolant is positive. The fuel has a calculated negative temperature coefficient because of the Doppler effect in the fertile material. Of the three temperature coefficients, the positive coefficient of the coolant is the one of most concern relative to control and safety.

The important coefficients of reactivity were computed by both ORNL and AI-CE and are listed in Table 5.8. Equilibrium fueling conditions were assumed, without consideration of changes in absorption resonances of fissile material. The AI-CE values are taken from Appendix A of the AI-CE reference report.<sup>1</sup>

It is of interest to note that a rather nominal rise in the mean temperature of the coolant would increase the reactivity by an amount greater than the effective delayed-neutron fraction of 0.49% listed in Appendix A of the AI-CE report. This temperature rise is approximately 120°F for the ORNL coefficient and approximately 93°F for the AI-CE coefficient. Also, a complete loss of the coolant or a displacement of the coolant by a void, such as steam, would increase the reactivity by an amount greater than that associated with the delayed-neutron fraction

Table 5.8. Reactivity Coefficients of HWOCR

	Reactivity Coefficient (%)	
	ORNL-Computed Value	AI-CE-Computed Value
Fuel temperature, $\Delta k_e / ^\circ\text{F}$	$-0.56 \times 10^{-3}$	$-0.48 \times 10^{-3}$
Coolant temperature, $\Delta k_e / ^\circ\text{F}$	$+0.41 \times 10^{-2}$	$+0.53 \times 10^{-2}$
Moderator temperature, $\Delta k_e / ^\circ\text{F}$	$+0.82 \times 10^{-4}$	$+4.4 \times 10^{-4}$
Coolant void, $\Delta k_e / \Delta\%$ void	$+0.58 \times 10^{-2}$	$+1.1 \times 10^{-2}$

for either the ORNL- or AI-CE-calculated void coefficient. Thus it is not surprising that the positive temperature and void coefficients of the coolant play an important role in the control and safety of the plant.

The moderator temperature coefficient will be of little significance in transients because of the large thermal capacity of the  $\text{D}_2\text{O}$ , together with the small amount of power absorbed by the moderator.

The power coefficient of reactivity may be either positive or negative, depending upon the changes in reactor fuel and coolant temperatures. If the temperature of the coolant entering the reactor and the coolant flow are both held constant while the reactor power is increased, the power coefficient is positive, as stated in the AI-CE report. However, if the plant is operated in such a manner that steam is produced in the steam generator at a constant temperature and at a constant pressure over the power range, the power coefficient will be negative. In this latter case, the coolant flow must be varied in almost direct proportion to the plant power and, since the reactor coolant inlet, outlet, and mean temperatures will remain almost constant, they will have little effect on reactivity. The rise in reactor fuel temperature with increased power will be the dominant characteristic and will contribute a negative reactivity. We found the power coefficient to be approximately  $-0.25 \times 10^{-2}\%$   $\Delta k_e / \%$  power change for this type of operation.

Although the power coefficient is negative for changes from one steady-state power level to another in the above operating mode, a power

increase without a corresponding coolant flow increase will produce an increase in reactivity. The reactor control system must continuously combat the effect of the positive temperature coefficient of the coolant. The ingredients of an unstable condition are always present, and failure of continuous control can lead either to a positive power excursion that requires prompt action of the safety system or to a negative power transient that shuts the reactor down.

Heat transfer information and temperature coefficients obtained from W. C. Coppersmith of Combustion Engineering were used in the analog computer study of the kinetic thermal characteristics of the HWOCR, as described in Appendix F. The results of a step increase in reactor power from 0 to 100% of rated value are illustrated in Fig. 5.14. The step rise in power provides an input variation for analytically examining the resultant temperature changes and reactivity variation. The coolant flow was held constant at 20% of its full value, and the reactor inlet temperature was held constant at 600°F. These values of coolant flow and inlet temperature represent the probable lower limit of operation in the

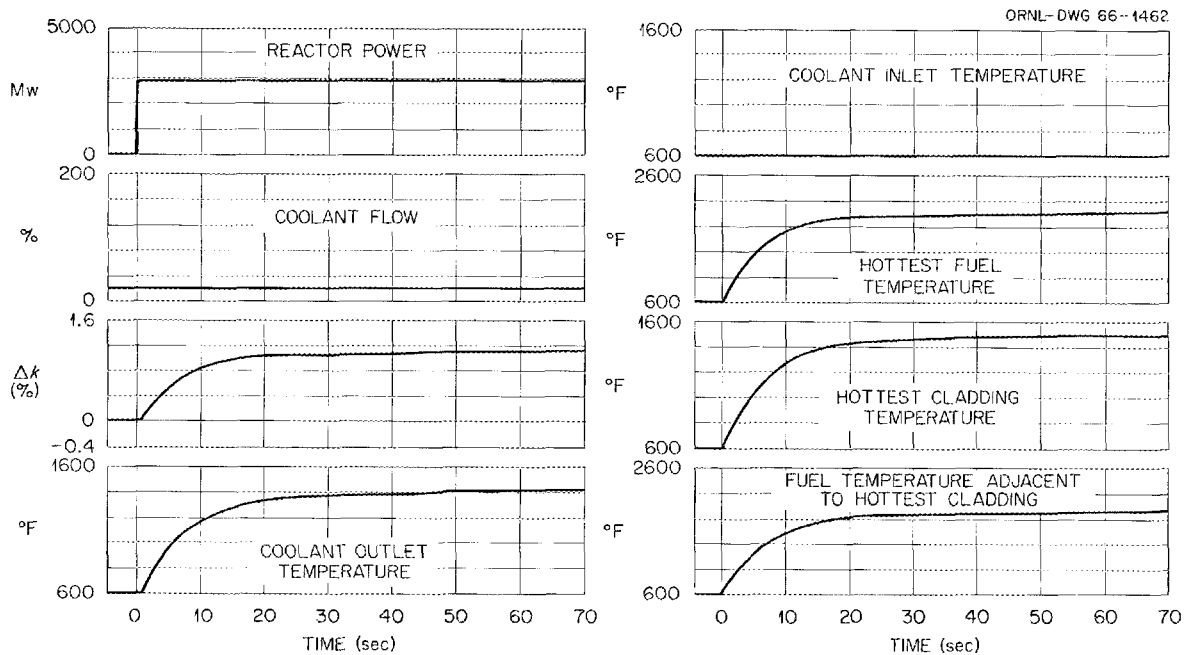


Fig. 5.14. Thermal Behavior Following Step Rise in Power.

power range. The effect of the reactivity variation on reactor power was not included in this set of curves, since we intended to observe only the thermal behavior of the fuel and coolant and to determine the effect of temperature changes on reactivity. As shown in the curves, the step increase in power produced a small initial decrease in reactivity of approximately 0.005% during the first half second while the fuel temperature was rising and before the coolant temperature increased significantly. The coolant temperature rise lagged behind the fuel temperature rise by less than 1 sec, and the net reactivity was positive and rising in less than 1 sec after the power step was initiated. Thus, although the prompt power coefficient is indeed negative, both the magnitude and duration of this negative aspect of reactivity are exceedingly small.

The temperature variations in Fig. 5.14 are quite similar to solutions of first-order linear differential equations, and it is logical to consider the time required for the temperature to reach 63% of its final value as a time constant. The time constants of these variations at 20% coolant flow are approximately 12.0 sec for the coolant outlet temperature and approximately 7.5 sec for the hottest fuel temperature. Since there was a delay of about 1 sec after the step in power before the outlet temperature of the coolant began its rapid increase, the time constant of the coolant has less physical meaning than that of the fuel. In other curves obtained at 100% flow, the difference between these time constants was negligibly small; both the fuel and coolant temperatures began to rise almost simultaneously, and both had a time constant of approximately 4.8 sec.

### 5.6.2 Reactor Startup

The manipulation of reactivity during startup is dictated by the requirements that the moderator must contain no boron at full power with equilibrium xenon and that the shutdown rods must be fully withdrawn before the reactor becomes critical. The vertical control rods lack sufficient reactivity to control the reactor over the range from zero power isothermal conditions at 190°F to full power at operating temperatures. Since the horizontal shutdown rods are fully withdrawn before the beginning of a power increase, almost all the necessary reactivity variations

must be accomplished by changes in boron concentration, while the control rods are allowed to maintain continuous fine control. Since the reference AI-CE report<sup>1</sup> gave no specific startup procedure, we suggest the following conditions and procedures for illustrative purposes:

1. The reactor system is initially assumed to be isothermal at 190°F. The moderator temperature is to be held constant at 190°F. One coolant pump is initially in operation at low speed, and it provides approximately 20% of full coolant flow.

2. The excess reactivity of the clean core (with no boron and isothermal conditions at 190°F) is at an initial value that will permit the reactor to be critical when operating temperatures are reached at full power with equilibrium xenon poisoning present and the vertical control rods inserted to their midpoints. We estimate this excess reactivity to be approximately 1.2%.

3. The moderator initially contains sufficient boron to keep the reactor from being supercritical with all the shutdown rods withdrawn completely and all the control rods withdrawn to their midpoints.

4. Those vertical control rods assigned to power control are placed in the center of their stroke to make reactivity changes available in both directions. The remaining vertical control rods are placed in suitable positions and are held in readiness for flux-distribution control.

5. The shutdown rods are withdrawn, not in unison, but in groups with successively fewer rods in each group as criticality is approached, until the last few shutdown rods are withdrawn individually. (A shutdown rod has no intermediate position; it is either fully inserted, fully withdrawn, or in motion.)

6. The moderator purifier system is placed in operation to increase reactivity by reducing the boron concentration.

7. The reactor is brought critical by boron removal from the moderator with the power level control rods withdrawn approximately to their midpoints. Under this condition the boron remaining in the moderator is estimated to be worth approximately 1.2% in reactivity.

8. The power level control rods are then moved to increase reactivity and initiate a reactor power rise. As the temperatures of the

fuel and coolant rise slowly, the control rods are inserted to control reactivity. (A flux servo to control these rods probably will be necessary; the plant operator would then raise the servo setpoint to increase the power.) The cooling system must be brought into operation to control the reactor coolant inlet temperature. The reactor must be brought to a steady-state condition before the control rods are fully inserted. Boron is then added to the moderator while the power is being held constant by withdrawal of control rods. The addition of boron must be stopped before the control rods are completely withdrawn.

9. The procedure of alternately raising the power and adding boron is continued until operating temperatures are reached with the reactor at 20% power. At this power level, the boron concentration is at its maximum value. The steam system must be in operation and the plant ready for automatic power control. Dumping of steam directly to the condenser may be required.

10. An increase in power from 20 to 100% requires an increase in reactivity to overcome the negative power coefficient of the normal mode of operation, as discussed in Section 5.6.1. Therefore, boron is removed from the moderator, and the coolant flow is increased while the coolant inlet and outlet temperatures remain nearly constant. While the boron is being removed, the plant power increases, and the control rods are maintained near the center of their stroke in order for them to be available to suppress reactivity transients. The two additional coolant pumps are started and all three pumps are at full speed when the plant reaches full power. When the plant first attains full power with little samarium or xenon poison in the reactor, the boron in the moderator should have a reactivity worth nearly equal to the equilibrium worth of xenon.

11. Boron is removed from the moderator to hold the reactor at full power and compensate for the reactivity decrease caused by the buildup of xenon until the xenon reactivity reaches its equilibrium value of 2.7%. At this point, no boron should remain in the moderator, and the fuel loading machine is then used to load the fresh fuel required to compensate for fuel depletion and buildup of samarium. The control rods are to be kept near the center of their stroke to allow the control system

to handle operating transients of either decreasing or increasing reactivity.

The above discussion illustrates, we believe, a reasonable procedure for bringing the plant from an isothermal subcritical condition to full power. The process requires the correct variation of boron dissolved in the moderator, together with the proper motion of the power level control rods. Correct manipulation of these two parameters will be especially important when the reactor temperatures begin to rise and the nonlinear relationship between power and reactivity becomes a complicating factor. The price of a miscalculation can be a reactor scram to stop a positive power excursion or a shutdown from a downward reactor power transient. Given sufficient training and time, an operator might be able to carry out the required procedure; however, this appears to be an appropriate area for computer control.

### 5.6.3 Restart After a Scram

One method of restarting after a scram requires a delay until the xenon has decayed to a low reactivity value. This restarting procedure would be quite similar to that described for startup in Section 5.6.2. After the xenon builds up to more than 2.7% reactivity after a scram, restart is not possible because there is insufficient excess reactivity in the core. The next restart must be delayed until after the xenon reactivity falls below 2.7% — a delay of about 34 hr. This delay, plus an additional delay of several hours in attaining full load, would result in the station being off the line for at least one and possibly two daily load peaks and should be avoided if possible.

Another method of restarting would eliminate the delay for xenon decay. This method uses control of the coolant heat removal system, together with afterheat generation, to make the reactor critical by temperature control with the shutdown rods withdrawn and no boron in the moderator. We have estimated the isothermal temperature at which the reactor will be critical immediately following a scram before the xenon concentration increases. This temperature is approximately 600°F based on the ORNL temperature coefficients. A rise of 100°F in this isothermal

temperature will add a reactivity of approximately 0.35%. Therefore xenon buildup after scram from its equilibrium value of 2.7% to a larger reactivity worth of 3.0% would require the isothermal temperature to be raised to approximately 685°F. During a rise to power from this critical condition, boron is not available for removal; thus, the only reactivity control possible is from motion of control rods and variation of coolant and fuel temperatures. Control of the steam system and coolant flow now become means for reactivity control, and steam temperature and steam pressure must be allowed to vary as required. A steam dump may be necessary if the steam conditions are not suitable for operation of the main turbine. The turbines driving the coolant pumps must be designed to operate on the steam pressure and temperature obtained during the rise to full power. We consider the restarting method important, since the acceptability of this plant in a power grid may depend on its ability to restart without a two-day delay in power operation following a shutdown.

#### 5.6.4 Safety System Requirements

The minimum performance requirements of the reactor safety system are established by considering the consequences of failures of the reactor control system. Since the HWOCR is an inherently unstable reactor, a loss of reactivity control can lead to an undesirable power excursion. Any imbalance between the rates of heat generation and heat removal will initiate a reactor power transient that continues to force a further divergence. Figures 5.15 and 5.16 show the results of power excursions that began with initial steady-state conditions of 20% power and 20% coolant flow. The reactor coolant inlet temperature and flow were held constant in both cases.

The curves in Fig. 5.15 show the result of permitting the power to drift upward for several seconds without corrective action. A power increase was not initiated intentionally; rather, the simulated reactor had been held at steady state by means of reactivity control for more than 2 min before this control was removed. The power rise began very slowly and was not perceptible on the power trace during the first 20 sec after the controller was turned off. The abscissa in Fig. 5.15 gives the time interval after control was removed. The last 5 sec of the curves

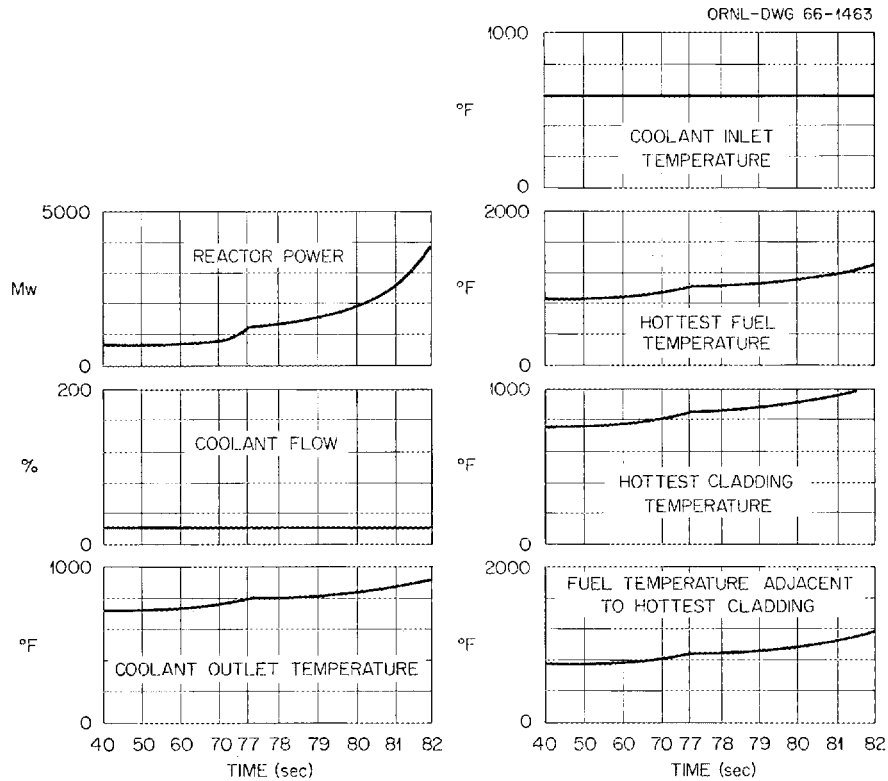


Fig. 5.15. Reactor Power Excursions — Controller Turned Off, No Excursion Initiated.

was recorded with a different time scale in order to show better the rapid rise of power during the final portion of the transient. The reactor period had shortened to approximately 1.8 sec at the instant the reactor power reached its 100% value of 3000 Mw(th). The coolant outlet temperature was 900°F. The rate of rise of the coolant outlet temperature was approximately 60°F/sec, and the rate was increasing. When the same procedure was tried with initial values of 100% flow and 3000 Mw(th), the period was 16.7 sec when the power reached 5000 Mw(th).

The curves shown in Fig. 5.16 show the result of a step increase in reactivity inserted at the moment the automatic power control was turned off. The magnitude of the step of reactivity was  $0.2\% \Delta k_e$ . Both the fuel and coolant temperatures at the time 3000 Mw(th) was reached were lower than the corresponding values in Fig. 5.15. The reactor period was also slightly shorter than in the previous case, being 1.7 sec at

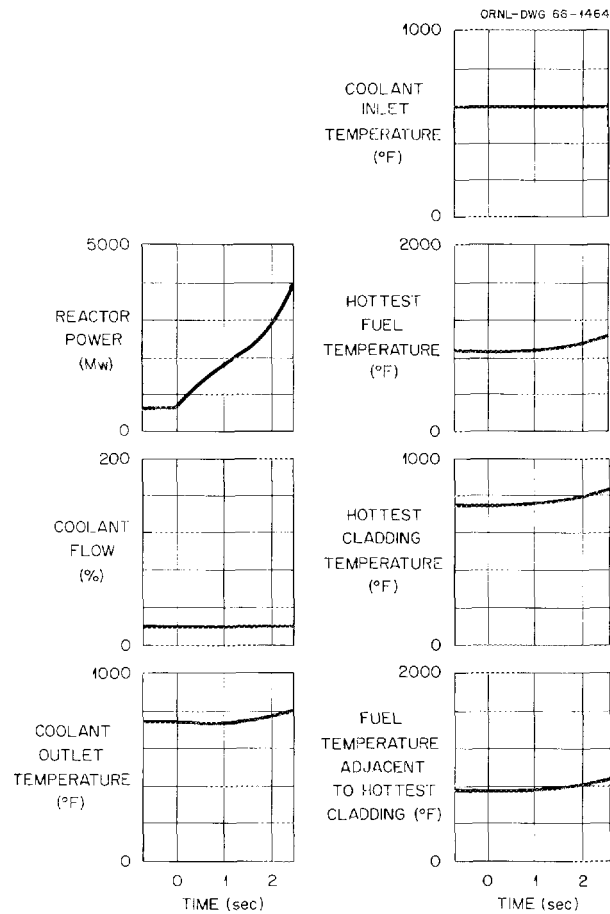


Fig. 5.16. Reactor Power Excursions — Step Increase of 0.2%  $\Delta k$  to Initiate Excursion.

3000 Mw(th) as compared with 1.8 sec. The increasing rate of power rise is quite apparent.

The curves in Fig. 5.16 qualitatively illustrate a startup accident. It is postulated that failure of the startup instrumentation and control system causes reactivity to be added at the maximum possible rate by withdrawal of control and/or shutdown rods, and criticality is reached before the rods are completely withdrawn. This accident could be quite severe in the HWOCR, and it establishes the minimum performance requirements of the safety system. The power excursion can be terminated only by insertion of the shutdown rods or by redistribution of the core into a less reactive configuration.

The startup accident could occur when most, or all, of the boron had mistakenly been removed from the moderator and the shutdown rods were withdrawn in preparation for going critical. If all the boron were removed, the reactor would be supercritical by about  $1.2\% \Delta k_e$  with all the shutdown rods withdrawn, the vertical control rods withdrawn to their midpoints, and the core isothermal at  $190^\circ\text{F}$ . If allowed to go unchecked, the excursion would cause the organic coolant to boil and the liquid to be expelled from the core. Our analysis of the results given in Figs. 5.15 and 5.16 shows that in a power excursion at low coolant flow rates the rate of reactivity addition associated with the positive coolant temperature coefficient is almost twice the rate of reactivity removal by the negative fuel coefficient. In order to control such excursions it will be necessary to retain the period trip in the power range or, alternatively, employ a rate trip or reset the flux level trip point as a function of the expected power. Since it is possible for the period of the excursion to be either quite short or only slightly larger than the trip setting, both the period trip (or rate trip) and level trip are required to perform reliably. A reset of the flux level trip point, if applied, must have a design reliability consistent with safety system requirements. Further analysis of power excursions will be needed to establish the required response time of the safety system, but it is probable that the proposed time of 3 sec to insert  $1\% \Delta k_e$  is too long.

The kinetic behavior of the HWOCR is such that failure to obtain prompt and adequate control response results in loss of control, with a high degree of certainty that a power excursion will follow. Thus, failure to act, rather than the commission of a series of misoperations, can require infallible operation of the safety system. Even a slight initial transient without safety action will lead to a power excursion that requires redistribution of the fuel or expulsion of the moderator to shut down the reactor. The containment structure appears unable to withstand the consequences of the failure of the safety system. Since both the reactor and the containment system require infallible performance on the part of the safety system, two complete and independent sets of instruments and shutdown rods are required. In order to minimize common failure modes, the two systems must be of different design and construction,

and both must have adequate time response. It is possible that the combined reactivity worth of both sets of rods will remain at  $4\% \Delta k_e$ ; however, more analyses are required to determine the response and reactivity needed. The correct operation of either group of shutdown rods must afford protection.

#### 5.6.5 Reactor Control System Requirements

The reactivity control of the HWOCR should be capable of keeping the reactor in operation in spite of probable reactor transients such as those arising from the insertion of one shutdown rod or the loss of one coolant pump. With 84 shutdown rods being held in the withdrawn position, failures causing insertion of individual rods could be expected to occur several times per year. The reactor power regulating system should therefore have the capacity and response to compensate for such a reactivity decrease with a minimal disturbance of reactor operation. Also, a loss of motive power to one of the three coolant pumps while the plant is at full power is quite likely. Simultaneously with coastdown of the pump, the control system must regulate the reactivity to reduce the reactor power as required to allow continued operation at reduced power.

Results obtained from our analog computer study (see Appendix F) of the effect of inserting one shutdown rod are given in Figs. 5.17, 5.18, 5.19, and 5.20. The most reactive shutdown rod is estimated to be worth approximately  $0.1\% \Delta k_e$ , and the time interval for insertion of the shutdown rods must be small to meet the safety system requirements discussed in Section 5.6.4. Therefore, a step reduction of  $0.1\% \Delta k_e$  was introduced to simulate the rapid insertion of such a rod. An automatic reactor power control system was used in an attempt to maintain the reactor power at its original value. In the run shown in Fig. 5.17, the reactivity rate addition of the control system was limited to  $\pm 0.005\% \Delta k_e / \text{sec}$ , with a maximum of  $\pm 0.10\% \Delta k_e$  available for control. The control system in this case was not capable of coping with the sudden reduction in reactivity, and the reactor was shut down. The curves in Fig. 5.18 show the effect of increasing the maximum reactivity available for control. When the reactivity of the control rods was changed from  $\pm 0.10$  to  $\pm 0.15\% \Delta k_e$ ,

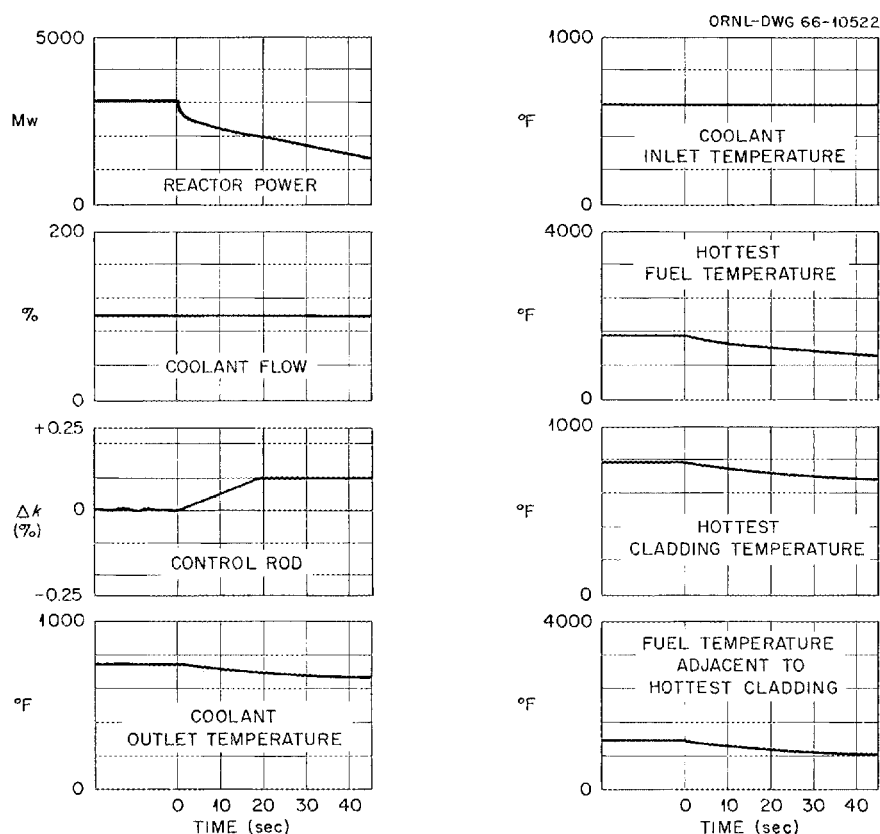


Fig. 5.17. Response to Step Decrease in Reactivity of  $0.1\% \Delta k_e$ ; Control of  $\pm 0.10\% \Delta k_e$  at  $\pm 0.005\% \Delta k_e/\text{sec}$ .

the system was able to recover in approximately 1.5 min, but the outlet temperature of the coolant suffered a  $50^\circ\text{F}$  variation during the transient. When the control system reactivity rate was increased from  $\pm 0.005$  to  $\pm 0.01\% \Delta k_e/\text{sec}$  with a maximum control system reactivity change of  $\pm 0.15\% \Delta k_e$ , the reactor was restored to normal conditions approximately 22.5 sec after the step decrease in reactivity. The outlet temperature varied approximately  $30^\circ\text{F}$ , as shown in Fig. 5.19. An increase in control system reactivity rate from  $\pm 0.01$  to  $\pm 0.015\% \Delta k_e/\text{sec}$ , with a maximum reactivity control of  $\pm 0.15\% \Delta k_e$ , decreased the variation in outlet temperature to  $20^\circ\text{F}$  and produced a recovery in approximately 10 sec, as shown in Fig. 5.20. These four sets of curves indicate that recovery of the reactor from a  $0.1\% \Delta k_e$  negative step is greatly enhanced by increasing the withdrawal rate from  $0.005\% \Delta k_e/\text{sec}$  to  $0.01\% \Delta k_e/\text{sec}$ .

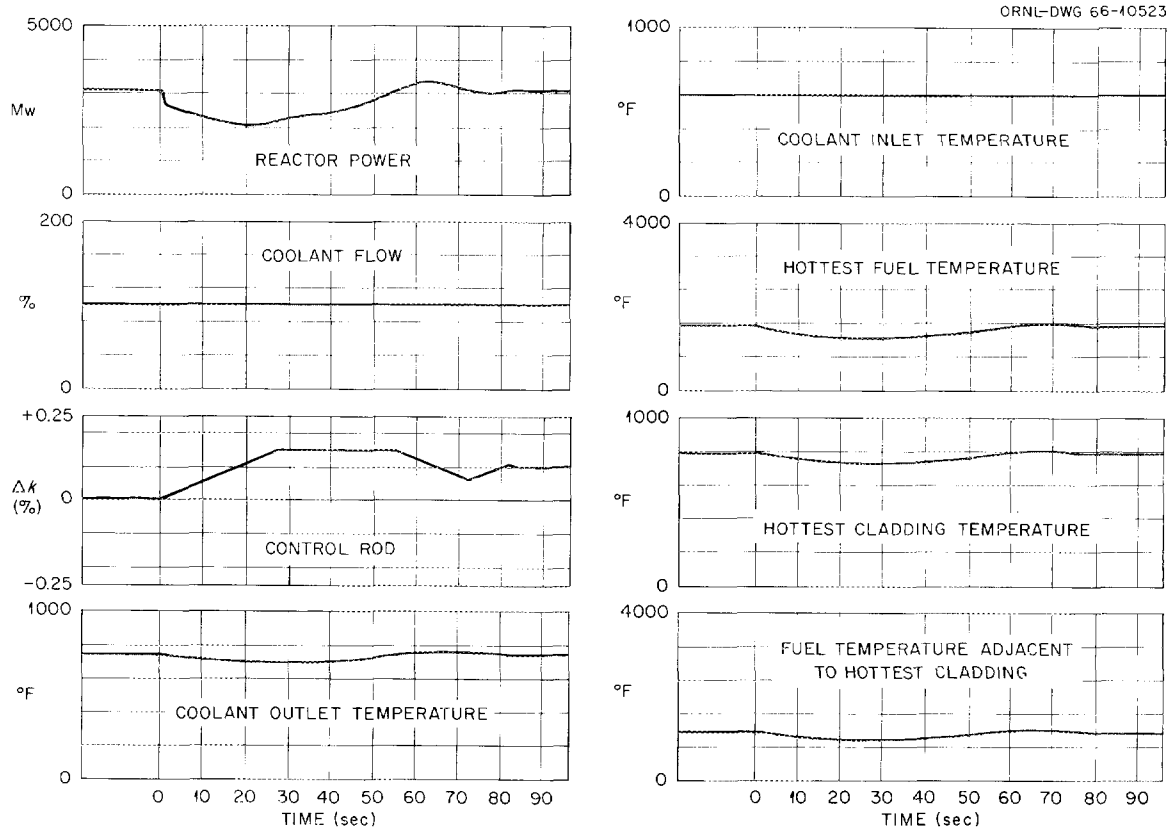
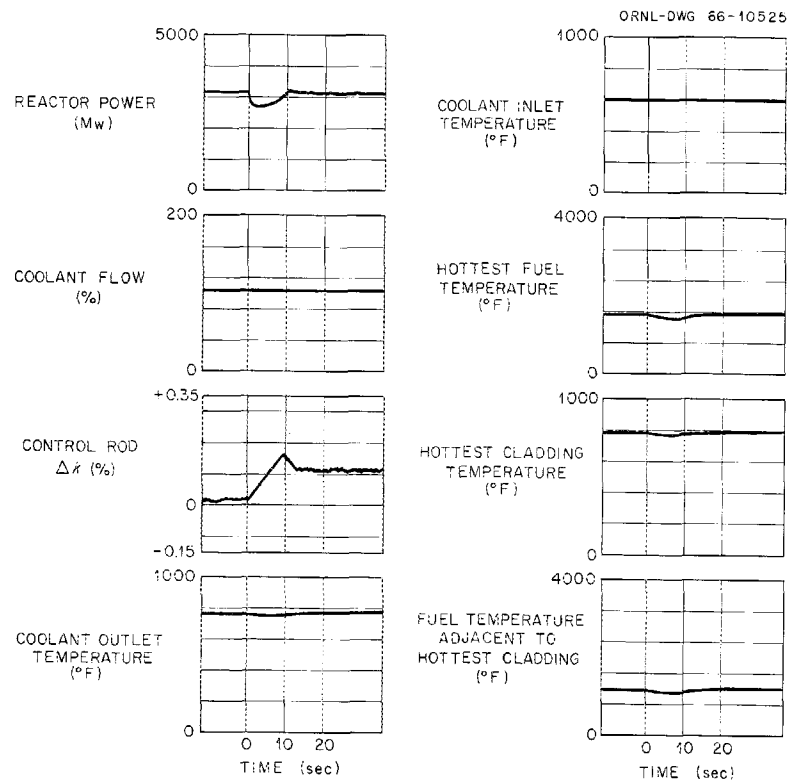
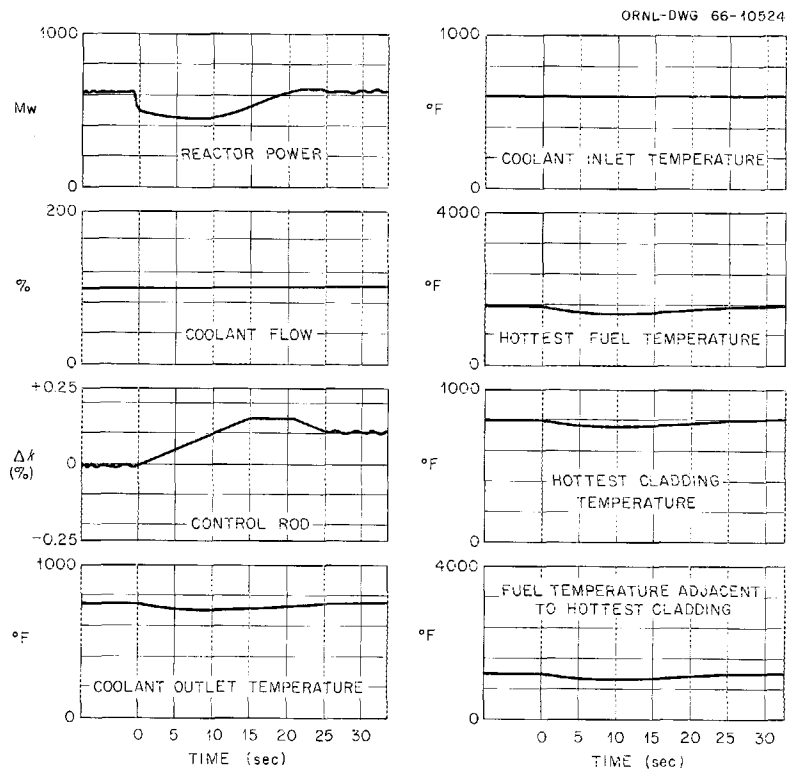


Fig. 5.18. Response to Step Decrease in Reactivity of  $0.1\% \Delta k_e$ ; Control of  $\pm 0.15\% \Delta k_e$  at  $\pm 0.005\% \Delta k_e/\text{sec}$ .

Provision of more regulating rod worth than  $\pm 0.15\% \Delta k_e$  would probably contribute little to the handling of a shutdown rod insertion.

We also examined the effects of a positive step of  $0.1\% \Delta k_e$ , as shown in Figs. 5.21 and 5.22. With a control system worth of  $\pm 0.15\% \Delta k_e$ , a control rate of  $\pm 0.01\% \Delta k_e/\text{sec}$  was insufficient, as shown in Fig. 5.21. A control rate of  $\pm 0.015\% \Delta k_e/\text{sec}$  limited the maximum power to 4200 Mw(th), the outlet temperature to  $790^\circ\text{F}$ , the cladding temperature to  $840^\circ\text{F}$ , and the fuel temperature to  $1800^\circ\text{F}$ . The transient was over in approximately 45 sec. It should be emphasized that a positive step of  $0.1\% \Delta k_e$  is an unusual condition arbitrarily imposed on the system and does not represent any specific incident.

The effects of coastdown of one of the three coolant pumps under various conditions are shown in Figs. 5.23, 5.24, 5.25, and 5.26. The



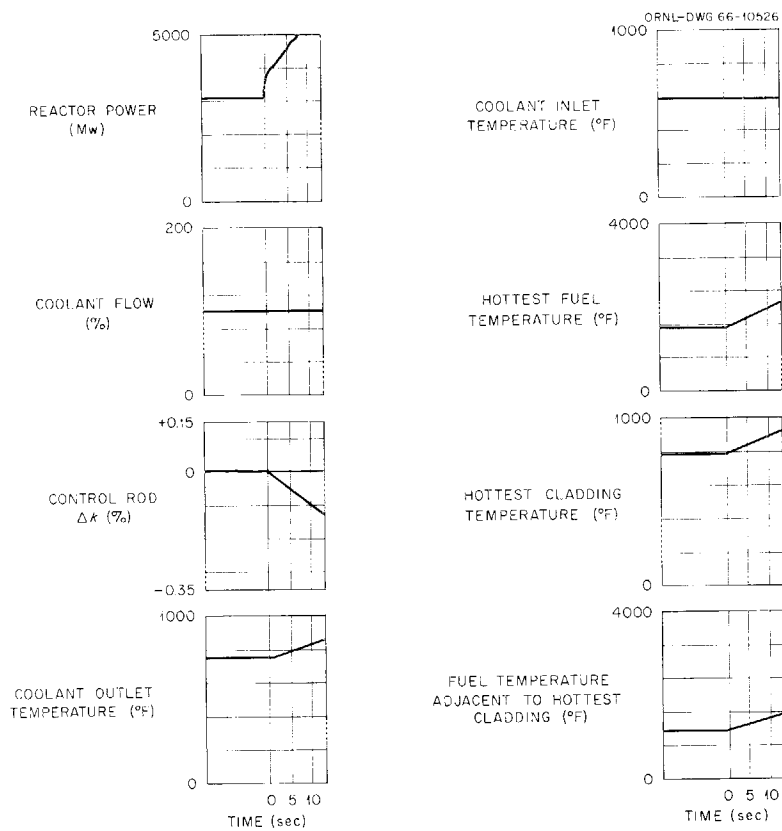


Fig. 5.21. Response to Step Increase in Reactivity of  $0.1\% \Delta k_e$ ; Control of  $\pm 0.15\% \Delta k_e$  at  $\pm 0.010\% \Delta k_e/\text{sec}$ .

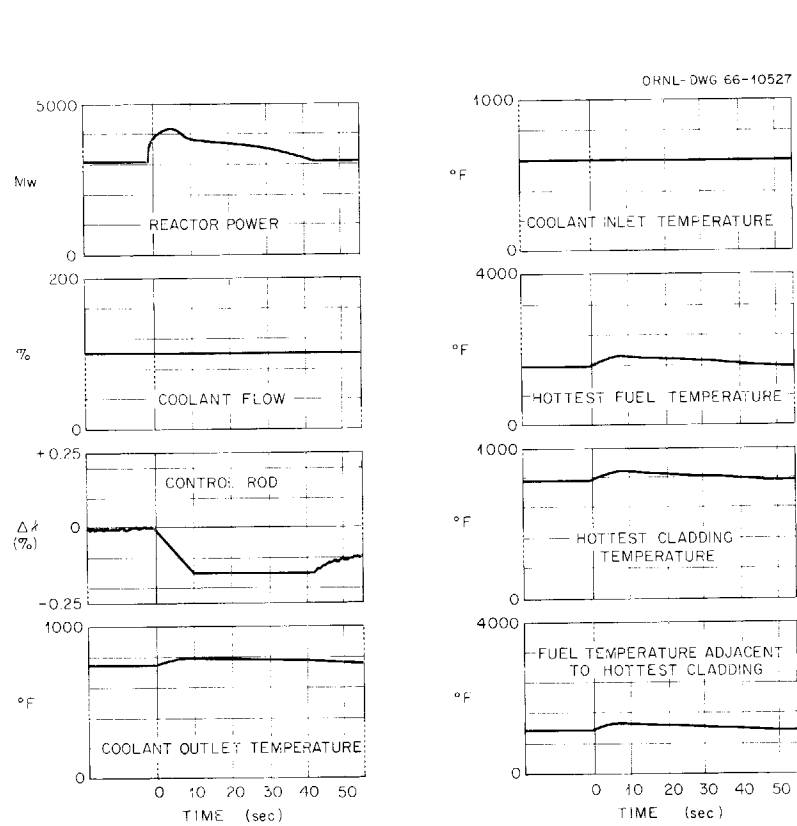


Fig. 5.22. Response to Step Increase in Reactivity of  $0.1\% \Delta k_e$ ; Control of  $\pm 0.15\% \Delta k_e$  at  $\pm 0.015\% \Delta k_e/\text{sec}$ .

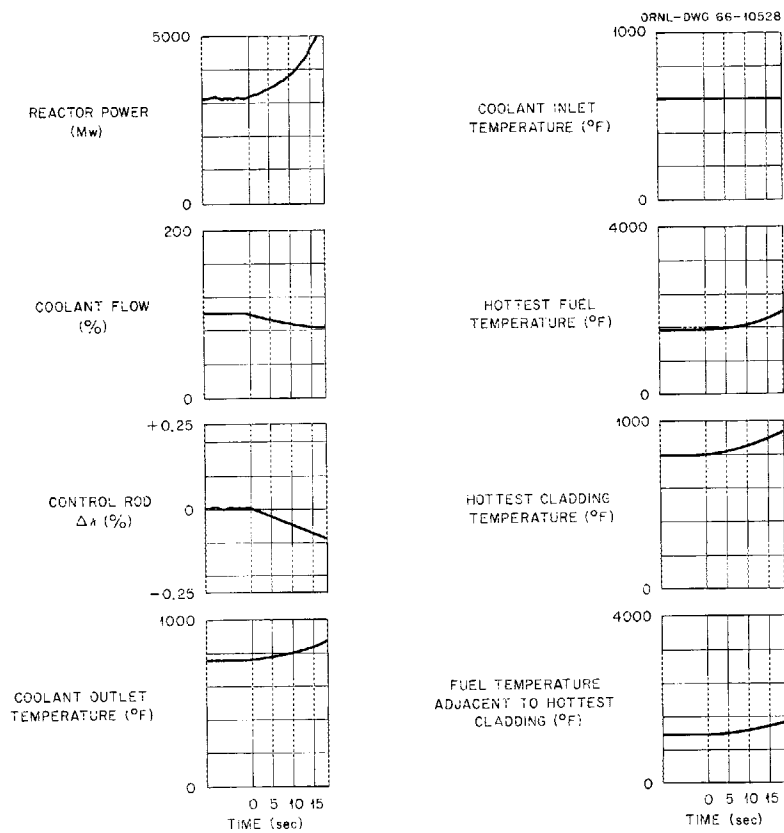


Fig. 5.23. Response to Coolant Pump Coastdown on 10-sec Time Constant; Control of  $\pm 0.15\% \Delta k_e$  at  $\pm 0.005\% \Delta k_e/\text{sec}$ .

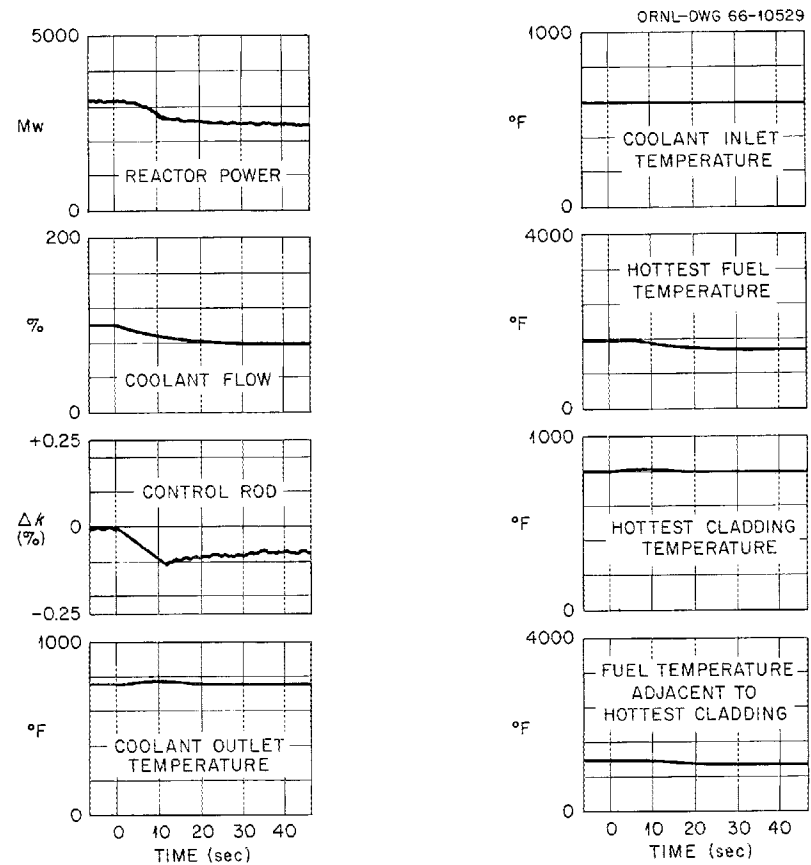


Fig. 5.24. Response to Coolant Pump Coastdown on 10-sec Time Constant; Control of  $\pm 0.15\% \Delta k_e$  at  $\pm 0.010\% \Delta k_e/\text{sec}$ .

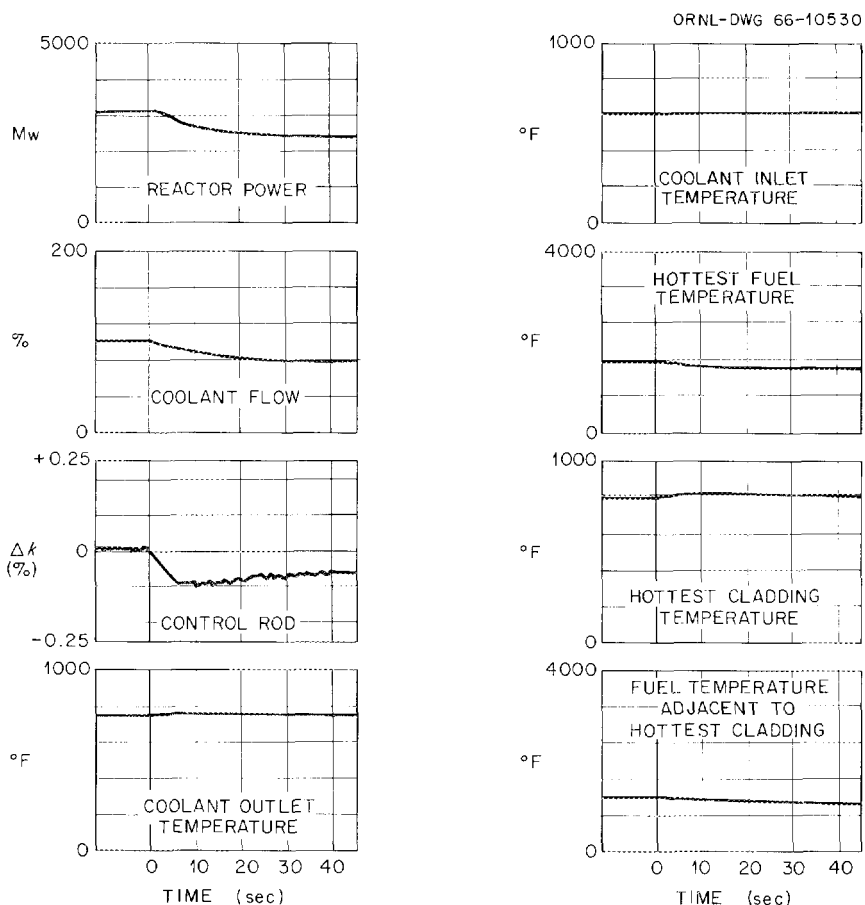


Fig. 5.25. Response to Coolant Pump Coastdown on 10-sec Time Constant; Control of  $\pm 0.15\% \Delta k_e$  at  $\pm 0.015\% \Delta k_e/\text{sec}$ .

simulated control system endeavored to adjust the reactor power to correspond to the coolant flow in each case. The coolant flow was assumed to decrease from 100 to 78% on a flow-time relationship described by a linear first-order differential equation. Three runs were made with a coastdown time constant of 10 sec and one with a time constant of 20 sec. It was necessary for the control system to decrease the reactivity to prevent a power excursion and to bring the power down to match the reduced coolant flow. The curves in Fig. 5.23 show that a reactivity rate of  $\pm 0.005\% \Delta k_e/\text{sec}$  was insufficient to cope with the results of a pump coastdown with a time constant of 10 sec. A scram would have been required to halt the ensuing excursion. An increase in the control reactivity to  $\pm 0.010\% \Delta k_e/\text{sec}$  was sufficient to prevent an excursion, as

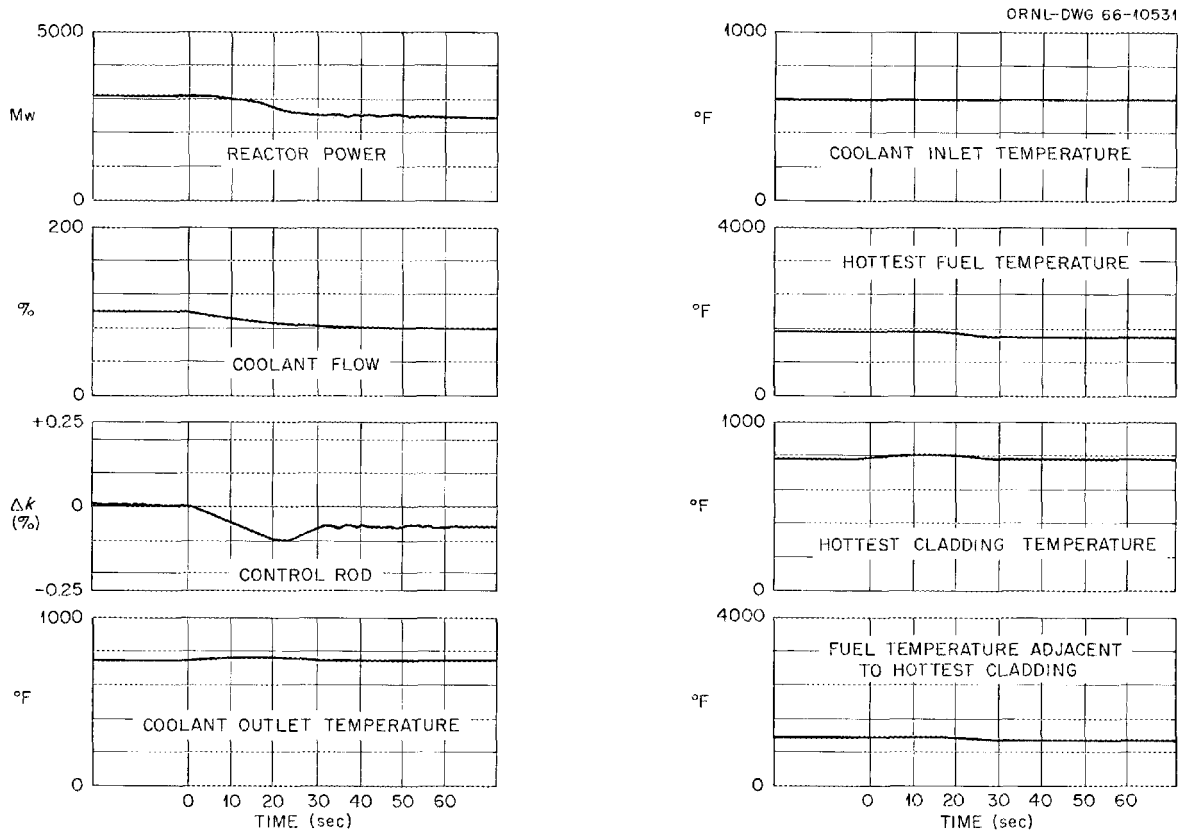


Fig. 5.26. Response to Coolant Pump Coastdown on 20-sec Time Constant; Control of  $\pm 0.10\% \Delta k_e$  at  $\pm 0.005\% \Delta k_e/\text{sec}$ .

shown in Fig. 5.24. Another increase in reactivity control rate to  $\pm 0.015\% \Delta k_e/\text{sec}$  provided an even smoother transition from 100 to 78% power in response to a pump coastdown, as shown in Fig. 5.25. In the last case, the coolant outlet temperature rose approximately  $20^\circ\text{F}$  before gradually decreasing to its design-point value. The temperature transient existed for less than 20 sec. An additional run was made with the slower pump coastdown time constant of 20 sec, and a reactivity control rate of over  $\pm 0.005\% \Delta k_e/\text{sec}$  was sufficient to cope with the transient, as shown in Fig. 5.26. In general, all these curves show that the transient due to a pump coastdown is much less severe than that of rapid insertion of a single shutdown rod.

Another type of transient requiring adequate reactivity control arises from a change of the temperature of the coolant entering the reactor. Such a temperature perturbation could be produced by a sudden

change in steam flow. Although no attempt has been made to describe the exact mechanisms for causing the particular coolant temperature variations that were examined, the control system needs sufficient capability in this area.

The transient was initiated by a steep ramp in coolant inlet temperature, with the flow held constant at its design value. The first change was a  $6^{\circ}\text{F}$  rise introduced in 1 sec, shown in Fig. 5.27. A control system reactivity rate of  $\pm 0.005\% \Delta k_e/\text{sec}$  handled the transient within approximately 12 sec. The power momentarily reached 3300 Mw, and the coolant outlet temperature rose about  $10^{\circ}\text{F}$  for a few seconds. The

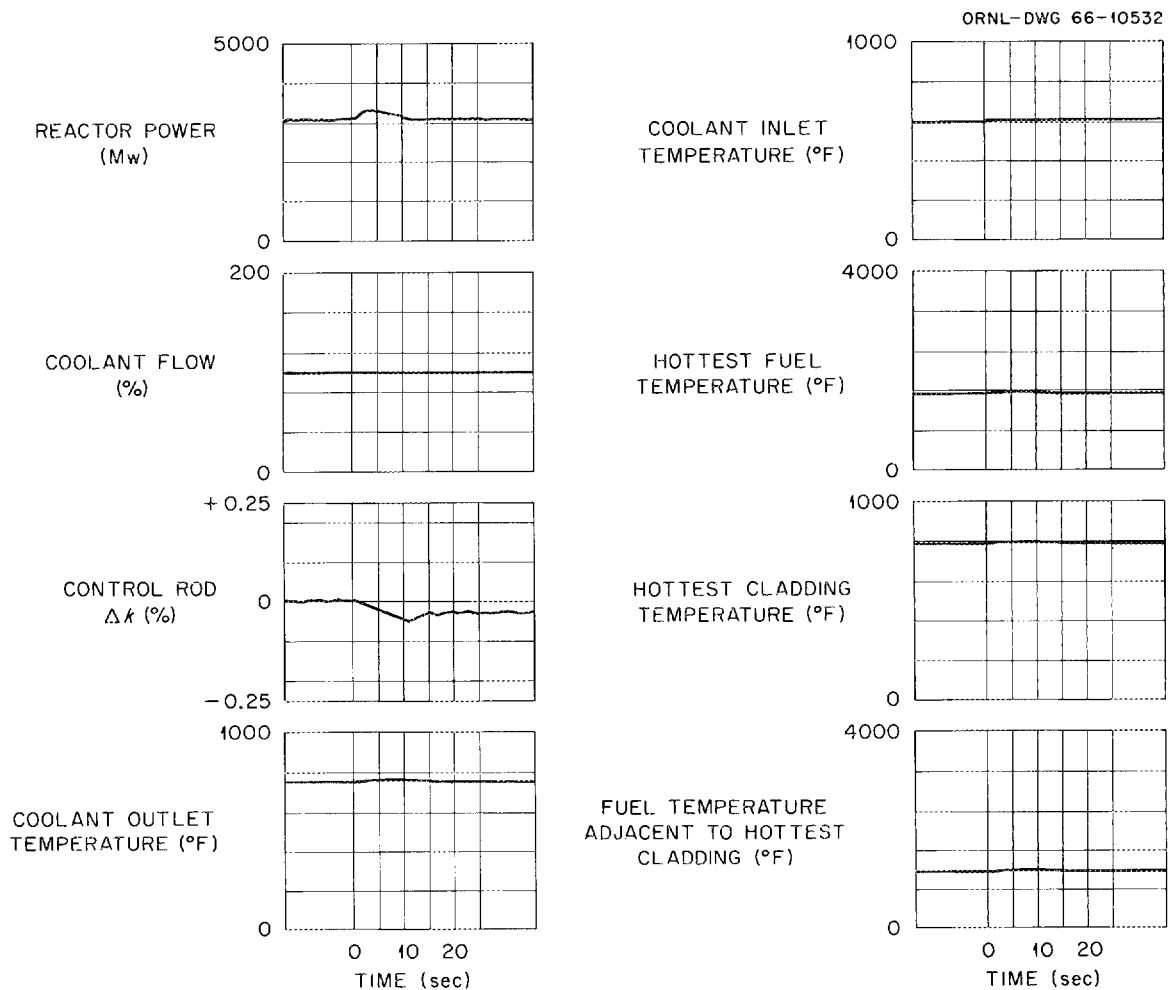


Fig. 5.27. Response to Rise in Coolant Inlet Temperature of  $6^{\circ}\text{F}$  in 1 sec; Control of  $\pm 0.15\% \Delta k_e$  at  $\pm 0.005\% \Delta k_e/\text{sec}$ .

next transient was initiated by a  $12^{\circ}\text{F}$  ramp rise in coolant inlet temperature, which was also introduced in 1 sec, as shown in Fig. 5.28. For this case, the reactivity control rate was  $\pm 0.010\% \Delta k_e/\text{sec}$ . This new control rate handled the  $12^{\circ}\text{F}$  rise in inlet temperature almost as well as the  $\pm 0.005\% \Delta k_e/\text{sec}$  rate handled the  $6^{\circ}\text{F}$  rise. The transient was over in approximately 12 sec. The reactor power went to a peak of 3700 Mw, and the coolant outlet temperature went to a high of  $780^{\circ}\text{F}$ . The curves in Fig. 5.28 also show the results of the same coolant inlet temperature change in a downward direction. The transient from a decrease in coolant temperature is much less pronounced than that from an increase in temperature.

A reactor control system having  $\pm 0.15\% \Delta k_e$  reactivity available at a rate of  $\pm 0.015\% \Delta k_e/\text{sec}$  was capable of coping with all the situations

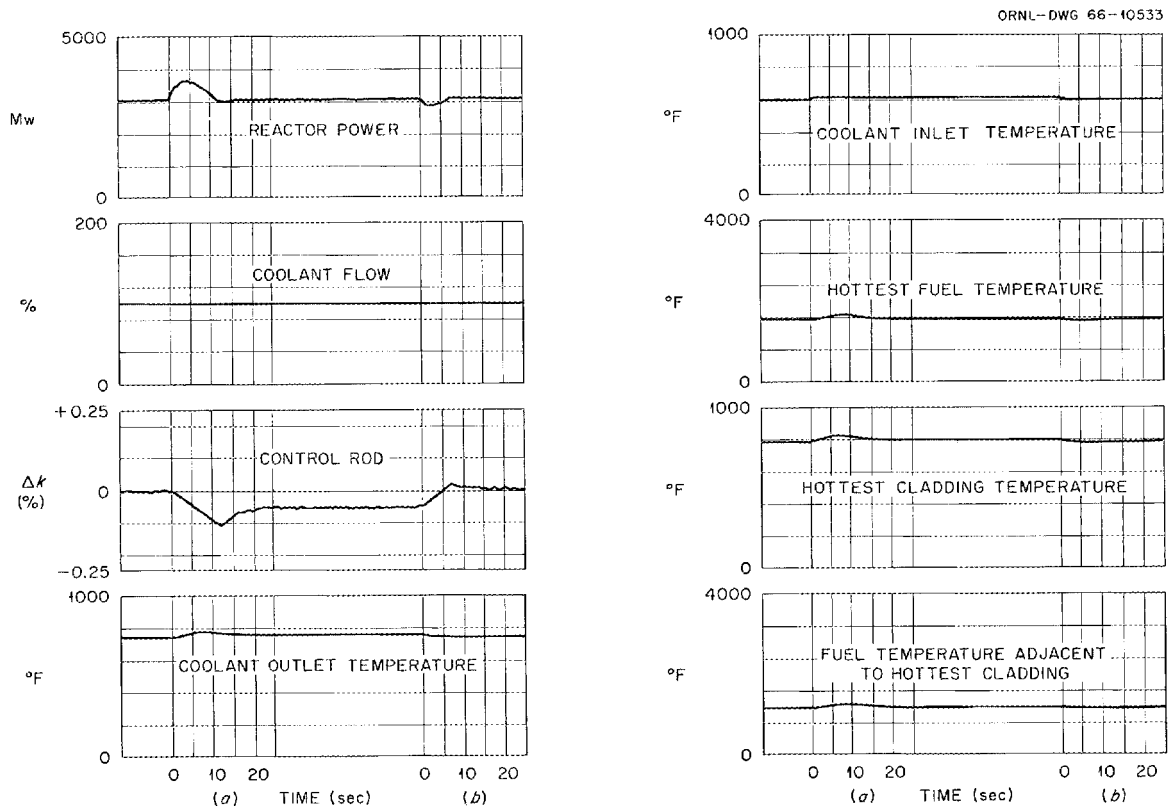


Fig. 5.28. Response to Change in Coolant Inlet Temperature of  $12^{\circ}\text{F}$  in 1 sec; Control of  $\pm 0.15\% \Delta k_e$  at  $\pm 0.010\% \Delta k_e/\text{sec}$ . (a) Temperature increase. (b) Temperature decrease.

examined. Since both positive and negative reactivity changes may be required, depending on the cause of the disturbance, a total control system reactivity of approximately  $0.3\% \Delta k_e$  appears necessary. To facilitate control without excessive power and temperature fluctuations, a reactivity rate of approximately  $\pm 0.015\% \Delta k_e / \text{sec}$  is needed.

Another factor that needs to be considered is the reactivity required for satisfactory suppression of the xenon spatial oscillations. Although of secondary importance to the problems discussed above, xenon control is needed in order to obtain the average fuel performance specified for the HWOCR.

There is considerable economic incentive in providing a control system for the HWOCR that will continue to operate the reactor despite failure of a system component. We recommend that the system use multiple controllers arranged to supply three similar error signals for control of the control rods. The median signal would then be selected by a controller for each rod drive. A failure of one error signal would be compensated by the remaining two signals, and a failure of one controller for one rod should be tolerable. This system is discussed in Section 6.8.2, and a block diagram of the arrangement is shown in Fig. 6.8.

#### 5.6.6 Reactor Shutdown Margin

In a reactor having positive coefficients, shutdown margin becomes a matter of urgent concern. When the shutdown rods are inserted, the reactivity decreases as the coolant temperature decreases. Addition of boron further reduces reactivity until the configuration becomes even more subcritical. Later, as for example when alterations are being made to the core and the rods, the reactor could again become critical and, with positive coefficients, be severely damaged. It is extremely important therefore that reserve negative reactivity be held in readiness to be inserted in order to buy time to remove fuel or moderator or take other suitable action.

With spare negative reactivity available for shutdown margin, the conditions and procedures given below are suggested for the HWOCR following a reactor shutdown:

1. A normal reactor scram should cause both groups of shutdown rods to be inserted.

2. Immediately following the scram, half the rods of each of the two rod groups should be withdrawn and remain in the withdrawn position throughout the shutdown period and subsequent restart. A reduction in coolant temperature and the addition of boron would supply the operating shutdown margin, leaving 2%  $\Delta k_e$  in one bank of rods as reserve against unplanned criticality.

Although the boron addition system is useful for its intended purpose, it has certain limitations. It is not capable of the fast response required of a safety system, and it may require the operation of auxiliary devices, such as moderator circulating pumps, in order for it to be used. Also, the amount of boron dissolved in the moderator is much more difficult to measure than is the position of each shutdown rod. One of our major reasons for recommending that spare negative reactivity be available in the form of withdrawn shutdown rods is that the boron concentration might slowly be reduced unknowingly until criticality was achieved.

Another aspect of shutdown margin is related to the maximum reactivity that can be introduced by optimum voiding. A reactivity increase of 1.1% for a complete loss of coolant was used by AI-CE in estimating the reactivity needed in the shutdown rods. However, complete voiding does not correspond to maximum reactivity control needs; rather, various spatial void distributions and coolant temperature distributions need to be considered. Thus further analyses are needed to determine the maximum reactivity addition possible from an optimum voiding in order to allow an evaluation of the reactivity needed in the shutdown rods. A satisfactory shutdown margin must be achieved by either of the shutdown systems discussed in Section 5.6.4.

#### 5.6.7 Conclusions

The positive coolant temperature coefficient of the HWOCR imposes severe demands on the operation of the safety and control systems. Further, the containment system is not independent of the safety system,

since performance of the containment system as proposed requires that the safety system shut down the reactor. The safety and control systems envisioned in the design report appear deficient in the areas of reliability and performance; however, we believe that these deficiencies can be corrected and satisfactory systems can be applied to the HWOCR.

The safety system should be split into two separate and independent shutdown systems. Two sets of instruments and shutdown rods are required. Each shutdown system should have sufficiently fast response and sufficient reactivity to give protection. The use of two highly reliable independent systems appears necessary to decrease the probability of shutdown failure to a satisfactory level. Further analyses will be required to establish the necessary response time and reactivity control, but the specified insertion speed of the shutdown rods appears too slow. The total reactivity control of  $4\% \Delta k_e$  presently available in the 84 shutdown rods may be sufficient but should be divided equally between the two shutdown systems to provide  $2\% \Delta k_e$  in each set of rods. The two sets of shutdown rods must have drive mechanisms of different design to reduce the probability of a common-mode failure.

Reserve negative reactivity should be available when the reactor is in a shutdown condition. Such reserve reactivity can be obtained by the withdrawal of a part of each set of shutdown rods after an evaluation of the situation following reactor shutdown. These rods should be maintained in the withdrawn position until the next reactor shutdown.

The rod control system for normal power regulation of the reactor should be made more reliable through the use of multiple controllers. In addition, both the amount and rate of reactivity change available for power control should be increased to provide for continued control of the reactor following possible reactivity perturbations during plant operation. An increase in the diameter, length, or number of vertical control rods allocated to power control will be needed. The necessary reactivity change rate appears readily obtainable.

References

1. Combustion Engineering, Inc., and Atomics International, Heavy Water Organic Cooled Reactor - 1000 Mwe Nuclear Power Plant Preliminary Conceptual Design, USAEC Report AI-CE-Memo-6, Vol. II, Oct. 1, 1965.
2. C. F. Colebrook, Turbulent Flow in Pipes with Particular Reference to the Transition Region Between Smooth and Rough Pipe Laws, Proc. Inst. Civil Engrs. (London), 11: 133 (1939).
3. L. F. Moody, An Approximate Formula for Pipe Friction Factors, Mech. Eng., 69: 1005-1006 (1939).
4. J. P. Waggner, Friction Factors for Pressure-Drop Calculations, Nucleonics, 19: 145 (1961).
5. I. E. Oldaker, Sheath Temperature - A G-20 Computer Program for Fuel Bundles, Canadian Report AECL-2269, May 1965.
6. Massachusetts Institute of Technology, In Pile Loop Irradiation Studies of Organic Coolant Materials, Report MIT-334-33, Nov. 1, 1965.
7. M. Silberberg and D. A. Huber, Forced-Convection Heat Transfer Characteristics of Polyphenyl Reactor Coolants, USAEC Report NAA-SR-2796, Atomics International, Jan. 15, 1959.
8. W. N. Bley, An In-Pile Loop Study of the Performance of Polyphenyl Reactor Coolants, USAEC Report NAA-SR-2470, Atomics International, Sept. 15, 1958.
9. F. Lanza, R. Ricque, and J. Villeneuve, Heat Transfer by Organic Liquids, paper presented at Third United Nations International Conference on the Peaceful Uses of Atomic Energy, Geneva, 1964, A/Conf 28/P/93.
10. Atomics International, Organic Heat Transfer Manual, USAEC Report NAA-SR-Memo-7343, Dec. 1, 1962.
11. H. Lurie and J. M. Robinson, Critical Heat Flux of Some Polyphenyl Coolants, USAEC Report NAA-SR-Memo-7524, Atomics International, Sept. 28, 1962.
12. T. C. Core and K. Sato, Determination of Burnout Limits of Santowax OMP, USAEC Report AGC-1672, Aerojet-General Corporation, Sept. 15, 1959.

13. D. G. Boxall et al., Development of Fuel and Coolant Tubes for a Reactor Cooled by Organic Liquid, paper presented at Third United Nations International Conference on the Peaceful Uses of Atomic Energy, Geneva, 1964, A/Conf 28/P/23.
14. J. T. Rogers and G. M. Barns, DNB Fluxes in an Annular Test Section for a Terphenyl Coolant Containing 30 Per Cent High Boilers, Report R63CAP67, Canadian General Electric Company, Ltd., June 1965.
15. J. T. Rogers, Heat Transfer Failure Mechanisms in Simulated Organic Cooled Fuel Bundles, Report R64CAP10, Canadian General Electric Company, Ltd., May 1965.
16. J. Howieson and G. D. McPherson, Cooling Mixing in 19-Element Fuel Bundles, Report TDSI-31, Atomic Energy of Canada, Ltd., July 1961.
17. H. Chelemer and L. S. Tong, Engineering Hot-Channel Factors for Open-Lattice Bores, Nucleonics, 20(9): 68-73 (September 1962).
18. J. E. Frank, R. D. Hahn, and P. S. Olson, Fuel Element Design Analysis, Specifications and Examination Procedures for HWOCR EXP-NRU-305 Experiments, USAEC Report NAA-SR-MEMO-11135, Atomics International, Mar. 9, 1965.
19. H. Pearlman and R. F. Dickerson, Carbide Fuel Fabrication and Performance, paper presented at Third United Nations International Conference on the Peaceful Uses of Atomic Energy, Geneva, 1964, A/Conf 28/P/234.
20. C. W. Wheelock, Carbide Fuels in Fast Reactors, USAEC Report NAA-SR-10751, Atomics International, Sept. 15, 1965.
21. A. Strasser, C. W. Wheelock, and L. Niemark, Uranium-Plutonium Carbide Fuels for Fast Breeder Reactors, p. 126 in Proceedings of Fast Breeder Reactor Conference, Detroit, April 1965, Report ANS-100, American Nuclear Society.
22. Personal communication from S. Arneson (Atomics International) to R. E. Adams (ORNL), Oct. 28, 1965.
23. Combustion Engineering, Inc., and Atomics International, Heavy Water Organic Cooled Reactor, USAEC Report AI-CE-Memo-25, Mar. 29, 1966.
24. R. S. Kemper et al., Fabrication of Zircaloy-2 Clad Thorium Uranium Alloy Fuel Elements, USAEC Report HW-79843, Hanford Atomic Products Operation, March 1964.

25. Hanford Atomic Products Operation, Quarterly Progress Report, Division of Reactor Development, December 1964, USAEC Report HW-84609.
26. S. R. Nemeth (Ed.), Thorium-1.4 wt Percent  $^{235}\text{U}$  Uranium Metal Fuel Tubes - Fabrication and Irradiation in HWCTR, USAEC Report DP-943 (Suppl.), Savannah River Laboratory, April 1965.
27. J. H. Kittel et al., Effect of Irradiation on Thorium and Thorium-Uranium Alloys, USAEC Report ANL-5674, Argonne National Laboratory, April 1963.
28. W. R. Thomas et al., Irradiation Experience with Zircaloy-2, paper presented at Third United Nations International Conference on the Peaceful Uses of Atomic Energy, Geneva, 1964, A/Conf 28/P/21.
29. Personal communication from P. H. Permar (Savannah River Laboratory) to R. E. Adams (ORNL), Feb. 3, 1965.
30. Personal communication from M. S. Picklesimer (ORNL) to R. E. Adams (ORNL), Dec. 28, 1965.
31. Hanford Laboratories, Progress in Plutonium Utilization, USAEC Report HW-83601, December 1964.
32. R. H. Hood (Comp.), Heavy Water Moderated Power Reactors Progress Report - March Through June 1965, USAEC Report DP-975, Savannah River Laboratory, August 1965.
33. M. F. Lyons et al., Post Irradiation Examination of High Burnup Molten  $\text{UO}_2$  Fuel Rods, Trans. Am. Nucl. Soc., 8(1): 42 (June 1965).
34. A. Biancheria and R. J. Allio, Fabricating  $\text{PuO}_2\text{-UO}_2$  Fuels - How Leading Processes Compare, Nucleonics, 23(12): 46 (December 1965).
35. J. S. Ballif III, W. H. Friske, and R. B. Gordon, Fabrication and Testing of Prototype APM-Clad  $\text{UO}_2$  Fuel Elements, New Nuclear Materials Including Non-Metallic Fuels, IAEA, Vienna, 1963.
36. D. G. Boxall et al., Development of Fuel and Coolant Tubes for a Reactor Cooled by Organic Liquid, paper presented at Third United Nations International Conference on the Peaceful Uses of Atomic Energy, Geneva, 1964, A/Conf 28/P/23.
37. A. R. Olsen et al., Properties and Prospects of Thoria-Base Nuclear Fuels, USAEC Report ORNL-TM-1297, Oak Ridge National Laboratory, November 1965.

38. H. Pearlman, Corrosion of Uranium, Thorium and Uranium Alloys in Sodium and Organics, USAEC Report TID-7546, Bk. 2, p. 565, November 1957.
39. Euratom's Scientific Activities - ORGEL Program Scientific Studies, EUR-1830.e, Pt. II, 1964.
40. Danish Atomic Energy Commission Research Establishment, Riso, Metallurgy Department, Annual Progress Report Ending March 31, 1965, Riso Report 110, July 1965.
41. A. Sawatzky, The Behavior of Zirconium Alloys in Santowax OM Organic Coolant at High Temperatures, Canadian Report AECL-2118, October 1964.
42. W. M. Campbell et al., Development of Organic Liquid Coolants, paper presented at Third United Nations International Conference on the Peaceful Uses of Atomic Energy, Geneva, 1964, A/Conf 28/P/15.
43. W. E. Parkins, Corrosion Effects with Organic-Liquid Reactor Coolants, Corrosion of Reactor Materials, Vol. 2, p. 503, IAEA, Vienna, 1962.
44. J. E. Cunningham et al., Fuel Dispersions in Aluminum-Base Elements for Research Reactors, USAEC Report TID-7546, Bk. 1, p. 269, November 1957.
45. N. Hansen et al., Sintered Aluminum Products for Organic Reactor Applications, paper presented at Third United Nations International Conference on the Peaceful Uses of Atomic Energy, Geneva, 1964, A/Conf 28/P/421.
46. R. C. Waugh, The Reaction and Growth of Uranium Dioxide-Aluminum Fuel Plates and Compacts, USAEC Report ORNL-2701, Oak Ridge National Laboratory, March 1959.
47. A. S. Kaufmann (Ed.), Nuclear Reactor Fuel Elements - Metallurgy and Fabrication, p. 287, Interscience, New York, 1962.
48. J. A. Milko, Diffusion Characteristics of Thorium and Aluminum, USAEC Report ORNL-1774, Oak Ridge National Laboratory, December 1954.
49. D. G. Boxall and D. J. Fleming, Applications of Oxide Dispersion-Strengthened Aluminum Alloys in Organic Cooled Power Reactors, p. 407 in Can. Mining Met. Bull., April 1965.

50. D. Gualandi and P. Jehenson, Contribution to the Studies of the Technology of Al-Al<sub>2</sub>O<sub>3</sub> Compounds with Regard to Nuclear Application, paper presented at Third United Nations International Conference on the Peaceful Uses of Atomic Energy, Geneva, 1964, A/Conf 28/P/733.
51. J. A. Van Echo and S. W. Porembko, Long-Term Creep Rupture of Sintered Aluminum Powder and Zircaloy-2 Alloys, USAEC Report BML-X-10113, Battelle Memorial Institute, June 1965.
52. R. A. Harlow (Ed.), SAP Materials Handbook -- Draft (no date).
53. J. E. Dorn (Ed.), Mechanical Behavior of Materials at Elevated Temperatures, McGraw-Hill, New York, 1961.
54. Design Practice: The Carolinas-Virginia Tube Reactor, Power Reactor Technol., 6(4): 63-81 (Fall 1963).
55. R. S. Makens (Ed.), Organic Coolant Summary Report, USAEC Report IDO-11401, pp. 8 and 135, Phillips Petroleum Company, December 1964.
56. L. E. Gardner, Catalytic Hydrocracking of High Boiler in Nuclear Reactor Coolant, USAEC Report IDO-16877, Phillips Petroleum Company, May 1963.
57. J. Libenthal, Preliminary Safety Analysis of the Piqua Hydrocracker Facility, attachment of a letter from J. P. Lyons of Phillips Petroleum Company, Idaho Falls to Idaho Operations Office, AEC, Nov. 8, 1965 (Ly-428-65A).
58. R. O. Bolt and J. G. Carroll, Radiation Effects on Organic Materials, pp. 294 and 302, Academic Press, New York, 1963.
59. T. H. Timmins, E. A. Mason, and D. T. Morgan, Effect of Reactor Irradiation on Santowax WR: Irradiations from 425°F to 800°F at 40% Fast Neutron Fraction, Report MIT-334-34, Massachusetts Institute of Technology, February 1966.
60. J. F. Zack, Jr., S. Berg, and N. M. Ewbank, In-Pile Capsule Experiments to Determine the Effect of Fast Neutrons on the Radiolytic Decomposition Rate of Terphenyls, USAEC Report NAA-SR-7395, Atomic International, 1963.
61. E. A. Mason and T. H. Timmins, Interpretation of Radiolysis of Terphenyls -- Apparent Kinetics and Fast Neutron Effect, Trans. Am. Nucl. Soc., 8(2): 420 (1965).

62. A. W. Boyd and H. W. J. Conner, The Radiolysis of Ortho and Meta Terphenyl, I: With a Mixture of Fast Neutrons and Gamma Rays at Dose Rates of 0.1 and 0.3 w/g, Canadian Report AECL-2258, May 1965.
63. W. G. Burns et al., The Radiation and Thermal Stability of Some Potential Organic Moderator-Coolants, VI: The Effect of Temperature on the Radiolysis of Biphenyl, Isopropyl Biphenyl, Metaterphenyl and Santowax R, British Report AERE-R 3989, August 1962.
64. R. T. Keen et al., Radiolysis Products of Polyphenyl Coolants, Part I. In-Pile Loop Irradiations, USAEC Report NAA-SR-3455, Atomics International, March 1962.
65. J. Chernick and H. Kouts, Nuclear Engineering Progress Report, May 1 to August 31, 1963, USAEC Report BNL-823, pp. 1-19, Brookhaven National Laboratory.
66. H. W. Schleicher, Corrosion Studies in Organic Coolants for Nuclear Reactors, Report EUR-379.3, Euratom, 1963.
67. W. E. Parkins, Corrosion Effects with Organic Liquid Reactor Coolants, IAEA Preprint CN-13/15.
68. G. Ito, F. Sawayanagi, and Y. Shimizu, Corrosion of Nuclear Metallic Materials in Organic Coolants, IAEA Preprint CN-13/9.
69. R. F. S. Robertson et al., Long Term Irradiation of SAP-Clad UO<sub>2</sub> Fueled, Trefoil Bundles in the X-7 Organic Cooled Loop, Canadian Report AECL-1782, May 1963.
70. A. R. Bancroff, D. H. Charlesworth, and J. H. Duerksen, Impurity Effects in the Fouling of Heat Transfer Surfaces by Organic Coolants, Canadian Report AECL-1913, May 1963.
71. Personal communications of P. R. Kasten and R. C. Olson (ORNL) with D. H. Charlesworth (AECL, Chalk River) and S. R. Hatcher (AECL, Whiteshell), Feb. 2, 1966.
72. D. H. Charlesworth, Fouling in Organic-Cooled Systems, Canadian Report CRCE-1096 (AECL-1761), April 1963.
73. Personal communication from C. A. Trilling (Atomics International) to L. B. Yeatts (ORNL).

74. Bureau of Mines, Division of Explosives Technology, Explosibility Characteristics of Irradiated Biphenyl and Terphenyl Isomers (OMRE Samples), Final Report 3747, 1959.
75. S. R. Hatcher and L. J. Cornett, Spontaneous Combustion Hazards of Organic Coolants, Canadian Report WDI-8, August 1963.
76. T. J. Haley et al., Toxicologic Studies on Polyphenyl Coolants Used as Atomic Reactor Moderator-Coolants, Toxicol. Appl. Pharmacol., 1(5): 515-523 (1959).
77. G. H. Hanson (Ed.), Experimental Organic Cooled Reactor Safety Analysis, p. vl.1, USAEC Report IDO-16820, Phillips Petroleum Company, March 1963.

## 6. ENGINEERING REVIEW OF PLANT DESIGN

The AI-CE design<sup>1</sup> was used as the overall plant reference design in this study, as mentioned previously, although there are essential differences between the AI-CE and B&W designs in the reactor vessels and re-fueling systems. The principal differences were discussed in Chapter 3.

This review of plant features is concerned primarily with

1. the feasibility of developing, building, and operating the plant under the specified conditions and applicable ground rules of this study,
2. a comparison of systems, where appropriate, with their counterparts in the heavy-water or pressurized-water plants of the advanced converter study<sup>2</sup> to establish bases for capital cost normalizations,
3. a comparison of AI-CE and B&W concepts where differences exist.

In the following discussions, principal features of the plant systems and major components are summarized; it is assumed that the reader will have access to the AI-CE and B&W conceptual design reports<sup>1,3,4</sup> for more detailed information. Along with the discussions, we have indicated where we were unable to verify design values as presented or where we think that modifications to the design may improve cost, reliability, or safety of the plant.

Comparisons of HWO CR systems with systems of other advanced-converter reactors relative to design and cost normalization were limited to comparisons of building requirements, turbine-generator facilities, and some of the moderator auxiliaries. The concepts most similar to the HWO CR are the two heavy-water reactor concepts discussed in Ref. 2. These heavy-water reactors operate with D<sub>2</sub>O coolant pressures in the range of 1800 to 1900 psia at a maximum temperature of approximately 580°F, and they have Zr-2 1/2% Nb pressure tubes. In comparison, the HWO CR operates with an organic coolant pressure of about 400 psi and a maximum temperature of 750°F, and it has SAP-895 pressure tubes. The distinct differences in reactor and heat transfer system designs due to the different coolants limit the extent to which normalization comparisons of these systems are meaningful.

## 6.1 Reactor Vessels and Internal Structures

### 6.1.1 Calandria and Shield

The AI-CE concept has a stainless steel calandria 25 ft in outside diameter and 20 ft high that is supported at the top tube sheet of the lower end shield and contains the D<sub>2</sub>O moderator fluid. The physical arrangement is indicated in Fig. 6.1. The Zircaloy tubes, which are mechanically rolled into the tube sheets, are sized to provide an annular clearance between them and the SAP process tubes. Additional vertical and horizontal penetrations are provided for instrumentation, control, and maintenance. This design has an emergency spray system that can bathe the top tube sheet with D<sub>2</sub>O from nozzles if a drop in moderator level occurs. A level-control tank maintains a pressure of 2 psig at the top tube sheet, and a helium cover gas is maintained in the tank. Bearing pads welded to the bottom of the calandria bear on mating pads welded to the top of the lower shield, and keys and keyways prevent rotation and displacement of the calandria due to thermal cycling. Since the structure associated with the proposed design is subject to significant stresses in both the tubes and calandria top corner welds, and a major shutdown is required to replace a defective tube (by semiremote procedures), it would be desirable to investigate other design approaches that either eliminate or reduce these problems.

The end and thermal shields are made of carbon steel and are cooled with treated light water. Eight curved sections form the cylindrical thermal side shield that surrounds the calandria. Flexible seals are used to contain the CO<sub>2</sub> atmosphere of the calandria vault. Seals must be used at all control rod penetrations, between the thermal-shield sections, and between the thermal and end shields. The seal to be used at the intersection of the side thermal shield and the end shields must simultaneously accommodate circumferential and axial expansion.

The design does not provide for inspection and/or replacement of the D<sub>2</sub>O spray nozzles of the emergency spray system. Since flow blockage in several nozzles would influence reactor safety, we feel that inspection and replacement provisions should be included. Also, a method and

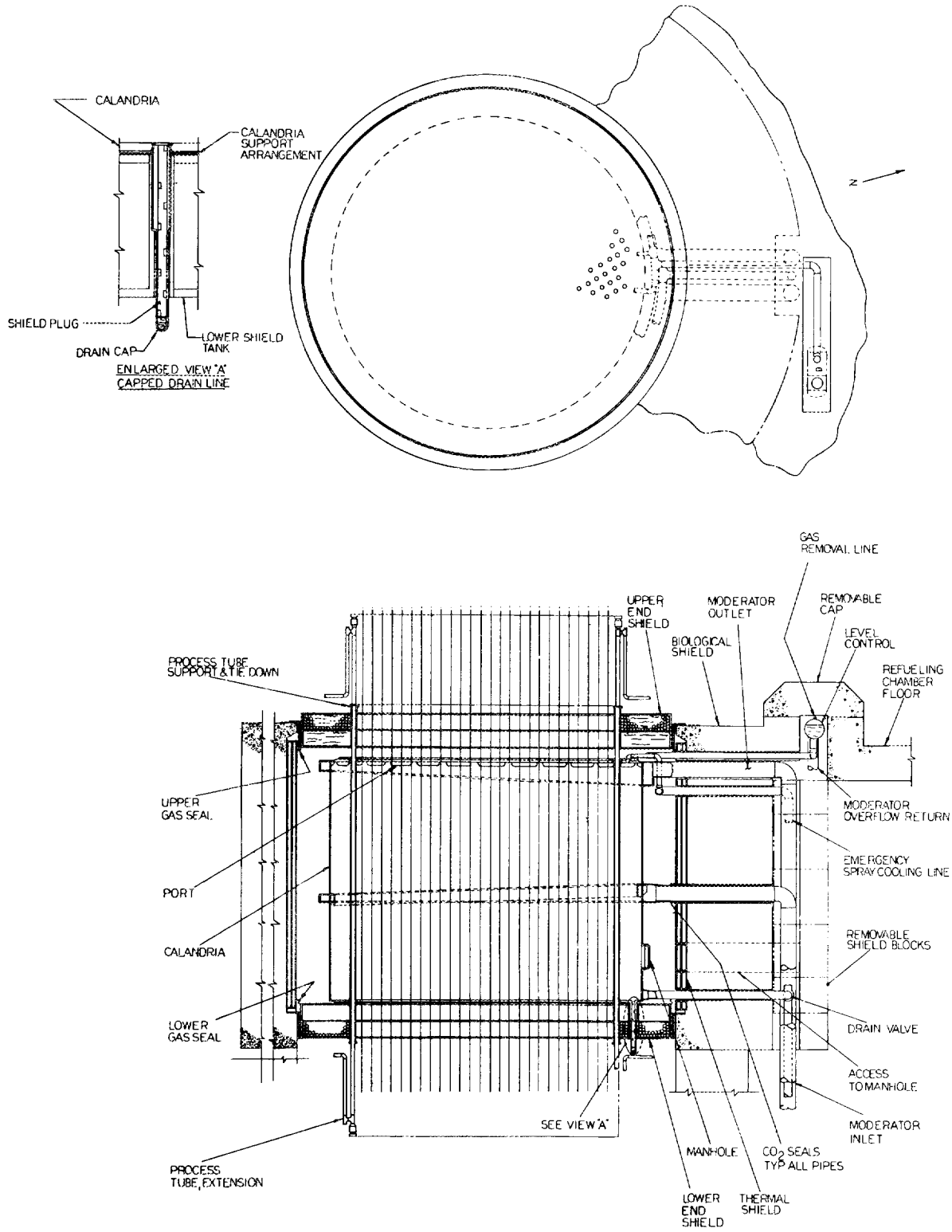


Fig. 6.1. AI-CE Reactor Components. (From Ref. 1.)

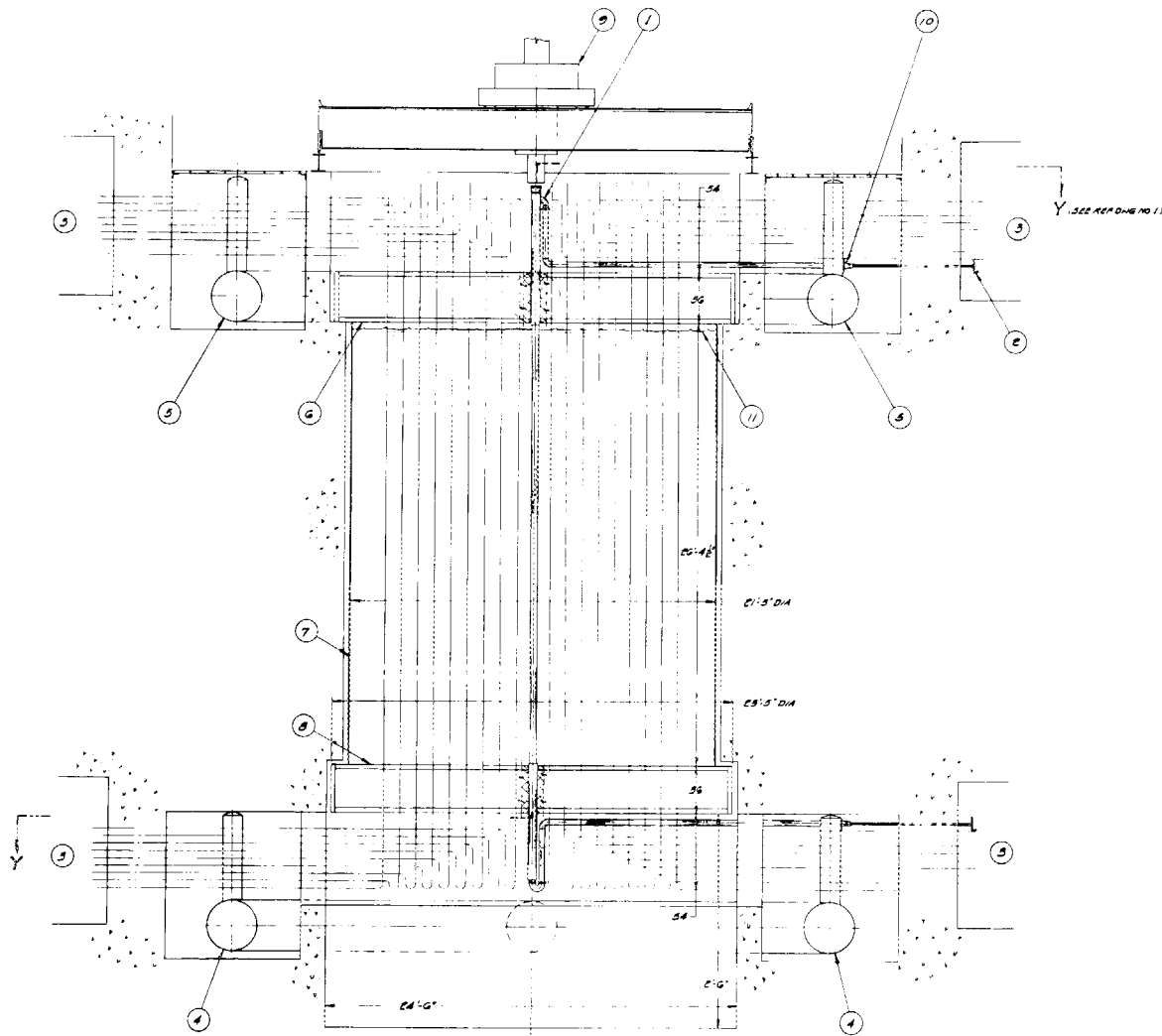
procedure should be established for the remote or semiremote replacement of a defective CO<sub>2</sub> bellows seal in a vertical control rod housing.

In the B&W design the cylindrical calandria tank and end shields are fabricated as one large unit and arranged as shown in Fig. 6.2. This design, coupled with the fuel channel assembly design, eliminates the calandria tubes as part of the calandria structure. The B&W shield-calandria vessel is approximately 22 ft in diameter and 32 ft high and is fabricated of stainless steel. Lead shot is used in the end shields, which are cooled with light water. No thermal side shield is shown in the B&W design, but we have assumed that one would be required as in the AI-CE design.

### 6.1.2 Fuel Channel Assemblies

AI-CE Assembly. The AI-CE fuel channel assembly, shown in Fig. 6.3, consists of a SAP process tube with stainless steel transition sections on each end, top and bottom carbon steel extensions to which the tube transition sections are welded, and mechanical end seal plugs at the top and bottom. Pigtail inlet and outlet piping is welded to the top and bottom extensions, and the top extension is bolted to and supported by the top tube sheet of the upper end shield. The process tube is supported by the upper extension, which passes through a stationary sleeve in the upper end shield. Alignment bearings are also located in this sleeve. The process tube passes through the Zircaloy-2 calandria tube and is welded to the lower extension. This lower extension passes through a sleeve in the lower end shield, which contains a sliding alignment bearing, and provides a packed gland to allow vertical thermal expansion and contraction of the fuel channel. This gland must seal the CO<sub>2</sub> gas used as a thermal barrier in the annular space between the pressure and calandria tubes. Both top and bottom extension pieces are provided with antirotational keys to resist torsion loads from the pigtail piping.

As shown, stainless steel-to-carbon steel welds are made between the pressure tube transition sections and the fuel channel extensions. These dissimilar metal welds could be avoided by welding a carbon steel piece to the transition sections during shop fabrication.



- LEGEND**
- ① FUEL CHANNEL ASSEMBLY
  - ② VALVE OPERATOR
  - ③ VALVE ACCESS ROOM
  - ④ OUTLET HEADER (TO PUMP)
  - ⑤ INLET HEADER (FROM STEAM GENERATOR)
  - ⑥ UPPER SHIELD
  - ⑦ MODERATOR TANK
  - ⑧ LOWER SHIELD
  - ⑨ FUEL TRANSFER MACHINE
  - ⑩ FUEL CHANNEL ISOLATION VALVES
  - ⑪ MODERATOR LEVEL

SECTION Z-Z  
(SEE REF DWG NO 1)

THE BABCOCK & WILCOX CO.		H.N.O.C.R.	
ATOMIC ENERGY DIVISION		REACTOR ARRANGEMENT - ELEVATION	
TOLERANCES	SEE DRAWING	SCALE	3/8" = 1'-0"
WELDING SYMBOLS	SEE DRAWING	DATE	10/15/57
SECTIONAL DIMENSIONS	SEE DRAWING	DRAWN BY	J. J. GIBSON
PRACTICAL DIMENSIONS	SEE DRAWING	CHECKED BY	J. J. GIBSON
ANGULAR DIMENSIONS	SEE DRAWING	APPROVED BY	J. J. GIBSON
BREAK ALL CORNERS	SEE DRAWING	PROJECT NO.	A30525
PROJECT NO.	A30525	REV.	0
PROJECT NAME	H.N.O.C.R.	DATE	10/15/57
PROJECT LOCATION	SEE DRAWING	SCALE	3/8" = 1'-0"
PROJECT ARCHITECT	SEE DRAWING	PROJECT NO.	A30525
DATE	10/15/57	REV.	0
DESIGNER	J. J. GIBSON	DATE	10/15/57
CHECKED BY	J. J. GIBSON	SCALE	3/8" = 1'-0"
APPROVED BY	J. J. GIBSON	PROJECT NO.	A30525
PROJECT NO.	A30525	REV.	0
PROJECT NAME	H.N.O.C.R.	DATE	10/15/57
PROJECT LOCATION	SEE DRAWING	SCALE	3/8" = 1'-0"
PROJECT ARCHITECT	SEE DRAWING	PROJECT NO.	A30525

Fig. 6.2. B&W Calandria. (From Ref. 4)

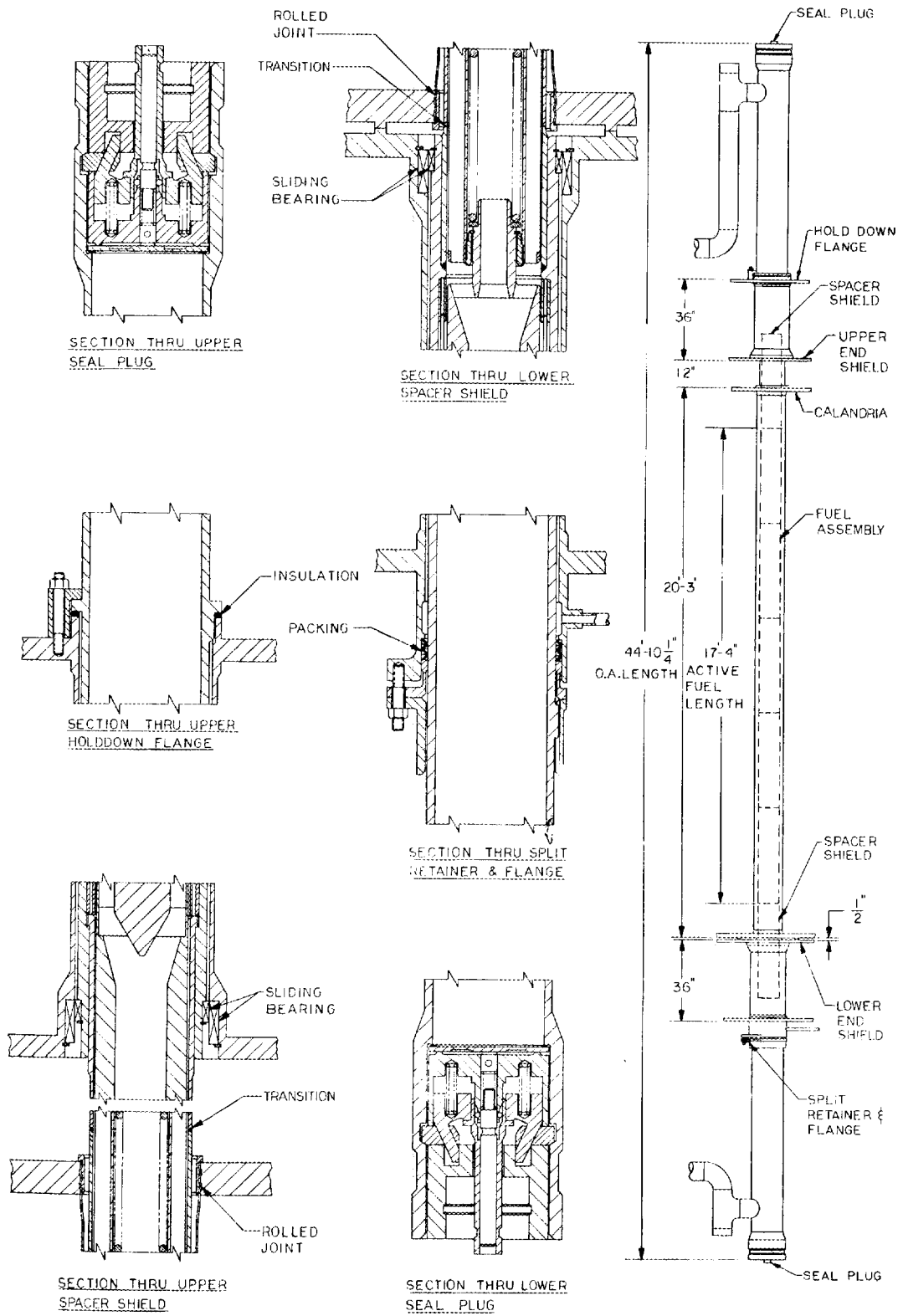


Fig. 6.3. AI-CE Process Tube Design. (From Ref. 1)

Latch assemblies, which position and support the fuel column, are mounted in the top and bottom extension pieces. These are spring-loaded cam-operated devices that must be activated by coordinated operations of both the top and bottom refueling machines. The present design should be revised to provide for replacement of the latch assemblies, and a latch assembly replacement device should be incorporated in the design of the refueling-machine head. The consequences of a latch failure must be evaluated with respect to refueling operations and dislocated fuel assemblies. Proper operation of the channel latches is imperative, since they must support the entire fuel column and act to retain the column during refueling operations when one machine ram is retracted.

The pressure tube replacement procedure requires the development of remotely operated cutting, welding, and inspection devices, which are difficult to manipulate. Nonetheless, the development of such devices appears feasible. The particular tube transition piece-to-extension weld joint configurations shown in Fig. 6.3 appear to be difficult to make and inspect remotely. While some success has been achieved in designing and testing equipment to perform similar operations,<sup>5,6</sup> additional design and development work will be required to tailor such machines and inspection devices to the exact joint configurations to be used. This type of program can greatly increase development costs. Remote field-welding, cutting, and inspection operations should be avoided whenever possible.

Commercial tubing tolerances will not maintain the radial clearance chosen for this design. It appears that due to accumulative tolerances, the radial clearance between the pressure and calandria tubes can be reduced to the point where the tubes touch. The lack of clearance would increase the chance of damaging a calandria tube during a pressure tube removal operation.

In the present design, the process tube is allowed to expand downward. In addition to a hoop-stress loading, the tube is subjected to an axial loading due to the weights of the fuel column, channel hardware, lower extension, and organic fluid and to compression from spring and hydraulic forces. These steady-state axial loads result in an axial stress that is below the allowable design stress chosen for the SAP

material. On the basis of maximum shear theory the equivalent rupture stress will be greater than the axial stress but less than the hoop stress used to calculate the process tube wall thickness; however, the hoop stress approaches the allowable stress based on 80% of the stress required to rupture the tube in 30 years. This allowable stress is based on an extrapolation of available experimental data. In addition to the steady-state axial loads, short-term loadings will be introduced by operations involving the attachment of the refueling machine and operation of the machine-head rams. Thus, while the design appears feasible based on present information and interpretations, additional data are needed to evaluate it adequately. An allowable design stress can be firmly established only after fabricating and testing actual pressure tubes over an extended period of time under simulated operating conditions.

A pressure tube ratchetting problem may develop due to thermal expansion and contraction of the tube associated with binding of the anti-rotational keys located in the bottom extensions. The 1/4-in. allowable deflection of the extensions (due to expansion of the pigtail piping) and the refueling-machine head-coupling operations could produce forces that would act to bind the keys and contribute to the ratchetting problem.

A procedure is needed for replacing a damaged calandria tube, and semiremotely operable devices that can reliably replace a tube must be designed, developed, and tested. This operation must follow removal of the associated process tube and its extensions. Though no time estimates for these operations are given in the AI-CE report, we estimate that at least 20 hr would be required to replace a calandria tube, including the time for D<sub>2</sub>O drainage and filling operations. Since the calandria must be drained to perform this operation, additional time will be required for the radiation level in other fuel tubes to decay sufficiently for the moderator to be drained. Equipment and procedures are also needed to limit the escape of the CO<sub>2</sub> gas during a process tube replacement operation and the escape of both CO<sub>2</sub> and helium gases during calandria tube replacement operations. During a process tube replacement operation, consideration must be given to the problems associated with induced and

airborne activity, decontamination, segmentation of the tube, negative pressure for semiremote operation, and shielded carrier handling.\*

B&W Assembly. The B&W channel assembly, shown in Fig. 6.4, is based on a unitized design in which both the pressure and calandria tubes are shop fabricated in one assembly. Axial thermal expansion of both tubes is accommodated by expansion joints located near the bottom of the lower end shield extension. Flow in all channels is downward; a closure plug is used at the top, and piping U-bends with mechanical joints are used at the top and bottom extensions. A cost savings could be effected and reliability increased by replacing the mechanical joints with welded closures.

A fuel channel is installed or replaced semiremotelly by field welding the top and bottom sections to the top and bottom end shield extension pieces, respectively. Provision is made for retaining the D<sub>2</sub>O in the calandria during a channel replacement operation by installing a maintenance can. During certain operations the moderator level would have to be lowered and consideration given to associated thermal stresses that might develop in the Zircaloy tubes or in other parts of the reactor structure. A method must be devised to limit the escape of the helium cover gas during channel replacement operations.

---

\*It has been noted that AI-CE report (Memo-25) on the 500-Mw(e) demonstration plant design presents several new features that improve the conceptual design of the process tube assembly and the calandria vessel.

The new proposed process-tube flow-turning and baffle arrangement improves the design, and the substitution of a bellows for the packing seal will prevent leakage of CO<sub>2</sub>. Of course the problem of reliability of a bellows will have to be investigated thoroughly. Increasing the lattice pitch from 10 1/2 to 11 in. should help alleviate accessibility problems. The introduction of an enlarged-diameter section near the top of the calandria vessel to accommodate expansion between the tubes and shell appears to improve the design.

The deflection of the process tube extensions at the refueling flanges has apparently increased from 0.25 to 0.33 in. The lower extension is to be designed to absorb this deflection.

The selection of a type 304 stainless steel section welded to the SA-213-T11 low-alloy steel for the extension piece permits a stainless steel-to-stainless steel field weld rather than a dissimilar-metal weld as previously required.

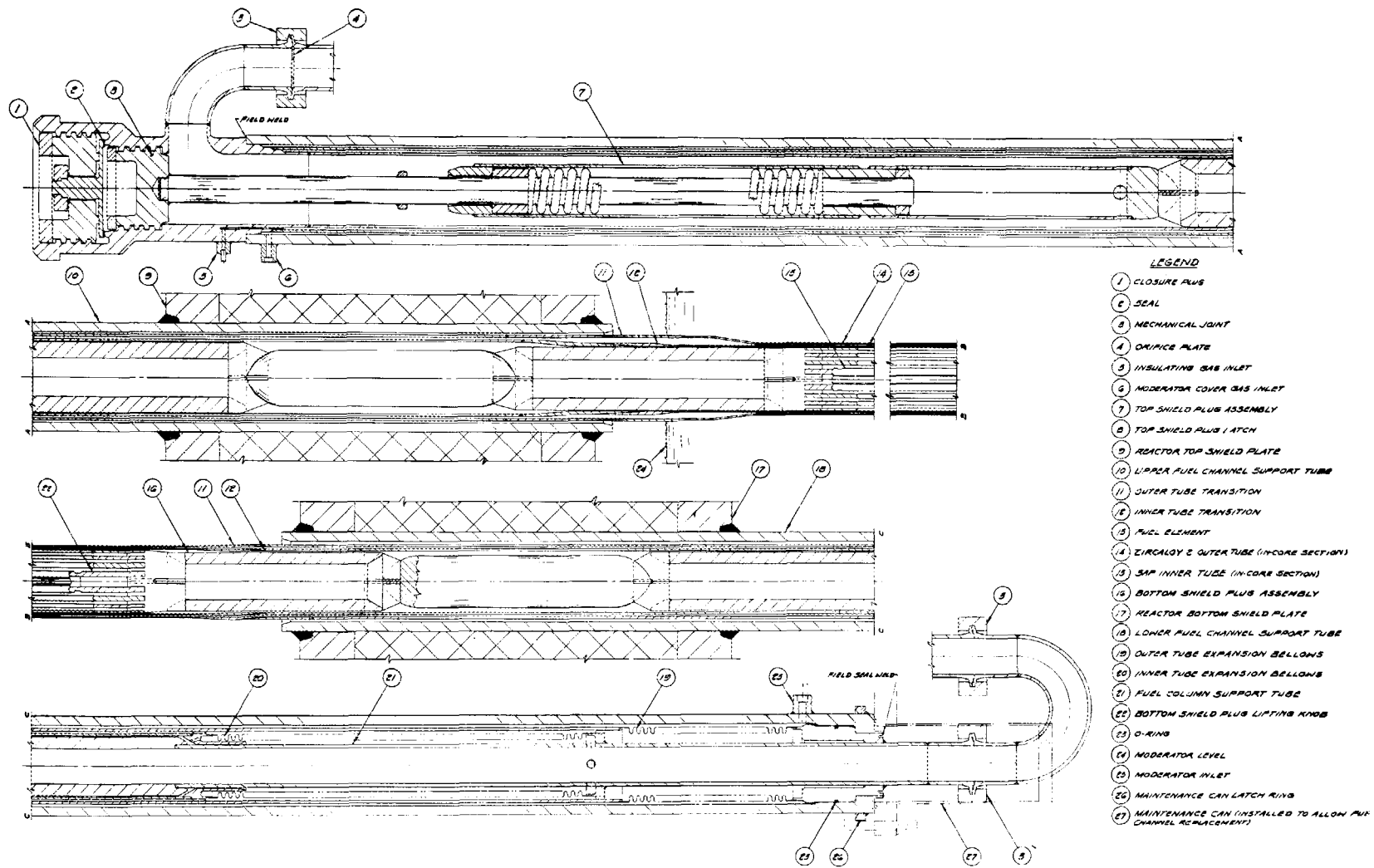


Fig. 6.4. B&W Fuel Channel Assembly. (From Ref. 3)

Shop fabrication of the entire assembly is an attractive feature of this design; however, it requires the installation of two long bellows to accommodate the thermal expansion of the tubes. Both bellows are installed within the lower end shield extension, and the inner bellows would be exposed to relatively stagnant organic coolant. Life testing of the bellows appears desirable, since failure of either bellows would require a reactor shutdown for removal of the entire channel assembly.

The 0.09-in. nominal radial clearance between the pressure and calandria tubes does not appear to be assured because of possible accumulative fabrication tolerances.

The 412-psi core inlet pressure given in Table 4.1 (and 416 psi in Table 5.1) of the B&W report<sup>4</sup> is incorrect. We find the core inlet pressure to be 281 psig for the pin-cluster design and 298 psig for the nested-cylinder design. The hoop stresses for the 5-in.-ID, 0.093-in.-wall SAP tubing with 281 or 298 psig internal pressures are about 7700 and 8170 psi, respectively. The maximum allowable stress for this material at 560°F, based on stress-rupture criteria, is 6800 psi. The thickness of the process tubes for both thorium-fueled concepts must therefore be increased about 25%. If the pressure tube ruptured or the bellows failed and permitted the Zircaloy calandria tube to be exposed to the 298-psig coolant pressure, a hoop stress of approximately 11,300 psi could be developed in the Zircaloy-2 tube. This is not an excessive stress, but it is not clear what thermal stresses would be introduced if hot organic coolant were to spray on the relatively cool Zircaloy tube.

## 6.2 Refueling and Fuel Handling

### 6.2.1 Refueling Operations

Both the AI-CE and B&W reactor concepts are dependent on reliable on-line bidirectional refueling. The AI-CE refueling assembly, shown in Fig. 6.5, is based on using two machines attached to the top and bottom extensions of the fuel channels, respectively. These machines are patterned after the CANDU prototype refueling machines, but there are significant differences due to the use of organic coolant instead of D<sub>2</sub>O

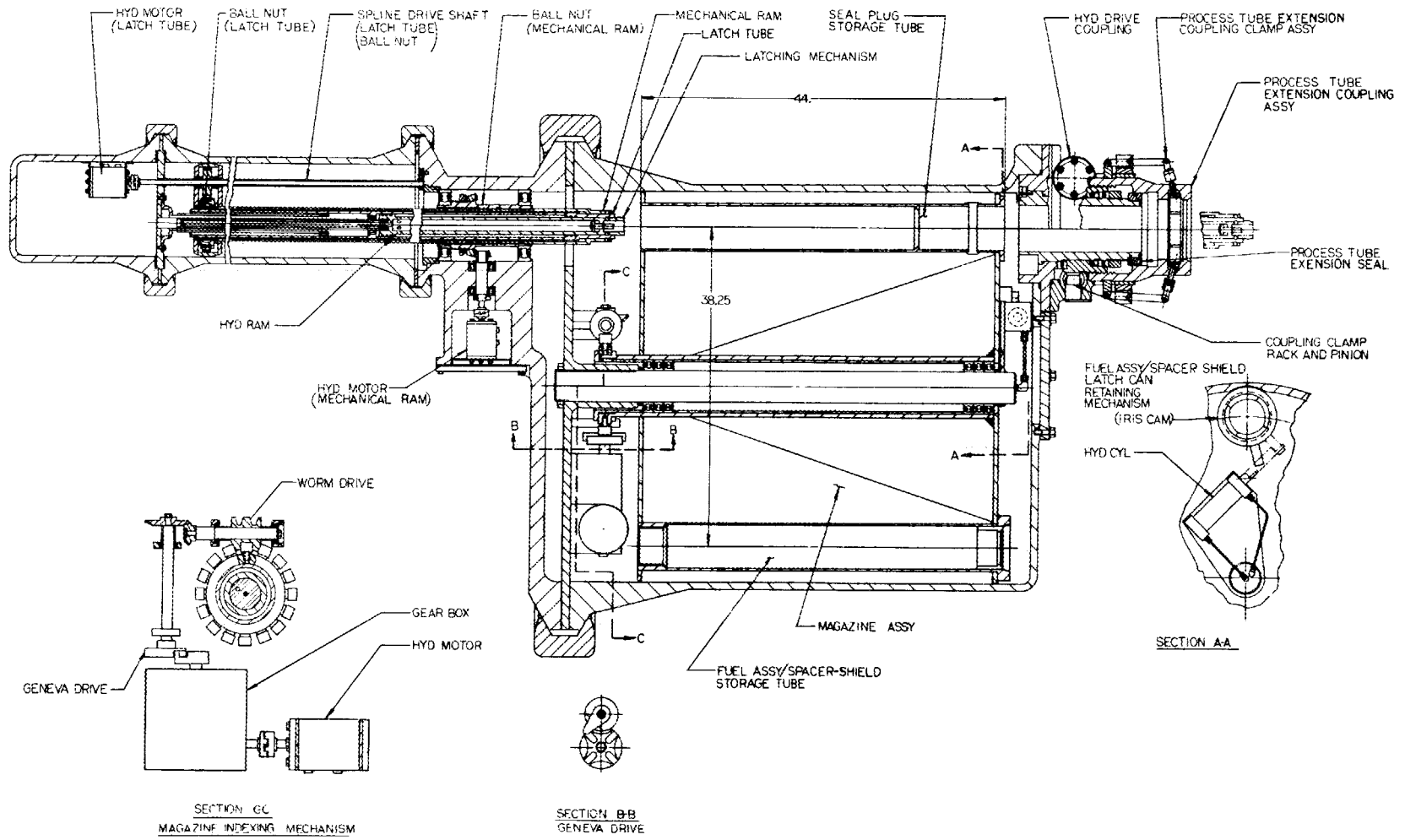


Fig. 6.5. AI-CE Refueling Machine Assembly. (From Ref. 1)

and the higher temperatures. The lubrication properties of the organic coolant are poorer than those of  $D_2O$ , and the higher temperatures present sealing and magazine-housing thermal stress problems. Life testing of the refueling-machine components and the control system will be required.

Latches in the channel normally retain the fuel column and spacer shields during the refueling operations indicated in Fig. 6.6. When the latches are released, the fuel column is supported by the refueling machine rams, which proceed to insert and remove the spacer shields and fuel assemblies by a series of coordinated axial motions and latching operations. Individual latch cans are used to transfer the spacer shields and fuel assemblies and to actuate the fuel channel latches. The top and bottom refueling-machine head-assembly controls must be carefully interlocked during refueling operations to avoid excessive ram forces on the fuel assemblies or the fuel-channel latches. Bidirectional coolant flow is used in the AI-CE concept to provide maximum cooling in the higher power regions of the core. New fuel is introduced in the coolant inlet end of each channel.

The refueling procedure must cope with problems associated with mechanical equipment failures during a refueling operation. Some postulated failures that would present serious problems are failure of the head-assembly magazine to index or failure of a ram mechanism to function with spent fuel already deposited in the magazine assembly. A failure of a refueling-machine organic-coolant line during refueling must also be considered.

Operator access to equipment under emergency conditions is not discussed in the report;<sup>1</sup> however, some degree of emergency access into the refueling area should be provided. Duplicate, or additional, instrumentation that would enable the operator to detect the cause of a failure in the automatic system and means to allow the operator to control the operations manually are desirable from the standpoints of operability and safety.

Remotely controlled television cameras would be invaluable in helping to guide the refueling machines during fuel-channel attachment operations. The lower attachment will be a sensitive operation, since the

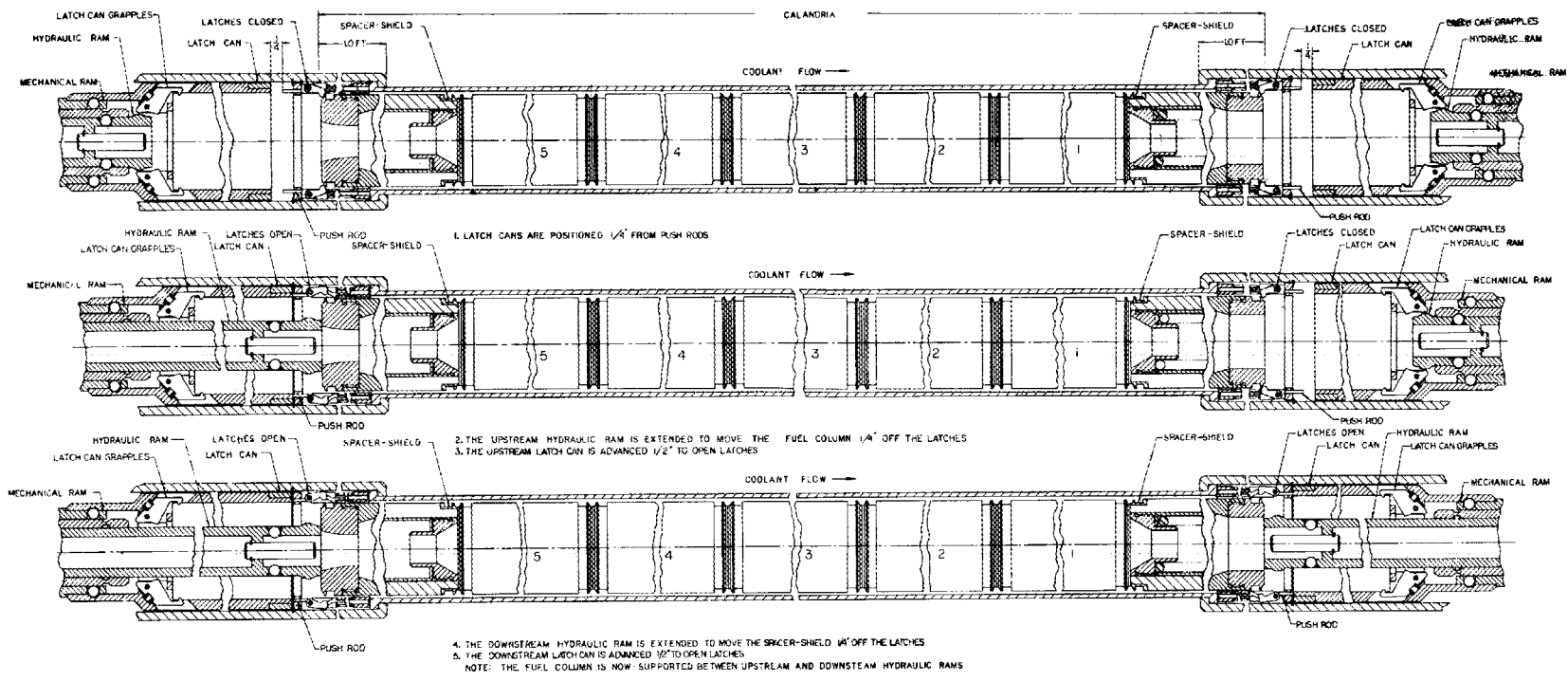


Fig. 6.6. AI-CE Refueling Sequence (Steps 1 through 5). (From Ref. 1)

extension ends, which can expand axially, may not all be in the same horizontal plane.

The time required for each fuel-assembly refueling operation is given by AI-CE as 45 min; however, we have estimated that from 90 to 180 min per fuel assembly may be required if difficulties are encountered in synchronizing the two machines and in checking procedures. Each fuel assembly is handled twice by each refueling machine, and during its life in the reactor it travels approximately 23 ft through a fuel channel pressure tube. For a complete core fuel change of 2460 assemblies and 984 spacer shields, each machine would be required to make 27,060 strokes. This includes all operations from loading a new element to discharging spent fuel. A machine stroke of approximately 185 in. is required for refueling; however, completely unloading a process tube for tube replacement requires a stroke of approximately 475 in. AI-CE indicates a maximum machine fuel ram travel of 340 in. During steps 2 through 20 (see Fig. II-39 of Ref. 1) it appears that the only cross-sectional area open for coolant flow is the 0.030-in. radial clearance between the process tube inner surface and the outer surface of the fuel-assembly end plates.

As mentioned previously, the B&W concept specifies bidirectional refueling; however, coolant flow is downward in all channels, and all refueling operations are performed by one machine operating at the top face of the reactor. Each fuel assembly is handled 12 times during its core life and, depending on the fuel-assembly concept, will travel either 162 or 170 ft through a fuel-channel pressure tube. For a complete core fuel change the refueling machine is required to make 43,056 strokes for the 299-channel concept or 48,240 strokes for the 335-channel concept. If two fuel assemblies, rather than one as stated in B&W's procedure, are loaded initially the corresponding numbers of machine strokes are reduced to 41,262 and 46,230, respectively.

Since the B&W report does not present a refueling-machine concept, we can only visualize the machine in terms of the operations required to handle the proposed fuel assemblies in the proposed fuel channels. A machine stroke of approximately 42 ft is required for refueling operations, and a stroke of approximately 46 ft will be needed to replace a

bottom shield plug. This machine must be capable of grasping either the one or two handling pins associated with the proposed fuel assemblies and of orienting the two-pin assembly. In addition to the grasping and translational motions the machine must also be able to rotate the top shield plug latch and the top closure (see Fig. 10.5.7 of Ref. 3). Latching assemblies must also be incorporated in the machine, and design consideration must be given to the manner in which components and mechanisms associated with on-line refueling operations can be repaired or replaced remotely. Consideration must also be given to the possibility of fuel elements sticking together because of coking in the stagnant regions around the alignment pins. (Piqua experience indicates that coking will take place in stagnant coolant.) If the refueling machine has a magazine for storing the shield plugs, it appears that it will have to be large enough to accommodate more than a 7-ft section. We assumed that the new and spent fuel-assembly auxiliary systems would be similar to those proposed by AI-CE.

No effort was made in this review to change the reactor vessel, internal structures, or refueling concepts proposed by AI-CE and B&W; however, an attempt was made to point out some design and development problem areas associated with each preliminary design proposal. Lack of detailed design and definitive information precluded a quantitative review. It appears that additional effort could be used profitably in preliminary and Title I design phases to examine alternate approaches in the design of these components that would improve reliability and reduce the number of development problems.

### 6.2.2 Fuel Handling

As described by AI-CE, the system for handling new fuel receives, inspects, stores, and prepares fuel assemblies for loading into the refueling machines, and the spent-fuel system receives spent assemblies from the refueling machines, transports them to the fuel storage pool tubes, where they are cooled, and then transfers them to shipping casks. The environmental control systems minimize fuel assembly thermal shock due to environmental changes. They also prevent contaminants from being

introduced into the reactor core and provide a means for dissipating spent-fuel decay heat during transfer from the core to the storage pool.

New fuel in the loading station is preheated in HB-40 fluid to 400°F before it is transferred into a refueling machine environmental system. In this system the fuel is maintained at 400°F in Santowax OM, and the pressure is increased from 50 to 300 psia. During transfer of fuel from the loading station to the refueling machine, the HB-40 and Santowax OM fluid pressures are equalized to minimize mixing. The HB-40 fluid in the spent-fuel unloading stations is maintained at 250°F during fuel-transfer operations. A heat exchanger is utilized to remove spent-fuel decay heat. Again the refueling-machine and unloading-station fluid pressures are equalized to minimize mixing. The spent fuel is then discharged into pool storage tubes, which are filled with HB-40. The AI-CE report does not explain how the new fuel is heated and maintained at the 130°F "ambient" temperature or how the fuel assemblies are transferred from storage to the loading stations.

A number of inconsistencies were noted in the AI-CE fuel-handling system, which is represented only schematically. Figures II-17, II-18, II-27, and II-28 of Ref. 1, which show new-fuel and spent-fuel facilities, are not in agreement. Provision for storing 120 fuel assemblies in each new fuel-storage area is required if a two-months supply is to be maintained as called for elsewhere in the report. Page II-83 and Fig. II-26 of Ref. 1 indicate provision for storing 60 fuel assemblies in each new fuel-storage area.

We feel that it should be feasible to work out the fuel-handling system along the lines described by AI-CE, but the present information is incomplete, and we cannot comment specifically on handling methods and equipment from the information available.

### 6.3 Plant Availability

The ground rules of this study call for the HWOGR to operate as a base-load power plant with a 0.8 load factor. It is assumed that the plant must be capable of an average availability of 0.9 over its 30-year life in order to qualify for a 0.8 load factor.

Plant availability was defined in the advanced-converter evaluation<sup>2</sup> as the product of four independent availability factors, which accounted for

1. refueling downtime and frequency,
2. reactor periodic maintenance and inspection for one week per year -- factor of 0.99,
3. steam-plant periodic maintenance and inspection for 30 days of every two years operating time -- factor of 0.964,
4. steam-plant forced outages for equipment repair -- factor of 0.977.

According to these assumptions, the maximum possible plant availability would be 0.931. Refueling downtime in excess of the time allowed for scheduled maintenance would be factored in and would further reduce the overall plant availability factor. The margin of plant availability above 0.9 gives an indication of how well the fuel-management scheme and refueling interval are coordinated with the requirements of the rest of the system. If the system barely meets the required 0.9 factor, modifications of the fuel-handling approach and equipment design are indicated, since there would be little or no margin available for forced outages of reactor equipment.

The HWOCR plant employs on-power refueling and thus has a high availability potential. In the advanced-converter evaluation<sup>2</sup> no attempt was made to evaluate the relative reliabilities of the reactor plants or to estimate the probability of reactor-plant forced outages and the effect of these outages on plant availability. Each of the concepts required development and demonstration of special features to establish their design performance requirements. The relative reliability of plant components therefore could not be assessed quantitatively from the information available. The same is true for the HWOCR; the present evaluation is restricted to considering possible failures of critical systems or components of the plant and the consequences of these failures on plant availability.

Downtime due to forced outages of reactor primary heat transfer equipment should be low, even though the HWOCR has only three loops. The equipment is accessible and can be readily repaired because of the very

low activity of the coolant under normal operation. Coolant and moderator purification facilities are sized to permit such facilities to be closed down for repair for a reasonable period of time without requiring a reactor shutdown; also, the coolant purification facilities can be used to clean up the coolant in case it becomes contaminated with fission products released from ruptured or leaking fuel elements. However, large releases of activity to the coolant could result in lengthy shutdown periods for cleaning the coolant and decontaminating equipment.

The reliabilities of the reactor control system, reactor components, and refueling operation are subject to question because of the high performance requirements of the system. Possible modes of failure are discussed in other parts of this section, but more complete analyses are required to establish the overall reliability to be expected.

A reactor shutdown from load changes, coolant system instability, malfunctioning of the reactor control system, or from other possible modes of failure could result in an offstream time of perhaps 40 hr to allow for xenon decay and subsequent startup time.

The durability of SAP tubes must be demonstrated before downtime for process tube replacement can be discounted as a factor to consider in plant availability. The probable frequency of process tube replacement and the average time required for replacement should be based on results from experimental studies.

Mechanical failure of the refueling machine during operation would require shutdown of the reactor to permit access to the refueling area to correct the failure. This system must, therefore, be essentially perfect mechanically to avoid an excessive number of shutdowns.

There is a margin of about 260 hr available for unscheduled outages of reactor equipment, according to assumptions made in this evaluation. Unscheduled reactor shutdowns for any of the above reasons or others would thus be limited to about six per year to comply with the average 0.9 plant availability factor. Assuming successful development of SAP and of refueling machines, we see no basic reason why the HWO CR could not easily attain a 0.8 load factor. At this point we consider a 0.9 load factor as feasible, although equipment reliability needs to be demonstrated to substantiate such operation.

## 6.4 Control Rod Systems

### 6.4.1 Shutdown Rods

Normally the reactor will be shut down by the insertion of 84 hydraulically actuated, hollow, cylindrical, neutron poison rods consisting of stainless steel tubes containing boron carbide. The rods are inserted horizontally into the moderator, and in order to minimize unwanted neutron losses no guide tubes are used. The total reactivity worth of all 84 rods is  $4\% \Delta k_e$ , and the time for 80% insertion is 5 sec, according to the AI-CE report. The rods will be maintained either in the fully withdrawn or fully inserted position.

The rods are normally fully withdrawn into a guide tube and, on insertion, are driven unsupported into the core. If a fault should occur in such a way as to separate the rod from the drive piston, failure would take place on the occurrence of a scram such that the rod would fall to the bottom of the calandria after it was pushed into the core. Since individual average rod worth is less than  $0.05\% \Delta k$ , the loss of a number of rods could pass unnoticed unless a routine test were available for detection of this type of failure. Such a test could consist of insertion and withdrawal of individual rods with the reactor at power. The movement of control rods required to keep the reactor at power would indicate the variation in poison caused by movement of a shutdown rod.

During reactor startup it would be helpful if the shutdown rods could be withdrawn individually. This would provide a more cautious approach to criticality and thereby reduce the amount of boron addition, and subsequent removal, required to guarantee subcriticality. Inasmuch as criticality must be reached through boron removal, it would be helpful to be able to withdraw and insert a single rod in order to observe changes in subcritical multiplication.

Figure II-47 of the AI-CE report<sup>1</sup> shows schematically the hydraulic system for withdrawing and inserting the shutdown rods. Valves are shown that will allow a rod drive to be isolated for maintenance purposes. If these valves were all closed because of confused maintenance or operating orders, the system would be unable to operate. This type of failure can

be made extremely improbable by careful monitoring of valve position, but this is cited as an example of a possible systematic failure that could cause all identical units to fail from a single cause. With positive coefficients, the most trivial loss of control followed by failure to shut down could result in destruction of the core. In order to minimize the possibility of a systematic failure immobilizing all rods, we propose that the 84 rods and drives be made up of two groups of different design and incorporated into two independent systems. Also, the results shown in Figs. 5.13 and 5.14, as discussed in Section 5.6.4, require the time for insertion of the shutdown rods to be decreased below the present design value.

#### 6.4.2 Control of Spatial Power Distribution and Power Level

The AI-CE report states that control of spatial flux oscillations and small power transients will be accomplished by means of 60 absorber rods, each 1/2 in. in diameter and 8 ft long, suspended by stainless steel tapes. Since the rods are short with respect to the 20-ft height of the core, they may be positioned at will within the core with relatively small net change in reactivity. Thirty-four rods with a combined worth of 0.2%  $\Delta k$  are designated for spatial flux control. The remaining 26 rods, with a combined worth of 0.1%  $\Delta k$ , will be operated partially inserted in the core for power level control. In operation, a digital computer will designate rod positions for optimum spatial control. The computer will also direct the fuel loading so as to maintain the power level control rods in their operating range. The plant control system will independently position the power control rods.

It is proposed in the AI-CE report that all the rods be available for reactor startup; however, several considerations dictate that the two groups of rods function separately and that the worth and velocity capability of the power control rods be increased to control a variety of probable transients. As developed in Section 5.6.5, the flux servo will require  $\pm 0.15\% \Delta k_e$  control at a rate of approximately  $0.015\% \Delta k_e / \text{sec}$ . The existing combined worth of the 60 vertical control rods is 0.3%  $\Delta k$ ; however, the rods assigned to spatial flux control are unsuitable for transient control. Their use during a power transient would upset the spatial

flux distribution. Although withdrawing some of the rods through the entire length of the core would cause little reactivity change, the reactivity change would go first negative and then positive if starting from the lower part of the core.

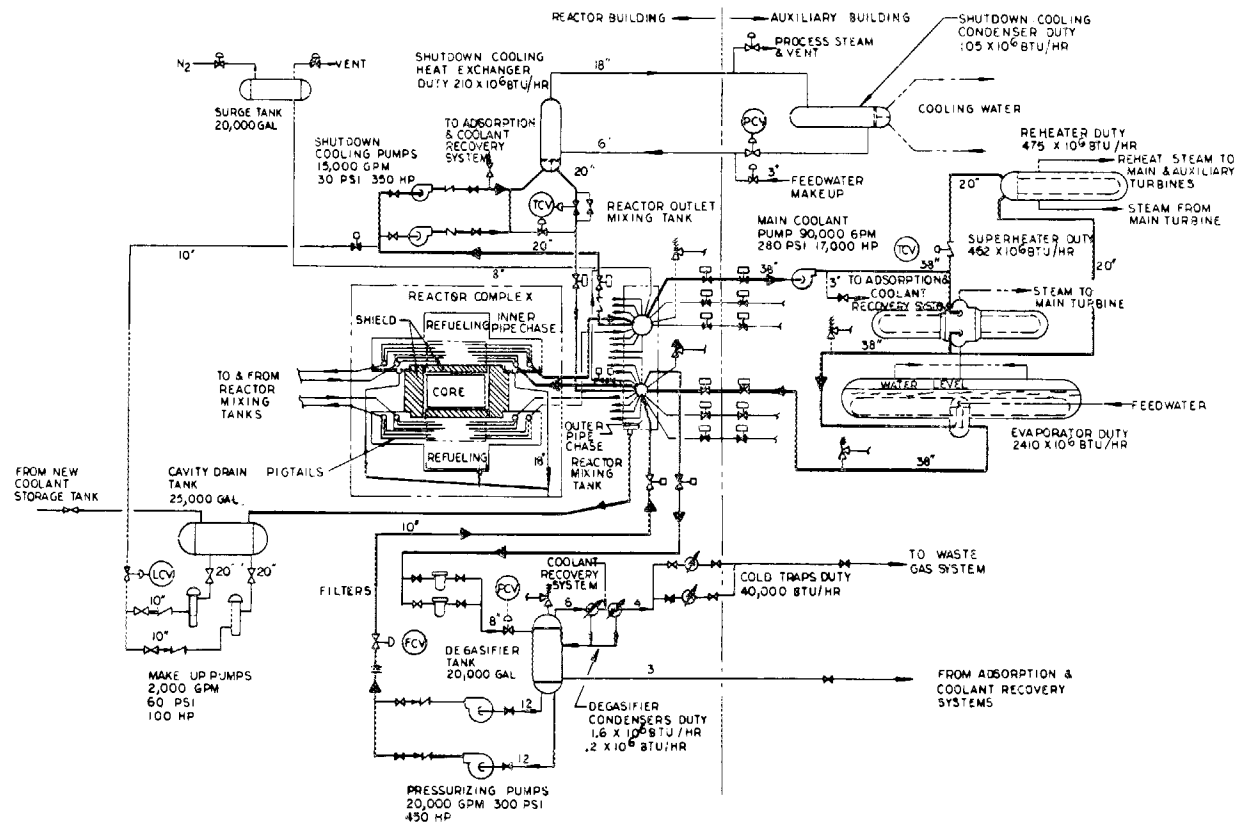
It will be necessary to increase the diameter, length, or number of vertical absorber rods allocated to power control to raise their worth from their present value of approximately  $0.1\% \Delta k_e$  to a new value of  $0.3\% \Delta k_e$ . Inasmuch as the control requirements are affected by the heat transfer coefficient through the gas gap between the  $UO_2$  fuel slugs and the cladding, and since the value of this coefficient is not well known and varies with fuel burnup, the value of  $0.3\% \Delta k_e$  should be considered minimal.

### 6.5 Primary Heat Transfer Systems

A flow diagram of the HWOCR primary heat transfer system is shown in Fig. 6.7, and the AI-CE and B&W design conditions are compared in Table 6.1. The HWOCR heat transfer system consists of three parallel loops, each with an evaporator, superheater, and reheater, a coolant circulating pump, isolation valves, and interconnecting piping. Carbon steel components are used throughout the system, except for some of the rotating parts of the pump.

Coolant pumps and heat exchangers are located in a building separate from the reactor building. Each loop is connected across reactor inlet and outlet mixing tanks, which serve as coolant collection headers. The outlet mixing tank also serves to provide a time delay for the coolant leaving the reactor. Motor-operated gate valves are used to isolate the loops if fission products are detected in the coolant leaving the reactor. Upon loop isolation, the reactor would be scrammed and the emergency cooling loop would remove shutdown decay heat.

The main coolant pumps are turbine driven and each is designed to deliver 90,000 gpm of coolant at  $750^\circ\text{F}$  against an 800-ft total dynamic head. (The B&W concepts require pumps of lower capacity but higher head.) The pumps are located in the loop hot legs to reduce the pressure in the fuel channel pressure tubes. According to an AI-CE report,<sup>7</sup> this reduced



LEGEND

	GATE VALVE
	CHECK VALVE
	DIAPHRAGM OPERATED VALVE
	SOLENOID OPERATED
	ELECTRICALLY OPERATED GATE VALVE
	RELIEF VALVE
	LEVEL CONTROL VALVE
	TEMPERATURE CONTROL VALVE
	PRESSURE CONTROL VALVE
	FLOW CONTROL VALVE
	ORIFICE

Fig. 6.7. Organic Coolant Systems Flow Diagram. (From Ref. 1)

Table 6.1. B&W and AI-CE HWO CR Primary System  
Parameter Comparison<sup>a</sup>

	B&W Thorium- Fueled HWO CR	AI-CE Uranium- Fueled HWO CR
Reactor coolant inlet temperature, °F	560	595
Reactor coolant outlet temperature, °F	750	750
Coolant temperature rise across reactor, °F	190	155
Total reactor coolant flow, lb/hr	$89.9 \times 10^6$	$110 \times 10^6$
Total reactor fission power, Mw(t)	3082	3093
Net power to coolant, Mw(t)	2928	2943
Total system pressure drop, psi	312	284
Reactor pressure drop (header to header), psi	218	184
Main loop coolant velocity, fps	24.5	30
Total pumping power, Mw	34	38
Superheaters		
Total flow, lb/hr	$64 \times 10^6$	$79 \times 10^6$
Pressure drop, psi	15.3	15
Inlet temperature, °F	750	750
Outlet temperature, °F	714	721
Total heat transfer area, ft <sup>2</sup>	99,000	97,500
Total thermal duty, Mw	406	406
Reheaters		
Total flow, lb/hr	25.9	30.9
Pressure drop, psi	18	18
Inlet temperature, °F	750	750
Outlet temperature, °F	661	672
Total heat transfer area, ft <sup>2</sup>	97,200	97,200
Total thermal duty, Mw	405	420
Evaporators		
Total flow, lb/hr	$89.9 \times 10^6$	$110 \times 10^6$
Pressure drop, psi	45	35
Inlet temperature, °F	699.5	707
Outlet temperature, °F	560	595
Heat transfer area, ft <sup>2</sup>	261,000	202,000
Thermal duty, Mw	2117	2117

<sup>a</sup>Values given by sponsors.

pressure results in a fuel cost advantage that is greater than the additional cost of pumping the hotter coolant.

There should be no difficulty in designing and fabricating the main coolant pumps. Larger pumps have already been built by several pump manufacturers. For the particular conditions of this design, some model testing in water may be required to verify the pump performance characteristics, such as head, flow, net pressure suction head, etc., as well as the impeller radial thrust needed for the bearing design. Face-type seals have been used under conditions more exacting than those present in the HWOCR. Other factors that must be considered and which are recognized by experienced pump designers include thermal stresses, vibration, operation of radial and thrust bearings, rotor dynamics, maintainability, equipment fabrication, and application of design codes; none of these appear to present unsolvable problems for the HWOCR.

The large heat exchangers, evaporator, superheater, and reheater can be shop fabricated and shipped by barge to the site. The largest of these is the evaporator. Each of the reference design evaporators is 51 ft long and 13 ft in diameter, and it weighs 500 tons dry. The heat transfer surface area is 67,300 ft<sup>2</sup>.

In our review of the evaporator design, we calculated a thermal duty of 701 Mw instead of 706 Mw as shown in Table III-5 of Ref. 1. The log mean temperature difference in the preheater section was calculated to be 118°F instead of 108°F and the overall heat transfer coefficient in the preheater section was found to be 330 Btu/hr·ft<sup>2</sup>·°F compared with the value of 167 Btu/hr·ft<sup>2</sup>·°F reported by AI-CE. This discrepancy is primarily due to the value assumed for thermal conductivity of water on the shell side. The overall heat transfer coefficient in the boiling section was calculated to be 490 Btu/hr·ft<sup>2</sup>·°F compared with the AI-CE value of 400 Btu/hr·ft<sup>2</sup>·°F. As a result, the minimum required heat transfer surface area was determined to be 46,000 ft<sup>2</sup> compared with the design value of 62,300 ft<sup>2</sup>. We would allow about 10% additional to our figure for uncertainties. Thus, for the capital cost determination, we used an area of 51,000 ft<sup>2</sup> for each unit. Results of calculations of the reheater and superheater areas checked reasonably well with the reported values. Evaporator surface area required in the B&W concepts is about

30% greater than required in the AI-CE reference design, because of the lower coolant temperature leaving the heat exchanger.

The design assumes no fouling resistance on the organic side of the heat exchangers. Piqua maximum coolant temperature is some 175°F lower than the HWO CR design maximum coolant temperature. To establish that no fouling will occur, successful test experience under HWO CR design conditions will be required before the size of the units as specified can be considered firm.

The HWO CR system has fewer coolant loops than any of the advanced-converter concepts of Ref. 2. The larger unit size of components, plus the fact that the heat exchanger tubing is carbon steel rather than the Inconel used for the pressurized-water-cooled reactors, results in a significant cost advantage for the HWO CR. It will be noted, however, that recent pressurized-water reactor designs are using fewer loops (Indian Point No. 2 will have four loops), and this is a factor to consider in comparing costs of the HWO CR with those of the advanced-converter reactors evaluated previously.

## 6.6 Heavy-Water Systems

Some direct comparisons can be made between the heavy-water systems of the HWO CR and those of the DuPont heavy-water reactor designs evaluated in the advanced-converter study.<sup>2</sup> A high degree of system integrity must be maintained for all these systems to prevent D<sub>2</sub>O losses. Contamination must be held to a minimum by providing a cover gas to prevent air inleakage and purification facilities to remove particulate matter and corrosion products.

The important difference, however, between the HWO CR and DuPont heavy-water reactor systems is that the HWO CR uses heavy water at relatively low pressure, whereas in the other designs heavy water at 2000 psi is used as the coolant. Thus the HWO CR D<sub>2</sub>O inventory is comparatively low, and associated losses should be considerably less than in the pressure tube concepts.

Also, special features have been introduced in the HWOCR design:

1. The moderator heat is recovered in boiler feedwater instead of being rejected to cooling water; this improves the plant thermal efficiency.
2. Heavy water from the moderator is used to provide flow to the hydraulically actuated reactor shutdown system and as an injection fluid for the soluble-poison shutdown system.

A heavy-water loss rate of 10 lb per day has been assumed. At this rate 0.56% of the heavy-water inventory would be lost annually. This is in contrast to an annual loss of 2% of the inventory assumed for the DuPont heavy-water systems. In systems with heavy water for both coolant and moderator, as much as 95% of the total loss is attributed to losses from the high-pressure coolant system. The total annual D<sub>2</sub>O loss from the DuPont reactor systems was 33,000 lb for the HWR-Th concept and 27,000 lb for the HWR-U reactor. Thus, the loss rate of 10 lb per day for the HWOCR appears acceptable to assume for the purpose of this study.

AI-CE assumed that fresh D<sub>2</sub>O makeup to replace heavy-water losses would be sufficient to maintain the light-water content at an acceptable level. Therefore, distillation units are not provided at the site for isotopic upgrading. D<sub>2</sub>O from accidental spills or from demineralizer washes that has been downgraded below specification level for light-water content will be shipped to other facilities for recovery. Since a cover gas of helium is maintained on the system and presumably at locations where leaks from pumps and valves are collected, normal contamination by exposure to moist air should be negligible. However, it seems that an estimate of quantities of heavy water to be shipped out for recovery should be made to determine whether operating costs are appreciably affected.

A potential source of heavy-water loss is in the moderator cooler. Tritium detectors may be used to monitor the feedwater stream and thus detect gross leakage. However, the sensitivity of this device may be limited (estimated as ~1 ppm D<sub>2</sub>O from a solution near saturation with tritium) so that leakage several times the specified loss rate may occur without being detected. Other means of closely monitoring the D<sub>2</sub>O system inventory will be necessary to make sure that gross leakages will not occur for any appreciable period of time.

### 6.7 Organic Coolant Decomposition, Recovery, and Makeup

Calculations were made to verify the required throughput of the hydrocracking unit and to determine its effect on the equilibrium composition of the coolant. A check was also made of the process design of the hydrocracker. It was considered that the neutron, gamma, and thermal exposures of the coolant under full-power operation leads to terphenyl degradation at the rate of 1500 lb/hr. This corresponds to our calculated value with outlet coolant at 700°F, and also corresponds to the AI-CE calculated value with outlet coolant temperature at 750°F (see Section 5.5). The conclusions reached under these circumstances are given below. They indicate general agreement with the hydrocracker throughput and process design as given by AI-CE; the biphenyl concentration in the equilibrium coolant, however, was estimated at 12 to 20 wt %, rather than the 2% shown in Table III-1 of Ref. 1.

The coolant degradation rate of 1500 lb/hr corresponds to an absorbed neutron dose of about 10 Mw(th), an absorbed gamma dose of about 4.5 Mw(th), and an outlet coolant temperature of 700°F. Then, with an HB destruction rate of 1500 lb/hr in the hydrocracker, the rate of biphenyl production was estimated. A design conversion (disappearance) of HB of 30% per pass in the hydrocracker was assumed, in accordance with AI-CE.<sup>1</sup> With this conversion factor, the biphenyl production estimated by Phillips Petroleum Company is about 23 wt % of the HB disappearance,<sup>8</sup> this gives a biphenyl production rate of 345 lb/hr. At equilibrium, this must be equaled by the rate of biphenyl disappearance by radiolysis and pyrolysis, since there is no other removal of biphenyl from the system. The G value for the radiolysis of biphenyl is about 1.8 times that of terphenyl.<sup>8,9</sup> These considerations lead to an estimated biphenyl concentration of about 12 wt %. However, some of the data<sup>10</sup> indicate that the biphenyl yield in the hydrocracker could be as high as 40 wt % of the HB disappearance. On this basis, an equilibrium biphenyl concentration of about 20% might be reached. The vapor pressure of the equilibrium coolant (with 10% HB) was calculated to be 50 to 60 psia at 750°F, as compared with about 35 psia shown (by interpolation) in Table III-2 of Ref. 1. Because bench-scale runs on a once-through unit cannot completely duplicate actual

conditions of continuous operation, the determination of the actual equilibrium concentration will have to wait until hydrocracking data are obtained at the proposed Piqua installation. At present it is recommended that provisions be made to insure that the reactor cooling system is operable with a vapor pressure as high as 60 psia in the outlet mixing tank, if the outlet coolant temperature is 750°F.

A required makeup rate of about 200 lb/hr of fresh coolant was estimated, in substantial agreement with the AI-CE figure of 0.4 gpm. However, this does not include any allowance for mechanical leakage.

The process design and estimated cost of the hydrocracker appear to be well supported by the available data.<sup>10</sup> It may be expected that operation of the Piqua unit will lead to improvements and possibly to cost reduction. The cost of the HWOCR hydrocracker unit is estimated to be about \$800,000, in agreement with the AI-CE value. If the throughput were a different rate, we estimate the capital cost would vary as the 0.6 power of the throughput rate.

Calculations were made in order to estimate the time required to approach equilibrium coolant composition. About three or four months of operation at near-design conditions should bring the biphenyl buildup to within 90% of its equilibrium value.

The following points are suggested for consideration in the present design:

1. The vacuum flash column and the reactor feed tank could be combined into one vessel with a uniform diameter of 6 ft.
2. The flash-column distillate receiver could be reduced to about 4 ft in diameter by 12 ft in height, since there is no process requirement for a long surge time.
3. The high-pressure hydrogen-liquid separator might be increased to about 4 ft in diameter by 12 ft in height to give better disengaging. The proposed size of 750 gal appears to be small.
4. The low-pressure hydrogen-liquid separator (atmospheric degasifier) capacity could be reduced from 2400 gal to about 1200 gal ( $4 \times 12$  ft).
5. The suction cooler of the hydrogen recycle compressor might be more efficient and cheaper if removed from the separator vessel and made a separate unit.

## 6.8 Instrumentation and Controls

### 6.8.1 Plant Controls

The requirements for reactor control were discussed in Section 5.6. The desirability, if not a need, for computer control during startup was indicated in Section 5.6.2, and the need for the capability of the control system to keep the plant in operation following probable plant malfunctions was discussed briefly in Section 5.6.5.

In our analog computer studies of the HWOCR, we were able to maintain the reactor at a fairly constant power level by manual control of reactivity when the plant was operating normally; however, constant attention was required, and any relaxation of effort often lead to results similar to those in Fig. 5.15. We do not recommend manual operation of the HWOCR plant, although a statement on page VI-1 of the AI-CE report<sup>1</sup> indicates that manual control from zero to 100% power is a design criterion.

It should be possible for an automatic plant control system to meet the design criterion of constant steam pressure and temperature (900 psig and 725°F) at the turbine throttle over a limited range of power with a limited rate of power change. This limitation of power range is required by the limited reactivity that can be made available in the control rods to compensate for the negative power coefficient discussed in Section 5.6.1. The total reactivity of the control rods assigned to power control must never be consumed in maintaining steady-state power levels. Rather, these control rods should be kept near the midrange of their stroke in order that reactivity is always available for control of transients, as discussed in Section 5.6.5. Either changes in fuel loading or the use of boron in the moderator must provide the reactivity changes needed for a variation in operating power of more than a few percent. Although the  $-0.15\%$   $\Delta k$  available from complete insertion of the control rods from their midposition is sufficient to reduce the power from 100 to 40%, it would be unwise to operate with these rods fully inserted for more than a very short time. Further analyses and computer studies of the plant will be required to establish the design of the plant control system.

Any plant control system in which the reactor power is a slave to turbine output will require a reactivity variation capable of changing the reactor power to meet whatever change in load is imposed on the turbine. The HWOCR does not have this inherent capability; therefore, this plant should probably have a control system of the type such that the turbine is a slave to the reactor, and the reactor power is ultimately varied to meet the requirements of the power system. Rod control would be by means of a flux servo, with the setpoint for this controller being obtained from the measurement of certain process variables. One of the measured process variables would be coolant flow; thus, variations in coolant flow for any reason would be reflected by changes in reactor power. Steam temperature could be controlled by signals that ultimately affected the setpoint of the flux servo. The turbine throttle would be controlled by steam pressure, and thus the turbine would be a slave to the reactor. The plant power setpoint would control the coolant pumps; therefore the plant power output would be determined, in actuality, by the rate of coolant flow. This power setpoint could be modified automatically by power system demand, provided the changes so produced were sufficiently limited in magnitude and rate. We do not recommend the use of multiple interdependent setpoints that must be varied simultaneously by a power computer, as indicated in Fig. VI-3 of the AI-CE report.<sup>1</sup>

In case the electrical load on the plant suddenly decreased because of some disturbance in the power network, the control system would have to change control of the turbine throttle from steam pressure control to speed governor control, with excess steam being dumped.

### 6.8.2 Nuclear Instrumentation

The nuclear instrumentation system proposed in the diagram of Fig. VI-2 of the AI-CE report<sup>1</sup> consists of 16 channels, as follows:

- 4 BF<sub>3</sub> source-range channels
- 4 compensated ion chamber intermediate channels
- 4 compensated ion chamber power-regulating channels
- 4 uncompensated ion chamber power-range (safety) channels

In order to more nearly match the reactor's characteristics and to take advantage of recent developments, we propose 12 channels, as shown in

Figs. 6.8 and 6.9. This nuclear instrumentation would provide the following channels:

- 3 fission chamber wide-range counting channels
- 3 uncompensated ion chamber power-regulating channels
- 6 uncompensated ion chamber safety channels  
(2 sets of 3 channels each)

Wide-Range Counting Channels. The AI-CE report<sup>1</sup> proposes BF<sub>3</sub> counters to cover the first five decades of operation on the assumptions that ten decades of range from source to full power are required and that no single instrument can satisfactorily cover the entire flux range. Because of statistical fluctuations of neutron pulses, the period signal from the source range channels is of an erratic nature and is employed only as an operating aid. No automatic corrective action would be taken because of the statistical fluctuations.

The assumptions underlying this choice do not take into account the following points:

1. The strong photoneutron source from  $\gamma$ -n reactions on D<sub>2</sub>O will produce an operating range much less than ten decades that will vary with the duration of shutdown. This strong source will permit the use of a fission chamber rather than the less-convenient BF<sub>3</sub> chamber.

2. A wide-range counting system is available that is capable of covering ten decades of operation,<sup>11</sup> and we recommend its use in the HWO CR. This system employs a servo-controlled moving detector in a water-filled attenuating tube and is routinely used for automatic reactor startup without interference from statistical fluctuations.

Power-Regulating Channels. Because failure to obtain prompt and adequate response will result in an uncontrolled excursion, it is required that unusual reliability be built into the flux-regulating servo and other controllers which, on failure, would cause the plant to go off the line. The problem is often met by employing setback — a controlled reduction in power — in order to avoid a reactor scram that would be brought about either by an excursion of some process variable or by an instrument malfunction. The AI-CE report<sup>1</sup> proposes, as setback, not a controlled reduction in power, but an insertion of the vertical control rods to continue

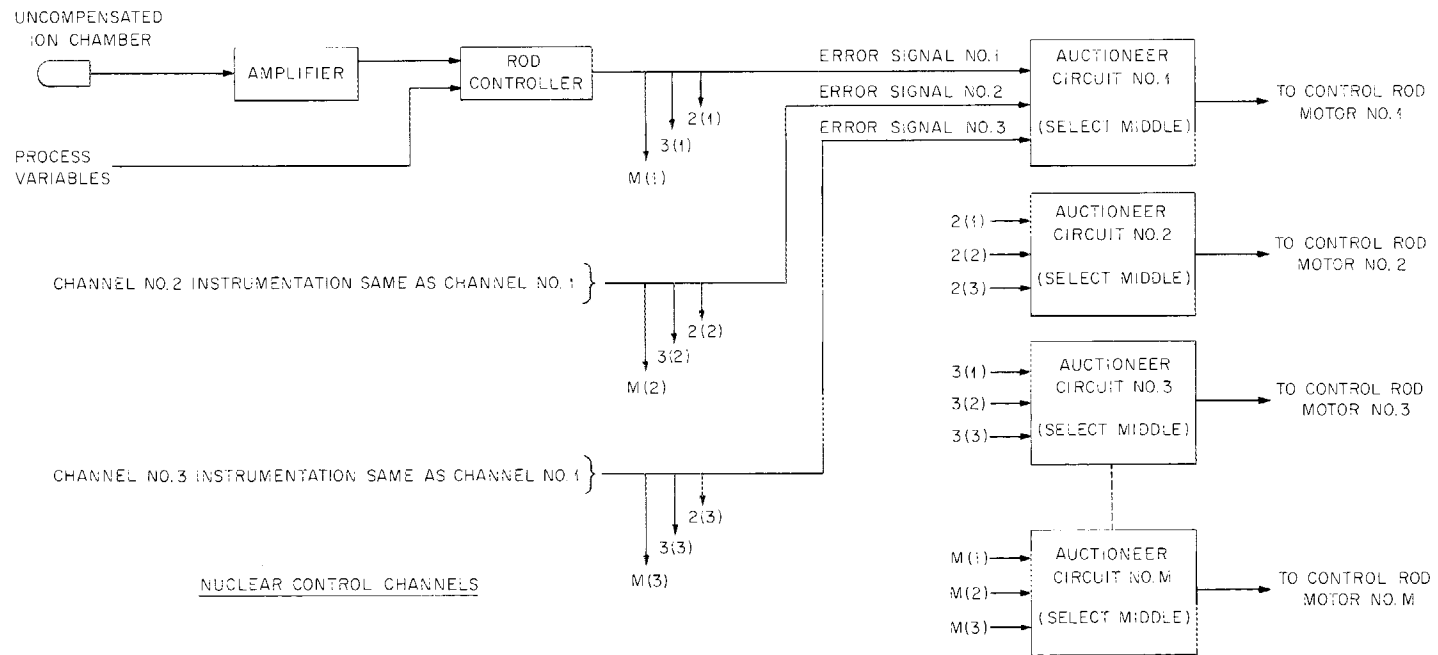
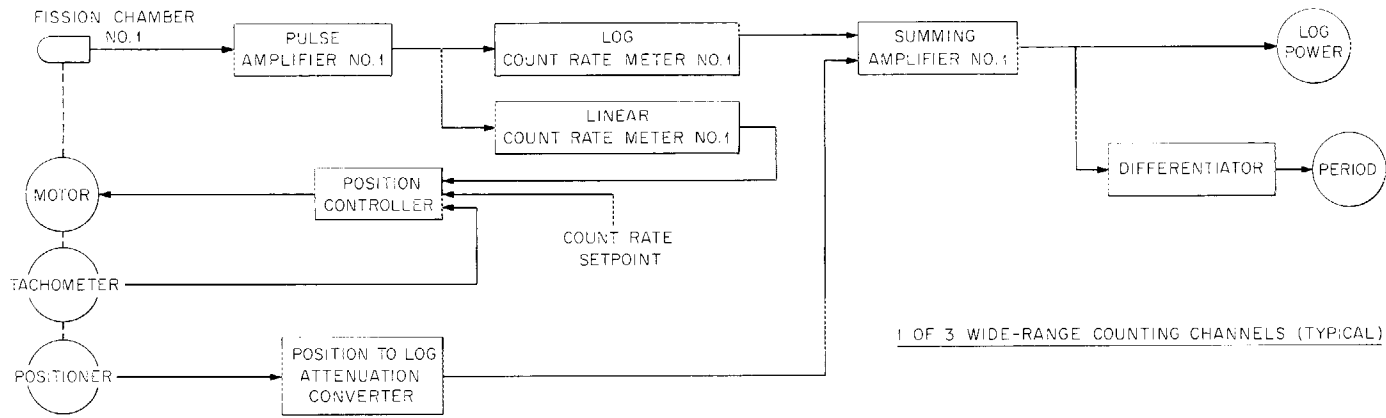


Fig. 6.8. Control System Nuclear Instrumentation.

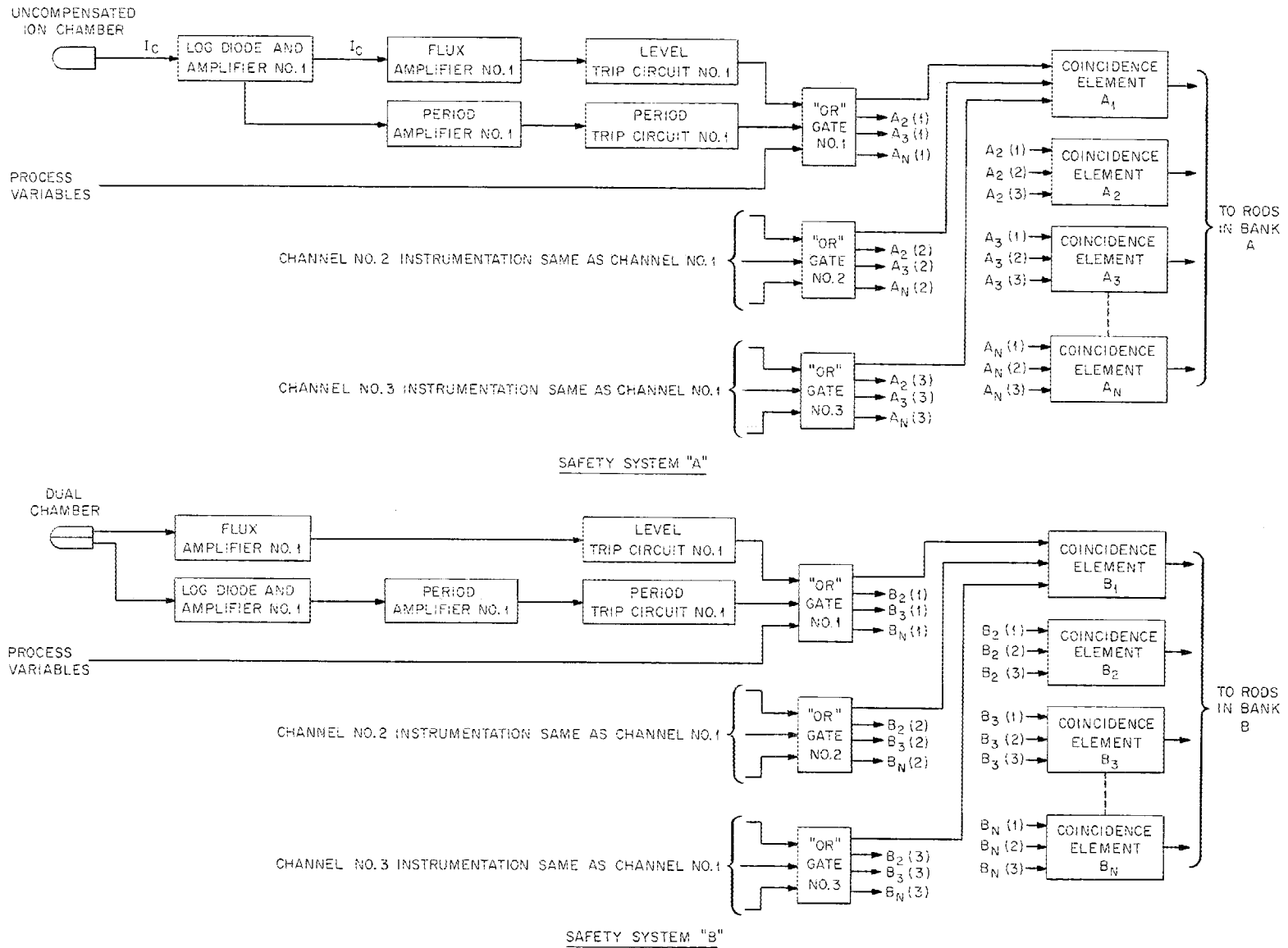


Fig. 6.9. Safety System Nuclear Instrumentation.

as long as the excursion persists, while at the same time automatic control is to be turned off. Since manual control would be difficult if not impossible in the power range, an unwanted turbine trip would probably result. Signals taken from the safety system and used in the control system to reduce power to prevent a scram are quite desirable, but such a reduction in power must not put the plant out of control. We do not recommend that setback be employed as proposed.

In order to obtain reliable control we propose that rather than the selection of one of four power channels as input for nuclear control, a multiple control system be employed to minimize the effect of failure of a controller or of failure of inputs to a controller. One version of such a system uses a full complement of inputs to each of three rod-drive controllers. The output velocities of the three controllers are added, and all control rods are moved with a velocity equal to the algebraic sum of the velocities of the three controllers.<sup>1,2</sup> Thus the failure of any one controller will be compensated by the remaining two. Another way of achieving the same end would be to auctioneer the signals from each of the three controllers so as to select the median signal for control.<sup>13</sup> This latter system is shown in Fig. 6.8.

Intermediate-Range Channels. The AI-CE report proposes four intermediate logarithmic channels overlapping the lower portion of the power range and the upper portion of the source range. The report states that the period circuitry used to initiate fast shutdown is to be cut out of service when the reactor power reaches a value somewhere between 2 to 20% of rated power in order to eliminate false period scrams in the range.

Again the assumptions do not fully take into account the reactor characteristics and available instrumentation techniques, as follows:

1. Overlapping of both the power and source ranges is a technique that is useful only for clean reactors (without appreciable gamma background) and is for reactors having a wide operating range. This reactor, once operated at power, will neither be clean nor have a wide operating range.

2. It is true that period circuitry is generally subject to spurious trips brought about by unrealistic trip settings in combination with

power-line transients. However, we have accumulated several years of operating experience without a single spurious trip of a log N period trip set at 1 sec.<sup>14</sup>

We propose to eliminate the intermediate channels and allow the wide-range counter channels to provide the logarithmic range and long-period control and to transfer the short-period protection function to the safety system.

Safety Channels. The AI-CE report<sup>1</sup> proposes four safety channels arranged so that scram and setback occur when reactor power exceeds pre-set limits in any two of the four channels. We propose a total of six safety channels arranged with three channels in each of two separate systems as shown in Fig. 6.9. Two complete and independent sets of safety channels are needed to meet the stringent requirements described in Section 5.6.4. The two sets of safety channels should be of different design so that causes of common failures of the two sets are reduced to a minimum.

Period trips are shown in Fig. 6.9; these period trips must remain in service at all times, as also discussed in Section 5.6.4. A safety system can be operated without spurious trips with the trip set at a 1-sec period,<sup>14</sup> whereas attempts to trip on longer periods result in many spurious scrams unless a long delay in response is acceptable. A period-trip circuit combined with the flux-level trip so that both functions can be obtained from a single chamber has been developed<sup>15</sup> and is shown in Safety System "A" in Fig. 6.9. Dual chambers in which the flux level and period signals originate separately are shown in Safety System "B" in Fig. 6.9. Uncompensated chambers can be used in the safety channels of the HWOCR because of the large photoneutron source.

## 6.9 Containment Structure

The reactor building provides the containment structure for the reactor, moderator cooling system, and refueling facilities. Primary coolant system pumps and heat exchangers are housed in separate buildings. Four fast-closing block valves, two in series in both the inlet and outlet lines, are provided to automatically isolate the loops in case of excessive

quantities of radioactive material in the coolant. This valve action will also maintain containment integrity in the event of an accident involving a break in a coolant line accompanied by a release of radioactivity to the reactor building atmosphere. This method of containment is similar to that used for direct-cycle reactor plants but is unique for an indirect-cycle reactor plant. In principle, this method of containment should be acceptable for the HWOCR system, since precedence for this method is already established for direct-cycle plants. Rates of leakage through isolation valves and other penetrations must, of course, be determined and shown to be within acceptable limits for containment structures of this type.

The containment structure is a vertical cylinder, 140 ft in diameter and 187 ft high above grade, with a hemispherical head and a concave base. It is a carbon-steel structure designed for an internal pressure of 15 psig at 165°F. The internal free volume is  $1.5 \times 10^6$  ft<sup>3</sup>.

AI-CE representatives have acknowledged that complete analyses of maximum critical accident (mca) conditions have not been made. However, AI-CE concluded from their preliminary studies that the containment design as proposed would provide adequate protection. These studies considered pressure resulting from large organic spills and fires with coincidental use of water pumps to control the fire.

One accident that bears consideration before the proposed containment design can be considered acceptable is a loss of coolant accident accompanied by a rupture of the reactor calandria, which would release heavy water. The heat content of a large quantity of hot coolant would be sufficient to vaporize heavy water in an amount that would cause a pressure buildup much in excess of the 15-psig design pressure. For example, we have calculated that a release of some 1,400,000 lb of coolant (~2/3 the coolant inventory) could result in a pressure buildup of approximately 75 psig if a large quantity of water were to come in contact with it. If the coolant spill were confined to half that amount, the pressure could build up to 45 psig. The organic spill would have to be limited to less than 230,000 lb (<35,000 gal), or the heavy-water release to less than 46,000 lb, to limit the pressure buildup to less than 15 psig. The proposed containment scheme must therefore be considered tentative until more

detailed investigations of possible accident conditions have been made. Pressure suppression in conjunction with the proposed containment scheme might be used to limit pressure buildup to an acceptable value.

#### 6.10 Turbine-Generator System

Turbine plant design data are summarized in Table 6.2. We have checked through the heat balances and calculational methods<sup>16</sup> furnished by AI-CE for this evaluation and are in general agreement with the reference design values listed. The selections of the reference design conditions are supported by AI-CE investigations of seven cycles ranging from a basic nonreheat system to a reheat arrangement. The effects of three pressure and temperature points on cycle components, efficiency, and plant thermal requirements were considered. From the three throttle steam conditions investigated,<sup>16</sup> namely, 600 psig and 675°F, 900 psig and 725°F, and 1200 psig and 775°F, the intermediate case was chosen as optimum. Areas where further optimization would be desirable were recognized; that is, investigations are needed to

1. confirm the selection of a single turbine-generator unit over two half size units for specific power system applications,
2. set final feedwater heater arrangement (number of heaters, heater terminal differences, the use of condenser deaeration, and utilization of generator heat losses),
3. set throttle and reheat steam conditions on a plant cycle basis,
4. consider noncondensing auxiliary turbine drives in half- and full-capacity sizes,
5. evaluate partial plant load operation for confirming equipment design selections and to establish plant control modes.

Our estimates of potential improvements in efficiency associated with several of these effects are given in Table 6.3. Although improvements in cycle efficiency are possible from these effects, they may not be practical to achieve for several reasons. Approximately \$300,000 capital expenditures are necessary to add one stage of feedwater heating. The final temperature must be acceptable for the reactor heat cycle, and the effect on reactor plant equipment costs must also be evaluated. Noncondensing

Table 6.2. Turbine Plant Design Summary

Reactor thermal output (including moderator and shield), Mw	3093
Reactor thermal power to coolant, Mw	2921
Evaporator and superheater thermal power, Mw	2524
Reheater thermal power, Mw	4.19
Gross generator electrical output (0.85 pf), Mw	1088
Plant auxiliary electrical power, Mw	12.0
Plant net electrical output, Mw	1076
Plant net heat rate, Btu/kwhr	9800
Plant net thermal efficiency, %	34.8
Turbine-generator	
Turbine arrangement	(a)
Throttle pressure, psia	915
Throttle temperature, °F	725
Throttle enthalpy, Btu/lb	1345.9
Throttle flow, lb/hr	$9.05 \times 10^6$
Reheat pressure, psia	167
Reheat temperature, °F	725
Reheat enthalpy, Btu/lb	1388.0
Reheat flow, lb/hr	$7.893 \times 10^6$
Condenser pressure, in. Hg abs.	1.5
Turbine exhaust flow, total, lb/hr	$6.437 \times 10^6$
Turbine exhaust enthalpy, <sup>b</sup> Btu/lb	1011.7
Condenser duty, total, Btu/hr	$6.13 \times 10^9$
Generator rating, kva	1,280,000
Generator terminal voltage, kv	24
Generator power factor	0.85
Generator hydrogen pressure, psig	60
Feedwater temperature, final, °F	420
Feedwater enthalpy, Btu/lb	397.5
Shaft-driven auxiliaries	None
Steam-driven auxiliaries, hot reheat	Main feedwater and main coolant pumps

<sup>a</sup>Tandem compound, six flow; 52-in. last-stage buckets.

<sup>b</sup>Used energy end point.

Table 6.2 (continued)

---

Main condensers	
Number of cooling-water pumps	6
Flow rate, each, gpm	108,000
Head, ft	30
Drive rating, hp	1000
Condenser type	Single pass
Number of units	3
Tube wall, BWG	18
Material	Admiralty
Size, in.	1
Length, ft	50
Design heat transfer surface, each, ft <sup>2</sup>	160,000
Design cooling-water temperature, °F	57
Design saturation temperature, °F	91.7
Cooling-water flow, each condenser, gpm	200,000
Feedwater system	
Feedwater demineralizing	None
Deaeration	Yes
Feedwater heaters, total number	13
Extraction closed	9
Extraction open	1
Moderator heat recovery	3
Number of banks	3
Drains	Cascade
Number of main feedwater pumps	3
Flow, each, gpm	6600
Feedwater temperature, °F	304.8
Total dynamic head, ft	2700
Driver type	Auxiliary steam turbine
Driver power, hp	6500
Number of auxiliary feedwater pumps	1
Flow, gpm	500
Total dynamic head, ft	2500
Driver type	Motor
Driver power, hp	400

---

Table 6.3. Estimates of Possible Efficiency Improvements in Steam Cycle

	Approximate Reduced Heat Rate Based on Selected Cycle (%)	Change in Plant Net Efficiency (%)	Remarks
High-pressure feed- water heater stage	0.5	+0.2	Steam flows affected; reactor plant must be considered
Reheat pressure, 5% change	>0.1	+0.005	Slightly higher pres- sure may be optimum
Noncondensing auxiliary drive turbines	None		Condensing usually more efficient
Generator regenera- tive heat exchanger		+0.1	Generator losses are 12.5 Mw; not all recoverable
Total		~+0.3	

auxiliary turbine drives are of doubtful benefit for efficiency improvement for the cycle such as the HWOCR, and costs cannot be assessed without extensive overall plant optimization. Since generator coolers are already provided, the cost of providing for cycle heat recovery in place of dumping the heat would probably not exceed \$50,000. In summary, efficiency improvements that can be justified on an economic basis are estimated to be of the order of 0.2%; this suggests a potential maximum net plant efficiency of 35.0% for the reference conditions.

The efficiencies for the HWOCR cycle are based on the nuclear heat balance calculation method developed by the General Electric Company.<sup>17</sup> Field experience with conventional units has often shown that manufacturer's calculational methods are on the conservative side.

A summary of the contributions to the plant thermal efficiency made by special features of the turbine-cycle design follows:<sup>16</sup>

Use of 52-in. last-stage buckets instead of 43 in.	+0.9%
Use of condensing auxiliary turbines instead of motor drives	+0.3
Use of hot reheat instead of cold reheat for auxiliary turbine drives	+0.1
Use of reheat instead of nonreheat	+1.7
Use of moderator heat exchanger	+0.3
	<hr/>
Total	+3.3%

The only items of equipment in the turbine-generator plant that require important development are the turbine (including the 52-in. last stage buckets), the generator, and the main exciter (if rectification is employed). The 60% extrapolation in turbine-generator size necessary for this study follows the generally accepted conclusion both by manufacturer and industry that this size equipment will be available when the demand is created. Reliability is not so easily predicted.

The main generator was designed with the conventional brush-type exciters (two one-half size units). However, brushless diode rectifier exciters are now available in ratings up to 5800 kw for 1000-mva generators.<sup>18</sup> A further increase to 1280 mva is considered by the manufacturers to be feasible for the operating period of this study. One arrangement being offered<sup>19</sup> that permits complete elimination of brushes, commutators, and collector rings has the fuse wheels, diode rectifier wheel, and rotors of the pilot exciter, ac exciter, and ac generator all on a single shaft. Output from the rotor (armature) of the exciter is rectified by the diodes and fed to the rotor (field) of the ac generator by leads through and along the directly connected shafts. Over five years operating experience to 1965 has shown less maintenance and higher reliability than for the brush-type or conventional exciter system. Approximately 20% more than rated diode capacity is provided to serve as "spare" in event individual diode systems fault. There is, therefore, no extra rotating equipment employed. The extra diode capacity serves this need. The exciter would be provided as part of equipment furnished with the turbine-generator unit and included in the cost in the usual manner.

The turbine-generator plant does not serve as an emergency heat dump for the nuclear plant; hence it is not encumbered with special backup

equipment and/or control for this purpose. Turbine steam bypass to the main condensers is provided, however, but this is for loss of electrical load or reactor decay heat removal after scheduled shutdown and is not related to nuclear plant emergency requirements. Transfer of moderator cooling to emergency cooling is independent of the feedwater system.

The use of hot reheat for steam supplied to the primary coolant pump and feedwater pump turbine drives appears to be justified, although cold reheat is more commonly used for auxiliary turbines. A balance of heat exchanger costs, auxiliary turbine costs, and piping costs would probably favor using hot reheat in the HWOCR system; however, we have not checked this point in detail.

The cost penalty for providing a speed reducer for the boiler feed pump is not clear, since turbine speed control can satisfy this requirement.

The heat balance shown in Fig. 6.10 closed with 0.15%. Steam conditions and net plant efficiency for the thorium-cycle design conditions are essentially the same as for the reference AI-CE design conditions.

As pointed out in Section 5.1, the present reactor designs do not appear capable of producing an outlet coolant temperature of 750°F and still meet other specified criteria. Thus, the effect on the overall plant efficiency of changing the temperature of the steam leaving the boiler-superheater and the reheater was evaluated.

The AI-CE data and flowsheet were used as the basis for comparing the different steam cycles. The total reactor heat chargeable against the plant thermal efficiency was 3093 Mw(t). There are heat losses from both the reactor and circulating coolant, and a reactor plant auxiliary electric load of 12 Mw(e) must be charged against the output. The AI-CE estimate of performance apparently assumed 162 Mw(t) of heat available to the steam system for feedwater heating in the D<sub>2</sub>O cooler. It has been judged that this is more correctly 156 Mw(t). The 725/725°F cycle performance was calculated based on this condition in order to give a correct basis of comparison for the 675/675°F case. As in the AI-CE estimate, it was assumed that 90% of the heat equivalent of the work done by the coolant pump is returned to the cycle. The overall results are listed below:

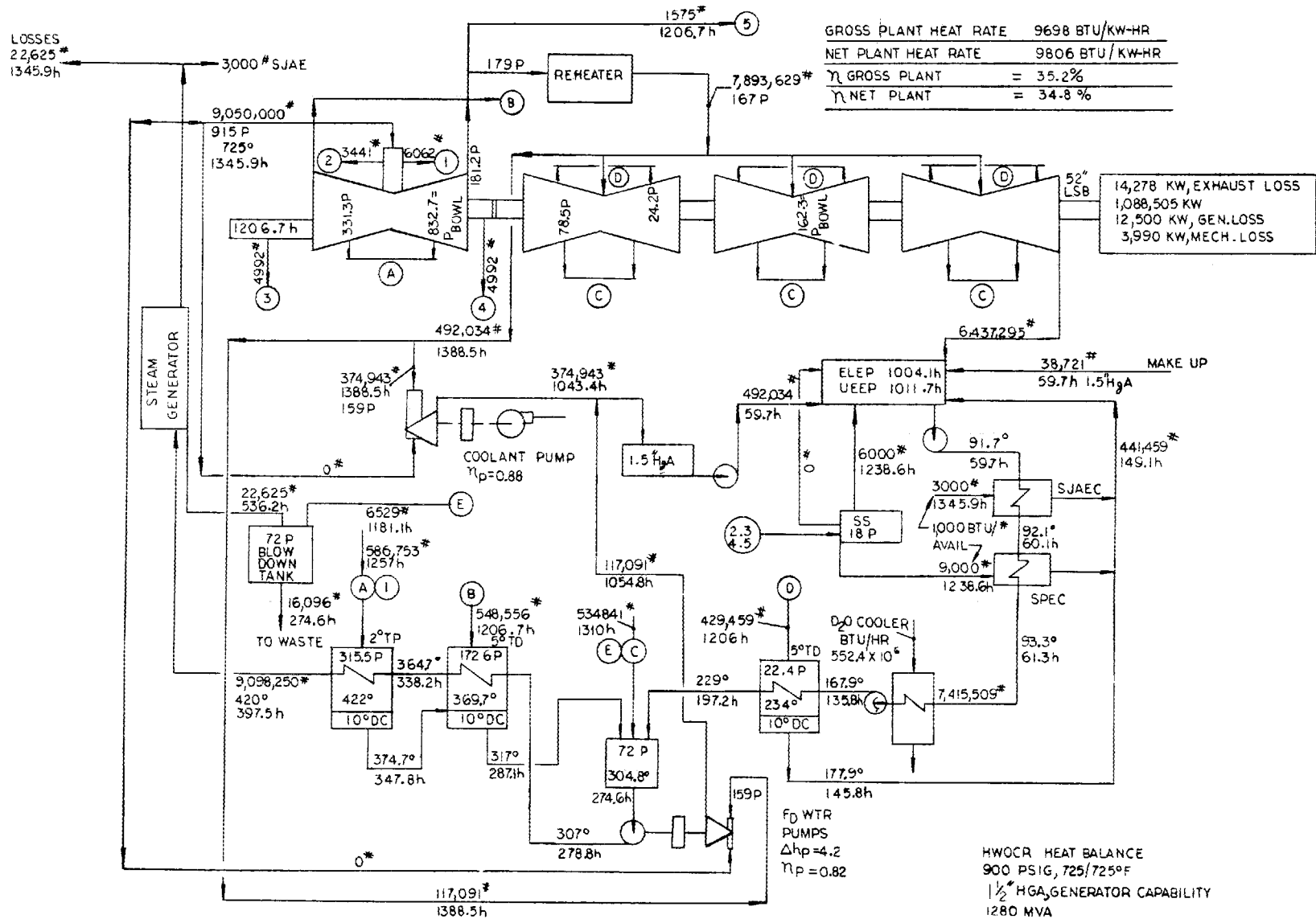


Fig. 6.10. HWOCR Heat Balance. (From Ref. 1)

<u>Steam Conditions to Turbine</u>	<u>Heat Available to Steam Cycle from D<sub>2</sub>O Cooler [Mw(t)]</u>	<u>Overall Plant Efficiency Based on 3093 Mw(t) Reactor Power (%)</u>
936 psia-725/725°F	162	34.81
936 psia-725/725°F	156	34.78
936 psia-675/675°F	156	34.08
815 psia-650/650°F	156	33.2

The conditions given above were associated with specific outlet coolant temperatures and particular heat exchanger design values. The 675/675°F steam conditions correspond to an outlet coolant temperature of 700°F and a steam generator having about twice the surface area of that given in the AI-CE design. The 650/650°F steam conditions correspond to using the same size heat exchange equipment as for the 675/675°F case with lowered feedwater temperatures in order to reduce "pinch-point" effects. Cost information on these aspects is given in Chapter 7.

The results given above were used in our evaluation of the HWOGR performance; specifically, with an average coolant outlet temperature of 700°F the thermal efficiency was taken as 34.1%. An efficiency value of 33.2% was associated with an average coolant outlet temperature of 675°F.

### 6.11 Electrical Systems

Auxiliary power requirements for the HWOGR are relatively low because all major pumps are turbine driven. If brushless exciters can be utilized, there will be no motor breaker requirements greater than 1000 hp.

The system is organized along conventional lines and employs 4160-v feeder breakers operating from four buses. The emergency ac and dc power provisions described are adequate for this plant.

### 6.12 Service Systems

Reactor service systems are provided for spent-fuel cooling, high- and low-temperature cooling water, nitrogen supply, carbon dioxide supply, reactor startup steam, radioactive waste disposal, refueling machine services, and new coolant handling. Functional requirements and capacities

of these systems given in the conceptual design report<sup>1</sup> were reviewed mainly for cost evaluation. We have no particular points to question as the result of the review that was made.

Plant service systems are comparable to equivalent systems of the concepts considered in the advanced-converter study.<sup>2</sup>

### 6.13 Site and Structures

The site for the reference plant is the AEC hypothetical Middletown. The features of the site have been described by the AEC.<sup>20</sup>

Because of the position of the turbine building with respect to the reactor building in the HWO CR plant layout, condenser cooling water inlet lines are longer than would be the case for parallel arrangement with the river. A rearrangement of the layout could reduce the cost of these lines somewhat but might result in higher costs elsewhere in the system. The savings, if any, would be too small to justify additional study of the building arrangements.

Structures appear to be adequately sized for the systems described. The type of construction for the turbine-generator building and auxiliary buildings is assumed to be the same for purposes of cost normalization as for equivalent buildings in the advanced-converter study.<sup>2</sup> However, the reactor building is of concrete-lined welded steel-plate construction, whereas in the advanced-converter studies most of the reactor buildings were constructed of reinforced concrete to withstand a high internal pressure.

The design of the turbine-generator building could be revised to reduce the volume. The turbine-generator equipment could be housed in a building of the same size as the pressurized-water reactor building used as a standard for normalization in the advanced-converter study.<sup>2</sup>

### 6.14 Plant Safeguards

Information presented on plant safeguards was not in sufficient detail for evaluation of the adequacy of the safeguards provided. Although

the design report<sup>1</sup> states that an accident analysis should consider the possibility of large organic spills and fires inside the containment building, with coincident use of the water-sprinkler system, no detailed analysis is presented of the consequences of such an accident. Even though a coolant release in itself would not result in a large increase in containment pressure, the transfer of the large amount of heat stored in the coolant to either the moderator or water from the spray system has the potential of causing a containment pressure higher than the design value.

We considered that use of double isolation valves on all main coolant lines penetrating the reactor building makes it feasible to locate the steam generators outside the reactor building. However, this philosophy may restrict this type of plant to remote sites, such as the AEC Middletown site assumed for this study. Although siting near urban areas was not a requirement in this study, consideration should be given to alternate designs that might be more acceptable than the present one from this viewpoint, such as arrangements using multiple containment of the reactor and associated coolant equipment. Plant safeguard requirements are dependent on the conditions associated with the maximum credible accident, which has not been defined or investigated.

#### References

1. Combustion Engineering, Inc., and Atomics International, Heavy Water Organic Cooled Reactor - 1000 Mwe Nuclear Power Plant Preliminary Conceptual Design, USAEC Report AI-CE-Memo-6, Vol. II, Oct. 1, 1965.
2. M. W. Rosenthal et al., A Comparative Evaluation of Advanced Converters, USAEC Report ORNL-3686, Oak Ridge National Laboratory, January 1965.
3. Babcock & Wilcox Company, Thorium Fuel Cycle for Heavy Water Moderated Organic Cooled Reactors, Quarterly Technical Report No. 2, April-June 1965, USAEC Report B&W-393-2, October 1965.
4. Babcock & Wilcox Company, 1000 MWe Thorium HWO CR - Preliminary Conceptual Design Data for ORNL Evaluation, USAEC Report (unnumbered), Nov. 15, 1965.

5. J. G. Roberts, Calandria Core Weld Joint Development, USAEC Report NAA-SR-9821, Atomics International, June 30, 1965.
6. Westinghouse Electric Corporation, Development of Pressure Tube Seal Welding and Cutting Equipment for CVTR, USAEC Report CVNA-99, March 1964.
7. Combustion Engineering, Inc., and Atomics International, HWOCR Quarterly Report through June 1965, USAEC Report AI-CE-3.
8. Private communications from Phillips Petroleum Company personnel.
9. R. F. Makens (Ed.), Organic Coolant Summary Report, USAEC Report IDO-11401, Phillips Petroleum Company, December 1964.
10. L. E. Gardner, Catalytic Hydrocracking of High Boiler in Nuclear Reactor Coolant, USAEC Report IDO-16877, Phillips Petroleum Company, May 20, 1963.
11. R. E. Wintenberg and J. L. Anderson, A Ten Decade Reactor Instrumentation Channel, Trans. Am. Nucl. Soc., 3(2): 454-455 (December 1960).
12. F. T. Binford and E. N. Cramer (Eds.), The High-Flux Isotope Reactor, USAEC Report ORNL-3572, Vol. 1, Oak Ridge National Laboratory, May 1964.
13. L. C. Oakes, High Reliability Servos, in Proceedings of the Seventh Tripartite Instrumentation Conference (Reactors), British Report AEEW-R 452, Vol. 1, August 1965.
14. E. P. Epler, Operating Experience with Coincident vs Noncoincident Reactor Safety Systems, USAEC Report ORNL-TM-738, Oak Ridge National Laboratory, Dec. 12, 1963.
15. J. L. Anderson, E. N. Fray, and S. J. Ditto, Log N and Period Safety Module, in Instrumentation and Controls Division Annual Progress Report, September 1, 1965, USAEC Report ORNL-3875, Oak Ridge National Laboratory (to be published).
16. J. H. Campo, Summary Report - 1000 Mwe HWOCR - Steam Cycle Investigations, Steam Generator and Reactor Thermal Power, and Net Plant Efficiency, informal AI-CE memorandum, October 1965.
17. 1965 Nuclear Heat Balance Calculation Method, Large Steam Turbine-Generator Department, General Electric Company, Schenectady, New York.

18. Advertisement in Power Engineering, p. 27, May 1965.
19. D. A. Oneil, Westinghouse Electric Corporation, telephone communication with M. L. Myers, Oak Ridge National Laboratory, Dec. 13, 1965.
20. Guide to Nuclear Power Cost Evaluation, USAEC Report TID-7025, Mar. 15, 1962.

## 7. CAPITAL COSTS

An evaluation of capital cost estimates for the reference uranium-fueled HWO CR plant was made, and capital cost differences between the uranium-fueled plant and the two thorium-fueled reactor concepts were estimated. The adjusted capital cost estimates we determined for the reference designs are compared with the costs reported by AI-CE for the uranium-fueled HWO CR plant in Table 7.1. The total direct construction costs are essentially the same, since the cost adjustments made in accounts 21, 22, and 23 offset each other. Except for the adjustment in reactor equipment costs, the adjustments of the reported costs resulted mainly from normalization of costs relative to the costs of the advanced-converter concepts.<sup>1</sup> No significant changes to the design described by AI-CE were considered in making these cost estimates. The influence of required design changes on costs is estimated separately. Also, possible compromises in the design to provide additional safety margins are discussed, but the effects of these compromises on capital cost were not evaluated.

Indirect costs were based on the same percentages as those used in the advanced-converter study. The breakdown of these percentages is given in Table 7.1.

The capital cost estimates for the thorium-fueled concepts were obtained by estimating the cost differentials associated with variations from the reference uranium-fueled design. The direct capital cost of the B&W nested-cylinder concept was \$3.9 million lower than that of the AI-CE uranium-fueled concept, and the direct capital cost of the B&W pin-cluster design was \$3.2 million lower.

### 7.1 Capital Cost Breakdown for AI-CE Reference Design Conditions

The breakdown of direct capital costs for the reference design was made in accordance with the AEC classification of accounts. Table 7.2 compares the breakdown of costs reported by AI-CE with the adjusted costs of this evaluation study for the reference design conditions. In arriving at the adjusted costs, correlations from the advanced-converter study

Table 7.1. Estimated Total Capital Costs for 1000-Mw(e) HWOOR Reference Plant

Thermal power: 3093 Mw  
Thermal efficiency: 34.8%

	Basis of In- direct Cost (% of direct cost)	Cost Reported by AI-CE	ORNL Adjusted Cost
Direct construction cost			
Account			
21 - Structures and improvements		\$ 11,926,000	\$ 11,463,000
22 - Reactor plant equipment		38,719,900	40,479,100
23 - Turbine-generator units		30,925,600	29,666,800
24 - Accessory electric equipment		3,345,300	3,345,300
25 - Miscellaneous power plant equipment		785,400	785,400
Total direct construction cost		\$ 85,702,200	\$ 85,739,600
Indirect construction cost			
General and administrative	6	5,142,100	5,144,400
Subtotal		\$ 90,844,300	\$ 90,884,000
Miscellaneous construction	1	908,400	908,900
Subtotal		\$ 91,752,700	\$ 91,792,900
Engineering design and inspection			
Architectural and engineering services	5	4,587,600	4,589,600
Subtotal		\$ 96,340,300	\$ 96,382,500
Nuclear engineering	2	1,926,800	1,927,700
Subtotal		\$ 98,267,100	\$ 98,310,200
Startup costs: 35% of annual operating and maintenance cost		695,400	605,400
Subtotal		\$ 98,872,500	\$ 98,915,600
Contingency	10	9,887,200	9,891,600
TOTAL DIRECT AND INDIRECT CONSTRUCTION COST		\$108,759,700	\$108,807,200
Customer cost			
Investor-owned plant			
Interest during construction	10.8	11,746,000	11,751,200
TOTAL DEPRECIABLE CAPITAL COST		\$120,505,700	\$120,558,400
20 - Land and land rights		360,000	360,000
TOTAL CAPITAL COST		\$120,865,700	\$120,918,400
Publicly owned plant			
Interest during construction	7.2	7,830,700	7,834,100
TOTAL DEPRECIABLE CAPITAL COST		\$116,590,400	\$116,641,300
20 - Land and land rights		360,000	360,000
TOTAL CAPITAL COST		\$116,950,400	\$117,001,300

Table 7.2. Breakdown of Estimated Direct Construction Costs for 1000-Mw(e) HWOCR Reference Plant

Account	Cost Reported by AI-CE	ORNL Adjusted Cost
20 - Land and land rights	\$ 360,000	\$ 360,000
21 - Structures and improvements		
211 Ground improvements	735,000	866,000 <sup>a</sup>
212 Buildings		
A-212 Steam generator building	612,400	556,400 <sup>a</sup>
B-212 Turbine-generator building	2,218,000	1,680,000 <sup>a</sup>
C-212 Auxiliary building	516,000	516,000
D-212 Administration building	220,000	220,000
E-212 Fuel-handling building	531,000	531,000
F-212 Service building	127,000	127,000
G-212 Screen well	551,000	551,000
H-212 D <sub>2</sub> O service building	315,000	315,000
I-212 Pump building	603,000	603,000
J-212 Gate house	10,000	10,000
K-212 Well pump house	2,600	2,600
Total cost, item 212	\$ 5,706,000	\$ 5,112,000 <sup>a</sup>
218 Stacks (in C-212)		
219 Reactor containment structure	\$ 5,485,000	\$ 5,485,000
Total cost, account 21	\$11,926,000	\$11,463,000 <sup>a</sup>
22 - Reactor plant equipment		
221. Reactor equipment		
.1 Reactor vessel	6,283,800	7,528,000 <sup>a</sup>
.2 Reactor controls	474,900	474,900
.3 Reactor shielding	1,460,200	1,460,200
.4 Reactor auxiliary cooling and heating systems	837,900	837,900
.5 Reactor plant containers (in 219)		
.6 Moderator and reflector (listed elsewhere)		
.7 Reactor plant cranes and hoists	160,500	160,500
Total cost, item 221.	\$ 9,217,300	\$10,461,500 <sup>a</sup>
222 Heat transfer systems		
.1 Reactor coolant system	4,799,000	5,202,000 <sup>a</sup>
.3 a) Steam generators	2,838,000	2,950,000 <sup>a</sup>
b) Superheaters	1,443,500	1,443,500
c) Reheaters	881,500	881,500
.4 Reactor coolant receiving, supply, and treatment	1,286,800	1,286,800
.5 Reactor moderator auxiliary systems	1,232,200	1,232,200
.6 Operating fluids	10,000	10,000
Total cost, item 222	\$12,491,000	\$13,006,000 <sup>a</sup>

<sup>a</sup>Specific items adjusted.

Table 7.2 (continued)

	Cost Reported by AI-CE	ORNL Adjusted Cost
22 -- Reactor plant equipment (continued)		
223 Nuclear fuel-handling and storage equipment	\$ 3,182,100	\$ 3,182,100
225 Radioactive waste treatment and disposal	137,500	137,500
226 Instrumentation and control	7,461,800	7,461,800
227 Feedwater supply and treatment	2,899,300	2,899,300
228 Steam, condensate, and feedwater piping	3,195,900	3,195,900
229 Other reactor plant equipment	135,000	135,000
Total cost, account 22	\$38,719,900	\$40,479,100 <sup>a</sup>
23 -- Turbine-generator units		
231 Turbine generators	\$26,291,100	\$25,473,900 <sup>a</sup>
232 Circulating-water systems	1,580,500	1,376,000 <sup>a</sup>
233 Condensers	2,677,100	2,440,000 <sup>a</sup>
235 Turbine plant boards, instruments, and controls	326,900	326,900
236 Turbine plant piping (in 228)		
237 Auxiliary equipment for generators	50,000	50,000
238 Other turbine plant equipment (in 232)		
Total cost, account 23	\$30,925,600	\$29,666,800 <sup>a</sup>
24 -- Accessory electric equipment	\$ 3,345,300	\$ 3,345,300
25 -- Miscellaneous power plant equipment	\$ 785,400	\$ 785,400

and related cost surveys were used as a check of the estimates submitted. To further assist in this evaluation, AI-CE provided second-order breakdowns separating labor and material costs, along with backup information, as requested, on data used in estimating costs of some of the major components. The following discussion of our evaluation of direct costs reported for each major account gives reasons for the adjustments we made.

The cost of ground improvements (account 21.1) was revised upward to agree with the cost used in the advanced-converter study.

Building costs reported by AI-CE were checked closely with unit cost correlations derived from the advanced-converter study. The turbine-generator building cost (account B-212) was reduced because the building volume of the pressurized-water reactor and other saturated-steam turbine

plants in the advanced-converter study would be adequate for the HWOCR plant. A slightly higher unit cost was used, however, since more recent cost data show unit costs reported for the pressurized-water reactor turbine-generator building to be low, even for a minimum estimate.

Correlations from studies of pressure-tube reactor costs and cost breakdowns submitted by AI-CE and B&W on their reactor plants were used in evaluating the reactor vessel costs (account 221.1). Unit costs reported by AI-CE and B&W for fabricated SAP and Zircaloy-2 tubes (approximately \$25 and \$32/lb, respectively) were based on manufacturer's quotations and were used in the adjusted cost estimate. However, the costs for assembly and other material charges were estimated to be some 30% higher than the AI-CE reported values. Our estimates of the calandria vessel and shields agreed closely with those reported by AI-CE.

We found little related cost information that could be applied to check the reported cost of reactor controls (account 221.2). The designs of both the regulating controls and shutdown rods are simple, and it seems reasonable to assume that they can be built for the costs reported. The necessity to change to a more sophisticated control rod system would significantly increase the cost in the subaccount.\*

We agreed with costs reported for the reactor coolant system (account 221.1) except that the cost of the reduction gear for the turbine-pump assembly did not appear to be accounted for. The cost was adjusted to account for this assembly.

Our calculations indicated that the heat transfer area of the steam generators (account 222.3a) could be reduced, but we estimated unit costs to be about \$19/ft<sup>2</sup> instead of the unit cost of \$15/ft<sup>2</sup> of the AI-CE estimate. The net result was a small increase in the cost of these units.

AI-CE estimates of the refueling machine (in account 223) were based on the cost of similar Canadian units and were used as reported.

---

\*The demonstration plant design<sup>2</sup> has 64 three-rod-cluster power-control rods as compared with 9 four-rod and 8 three-rod clusters in the reference plant. Based on a scaleup of the demonstration plant control rod system design and costs, we estimate that costs in this subaccount for the 1000-Mw(e) reactor controls would be increased more than one million dollars over the amount shown in Table 7.2.

The cost of equipment for radioactive waste treatment and disposal (account 225) appears low when compared with costs for similar systems for other large reactors, but it seems consistent with the simplicity of the system described in the conceptual design report. Thus we made no adjustment to the reported cost.

Instrumentation and control (account 226) costs were reviewed and checked against other cost data. The reported costs are believed to be conservative for this concept, even though modifications to the proposed control scheme appear to be required.

Costs of feedwater supply and treatment (account 227) and steam condensate and feedwater piping were estimated and found to agree closely with those reported by AI-CE.

In the advanced-converter study, estimated list prices of turbine-generator units (account 231) were discounted 22% to arrive at the adjusted costs. The cost of the turbine-generator unit for the HWOCR was obtained by AI-CE as a budgetary quote from Westinghouse for the selling price of a unit of this type and rating. It is assumed that Westinghouse applied a discount, but the amount of discount is not known. Due to the special design features of this unit, a probable selling price cannot be developed with much accuracy from existing price tables. Therefore, we made no adjustment to the reported cost for the turbine-generator units.

The cost of the exciter is included as part of the cost of the turbine-generator units and, in this case, it is assumed a brushless design with spare built-in capacity would be provided. The spare unit called for in the reference design would therefore be eliminated. The cost for this account was thus adjusted by subtracting the cost of the spare exciter and reducing the foundation and installation costs.

The circulating water system (account 232) costs were normalized to be consistent with the costs of this system in the advanced-converter study.

Normalization of the condenser (account 233) costs resulted in a 9% reduction in the cost reported for this account.

We agreed with other costs reported under account 23 and satisfactorily checked costs reported for accounts 24 and 25.

## 7.2 Capital Cost Normalization of B&W Concepts

The principal differences between concepts proposed by B&W for the thorium-fueled reactors and the reference AI-CE concept that affect costs are the following:

1. The reactor vessels for the B&W concepts are smaller in diameter because of fewer fuel channels but are longer than the AI-CE vessel. The B&W reactor calandria and process tubes are longer and larger in diameter than the AI-CE reactor tubes.

2. B&W proposes single-direction coolant flow and on-power refueling from one end instead of bidirectional flow and refueling from both ends as in the AI-CE reference plant concept.

3. Because of a higher coolant temperature rise and greater pressure drop across the core, the B&W concepts require about 0.8 of the coolant flow and 0.9 of the pumping power required by the AI-CE concept. The B&W concepts require steam generators about 30% larger in order to produce steam at the same pressure and temperature as in the reference design.

Estimated direct capital cost differences associated with these design variations are compared in Table 7.3. These differences were

Table 7.3. Capital Cost Differences Between AI-CE and B&W Designs

Account	Item	Adjusted AI-CE Base Cost	Cost Differential	
			B&W Nested- Cylinder Design	B&W Pin- Cluster Design
A212	Steam generator building	\$ 556,400	\$ +108,000	\$ +108,000
219	Reactor containment structure	5,485,000	-450,000	-450,000
221.1	Reactor vessel and shields	8,988,200	-2,481,000	-1,942,800
and 221.3				
221.2	Reactor controls	474,900	-94,900	-94,900
222.1	Reactor coolant system	5,202,000	-330,000	-330,000
222.3a	Steam generators	2,950,000	+600,000	+600,000
222.3b	Superheaters	1,443,500	+26,500	+26,500
223	Nuclear fuel-handling and storage equipment	3,182,100	-602,100	-602,100
226	Instrumentation and control	7,461,800	-665,000	-540,000
	Net direct capital cost difference		\$-3,888,500	\$-3,225,300

determined from normalizations of cost to the reference design conditions according to assumptions discussed below.

The B&W steam generator building (account 212) would be larger to accommodate larger steam generators. The reference design unit cost was used to make the adjustment for the increased building volume.

It was estimated that the reactor containment structure (account 219) could be reduced about 5 ft in diameter because of the more compact header arrangements of the B&W design. It is not clear how much reduction in height would be realized because of refueling from one end. Space requirements for fuel storage and for moderator facilities would be equivalent in all designs. More detailed layout studies would be necessary to determine minimum containment height for the B&W concepts; however, a reduction of 15 ft was assumed for this estimate. With the reduced volume, the containment vessel would be required to withstand a higher internal pressure for the same accident conditions and thus have a thicker steel shell than the base design.

A differential cost of \$450,000 less was estimated for net changes in substructure, pressure vessel, and internal concrete.

The end shields (account 221.3) for the B&W concepts are integral parts of the reactor vessel (account 221.1) but are separate components in the AI-CE reference design. For the purpose of cost normalization, the end closures were considered as being part of the reactor vessel, and the remainder was considered in the shielding costs. A summary of the normalized cost comparison of reactor vessels and shields is shown in Table 7.4. Side shields were assumed to be required for both concepts.

Differences in reactor control (account 221.2) requirements were not defined. An arbitrary reduction of 20% was assumed because of the fewer number of process tubes and control zones.

The reactor coolant system cost (account 221.1) was adjusted to account for reduced pumping requirements. Differential pump costs were evaluated at \$65/bhp.

The normalized cost of steam generators (account 223.a) was determined on a differential basis; it was scaled by the 0.7 power of size. This resulted in a differential cost addition of about \$600,000 for the

Table 7.4. Summary of Normalized Cost of Reactor Vessels and Shields - Accounts 221.1 and 221.3

	AI-CE	B&W Designs	
	Design Adjusted	Nested Cylinder	Pin Cluster
Vessel	\$ 966,500	\$ 827,500	\$ 845,500
Channel assemblies	5,195,500	3,638,700	4,076,900
Pigtails and headers	1,366,000	1,068,000	1,121,000
Shields	1,460,200	973,000	1,002,000
Total	\$8,988,200	\$6,507,200	\$7,045,400
Difference	Base	\$-2,481,000	\$-1,942,800

B&W concepts. The minor increase in superheater area was costed (account 223.b) at the base case value of \$14.80/ft<sup>2</sup>.

The single fuel-handling machine cost (account 223 - nuclear fuel-handling and storage equipment was arbitrarily taken at 80% of the reported cost for the two machines in the reference plant. There was not enough detailed information to identify cost differences for this account more accurately; however, since the storage length was relatively long and much more fuel handling was involved than for the AI-CE mechanism, improved reliability was required.

Reactor plant instrumentation (account 226) for the reference plant is estimated to cost \$4,310,000, of which about \$1,200,000 is for the computer complex. The difference of \$3,110,000 was adjusted for reactor volumes and number of fuel channels to arrive at the estimated costs for the B&W concepts.

### 7.3 Moderator and Coolant Investment

A summary of moderator and coolant inventories and corresponding investments for the uranium- and thorium-fueled HWOCR designs is given in Table 7.5. Coolant inventories reported for the uranium-fueled design were assumed to be applicable to all three concepts.

Table 7.5. Moderator and Coolant Investments

	AI-CE Uranium- Fueled Design	B&W Pin- Cluster Thorium- Fueled Design	B&W Nested- Cylinder Thorium- Fueled Design
Calandria D <sub>2</sub> O inventory, lb	588,000	567,000	555,000
Moderator auxiliaries D <sub>2</sub> O inventory, lb	66,000	66,000	66,000
Total D <sub>2</sub> O inventory, lb	654,000	633,000	621,000
Total D <sub>2</sub> O investment, \$	13,080,000	12,660,000	12,420,000
Coolant inventory, lb	2,300,000	2,300,000	2,300,000
Coolant investment, \$	276,000	276,000	276,000

#### 7.4 Cost Uncertainties

There are a number of difficulties in interpreting design requirements that can introduce cost uncertainties, aside from the uncertainties associated with normal estimating inaccuracies. Some specific items in question are

1. the additional cost of reactor containment if pressure suppression is required,
2. the special tools and services required for emergency operations which were not fully evaluated in this conceptual study,
3. the cost of the instrumentation and control systems required to adequately control an HWOCR with a positive temperature coefficient of reactivity,\*

---

\*Although this cost cannot be specified reliably without much more investigation, it is clear that a sophisticated control system is required. The total money provided for instrumentation, control rods, and drives is believed more than adequate based on needs specified by the design sponsor; considering our suggested changes, the funds allocated appear sufficient to cover the instrumentation and control needs. However, safety considerations, maximum-credible-accident studies, and associated containment requirements need to be investigated in detail, and results of these studies could influence reactor costs.

4. the reliability of on-line refueling and fuel-handing equipment relative to maintaining a high load factor,
5. the turbine-generator costs, which may not have been discounted to the same extent as the turbine-generator costs used in the advanced-converter study.

#### 7.5 Effect of Recommended Design Changes on Estimates of Capital Costs

The design changes that appear necessary for plant feasibility have an influence on the cost estimates; the most significant one relative to power costs is the lower coolant temperature required because of heat transfer, fluid flow, and fouling considerations. It is estimated that for the specified design conditions, the fuel surface temperature is about 880°F with no fouling film present, and the temperature drop through the fouling film associated with fuel at the maximum surface temperature will raise the maximum fuel temperature an additional 25 to 50°F. While the influence of these factors can be incorporated in several ways, the most direct is to consider a change in coolant temperature for essentially the same design. Under such conditions the reactor inlet and outlet temperatures would be lowered, and the steam conditions would be those given previously in Chapter 6. The thermal efficiency of the plant would then drop from 34.8 to about 33.2 to 34.1%. The above changes in temperatures would be accompanied by an increase in heat exchanger sizes in order to minimize changes in steam conditions. We estimate that decreasing the outlet coolant temperature from 750 to 700°F would increase the direct costs of the heat exchangers and associated equipment about \$2,500,000 and lead to a plant thermal efficiency of 34.1%. By taking into consideration the direct costs plus indirect costs for the above items, the adjusted cost estimate in Table 7.1, and the change in thermal efficiency, our lower estimate of capital costs for the AI-CE plant is \$124,400,000 for a plant producing 1052 Mw(e) or \$118/kw(e) for an investor-owned plant; the corresponding number for a publicly owned plant is \$114/kw(e).

Based on an outlet coolant temperature of 675°F, the thermal efficiency would be reduced to 33.2%, and the capital costs would remain as

adjusted above (increasing the size of the heat exchanger beyond that considered above does not appear to be advantageous because of transportation limitations). Under these circumstances, the capital costs for the AI-CE design correspond to \$121/kw(e) for investor-owned plants and \$117/kw(e) for publicly owned plants.

Similar changes in heat exchanger costs and thermal conditions apply to the B&W designs. However, the situation is more involved, since the power-peaking factors in the thorium-fueled cases can be improved by using an "out-in" type of fueling scheme. Such a change is feasible, but a new design study would be required to determine the design parameter values that would apply. Also, using bidirectional coolant flow lowers peak temperatures; we consider such coolant flow desirable and applicable.

For the B&W nested-cylinder fuel design, the outlet organic coolant temperature is estimated to be 675 to 700°F. For such conditions the heat exchanger systems would be enlarged above the base case to maintain a high thermal efficiency for the plant. The associated changes in coolant temperatures and heat exchanger sizes are estimated to add about \$1,800,000 to the direct costs given in Table 7.3, while the associated increase in coolant pumping requirements would add about \$500,000. Thus the direct cost changes given in Table 7.3 for the nested-cylinder design would be increased by \$2,300,000. Applying indirect costs and the ORNL adjusted costs of Table 7.1 gives total capital costs of \$118,700,000 for an investor-owned plant. The associated thermal efficiency would be in the range of 33.2 to 34.1% and would give unit costs of \$113 to 116/kw(e) for the B&W investor-owned nested-cylinder reactor. Based on public ownership accounting, the unit capital costs would be in the range \$109 to 112/kw(e).

Similarly, the total capital costs for the B&W pin-cluster design would be \$119,600,000 for investor-owned utilities and \$115,700,000 for publicly owned plants. The outlet coolant temperature would be 660 to 690°F and would give an estimated plant thermal efficiency in the range of 32.5 to 33.9%. The unit capital costs for the B&W pin-cluster design would then be \$114 to 119/kw(e) for investor-owned plants and \$110 to 115/kw(e) for publicly owned facilities.

The above estimates of capital costs for 1000-Mw(e) stations are summarized in Table 7.6. These costs are based on requirements of a feasible system; they imply that special features of the plant will be successfully demonstrated through the development programs now in progress.

Table 7.6. Summary of Unit Capital Cost Estimates for 1000-Mw(e) HWOCR Plants

	Total Capital Costs [\$/kw(e)]	
	Investor-Owned Plant	Publicly Owned Plant
AI-CE design, uranium cycle	118-121	114-117
B&W design, thorium cycle		
Oxide fuel	114-119	110-115
Metal fuel	113-116	109-112

#### References

1. M. W. Rosenthal et al., A Comparative Evaluation of Advanced Converters, USAEC Report ORNL-3686, Oak Ridge National Laboratory, January 1965.
2. Combustion Engineering, Inc., and Atomics International, Heavy Water Organic Cooled Reactor, USAEC Report AI-CE-Memo-25, Mar. 29, 1966.

## 8. OPERATION AND MAINTENANCE COSTS

The total operation and maintenance costs reported by AI-CE are consistent with the total operation and maintenance costs used for the advanced-converter comparisons.<sup>1</sup> We have no general basis for modifying the costs as presented for this evaluation study, but we recommend that more detailed evaluations and breakdowns of these costs be made as operation and equipment maintenance requirements become better established. The breakdown of operation and maintenance costs is listed below:

	Annual Cost
	<u>                    </u>
Total payroll	\$ 680,000
Repair and maintenance materials and contract services	1,050,000
Insurance	353,000
Coolant makeup cost*	168,000
Heavy-water makeup cost	73,000
	<u>                    </u>
Total	\$2,324,000

The total payroll cost reported above is based on a permanent staff of about 70 people with an allowance of 25% for payroll fringe benefits and 20% for general and administrative expense. Although these costs are consistent with the values used in the advanced-converter study, we now believe the staff cost to be underestimated by as much as 30 to 40%, based on preliminary information in Brookhaven National Laboratory's proposed revision to Section 530 of the AEC "Guide to Nuclear Power Cost Evaluation."<sup>2</sup> Increasing the total payroll cost by 35% increases the total cost figure in the above tabulation from \$2,324,000 to \$2,562,000. Under the above circumstances, the operation and maintenance cost contribution to power production cost increases from 0.332 to 0.366 mill/kwhr(e).

The costs associated with coolant makeup and heavy-water losses are nearly the same for the uranium- and thorium-fueled reactors, so only a single value is considered here. The cost for coolant makeup depends on the successful development of a catalytic hydrocracker to produce coolant

---

\*Based on 0.8 load factor and coolant cost of 12¢/lb.

of the required properties. The coolant makeup costs are based on requirements of 200 lb/hr at full-power operation; the heavy-water losses are estimated to be 0.56% of the total D<sub>2</sub>O inventory per year.

#### References

1. M. W. Rosenthal et al., A Comparative Evaluation of Advanced Converters, USAEC Report ORNL-3686, Oak Ridge National Laboratory, January 1965.
2. Guide to Nuclear Power Cost Evaluation, USAEC Report TID-7025, Mar. 15, 1962.

## 9. FUEL PREPARATION COST

Fuel preparation consists of those operations necessary to convert makeup and/or recycle material to the proper chemical and physical form needed for fuel fabrication. The complexity of these operations varies with the fuel cycle envisioned. Fuel preparation is defined here to include the preparation of ceramic-grade oxide powder, arc-fused oxide fragments, sol-gel oxide fragments, sol-gel oxide fragments containing carbon, thorium-metal powder or sponge, or uranium-metal billets, as appropriate. The preparation of UC from ceramic-grade oxide is not considered here but is included in fuel fabrication (Chapt. 10).

Fuel material preparation for the proposed AI-CE UC-fueled reactor consists of the conversion of slightly enriched  $UF_6$  to  $UO_2$ . Normal processing methods for feed material production may be used for this conversion. No recycle of plutonium or depleted uranium is considered.

B&W considered two alternate fuels in their studies; namely, uranium-thoria in clustered SAP-clad pins or uranium-thorium metal in Zircaloy-clad nested cylinders. Fuel preparation consists of conversion of partially decontaminated nitrate product solutions from the reprocessing plant to uranium-thoria for the pins or to pressed thorium powder and uranium billets for the nested cylinders. Makeup uranium of high enrichment is converted from  $UF_6$  to purified  $UO_3$  for the oxide cycle or to  $UF_4$  for the metal cycle. The appropriate compound is then added to the single "sol-gel" line required for uranium-thoria preparation or to the metal line. Thorium compounds (as purchased) may be added directly to these alternate fuel-preparation lines. The chemical conversion of recycle thorium and  $^{233}U$  requires remote operations in a highly shielded facility.

### 9.1 Estimating Method

The total estimated cost of production is the sum of the direct operating costs and a capital charge of 22% or 15% per year on the total estimated capital cost.

The steps in obtaining the estimated capital cost are to

1. prepare process flowsheet,
2. size individual process equipment items,
3. size building to house process equipment,
4. estimate cost of installed process equipment items and the building, including normal services, and
5. estimate complete cost by multiplying item 4 costs by factors that take into account the requirements for a complete plant.

Operating costs are based on the required staff, overhead, and other needs, such as chemicals, other supplies, services, and utilities.

The fuel preparation plant is considered to be an integral portion of the processing-fabrication facility. An onstream factor of 260 days per year is assumed. The preparation plant is assumed to share items such as site, service, and utility services, as well as certain manpower, with the reprocessing or fabrication plants as appropriate, and this is reflected in estimated costs.

## 9.2 UF<sub>6</sub>-to-UO<sub>2</sub> Conversion for AI-CE Fuel

The AI-CE fuel cycle starts with slightly enriched UF<sub>6</sub>, and the fuel preparation step provides for the conversion of this material to ceramic-grade UO<sub>2</sub>. In estimating the cost of fuel preparation, the process was subdivided as follows:

1. UF<sub>6</sub> is oxidized to U<sub>3</sub>O<sub>8</sub> by reaction with steam at 500°F, followed by pyrohydrolysis in a propane-oxygen flame.
2. The impure U<sub>3</sub>O<sub>8</sub> is dissolved in nitric acid, passed through a solvent extraction cycle, and converted to UO<sub>3</sub> by steam denitration.
3. UO<sub>3</sub> is converted to UO<sub>2</sub> by hydrogen reduction in a fluid bed.

The estimated costs for the installed equipment and direct operations for steps (1) and (2) are taken directly from a previous study.<sup>1</sup> New estimates were made for step (3). All three steps are performed in the same building. Table 9.1 summarizes the costs for these operations, including building, auxiliaries, operating, and service costs.

Table 9.1. Estimated Cost of Converting UF<sub>6</sub> to UO<sub>2</sub> for AI-CE Fuel

Item	1-MT/Day Plant	10-MT/Day Plant
Plant costs, \$		
Installed equipment		
UF <sub>6</sub> to U <sub>3</sub> O <sub>8</sub>	172,000	787,000
U <sub>3</sub> O <sub>8</sub> to UO <sub>3</sub>	626,000	1,783,000
UO <sub>3</sub> to UO <sub>2</sub>	427,000	1,467,000
Subtotal	1,225,000	4,037,000
Building	518,000	1,110,000
Total physical cost	1,743,000	5,147,000
With yard improvements (15%)	2,004,000	5,919,000
With construction overhead (30%)	2,605,000	7,695,000
With architect-engineer fees (15%)	2,996,000	8,849,000
Total estimated capital cost (with 1.0% contingency)	3,295,000	9,732,000
Unit operating costs, \$/kg		
Direct operating costs		
UF <sub>6</sub> to U <sub>3</sub> O <sub>8</sub>	0.67	0.20
U <sub>3</sub> O <sub>8</sub> to UO <sub>3</sub>	1.52	0.40
UO <sub>3</sub> to UO <sub>2</sub>	1.43	0.42
Subtotal	3.62	1.02
Capital charges		
At 22% per year	2.79	0.82
At 15% per year	1.90	0.56
Total estimated cost		
At 22%	6.41	1.84
At 15%	5.52	1.58

### 9.3 Preparation of Thorium Fuels for B&W Designs

Preparation of the two B&W fuels consists essentially of (1) conversion of partially decontaminated nitrate product solutions from the reprocessing plant to urania-thoria or to pressed thorium-metal powder and uranium billets, and (2) conversion of makeup  $UF_6$  to purified  $UO_3$  or to  $UF_4$ .

The reprocessing plant consists of a single-cycle solvent extraction unit. Conversion of the recovered nitrate products to the form desired for fabrication requires remote operations in a highly shielded canyon. The required makeup  $^{235}U$  is converted to the desired form in a nonshielded area; the resulting material is then added to the remote-operations facility at the appropriate step.

In estimating the cost for the oxide facility, an earlier estimate<sup>2</sup> was used, along with modifications. The principal changes were increases in the factors converting total physical cost to total capital cost, an increase in labor overhead to 100%, and a decrease in operating time to 260 onstream days per year. The results are summarized in Table 9.2.

The metal-fuel facility consists of a heavily shielded thorium-metal powder line based on the Nuclear Fuel Services<sup>3</sup> approach and an

Table 9.2. Preparation Costs for B&W Oxide Fuel

Item	1-MT/Day Plant	4-MT/Day Plant
Capital cost		
Total, \$	5,819,000	10,973,000
\$/yr at 22% per year capital charge	1,280,000	2,414,000
\$/kg for 260 days per year	4.92	2.32
\$/kg at 15% per year capital charge	3.35	1.58
Operating cost		
Direct, \$/kg	4.83	1.98
Total		
\$/kg at 22%	9.75	4.30
\$/kg at 15%	8.18	3.56

enriched-uranium billet line based on information from Y-12.<sup>4</sup> Table 9.3 summarizes the fuel preparation costs associated with the required facilities.

Table 9.3. Preparation Costs for B&W Metal Fuel

Item	1-MT/Day Plant	4-MT/Day Plant
Capital cost		
Total, \$	6,837,000	12,126,000
\$/yr at 22% per year capital charge	1,504,000	2,668,000
\$/kg for 260 days per year	5.78	2.56
\$/kg at 15% per year capital charge	3.94	1.74
Operating cost		
Direct, \$/kg	7.71	4.34
Total		
\$/kg at 22%	13.49	6.90
\$/kg at 15%	11.65	6.08

#### 9.4 Summary

Table 9.4 summarizes the estimated preparation costs for the fuels and conditions considered. The reported point estimates may be connected by a straight line on a log-log graph to obtain the costs for fuel throughput rates different than those investigated; the resulting graph is given in Fig. 9.1.

In the advanced-converter evaluation,<sup>5</sup> fuel preparation costs were based on a "cold sol-gel" process and were included as part of the fabrication costs. To make a comparison of the above results with those of the advanced-converter study, the fuel preparation costs used in the advanced-converter study have been identified.<sup>6</sup> These are given in Table 9.5 based on use of "cold sol-gel" oxide preparation. Metallic fuel was not considered in the advanced-converter study, so no associated costs can be given.

Table 9.4. Summary of Estimated Fuel Preparation Costs

	Annual Capital Charge (%)	Costs (\$/kg)		
		1-MT/Day Plant	4-MT/Day Plant	10-MT/Day Plant
AI-CE fuel	22	6.41		1.84
	15	5.52		1.58
B&W fuel				
Urania-thoria	22	9.75	4.30	
	15	8.18	3.56	
Uranium-thorium	22	13.49	6.90	
	15	11.65	6.08	

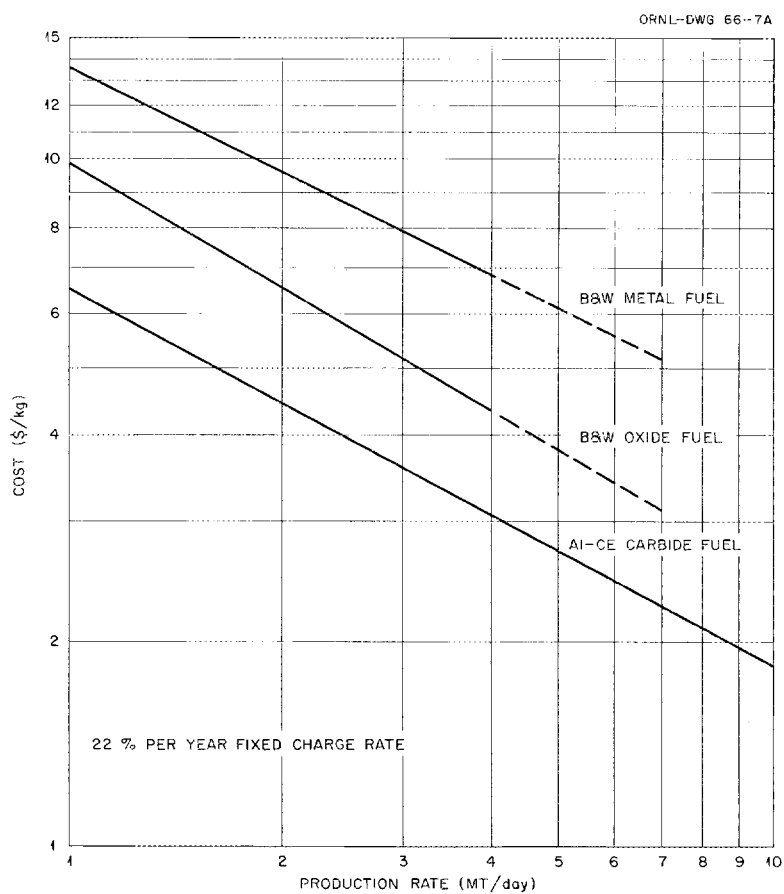


Fig. 9.1. Estimated Fuel Preparation Costs as Function of Production Rate.

Table 9.5. Estimated Costs for Producing Oxide Fuels  
Based on 22% Annual Capital Charge Rate and Costs  
Given in Advanced-Converter Evaluation

	Fuel Costs (\$/kg)	
	1-MT/Day Plant	10-MT/Day Plant
AI-CE	10.61	3.13
B&W with oxide fuel	6.50	1.71

#### References

1. F. E. Harrington et al., Fuel Cycle Costs for a Plutonium Recycle System, USAEC Report ORNL-3501, Oak Ridge National Laboratory, January 1964.
2. J. M. Chandler and F. E. Harrington, A Study of Sol-Gel Fuel Preparation Costs for SSCR and HTGR Reactors, USAEC Report ORNL-TM-1109, Oak Ridge National Laboratory, Apr. 8, 1965.
3. Private communication, E. L. Nicholson, J. M. Chandler, and T. N. Washburn to M. W. Rosenthal, "Meeting at Nuclear Fuel Services, Inc., Erwin, Tennessee, May 18, 1965."
4. Private communication, J. J. Kurtz to F. E. Harrington, "Chemical Preparation and Reduction Facility for Enriched Uranium Metal," Oct. 27, 1965.
5. M. W. Rosenthal et al., A Comparative Evaluation of Advanced Converters, USAEC Report ORNL-3686, Oak Ridge National Laboratory, January 1965.
6. Private communication, F. E. Harrington to A. L. Lotts, "Cost Equations," June 5, 1964.

## 10. FUEL FABRICATION COSTS

### 10.1 General Procedure for Cost Estimating

The method of estimating fuel fabrication costs for this evaluation is consistent with and similar to that used in the advanced-converter evaluation.<sup>1</sup> In brief, this method makes use of a computer program to perform the many calculations required in estimating fabrication costs. Both operating and capital costs are stored in the program for performing each step of the fabrication process over a wide range of production rates. Costs of tubing, end caps, and other items of fuel element hardware are specified, with values covering the ranges of physical dimensions, quality level, and procurement rates required for different evaluations. Input data for each particular case include a specification of the fuel element parameters, the fabrication process selected, rate of capital amortization, an estimated reject rate, a plant utilization factor, and the production rates of interest. The computer program then selects the appropriate cost for each step of the process and accumulates and manipulates these costs for each specified set of conditions to calculate the fuel fabrication cost in dollars per kilogram of heavy metal.

In this study, fabrication costs are divided into three principal parts: operating expenses, capital charges, and hardware costs. Costs of fuel preparation, which were included in fabrication in the advanced-converter evaluation, are given in Chapter 9. The general ground rules used in estimating fabrication costs are given in Chapter 2.

### 10.2 Fabrication Costs for AI-CE Fuel

The AI-CE uranium carbide fuel assembly is described in Chapter 3. The fuel fabrication flowsheet that would be associated with the AI-CE assembly is shown in Fig. 10.1. Input material to the fabrication plant is ceramic-grade  $UO_2$  supplied by the fuel preparation plant; the output of the fabrication plant would be fuel assemblies packaged for shipment.

The fuel production rate required in the fabrication plant for reference conditions is 3475 kg of uranium per day; this corresponds to a

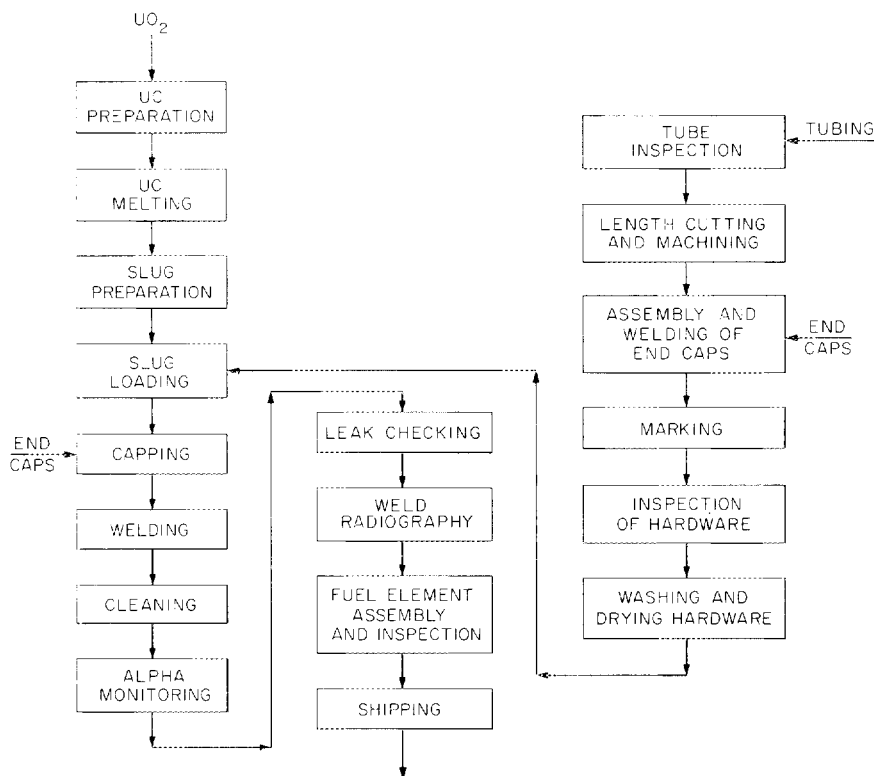


Fig. 10.1. Flowsheet for Fabrication of Uranium Carbide Fuel for HWO CR.

fuel exposure of 15,000 Mwd per metric ton of uranium, a reactor on-line factor of 0.8, operation of the fabrication plant 260 days per year, and furnishing the fueling needs of a 15,000-Mw(e) industry. This scale of production is a large extrapolation of existing technology and experience; thus, the cost estimates obtained are based primarily on engineering estimates and judgments. A major unknown is the future price of SAP cladding for large orders. Based on information supplied by AI-CE, B&W, other sources, and our own interpretations, an average SAP price of \$1.95 per foot of tubing was assigned to the AI-CE fuel element.

The estimated fuel fabrication cost for AI-CE fuel assemblies at various production rates is shown in Fig. 10.2 for equilibrium-fueled cores. For a production rate of 3475 kg per day and a 22% per year fixed charge

rate, the fabrication cost breakdown is that given below:

	<u>Cost (\$/kg of uranium)</u>
Capital charges	8.50
Operating expenses	13.46
Hardware costs	<u>6.46</u>
Total	28.42

Since the initial core of the AI-CE design uses fuel of nine different enrichments, fabrication of the initial cores would involve losses of time for changing over from one enrichment to another. Additional work would also be involved in identification and materials control. For these reasons, a penalty of 10% was assigned to the operating costs of the plant when fabricating initial cores; the resulting initial core fabrication costs are given in Fig. 10.3.

### 10.3 Fabrication Costs for B&W Fuels

The two B&W thorium fuel assembly designs are described in Chapter 3. The fuel fabrication flow sheet for the oxide-containing assembly is shown in Fig. 10.4, and Fig. 10.5 gives the same information for the metallic fuel assembly. Material fed to the fabrication plant is sol-gel-produced high-density thoria-urania fragments for the oxide fuel and thorium powder briquettes and fully enriched uranium metal for the metallic fuel. For both fuels, output of the fabrication plant consists of fuel assemblies packaged for shipment.

The fuel fabrication rate required for the reference conditions is 2590 kg of heavy metal per day; this is based on a fuel exposure of 20,000 Mwd per metric ton of heavy metal, a reactor load factor of 0.8, operation of the fabrication plant for 260 days per year, and furnishing the fueling needs of a 15,000-Mw(e) industry.

The above production rate, when fabricating virgin material, is not so large an extrapolation of current experience as that for the carbide fuel. The major area of extrapolation for fabrication of the thorium cores is the large-scale application of remote operations required for

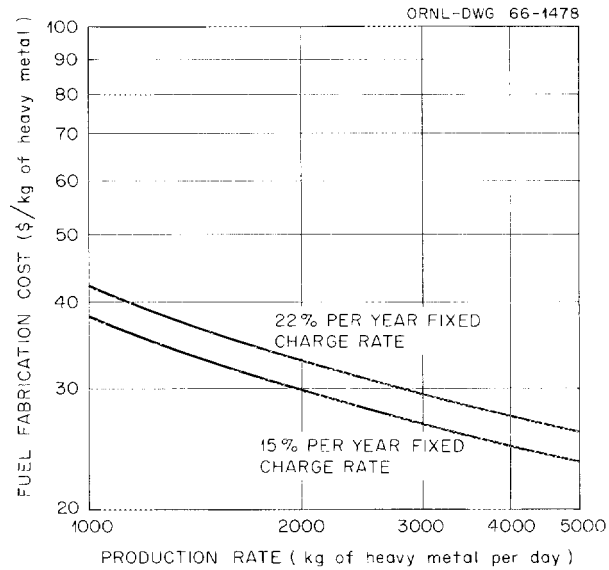


Fig. 10.2. Fabrication Cost for HWO CR Uranium Carbide Fuel -- Equilibrium Cores.

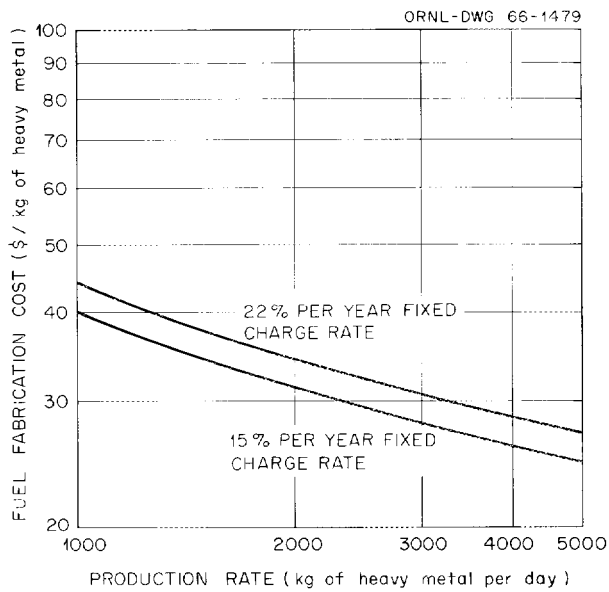


Fig. 10.3. Fabrication Cost for HWO CR Uranium Carbide Fuel -- Initial Cores.

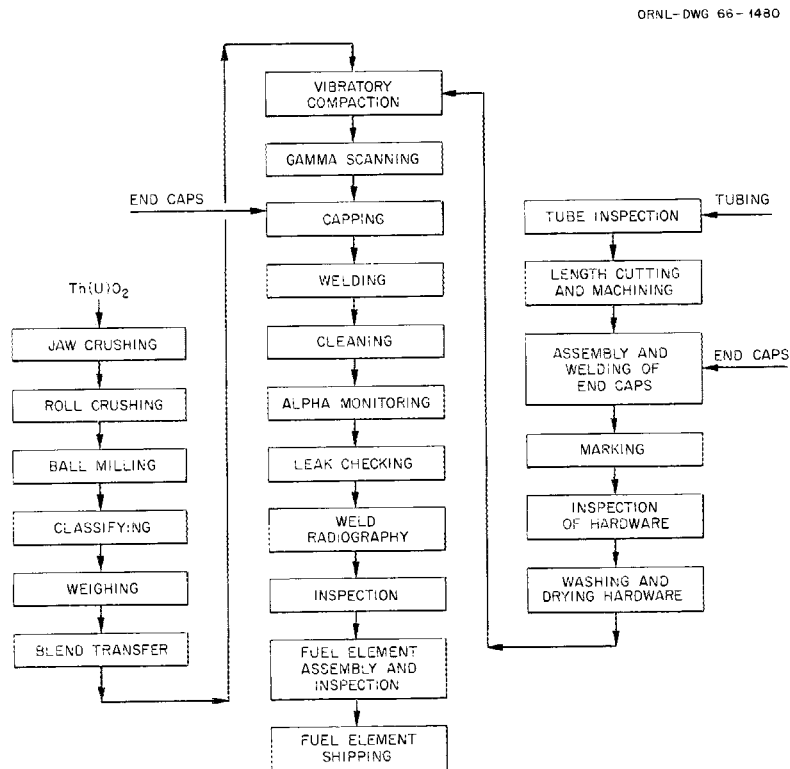


Fig. 10.4. Flowsheet for Fabrication of Thorium-Uranium Oxide Fuel by Vibratory Compaction.

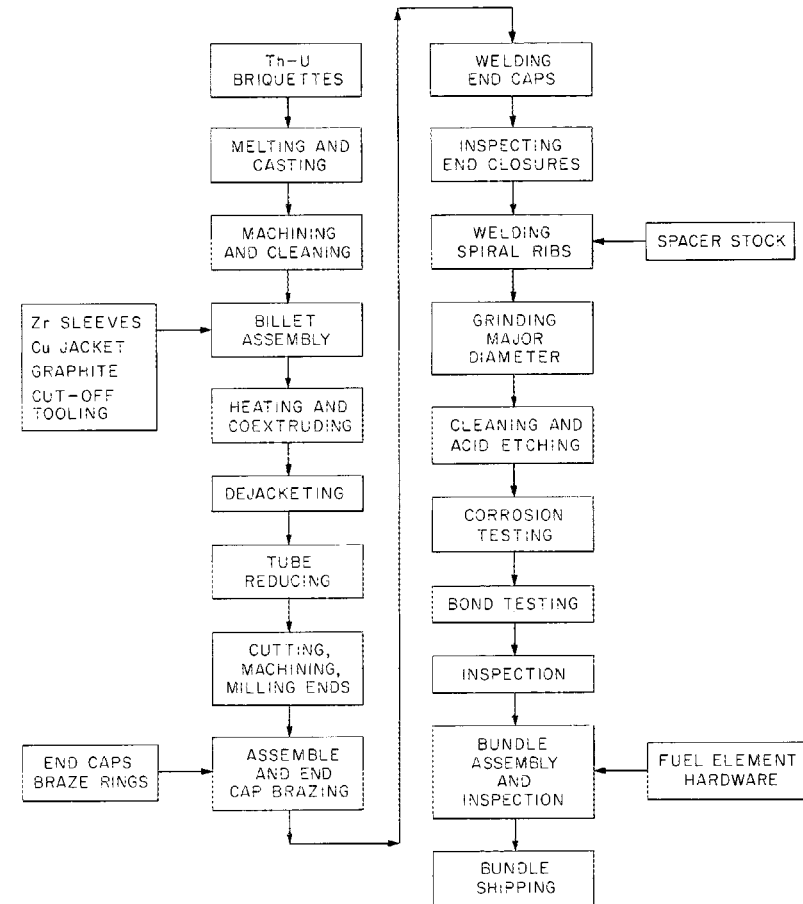


Fig. 10.5. Flowsheet for Fabrication of Thorium-Uranium Alloy Fuel Coextruded with Zircaloy-2 Cladding.

recycle fuel. While vibratory compaction of sol-gel thorium-uranium fuel has been performed in ORNL's Kilorod Facility<sup>2-4</sup> and B&W has evaluated the process on a pilot-plant scale in a hooded facility,<sup>5</sup> there is no experience to date with a remotely operated fabrication plant of the type envisioned. However, a detailed engineering design of both facilities and equipment for remote fabrication was made for the Thorium Uranium Recycle Facility (TURF) at ORNL.<sup>6</sup> In addition, design studies and evaluation of factors involved in plant extrapolations have been done extensively in other work at ORNL. Thus, the projection of fabrication costs in remotely operated large-scale plants for oxide fuels appears reasonably well founded.

The coextrusion of uranium metal with Zircaloy cladding on a production basis has been done successfully for a number of years. Also, thorium-uranium alloys have been coextruded with Zircaloy cladding at Hanford<sup>7</sup> and by Nuclear Metals, Inc., for Savannah River Laboratory.<sup>8</sup> There is no experience, however, relative to "remote" fabrication by this process. Therefore, the accuracy of the cost estimate for the metallic fuel assembly is probably less than that for the oxide pin assembly.

The price of SAP cladding for the oxide pin design was considered to be \$1.57/ft. This price is consistent with that used for the AI-CE carbide fuel cladding. Due to the smaller pin diameter and fewer fins (6 versus 12), cladding cost per foot of length is 20% less for the oxide pin design.

Estimated fabrication costs for the oxide fuel design are given in Fig. 10.6, and those for the metal fuel design are shown in Fig. 10.7. For the reference conditions of 2590 kg per day production and a 22% per year fixed charge rate, the cost breakdown is as follows:

	Unit Cost (\$/kg of heavy metal)	
	Metal	Oxide
Capital charges	15.07	21.31
Operating expenses	10.81	18.58
Hardware costs	16.27	23.63
Total	42.15	63.52

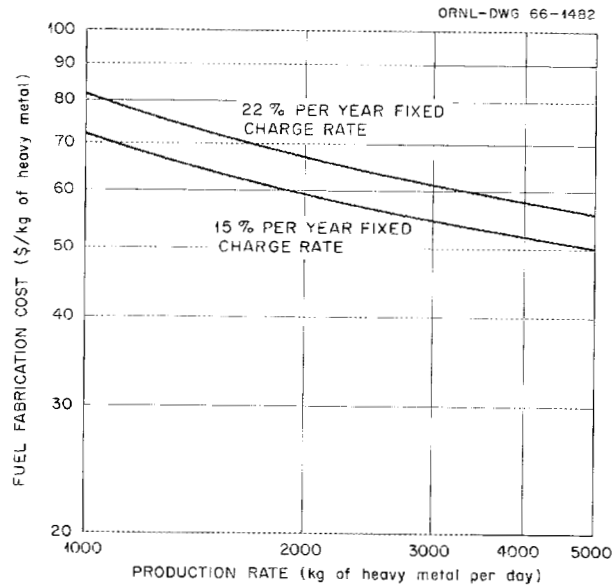


Fig. 10.6. Fabrication Cost for HWOOCR Thorium-Uranium Oxide Fuel — Equilibrium Cores, Remote Fabrication.

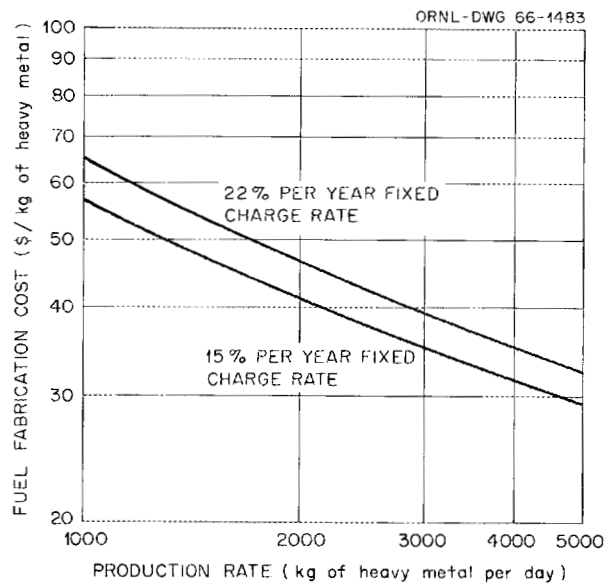


Fig. 10.7. Fabrication Cost for HWOOCR Thorium-Uranium Alloy Fuel — Equilibrium Cores, Remote Fabrication.

Our estimate of the fuel fabrication cost for the metallic fuel assemblies is in reasonable agreement with the B&W estimate. However, our estimate for the oxide fuel is substantially higher than that reported by B&W. There are three major items associated with these different estimates. B&W has estimated a lower unit fabrication time, less operating cost per operator man-year, and less capital investment than allowed for in the ORNL estimate. In recent discussions, the difference in operating cost per operator man-year has been resolved in favor of our value; however, the differences in the other items still exist. With regard to required unit fabrication time, a judgment is required, since actual experience is lacking. We estimate higher required times than does B&W. The capital cost difference is associated with capital cost estimates themselves and also with the type of fuel-recycle facility. Our estimates are based on separate fuel processing and fabrication plants located at the same site. B&W considered an integrated processing-fabrication complex with shared manpower, facilities, and services. We agree that under such circumstances there would be cost savings relative to fabrication costs; however, the ground rules for this study did not consider this situation. If an integrated facility were used, we would reduce our fabrication cost estimates, but we doubt whether they could be reduced as much as \$10/kg of heavy metal.

#### 10.4 Summary

An overall comparison of the estimated fabrication costs per kilogram of heavy metal for the three designs, based on reference conditions, is given in Fig. 10.8. The specific design parameters associated with the different fuel assemblies are given in Table 10.1. On a relative basis, the oxide pin design is "penalized" by its small fuel diameter and low fuel density. The metal fuel design is likewise "penalized" by its thin fuel section and low density relative to that of uranium carbide. The carbide fuel design has relative cost advantages due to the high fuel density and large pin diameter; both these factors contribute to a high fuel loading per unit length, which decreases the number of fuel-bearing components per unit weight of fuel material.

Table 10.1. Comparison of Fuel Element Parameters and Fuel Fabrication Costs

	AI-CE UC Fuel		B&W (Th-U) <sub>2</sub> O <sub>3</sub> Fuel	B&W Th-U Alloy Fuel				
	Large Rods	Small Rods		Ring 1	Ring 2	Ring 3	Ring 4	Ring 5
Fuel dimensions								
Outside diameter, in.	0.472	0.275	0.316	2.606	3.116	3.638	4.176	4.750
Inside diameter, in.				2.406	2.916	3.438	3.976	4.550
Length, in.	41.5	41.5	44	48	48	48	48	48
Thickness, in.				0.100	0.100	0.100	0.100	0.100
Fuel density								
Theoretical, g/cc	13.4	13.4	10.0			11.85		
Attained, %	100	100	88			100		
Fuel per piece, kg of heavy metal	1.52	0.52	0.44	7.34	8.83	10.36	11.94	13.62
Fuel per foot, kg of heavy metal	0.44	0.15	0.12	1.84	2.21	2.59	2.99	3.41
Number of rods (rings) per assembly	31	6	66	1	1	1	1	1
Fuel per assembly, kg of heavy metal		50.09	29.07			52.09		
Fuel element autoclaved		No	No			Yes		
Type of fabrication		Hooded	Remote			Remote		
Fuel fabrication cost, \$/kg of heavy metal		28.4	63.5			42.1		

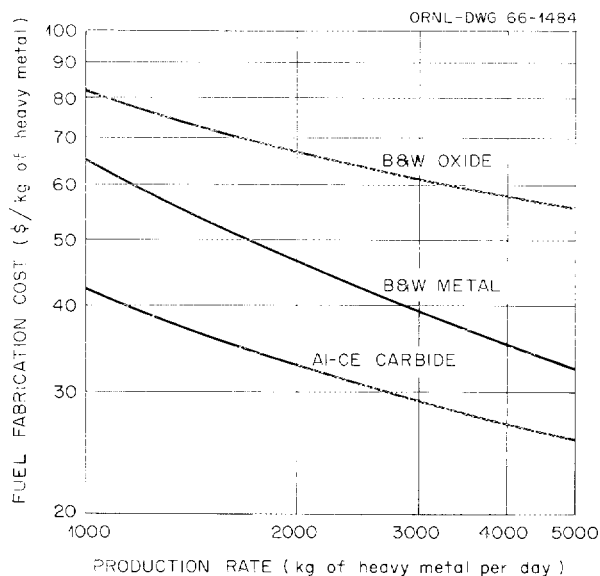


Fig. 10.8. Comparison of Fuel Fabrication Costs for HWOCR Equilibrium Cores Based on Fixed Charge Rate of 22% per Year.

Table 10.2. Fuel Fabrication Cost Per Core for Fabrication Plant Capacities Associated with Different Burnup Levels

Fixed charge rate: 22% per year

Fuel Material	Burnup (Mwd/MT)	Fuel per Core <sup>a</sup> (kg of heavy metal)	Fabrication Cost	
			\$/kg of Heavy Metal	10 <sup>6</sup> \$ per Core
Uranium carbide	15,000 <sup>b</sup>	123,000	28.41	3.5
Th-U metal	20,000 <sup>b</sup>	93,400	42.14	3.9
Th-U oxide	20,000 <sup>b</sup>	58,160	63.50	3.7
Uranium carbide	15,000 <sup>b</sup>	123,000	28.41	3.5
Th-U metal	15,000	93,400	37.25	3.5
Th-U oxide	15,000	58,160	60.00	3.5
Uranium carbide	20,000	123,000	30.50	3.8
Th-U metal	20,000 <sup>b</sup>	93,400	42.14	3.9
Th-U oxide	20,000 <sup>b</sup>	58,160	63.40	3.7

<sup>a</sup>Specified by sponsor.

<sup>b</sup>Burnup specified by sponsors; this value determines fabrication plant capacity.

These results show that for the three fuel assembly designs evaluated, the fabrication cost per kilogram of heavy metal is least for the carbide (\$28.42), intermediate for the metal (\$42.15), and greatest for the oxide (\$63.52). However, when converted to a fabrication cost per reactor core, the spread in cost is within 12% at reference design conditions because of the large differences in quantity of fuel for the different cores. If an exposure of 15,000 Mwd/MT is assumed to apply to each of the fuels, the fabrication costs per core are essentially the same. If an exposure of 20,000 Mwd/MT is assumed for each of the fuels, the cost per core is within 6%. These points are illustrated in Table 10.2.

#### References

1. M. W. Rosenthal et al., A Comparative Evaluation of Advanced Converters, USAEC Report ORNL-3686, Oak Ridge National Laboratory, January 1965.
2. J. D. Sease, A. L. Lotts, and F. C. Davis, Thorium-Uranium-233 Oxide Fabrication Process and Equipment, USAEC Report ORNL-3539, Oak Ridge National Laboratory, April 1964.
3. C. C. Haws et al., Summary of the Kilorod Project - A Semiremote 10 kg/Day Demonstration of  $^{233}\text{UO}_2\text{-ThO}_2$  Fuel Element Fabrication by the ORNL Sol-Gel Vibratory Compaction Method, USAEC Report ORNL-3681, Oak Ridge National Laboratory, August 1965.
4. J. E. Van Cleve, Jr., J. J. Varagona, and A. L. Lotts, Time Study of Fuel Rod Fabrication in the Kilorod Facility, USAEC Report ORNL-3740, Oak Ridge National Laboratory, October 1965.
5. G. Schileo and L. R. Weissert, A Pilot Plant for the Production of Th-U $^{233}$  Recycle Fuels, paper presented at the VIII Congresso Nucleare of the Comitato Nazionale per L'Energia Nucleare, Rome, Italy, June 17-23, 1963.
6. A. R. Irvine, A. L. Lotts, and A. R. Olsen, The Thorium-Uranium Recycle Facility, Proceedings of the 13th Conference on Remote Systems Technology, Washington, D.C., American Nuclear Society.

7. R. S. Kemper et al., Fabrication of Zircaloy-2 Clad Thorium-Uranium Alloy Fuel Elements, USAEC Report HW-79843, Hanford Atomic Products Operation, March 1964.
8. S. R. Nemeth (Ed.), Thorium-1.4 wt %  $^{235}\text{U}$  Uranium Metal Fuel Tubes - Fabrication and Irradiation in HWCTR, USAEC Report DP-943, Supplement, Savannah River Laboratory, April 1965.

## 11. SPENT-FUEL PROCESSING COSTS

The HWO CR fuel-processing costs were estimated on two bases: one was exactly the same as that used for the advanced converter evaluation,<sup>1</sup> and the other was a revised basis that is felt to be more realistic. The estimates obtained on the latter basis were used in this evaluation.

The HWO CR estimates are presented in Tables 11.1 and 11.2 for the reference-burnup throughputs on both old and new bases. They are not very different from the numbers for the corresponding HWR-U and HWR-Th cases (see Appendix G), except that the higher thermal efficiency of the HWO CR requires lower fuel throughput for the same power generation and, hence, lower total costs. Comparison of fuel-processing costs for advanced converters other than the HWO CR on the old and new bases are given in Appendix G.

### 11.1 Cost Bases and Assumptions

The advanced converter evaluation estimates were based on Du Pont estimates for 0.907- and 9.07-MT/day remote-maintenance processing plants,<sup>2</sup> with adjustments estimated by us to cover escalation and competitive conditions, differences in head-end treatment, throughput rates (fertile, fissile, and fission product), and cost items not included in the original estimates (land, startup costs, working capital, and ultimate disposal of radioactive wastes). The revised estimates are based on Du Pont estimates for a 9.07-MT/day limited-maintenance processing plant,<sup>3</sup> plus new Du Pont estimates made for the HWO CR evaluation,<sup>4,5</sup> and also on our interpretation and evaluation of published Nuclear Fuel Services (NFS) capital and operating costs for a 1.0-MT/day limited-maintenance plant.<sup>6,7</sup> We have modified these basic estimates by adjusting them to the same basis with respect to escalation, competition, head-end treatment requirements, throughput rates, land, startup, working capital, and ultimate waste disposal. For ultimate waste disposal costs we have used 1965 ORNL Chemical Technology Division estimates<sup>8,9</sup> rather than those used in earlier studies.<sup>10</sup>

Table 11.1. Spent-Fuel Processing Cost Estimates for HWOCR-U Evaluation

Basis: Single-purpose processing plants serving 15 reactors of a given concept; 1000 Mw(e) each; 0.8 load factor; 34.1% thermal efficiency

	Previous Basis <sup>a</sup>		Revised Basis	
Burnup, Mw $\bar{d}$ /MT	15,000	20,000	15,000	20,000
Throughput, MT/yr	856	642	856	642
Processing days per year	155	155	260	260
Processing rate, MT/day	5.52	4.14	3.29	2.47
Total capital investment, \$	$61.3 \times 10^6$	$58.3 \times 10^6$	$46.8 \times 10^6$	$42.2 \times 10^6$
Operating cost, \$/yr	$5.18 \times 10^6$	$4.86 \times 10^6$	$4.68 \times 10^6$	$4.22 \times 10^6$
Total waste disposal charge, \$/yr	$2.38 \times 10^6$	$2.38 \times 10^6$	$3.02 \times 10^6$	$3.02 \times 10^6$
Unit cost at 15% per year FCR <sup>b</sup>				
\$/kg	19.6	24.9	17.2	21.1
Mill/kwhr(e)	0.159	0.152	0.140	0.129
Cost expressed as per cent of Ref. 1 basis	100	100	88.1	84.9
Unit cost at 22% per year FCR <sup>b</sup>				
\$/kg	24.6	31.3	21.0	25.7
Mill/kwhr(e)	0.200	0.191	0.171	0.157
Cost expressed as per cent of Ref. 1 basis	100	100	85.5	82.2

<sup>a</sup>See Ref. 1.

<sup>b</sup>Fixed charge rate.

Table 11.2. Spent-Fuel Processing Cost Estimates for HWOCR-Th Evaluation

Basis: Single-purpose processing plants serving 15 reactors of  
a given concept; 1000 Mw(e) each; 0.8 load factor;  
34.1% thermal efficiency

	Previous Basis <sup>a</sup>		Revised Basis			
			Oxide Fuel		Metal Fuel	
Burnup, Mwd/MT	15,000	20,000	15,000	20,000	15,000	20,000
Throughput, MT/yr	856	642	856	642	856	642
Processing days per year	155	155	260	260	260	260
Processing rate, MT/day	5.52	4.14	3.29	2.47	3.29	2.47
Total capital investment, \$	66.8 × 10 <sup>6</sup>	63.4 × 10 <sup>6</sup>	42.1 × 10 <sup>6</sup>	38.2 × 10 <sup>6</sup>	42.1 × 10 <sup>6</sup>	38.2 × 10 <sup>6</sup>
Operating cost, \$/yr	5.82 × 10 <sup>6</sup>	5.42 × 10 <sup>6</sup>	4.21 × 10 <sup>6</sup>	3.82 × 10 <sup>6</sup>	4.21 × 10 <sup>6</sup>	3.82 × 10 <sup>6</sup>
Total waste disposal charge, \$/yr	2.38 × 10 <sup>6</sup>	2.38 × 10 <sup>6</sup>	3.02 × 10 <sup>6</sup>	3.02 × 10 <sup>6</sup>	2.21 × 10 <sup>6</sup>	2.21 × 10 <sup>6</sup>
Unit cost at 15% per year FCR <sup>b</sup>						
\$/kg	21.3	27.0	15.8	19.6	14.9	18.3
Mill/kwhr(e)	0.173	0.165	0.129	0.120	0.121	0.112
Cost expressed as per cent of Ref. 1 basis	100	100	74.6	72.7	69.9	67.9
Unit cost at 22% per year FCR <sup>b</sup>						
\$/kg	26.8	33.9	19.3	23.7	18.3	22.5
Mill/kwhr(e)	0.218	0.207	0.157	0.145	0.149	0.137
Cost expressed as per cent of Ref. 1 basis	100	100	72.0	70.0	68.3	66.2

<sup>a</sup>See Ref. 1.

<sup>b</sup>Fixed charge rate.

### 11.1.1 Capital Investment

The original Du Pont estimates were  $\$43 \times 10^6$  for a 0.907-MT/day plant and  $\$60 \times 10^6$  for a 9.07-MT/day plant (Ref. 2, Cases I and III, remote maintenance), corresponding to a scaling factor of about 0.15. For the advanced converter evaluation, we adjusted these numbers to reflect escalation, competitive pressures and technological improvements, land costs, startup costs and working capital, and flowsheet and throughput differences to get the numbers shown in Table G.1 of Appendix G. For both the uranium and the thorium fuels we assumed complete decontamination from fission products; and since there is a throughput rate penalty for thorium in that it can be processed at only 50 to 60% of the uranium throughput in the same size dissolvers and solvent extraction columns, this led to a cost penalty of 10 to 15% for the same throughput in different single-purpose plants.

A later Du Pont estimate gave  $\$58 \times 10^6$  for a 9.07-MT/day limited-maintenance plant (Ref. 3, Case VII), that is,  $\$2 \times 10^6$  less than for the remote-maintenance plant. For the present evaluation, Du Pont estimated that for HWO-CR-Th fuel a 9.07-MT/day remote-maintenance plant would cost very nearly the same as their original 9.07-MT/day uranium plant, that is,  $\$60 \times 10^6$  on the original basis,<sup>4</sup> after taking into consideration that larger equipment was needed but that fewer cycles of decontamination were required, since remote fabrication of the recycle thorium and uranium would be practiced in any event because of the presence of the gamma-active daughters of  $^{228}\text{Th}$  and  $^{232}\text{U}$ . In other words, there is no thorium processing cost penalty on this basis. For the HWO-CR-U fuel, Du Pont estimated  $\$65 \times 10^6$  (Ref. 5), that is,  $\$5 \times 10^6$  more than for the original basic plant, for a complete decontamination remote-maintenance plant, after adding extra costs for a uranium carbide head-end treatment and for converting the recovered depleted uranium nitrate to oxide and storing it. (There were two additional Du Pont estimates for HWO-CR-U fuel,<sup>5</sup> one for recovering only the plutonium while leaving the uranium in the high-level waste, and the other for plutonium recovery plus recovery and storage of partially decontaminated uranium. The first-mentioned alternative gave a lower estimated processing plant cost but

high waste disposal costs and has undesirable fuel-utilization implications; hence we chose not to consider it for our evaluation. The second-mentioned alternative had the highest processing plant cost, and we eliminated it on this basis.) The Du Pont estimates mentioned include about  $\$5 \times 10^6$  for interim waste storage facilities. For the advanced converter evaluation, we left this item in the processing plant cost; for the HWO CR evaluation we removed it and included all waste disposal costs under a separate heading (see Sect. 11.1.3).

For our revised processing cost basis, we scaled from "modified-Du Pont" limited-maintenance cost estimates at 9.07 MT/day down to "modified-NFS" limited-maintenance cost estimates at 1.0 MT/day. For the reference PWR fuel, for example, the two estimates were:

	1.0-MT/Day Plant	9.07-MT/Day Plant
	× 10 <sup>6</sup>	× 10 <sup>6</sup>
Basic project cost	\$27.5	\$58.0
Less interim waste storage	-3.0	-5.0
	-----	-----
	\$24.5	\$53.0
Plus PWR modifications	+1.5	+3.0
	-----	-----
	\$26.0	\$56.0
Plus land, startup, and working capital	+3.0	+6.0
	-----	-----
	\$29.0	\$62.0

The scaling factor is about 0.34, which is much higher than the Du Pont scaling factor (for remote-maintenance plants) of 0.15 but almost the same as a published French estimate of 0.4.<sup>11</sup> The numbers represent 1965 dollars, with escalation of the 1961 Du Pont estimates having been assumed to be offset by competitive conditions and technological improvements. (See also Sect. 11.2, "Cost Estimates.")

#### 11.1.2 Annual Operating Costs

The Du Pont estimates of annual operating costs for the basic 0.907- and 9.07-MT/day remote-maintenance plants were  $\$3.73 \times 10^6$  and  $\$6.23 \times 10^6$  per year, respectively, corresponding to a scaling factor of about 0.22.

For our revised estimates we arrived at numbers approximately equal to 10% of the total capital investment for the reference PWR fuel, and we decided to apply this percentage in all cases rather than estimate each case individually. This gives the same scaling factor as that for the capital costs, about 0.34, which is higher than the corresponding Du Pont figure mentioned above but in rough agreement with French estimates of 0.3 on labor and 1.0 on materials.<sup>11</sup>

### 11.1.3 Radioactive Waste Disposal Costs

The Du Pont estimates include only an initial investment in liquid-waste storage tanks. For the purposes of the advanced converter evaluation we assumed that the Du Pont estimates adequately covered low- and intermediate-level waste disposal but provided for only a minimum of interim storage for high-level liquid wastes. To allow for the eventual ultimate disposal of high-level wastes, we added a sum based on estimates<sup>10</sup> for a scheme consisting of (1) interim acidic-liquid storage, (2) calcination to a thermally stable solid in stainless steel pots, (3) interim storage of the calcined solids at the processing plant, (4) shipment to a salt-mine disposal facility, and (5) ultimate disposal in a deep rock-salt formation. At the time of the advanced converter evaluation, this disposal scheme had not been optimized, and thus the estimated cost used was only a first approximation.

For the present evaluation, our revised estimates show an item for total waste disposal costs, including capital and operating costs incurred during the period of operation of the processing plant, as well as the subsequent "perpetual-maintenance" costs. We have assumed some form of government (city, state, or federal) ownership of the waste disposal facilities in that we have used a 4% cost of money, tax free, and we have assumed that the total waste cost is charged to the processing plant on an amortized equal annual payment basis. Thus the costs are treated as an operating cost of the processing plant (privately owned) instead of as a combination of capital and operating costs. This is something like the arrangement between NFS and New York State and hence is felt to be reasonably realistic.

We used the cost estimating bases developed for two recent studies of optimized costs of perpetual liquid storage<sup>8</sup> and of conversion to solids for salt-mine disposal<sup>9</sup> for a particular mixture of uranium and thorium converter reactors totaling 22,400 Mw(e). We calculated optimized perpetual liquid storage costs with the TASC0 computer code<sup>8</sup> for a variety of possible cases, including acidic and neutralized storage, with and without the uranium or thorium left in the high-level fission-product waste and with the clad material assumed to be either in the high-level liquid waste or in a separate chemical-declad liquid waste or in a separate leached-hulls solid waste. The most economical realistic cases were the following:

1. HWOCR-U. Dissolve SAP cladding with fuel. Recover uranium and plutonium. Store neutralized aluminum-containing waste.
2. HWOCR-Th (oxide). Dissolve SAP cladding with fuel. Recover thorium and uranium. Store neutralized aluminum-containing waste.
3. HWOCR-Th (metal). Use shear-leach head-end treatment. Dissolve only 5 to 10% of the zirconium cladding with the fuel. Store acidic solution.

The cost for each of the three cases was estimated to be about  $\$2.0 \times 10^6$  per year. Leaving the uranium or thorium in the wastes (acidic) increased the cost by  $\$1.1$  to  $2.4 \times 10^6$  per year, and separate chemical decladding added a similar amount. Though the cheapest liquid-disposal scheme is economically competitive with the solid-disposal scheme, the latter is felt to be inherently safer and was used as the reference basis for comparison in this study. The revised-basis total waste-disposal charges represent the five-step scheme described earlier, with allowance for the varying amounts of fission products, because of differing thermal efficiencies, and for the varying amounts of inert solids in the wastes (especially the aluminum for SAP-clad fuels and 5 to 10% of the zirconium for zirconium-clad thorium fuels), because of differences in chemical flowsheets. The revised solid-disposal scheme costs are, in general, lower than those for the advanced converter evaluation because further study has produced more nearly optimized conditions.

#### 11.1.4 Plant Sizing

The primary reason for the difference in plant sizes between the advanced converter evaluation and the revised basis is that the "turn-around time" allowance has been changed. On the old basis, processing batches were kept separate, and the time required for plant cleanout between batches was equal to the processing time within limits of two days minimum and eight days maximum per batch. This rule is not too burdensome for large power reactors in a small processing plant. For example, at NFS a 24-MT batch of standard PWR fuel pays for 24 processing days plus eight turn-around days, but in the advanced converter evaluation the large number of batches per year in most cases called for an equal number of processing and turn-around days. The cost penalty associated with oversizing a plant by a factor of 2 to get the required annual production in only 155 processing days was only about 13% because of the low cost-scaling factor used; but it would be about 26% with the revised factor, and either 13 or 26% is a questionably high price to pay for batch segregation, especially in a single-purpose processing plant. While it might be argued that turn-around time for processing fuel from 15 identical reactors could be eliminated completely to give 310 processing days per year (85% plant availability), we have compromised on 260 processing days per year for our revised estimating basis. This allows for some turn-around time for fuel batches that may need to be segregated, for one reason or another, and allows also for the possibility that we might have a somewhat smaller plant availability factor in limited-maintenance plants. The 260-day figure also has the merit that it is the same as the number used in the fuel preparation and fabrication estimates. Other factors affecting plant sizing were kept the same as in the advanced converter evaluation.

#### 11.2 Cost Estimates

The HWOCR cost estimates for the reference burnups have already been presented in Tables 11.1 and 11.2. Processing cost estimates for other advanced converters are given in Appendix G. The sizing and cost

estimating on the advanced converter evaluation basis was done with a subroutine of the NORA computer code<sup>12</sup> (see Chapt. 12). For the revised estimates, the size was calculated for 15,000 Mw(e) at a 0.8 load factor and at the specified thermal efficiency and burnup for 260 processing days per year. The total capital investment was obtained as already described above. Capital investment costs are summarized in Fig. 11.1 as a function of plant throughput for the HWOCR systems and compared with costs for other advanced converter reactors. The annual operating costs were estimated at 10% of the total capital investment; these, together with the capital charges and the waste disposal costs, were added to give the unit processing costs shown in Fig. 11.2.

Cost estimates for dual-purpose plants were not prepared for the present evaluation because the ground rules had changed since the advanced converter evaluation. The difficulties, both practical and theoretical, of cost division in dual-purpose plants were mentioned in the previous report.<sup>1</sup> Similar cost division questions have arisen in other economic studies — for example, in the case of nuclear reactors for producing both electric power and heat for water desalination.

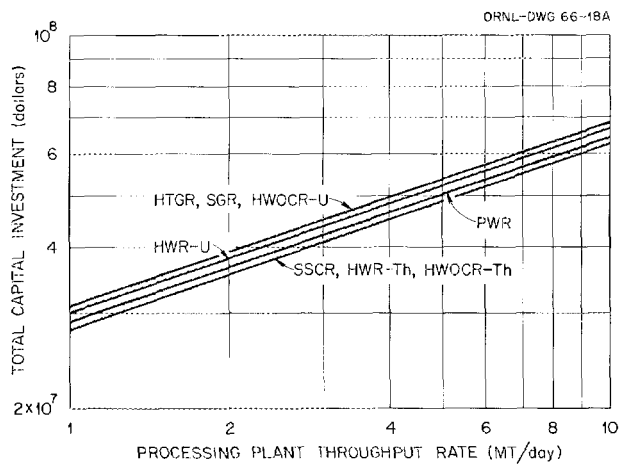


Fig. 11.1. Total Capital Investment for Single-Purpose Spent Fuel Processing Plants Exclusive of Waste Disposal Costs.

ORNL DWG 66-32

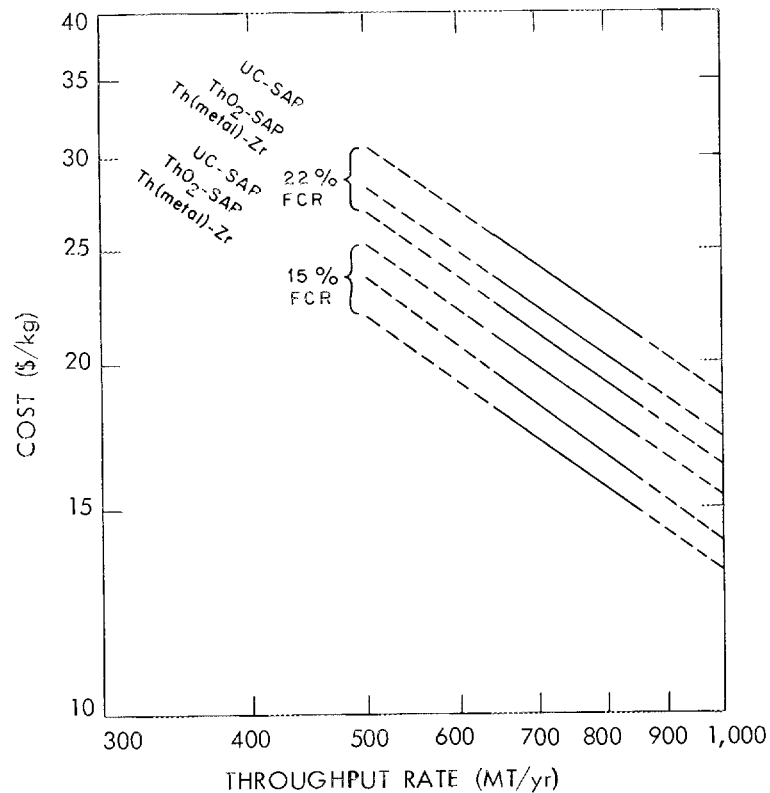


Fig. 11.2. Processing Costs, Including Ultimate Waste Disposal, for HWO CR Fuels.

#### 11.2.1 Throw-Away Fuel Cycle

The uranium and plutonium in some of the first fuel discharged from the HWO CR-U may not be worth recovering at the processing and conversion charges estimated. In this case, probably at least the shipping cost plus ultimate waste disposal charge should be assigned to the fuel. Detailed studies of such a throw-away fuel cycle were not made for this evaluation; but the suggested assignment probably would pay for at least interim storage until processing and conversion costs were reduced as the scale of operations increased with time.

#### 11.2.2 Comparison with B&W and AI-CE Estimates

The summary report on HWO CR-U, by Combustion Engineering and Atomic International,<sup>13</sup> allowed \$18/kg of uranium for spent fuel processing

without going into the details of how this number was calculated. This is approximately the same as the value we show in Table 11.1 on the revised basis.

The summary report on HWOCR-Th by Babcock & Wilcox<sup>14</sup> allows \$57 to \$66/kg for the sum of spent fuel processing, fuel preparation, and fuel refabrication in a completely integrated fuel-cycle facility, with an indication that reprocessing accounts for about one-third of the total, that is, presumably \$19 to \$22/kg. These numbers also are within the limits of accuracy of our revised estimates in Table 11.2.

### 11.2.3 Comparison with NFS Processing Charges

Present-day NFS processing charges<sup>6</sup> for PWR-type fuels are \$31.3/kg for fuels of less than 3% enrichment, with 20,000-Mwd/MT exposure or less, in 24 MT or greater batches. For 31% thermal efficiency this corresponds to 0.21 mill/kwhr(e) or greater. For similar thorium fuels containing 8.5% uranium or less, with 40,000-Mwd/MT or less exposure, in 12 MT or greater batches, the NFS charge is \$62.6/kg plus any special costs of storing the high-level radioactive waste because of the presence of thorium. Our new estimating basis predicts numbers similar to these for a 15% per year fixed charge rate and a 1.0-MT/day plant size for uranium or 0.5 MT/day for thorium, and thus our new estimates are more nearly comparable with NFS charges than our old ones. On the other hand, NFS is not now equipped to handle carbide fuels; in addition, the NFS charges amount to a significant penalty for thorium in comparison with uranium, whereas in our estimates the penalty is small or nonexistent because the processing plants are assumed to match the fuel type instead of being designed for uranium and being able to process thorium only at a much lower rate.

## 11.3 Summary and Conclusions

Spent-fuel processing costs were estimated for HWOCR-U and HWOCR-Th fuels on the basis previously used for the advanced converter evaluation and also on a revised basis believed to be more realistic for future conditions. On the same annual throughput basis, the processing costs would

be quite similar to the numbers developed previously for the HWR-U and HWR-Th, but the higher thermal efficiency of the HWO CR requires a lower refueling rate and hence lower overall costs. The HWO CR-U carbide fuel requires a more elaborate head-end treatment than  $UO_2$  or U-metal fuels but probably can be handled with no outstanding difficulties by methods now demonstrated on a laboratory scale.<sup>15</sup> The SAP cladding material on HWO CR-U and HWO CR-Th (oxide) fuel probably could be removed separately by chemical decladding with NaOH,<sup>15</sup> but our estimates of waste-handling costs (under our ground rules) seem to indicate that dissolution of the SAP cladding with the fuel is preferable. The Zircaloy cladding on the HWO CR-Th (metal) fuel apparently will dissolve with the fuel to the extent of 5 to 10% in Thorex dissolution reagent. This does not seem to seriously interfere with processing,<sup>15,16</sup> though the cost of waste disposal is increased slightly. Our estimated total processing costs do not differ significantly ( $\pm 20\%$ ) from those of the AI-CE and B&W evaluations.

#### References

1. M. W. Rosenthal et al., A Comparative Evaluation of Advanced Converters, USAEC Report ORNL-3686, Oak Ridge National Laboratory, January 1965.
2. W. H. Farrow, Jr., Radiochemical Separations Plant Study, Part II -- Design and Cost Estimates, USAEC Report DP-566, Savannah River Laboratory, March 1961.
3. R. J. Christl, J. E. Crawley, and C. S. Otto, Radiochemical Separations Plant Study, Limited Maintenance -- Case VII, USAEC Report DP-730, Savannah River Laboratory, September 1964.
4. V. R. Thayer, E. I. du Pont de Nemours and Company, personal communication with R. A. Webb, The Babcock & Wilcox Company, June 22, 1965.
5. V. R. Thayer, E. I. du Pont de Nemours and Company, personal communication with S. Golan, Atomics International, September 2, 1965; with attached memo DPST-65-417 from J. F. Proctor to V. R. Thayer, Aug. 31, 1965.

6. Chemical Processing Plant, Hearing Before Joint Committee on Atomic Energy, 85th Congress of the United States, May 14, 1963.
7. Davison Details Reprocessing Plants at Nuclear Congress, news item in Nucleonics, p. 20, July 1962.
8. J. O. Blomeke et al., The Costs of Permanent Disposal of Power-Reactor Fuel-Processing in Tanks, USAEC Report ORNL-2873, Oak Ridge National Laboratory, September 1965.
9. J. O. Blomeke et al., Estimated Costs of High-Level Waste Management, to be published in the Proceedings of the Symposium on Solidification and Long-Term Storage of Highly Radioactive Wastes, Richland, Washington, Feb. 15-18, 1966.
10. J. O. Blomeke et al., Estimated Costs for Management of High-Activity Power Reactor Processing Wastes, USAEC Report ORNL-TM-559 (A summary of USAEC Reports ORNL-3128, -3192, -3355, -3356, and -3358), Oak Ridge National Laboratory, May 13, 1963.
11. L. Thiriet, C. Oger, and P. de Vaumas, Long-Term Developments in Irradiated Natural Uranium Processing Costs - Optimal Size and Siting of Plants, French Report CEA-R-2642, August 1964; also published as Paper A/Conf. 28/P/98, Third United Nations International Conference on the Peaceful Uses of Atomic Energy, Geneva, 1964.
12. R. Salmon, Economics of Irradiated Fuel Shipments, Chem. Eng. Progr. Symp. Ser., 56, 65: 7-15 (1965).
13. Combustion Engineering, Inc., and Atomics International, Heavy Water Organic Cooled Reactor - 1000 Mwe Nuclear Power Plant Preliminary Conceptual Design, USAEC Report AI-CE-Memo-6, Vols. I and II, Oct. 1, 1965.
14. Babcock & Wilcox Company, 1000 MWe Thorium HWOCR - Preliminary Conceptual Design Data for ORNL Evaluation, USAEC Report (unnumbered), Nov. 15, 1965.
15. Personal communication with L. M. Ferris, Oak Ridge National Laboratory, December 1965.
16. Personal communication with R. H. Rainey, Oak Ridge National Laboratory, December 1965.

## 12. FUEL SHIPPING COSTS

The costs of shipping fresh and irradiated fuel elements are reported here in dollars per kilogram of reference material charged to the reactor. The reference materials are total uranium for the AI-CE fuel element and total uranium plus thorium for the B&W fuel elements. The ground rules and assumptions were patterned closely after those used in the advanced-converter evaluation.<sup>1</sup>

The shipping cost is the total of the following four items:

1. the handling cost, which covers the cost of loading, unloading, rigging, testing, and decontamination,
2. the insurance cost, which covers insurance against loss of or damage to the fuel in transit,
3. the freight cost, which covers the cost of transportation charged by the railroad or other carrier, and
4. the cask cost, which covers the annual fixed charges on the shipping casks or containers (recovery of investment, return on investment, taxes, and maintenance).

Costs were calculated for fuel shipments of the following types:

1. irradiated (spent) fuel of high gamma activity shipped from reactor to reprocessing plant,
2. recycled fresh fuel of moderate gamma activity shipped from fabrication plant to reactor, and
3. nonrecycled fresh fuel of zero gamma activity shipped from fabrication plant to reactor.

The results are summarized in Tables 12.1, 12.2, and 12.3.

### 12.1 Spent-Fuel Shipping Costs

Shipping Costs for spent fuels were calculated with the computer code NORA.<sup>2</sup> This code is similar to an earlier code, MYRA,<sup>3</sup> but contains additional optimizing features. Table 12.4 summarizes the input data. The bases and assumptions were the following:

1. Shipment is by rail. Distance is 1000 miles each way.

Table 12.1. Spent Fuel Shipping Costs

Cooling time: 120 days  
 Rail shipment distance: 1000 miles each way  
 Maximum weight of loaded cask: 240,000 lb  
 Reactors serviced: 15

Fuel Type	Burnup (Mwd/MT) <sup>a</sup>	Cask Weight When Full (lb)	Reference Material per Cask (kg)	Shipping Cost (\$/kg) <sup>b</sup>	Shipping Cost [mills/kwhr(e)]
AI-CE 37-rod clusters	10,000	139,000	3200	2.31	0.028
	15,000	140,000	3200	2.37	0.019
	20,000	135,000	2800	2.70	0.016
	25,000	132,000	2400	2.96	0.014
B&W 66-pin clusters	15,000	165,000	1852	4.78	0.038
	20,000	167,000	1852	4.82	0.029
	25,000	159,000	1620	5.58	0.027
B&W 5-ring nested cylinders	15,000	169,000	2916	3.21	0.026
	20,000	165,000	2499	3.56	0.021
	25,000	168,000	2499	3.62	0.017

<sup>a</sup>Burnup of reference material.

<sup>b</sup>Costs are in \$/kg of reference material charged to reactor.

Table 12.2. Recycled Fresh-Fuel Shipping Costs

Rail shipment distance: 1000 miles each way  
 Maximum cask weight: 240,000 lb  
 Cask length: four elements end to end  
 Reactors serviced: 15

	B&W 66-Pin Clusters	B&W 5-Ring Nested Cylinders
Cost, \$/kg of U + Th		
Handling	0.11	0.08
Insurance	0.14	0.14
Freight	1.38	0.91
Cask amortization	0.43	0.40
Total shipping cost	2.06	1.53
Cask weight when full, lb	179,000	172,000
U + Th per cask, kg	4630	6665
Heat removal per cask, kw	0.6	0.9

Table 12.3. Nonrecycled Fresh-Fuel Shipping Costs

Item	Cost (\$/kg of reference material)		
	AI-CE 37-Rod Clusters	B&W 66-Pin Clusters	B&W 5-Ring Nested Cylinders
Handling	0.04	0.05	0.05
Insurance	0.03	0.08	0.06
Freight	0.20	0.21	0.19
Containers	0.06	0.10	0.08
Total shipping cost	0.33	0.44	0.38

Table 12.4. Input Data for Spent-Fuel Shipping Cost Calculations

	AI-CE 37-Rod Clusters	B&W 66-Pin Clusters	B&W 5-Ring Nested Cylinders
Reference material	U	U + Th	U + Th
Reactor power, Mw(t)	3093	3082	3082
Specific power, Mw/Mt of reference material	24.8	53.0	33.0
Cooling time, days			
Minimum	90	90	90
Maximum	150	180	150
Element length, ft			
Overall	3.67	3.90	4.12
Active	3.46	3.67	4.00
Element weight, lb/ft	27	23.1	36.4
Element outside surface area, ft <sup>2</sup>	15.5	22.6	5.03
Reference material per element, kg	50	28.93	52.07
Pins per element	37	66	1
Pin outside diameter, in.	0.521	0.356	4.94
Pin spacing, center to center, in.	0.615	0.486	
Thermal conductivity of divider plate, Btu/ft·hr·°F	210	210	210
Box size, inside, in.	4.76	5.44	5.44
Elements per process batch	400-1200	320-800	192-480
Peaking factor	1.2	1.2	1.2
Pa in spent fuel, g/kg of U + Th		1.84	1.32
Allowable cladding temperature, <sup>a</sup> °F	850	850	950
Reactor thermal efficiency	0.348	0.349	0.349
Burnup, minimum, Mwd/Mt of reference material	10,000	15,000	15,000
Burnup, maximum, Mwd/Mt of reference material	25,000	25,000	25,000
Fuel value, <sup>b</sup> \$/kg of reference material	32	202	218

<sup>a</sup>At hottest surface of fuel element.

<sup>b</sup>Before subtracting reprocessing cost.

2. Shipments comply with the proposed AEC regulations, 10CFR72, with a dose limit of 10 mr/hr at a distance of 1 meter from the cask.<sup>4</sup>
3. Round-trip time is 16 days.
4. Casks are empty on the return trip.
5. Handling cost is \$500 per round trip.
6. Insurance charge is 0.0005 times the value of the cask and fuel.
7. Freight cost is \$0.0193/lb for the loaded cask and \$0.0181/lb for the empty cask.
8. Maximum weight of cask, fuel, mountings, and tie-downs is 240,000 lb.
9. Casks are purchased and are shared among 15 identical reactors of 1000-Mw(e) capacity each. Cask cost is \$1.00/lb of cask weight. Fixed charge rate is 22% per year for shared casks. Utilization time is limited to not more than 80%.
10. Individual canning of fuel elements is not required.
11. Maximum allowable temperature of fuel element cladding is as follows:

AI-CE 37-rod cluster	850°F
B&W 66-pin cluster	850°F
B&W 5-ring nested cylinder	950°F

12. Peaking factor for shipping purposes, defined as specific power during exposure divided by average design specific power, is 1.20. All elements in a cask are assumed to have the same exposure.

Criticality calculations were not made. It was assumed that criticality could be avoided by using boron-containing divider plates.

#### 12.1.1 Description of Cask

The cask is a right circular cylinder with an opening at one end. Outer and inner shells are steel, 1.25 and 0.50 in. thick, respectively. Lead shielding, approximately 8 in. thick, is placed between the shells. The space inside the inner shell is divided into a gridwork of square pigeonholes by means of copper-boron divider plates. Each pigeonhole contains four fuel elements (fuel assemblies), placed end to end.

Heat removal is by natural convection and radiation. The outer surface of the cask is finned. There is no mechanical cooling system.

### 12.1.2 Method of Calculation

A block flow chart of NORA is shown in Fig. 12.1. Besides calculating the cask dimensions and shipping costs, NORA goes through certain optimization procedures to find conditions that give minimum total cost. The conditions sought are combinations of cooling time, the number of elements per cask, the number of casks, and the number of fuel elements per reprocessing batch which minimize fuel-cycle costs.

Input Data. The required input data include

1. fuel dimensions, weights, value, and other pertinent characteristics,
2. burnup and specific power,
3. cooling time (minimum, maximum, and increment),
4. number of reactors,
5. cost factors associated with shipping,
6. cost factors associated with reprocessing,
7. inventory charge rate and other economic factors,

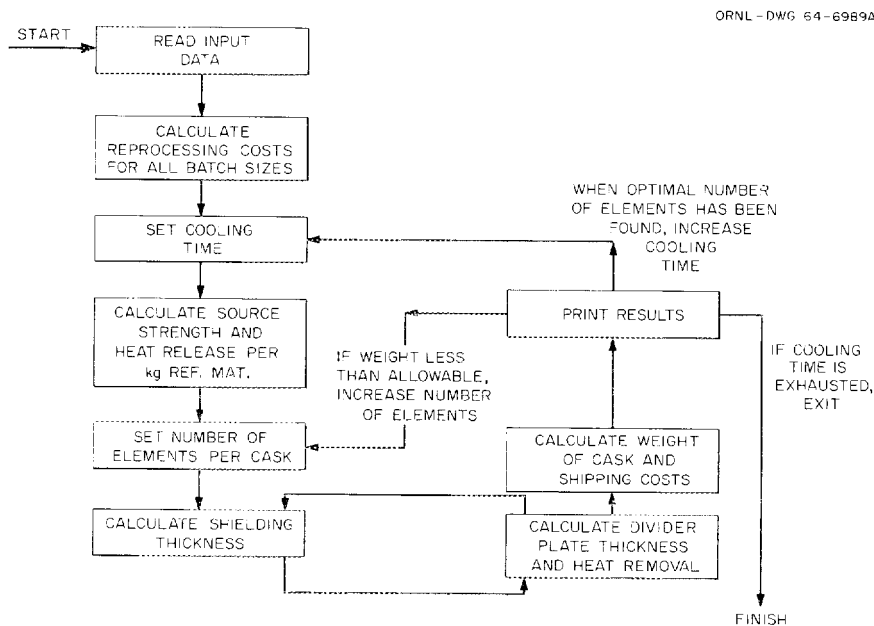


Fig. 12.1. Block Flow Diagram of NORA Code.

8. elements per reprocessing batch (minimum, maximum, and increment),
9. material properties,
10. maximum allowable temperature of fuel cladding.

Description of Code. When all the input data are received, NORA proceeds as follows:

1. Reprocessing costs are calculated for each batch size.
2. The cooling time is set at the minimum specified.
3. Using the burnup, specific power, peaking factor, and cooling time, the gamma source strength and decay heat release are calculated per fuel element. The subroutine used here is the PHOEBE code of Arnold,<sup>5</sup> which is based on the data of Blomeke and Todd<sup>6</sup> and of Knabe and Putnam.<sup>7</sup>
4. The number of elements per cask is set at one.
5. The shielding thickness is calculated by trial and error until the dose is between 90 and 100% of the allowable dose.
6. The thickness of the copper-boron heat-conducting divider plates is calculated by trial and error until the required rate of heat removal is achieved without exceeding the permissible temperature.
7. When the shielding and heat-removal relationships have been simultaneously satisfied, the cask design is complete. The cask weight and all costs are calculated. The optimal number of casks is found. The results are printed out.
8. The number of elements per cask is doubled, and steps 5, 6, and 7 are repeated.
9. When the number of elements per cask becomes so large that the weight limit is exceeded, and interpolation procedure takes over, and the calculation converges toward the maximum number of elements that can be carried within the weight limit. The optimal number of elements per cask is then searched for and reported.
10. The cooling time is increased by the specified increment, and steps 3 through 9 are repeated.
11. When the calculations at the maximum cooling time are completed, the calculation ends.

### 12.1.3 Optimization Procedures

The cooling time, number of elements per cask, number of casks purchased, and reprocessing batch size were chosen so as to minimize the total shipping, inventory, and reprocessing costs. The associated parameter value is termed its optimal value. In doing this, it was assumed that the reprocessing batches of each reactor were kept separate. Inventory charges covered the time used for cooling, delivery of reprocessing batch, and reprocessing and were based on a charge rate of 10% per year times the value of the spent fuel. Reprocessing cost was subtracted in arriving at the fuel value. A preprocessing lag of 30 days per batch was assumed in all cases.

Optimal Number of Casks. NORA starts with the minimum number of casks and then checks to see whether savings can be effected by using more casks. It chooses the number of casks that gives the minimum sum of cask cost and delivery time cost. In all cases it was found that the optimal number of casks was the minimum number necessary to keep up with the rate of discharge of the 15 reactors.

Optimal Cooling Time. For highly irradiated fuels, there is some minimum cooling time below which it is impossible to ship even one fuel element in a cask of the type described. The limiting factor is heat removal; the decay heat cannot be removed at the required rate without exceeding the allowable cladding temperature. Increasing the cooling time above this minimum reduces the amount of shielding needed and may also make it possible to ship a greater number of elements per cask. On the other hand, after lengthy cooling the incremental gain is small and tends to be outweighed by the increase in cooling cost (inventory charges for the cooling period). In the cases studied here, a cooling time of 120 days appeared to be about optimal and was used for the final costs.

Optimal Cask Length. Because of the small length of a single fuel element, the cask designs investigated included stacking of elements end to end in single, double, triple, and quadruple lengths. Quadruple length gave the lowest costs.

Optimal Reprocessing Batch Size. The delivery time can be reduced by reducing the number of elements per process batch. This tends, however, to increase reprocessing costs, because small batches are penalized by higher turnaround costs per kilogram. An optimal process batch size may therefore be found. Generally, the optimal cask size will be such that the optimal reprocessing batch size is an integral number of full cask loads. If it becomes necessary to ship partially loaded casks, this tends to increase the shipping cost. The reprocessing batch size may therefore affect the shipping cost. Ordinarily, however, the batch size is considerably larger than one cask load. It becomes possible therefore, by adjusting the batch size slightly, to make it equal to an integral number of cask loads. The resultant saving in shipping cost usually is greater than the additional cost incurred by the slight departure from the optimal batch size. Accordingly, in the present evaluation, shipping costs were based on the use of full cask loads in all cases. Since continuous discharge was used for all fuels, the problem of matching the process batch size to the discharge batch size did not arise.

## 1.2.2 Recycled Fresh-Fuel Shipping Costs

The B&W reactor, which uses a thorium fuel cycle, requires shielded casks for the shipment of fresh fuel containing recycled material. The gamma activity of the recycled thorium fuels is due to the decay products of  $^{232}\text{U}$ , principally  $^{212}\text{Bi}$  and  $^{208}\text{Tl}$ . The  $^{232}\text{U}$  is produced in the reactor by a series of reactions initiated by an  $(n,2n)$  reaction on  $^{232}\text{Th}$ . The  $^{232}\text{U}$ , which has a half-life of 74 years, decays to  $^{228}\text{Th}$ , so both of these nuclides are present at the time the fuel leaves the reactor.

In chemical reprocessing of the irradiated fuel, the  $^{232}\text{U}$  is removed with the finished  $^{233}\text{U}$  product, and the  $^{228}\text{Th}$  comes out with the finished  $^{232}\text{Th}$  product. The subsequent members of the decay chain (those following  $^{228}\text{Th}$ ) are eliminated with the fission products. Immediately after reprocessing, however, the decay products start to build up again, and both the  $^{233}\text{U}$  and the  $^{232}\text{Th}$  soon become gamma active. This activity changes with time after reprocessing, so the amount of shielding required

depends on how soon the shipment is made. Fabrication may require from 20 to 60 days. In addition, there may be a waiting period after fabrication, because it may take some time to accumulate a full cask load of fuel elements. Calculations showed, however, that the change of activity in the time range 30 to 100 days was small enough so that the effect on shipping cost was negligible. The costs shown in Table 12.3 are based on time lags of 150 days from discharge to reprocessing and 35 days from reprocessing to shipping. At the time of discharge from the reactor, the fuel was assumed to contain 25 ppm of  $^{232}\text{U}$  and 0.65 ppm of  $^{228}\text{Th}$ , both expressed per million parts of total U + Th.

The type of cask and the assumptions used in the cost calculations are the same as for the spent fuel. It was assumed that casks must be provided independently of those used for shipping spent fuel.

### 12.3 Nonrecycled Fresh-Fuel Shipping Costs

Fresh fuel elements of the non-gamma-active type will be shipped in nonshielded containers designed to protect the fuel assemblies against mechanical damage during transit. In the AI-CE case, all fresh-fuel shipments are of this type; in the B&W case, only the fresh nonrecycled fuel can be shipped this way. Cost calculations were based on the following assumptions:

1. Shipment is by truck, a distance of 1000 miles each way. Empty containers are returned and reused.
2. Container cost is \$1.00/lb of container weight. Container weight is equal to fuel assembly weight. Containers are shared among 15 reactors.
3. Trucking charges are \$0.75 per mile or \$1500 per round trip.
4. Shipments are made in full truck loads of 46,000 lb each.
5. Handling costs are \$400 per round trip.
6. Insurance costs are 0.0005 times value of shipment.

### 12.4 Discussion of Results

The spent-fuel shipping costs are given in Table 12.1 for the three types of fuel. The AI-CE uranium carbide element has the lowest cost,

the B&W 5-ring nested cylinder cost is intermediate, while the cost of the B&W 66-pin cluster is highest. The costs (in \$/kg of reference material) are roughly in inverse proportion to the payload in kilograms of reference material per cask. The payload was limited in every case by the heat-removal capacity of the cask; the total weight limitation of 240,000 lb was not reached in any of the cases. The lower shipping cost of the AI-CE fuel is largely due to the associated lower specific power, which made possible the shipping of larger payloads without exceeding the heat-removal limitations.

Comparing the two B&W elements, the 5-ring nested cylinder has the advantages of lower specific power (33 versus 53) and larger mass of reference material per element (52 kg versus 29 kg). The latter advantage permits the shipping of larger payloads in a cask of a given interior volume.

The fresh-fuel shipping costs (nonrecycled) are relatively small and therefore of lesser importance. The AI-CE fuel is shipped in large quantities throughout the reactor lifetime and thereby gains a slight cost advantage. The B&W 5-ring nested cylinder cost again is lower than the cost for the 66-pin cluster, chiefly because of its greater payload per unit volume.

#### References

1. M. W. Rosenthal et al., A Comparative Evaluation of Advanced Converters, USAEC Report ORNL-3686, Oak Ridge National Laboratory, January 1965.
2. R. Salmon, Economics of Irradiated Fuel Shipment, Chem. Eng. Progr. Symp. Ser. 56, 61: 7-15 (1965).
3. R. Salmon, A Computer Code (CDC 1604A or IBM 7090) for Calculating the Cost of Shipping Spent Reactor Fuels as a Function of Burnup, Specific Power, Cooling Time, Fuel Composition, and Other Variables, USAEC Report ORNL-3648, Oak Ridge National Laboratory, August 1964.
4. Regulation to Protect Against Radiation in the Shipment of Irradiated Fuel Elements, U.S. Code of Federal Regulations, Title 10, Part 72, proposed, as issued in Federal Register, Sept. 23, 1961.

5. Private communication with E. D. Arnold, Oak Ridge National Laboratory.
6. J. O. Blomeke and Mary F. Todd,  $U^{235}$  Fission Product Production as a Function of Thermal Neutron Flux, Irradiation Time, and Decay Time, USAEC Report ORNL-2127, Oak Ridge National Laboratory, November 1958.
7. W. E. Knabe and G. E. Putnam, The Activity of the Fission Products of  $U^{235}$ , USAEC Report APEX-448, General Electric Company, Oct. 31, 1958.

### 13. FUEL-CYCLE COSTS

#### 13.1 Calculation of Average Lifetime Fuel-Cycle Costs

Fuel-cycle costs were calculated by the present-value discounting technique to obtain average 30-year-lifetime costs. The average fuel cost is determined by computing the present value (value discounted to reactor startup) of all future costs and dividing it by the discounted amount of the energy sold during the life of the plant. This levelized cost represents the fixed price that must be received per unit of electrical energy in order to pay for all the costs associated with the fuel cycle. It was assumed that neither the reactor load factor nor the unit costs of purchased materials varied during the lifetime of the reactor.

The advantage of present-value discounting is that it implicitly includes the effect of time displacements between investments and returns. The levelized cost includes applicable interest charges caused by these time displacements.

In making the fuel-cycle cost calculation we first determined the direct cost, which is the contribution that an item would make if interest charges and taxes were zero. The direct-cost contribution to the fuel-cycle cost is obtained by summing all the money invested in an item during the reactor history and dividing by the total energy sold, with no discounting. Thus, for the same total investment, the direct-cost contribution is the same regardless of whether the money is spent at the start of the history, at the end of the history, or in smaller payments spaced during the history.

For the computation of the interest cost we must consider that some items contribute to the outstanding indebtedness of a utility company. These costs must be financed out of capital funds, and the charge rate applied to them must include taxes. In this study we assumed that fuel purchase, fuel fabrication, coolant purchase, and D<sub>2</sub>O purchase are in this category and applied a capital charge rate of 10% per year in these costs. Other costs of the fuel cycle may be covered out of current revenues and treated as operating costs rather than as capital investment. Since operating costs are paid before taxes, the applicable rate is simply

the net cost of borrowing money. In this study we treated spent-fuel shipping and reprocessing in this manner, with a charge rate of 6% per year. This assignment of charges to capital is the same as that used in the advanced-converter study.<sup>1</sup> For all items we calculated the present-value discount factor with a rate equal to the cost of borrowing money; that is, 6% per year. The discounting was calculated with semiannual compounding. For the calculations we assumed that income from energy generated during a six-month accounting period is received at the end of the period. Other costs and credits were taken at the time they occurred, with discounting to reactor startup.

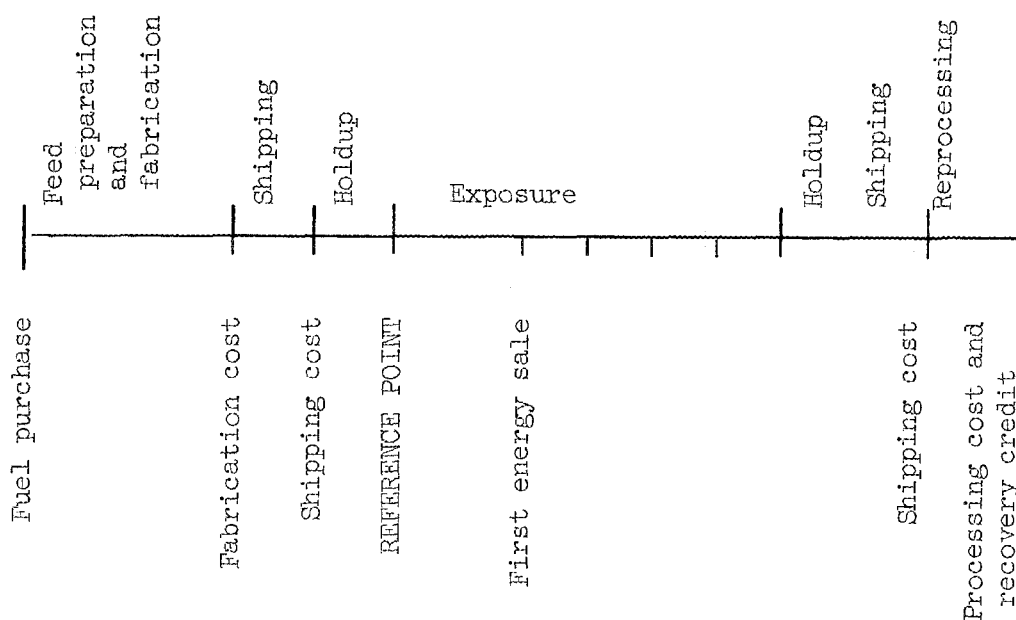
To calculate the interest charges associated with an item of cost, we determined the total discounted present value of all direct costs and credits for the item over the reactor lifetime and divided this by the amount of energy delivered, also discounted, over the same period. The result is the total cost for the item, including interest charges if the interest rate is equal to the discount rate. The interest charge is the difference between the above total cost and the direct cost multiplied by the ratio of the capital charge rate to the discount rate.

The interest charge on an item may be either positive or negative, depending on whether the investment is made before or after revenue is received. In any case it is convenient to have the results presented in a form in which direct costs and interest costs are separate so that the effect of any changes in direct unit costs or interest rates can easily be determined.

With discounting to a fixed point in time (for example, reactor startup), the interest cost depends strongly on whether the investment occurred at the start or end of the history due to time displacement between expenditures and receipts. It is noteworthy that with 6% discounting and 10% charges, credit for fuel or unused fabrication at the end of a 30-year life makes essentially no net contribution and could be neglected. The contribution to direct cost is largely offset by a nearly equal interest charge of opposite sign.

### 13.2 Calculation of Equilibrium Fuel-Cycle Cost

In the calculation of equilibrium fuel-cycle cost, a present-value discounting method is used that takes account of time displacements between costs and revenues in a typical cycle; that is, a cycle late enough in the reactor lifetime that it is not greatly affected by startup assumptions (although feed and discharge rates for such a cycle are not always at a true equilibrium). The history of a particle of fuel fed to the reactor is followed through the entire fuel cycle, as shown schematically below. Note that the present-value reference point is at the start of exposure, a lead time (holdup period) is indicated that allows for out-of-core inventory, and revenue from energy sale is credited at the end of each accounting period.



### 13.3 Special Aspects of HWO CR Fuel-Cycle Economics

In the calculation of 30-year histories by present-value discounting, considerable importance is associated with the startup cycles that have the highest present value. We have not attempted to optimize the startup cycle. In the point-depletion calculations of the AI-CE design we used

the same length of cycle for startup as for subsequent exposures. In the one-dimensional calculation, advantage was taken of the initial increase in reactivity during plutonium buildup, and the initial refueling was not made until 148 calendar days of exposure. For the B&W designs we chose an initial set of enrichments sufficient to give 3000 to 5000 Mwd/MT before initial refueling. We have not investigated the effect of other choices.

Charges for interest on D<sub>2</sub>O and organic coolant at 10% per year, as well as losses of these materials, were included as a separate item in the total fuel-cycle cost for direct comparison with other concepts.

Fabrication and processing plants were sized for a projected 1980 industry of 15,000-Mw(e) installed capacity of a given concept based on makeup requirement only. Considering the strong dependence of unit costs on plant size, it should be noted that fueling of new reactors going on-stream would initially increase the fabrication plant requirements considerably in relation to processing plant requirements.

In instances in which slightly enriched uranium fuel was below an optimum blend enrichment from a cascade, credit was given for blending with natural uranium. Material discharged below 0.25% enrichment was assigned a zero value. Costs were calculated at the design power level of 1076 Mw(e) rather than the 1000 Mw(e) indicated by the ground rules. This difference in power level had no significant influence on the fuel-cycle cost.

#### 13.4 AI-CE Design Fuel-Cycle Costs

Our calculated fuel-cycle costs for the uranium-loaded HWOCR are listed in Table 13.1. The results from point-depletion calculations indicate that the optimum enrichment is slightly above 1.26% with an associated exposure of 17,000 Mwd/MT of heavy metal. Our 30-year cost of 0.856 mill/kwhr(e) (D<sub>2</sub>O and coolant inventories not included) at 17,000 Mwd/MT is close to the 0.85 mill/kwhr(e) obtained by AI-CE, although we used slightly higher interest charges on fabrication and higher plutonium credit than AI-CE.

Table 13.1. Fuel-Cycle Costs for a 1076-Mw(e) Uranium-Loaded Heavy-Water Moderated Organic-Cooled Reactor (HWOCR-U)

Thermal efficiency: 34.8%

	Cases							
	Q-1		Q-2		Q-3		R-1	
Core behavior calculation	15-zone point depletion		15-zone point depletion		15-zone point depletion		15-zone one-dimensional depletion	
Equilibrium-cycle data								
Exposure, Mwd/MP	12,869		14,842		16,801		16,003	
Fuel lifetime, full-power days	517		596		676		607	
Fuel enrichment, wt % <sup>235</sup> U	1.0879		1.1685		1.2510		1.159	
Fuel handling plant size, MP of U per year for 15,000-Mw(e) capacity	978		849		749		787	
Fabrication cost, \$/kg of U	31.2		32.1		32.9		32.5	
Processing cost, \$/kg of U	19.1		21.1		23.1		22.3	
Fuel shipping cost, total \$/kg of U	2.74		2.74		2.74		2.74	
Preexposure fuel holdup, days	93		93		93		93	
Postexposure holdup through processing, days	206		206		206		206	
Initial fissile inventory, kg	973		973		973		1018	
First core fuel inventory cost, \$	3.623 × 10 <sup>6</sup>		3.623 × 10 <sup>6</sup>		3.623 × 10 <sup>6</sup>		3.815 × 10 <sup>6</sup>	
First core fabrication cost, <sup>a</sup> \$	4.16 × 10 <sup>6</sup>		4.34 × 10 <sup>6</sup>		4.50 × 10 <sup>6</sup>		4.46 × 10 <sup>6</sup>	
Fuel-cycle cost, mills/kwhr(e)	<u>Equilibrium</u>	<u>30 Years</u>	<u>Equilibrium</u>	<u>30 Years</u>	<u>Equilibrium</u>	<u>30 Years</u>	<u>Equilibrium</u>	<u>30 Years</u>
Burnup and losses	0.519	0.537	0.511	0.529	0.507	0.524	0.506	0.510
Preparation plus fabrication	0.290	0.300	0.258	0.268	0.234	0.244	0.262	0.263
Processing	0.175	0.180	0.167	0.171	0.161	0.167	0.178	0.180
Shipping	0.025	0.026	0.022	0.023	0.019	0.020	0.022	0.022
Uranium inventory	0.075	0.061	0.080	0.061	0.087	0.062	0.076	0.060
Interest on fabrication	0.039	0.073	0.038	0.072	0.038	0.072	0.039	0.065
Interest on processing and shipping	-0.014	-0.012	-0.014	-0.012	-0.015	-0.012	-0.015	-0.011
Fissile plutonium credit	-0.297	-0.305	-0.267	-0.276	-0.242	-0.252	-0.268	-0.275
Plutonium inventory	<u>0.033</u>	<u>0.034</u>	<u>0.033</u>	<u>0.032</u>	<u>0.033</u>	<u>0.031</u>	<u>0.034</u>	<u>0.033</u>
Net fuel-cycle cost	0.845	0.894	0.828	0.868	0.822	0.856	0.834	0.847
B <sub>2</sub> O and coolant inventory at 10% per year	0.191	0.191	0.191	0.191	0.191	0.191	0.191	0.191
Total	1.036	1.085	1.019	1.059	1.013	1.047	1.025	1.038

<sup>a</sup>8% extra charge on first loading.

The effect of fissile plutonium sale price on the fuel-cycle cost is shown in Fig. 13.1. Processing is not economical below a price of about \$7/g of fissile material.

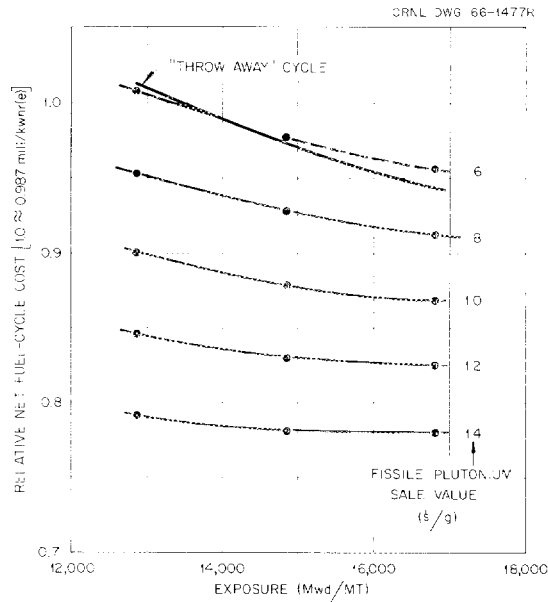


Fig. 13.1. Effect of Fissile Plutonium Value on Fuel-Cycle Cost of HWOCR-U.

### 13.5 B&W Design Fuel-Cycle Costs

Our calculated fuel-cycle costs for the thorium-loaded HWOCR are listed in Tables 13.2 and 13.3.

The costs for these particular designs are clearly too high to be attractive. We obtained a net fuel-cycle cost of 1.48 mills/kwhr(e) for the thorium oxide design and 1.35 mills/kwhr(e) for the thorium-metal design, both at 20,000 Mwd/MT. B&W obtained a fuel-cycle cost of 1.08 mills/kwhr(e) in both bases at the same burnup. The differences between the B&W costs and ours come principally from the differences in conversion ratios and fabrication cost estimates. For the thorium oxide design we estimated an equilibrium cycle conversion ratio of 0.72, while B&W obtains 0.79. The resulting difference in burnup costs over the 30-year lifetime is 0.15 mill/kwhr(e). For the thorium-metal design, we

Table 13.2. Fuel-Cycle Costs for B&W HWO CR Fueled with ThO<sub>2</sub>-UO<sub>2</sub> in Pin-Cluster Elements

Thermal efficiency: 34.8%

	Case					
	W-1		W-2		W-3	
Core behavior calculation	12-zone point depletion		12-zone point depletion		12-zone point depletion	
Last-cycle data	74th fueling		74th fueling		74th fueling	
Exposure, Mwd/MP	14,794		19,940		22,883	
Fuel lifetime, full-power days	279		377		434	
Fuel enrichment, wt % <sup>235</sup> U + <sup>233</sup> U	2.332		2.513		2.620	
Fuel handling plant size, MP of U + Th per year for 15,000-Mw(e) capacity	851		631		550	
Fabrication cost, \$/kg of U + Th	67.0		70.1		71.6	
Processing cost, \$/kg of U + Th	19.4		24.0		26.5	
Fuel shipping cost, total \$/kg of U + Th	6.88		6.88		6.88	
Preexposure fuel holdup, days	93		93		93	
Postexposure holdup through processing, days	201		201		201	
Initial fissile inventory, kg	1277		1277		1277	
First core fuel inventory cost, \$	16.04 × 10 <sup>6</sup>		16.04 × 10 <sup>6</sup>		16.04 × 10 <sup>6</sup>	
First core fabrication cost, \$	3.772 × 10 <sup>6</sup>		4.138 × 10 <sup>6</sup>		4.231 × 10 <sup>6</sup>	
Fuel cycle cost, mills/kwhr(e)	<u>Last Cycle</u>	<u>30 Years</u>	<u>Last Cycle</u>	<u>30 Years</u>	<u>Last Cycle</u>	<u>30 Years</u>
Burnup and losses <sup>a</sup>	0.491	0.480	0.501	0.472	0.507	0.510
Preparation plus fabrication	0.542	0.548	0.421	0.427	0.376	0.382
Processing	0.154	0.156	0.141	0.144	0.130	0.133
Shipping	0.055	0.056	0.041	0.042	0.035	0.036
<sup>235</sup> U and <sup>232</sup> Th inventory <sup>a</sup>	0.038	0.307	0.026	0.318	0.022	0.312
Interest on fabrication	0.051	0.082	0.048	0.079	0.045	0.078
Interest on processing and shipping	-0.008	-0.006	-0.008	-0.006	-0.009	-0.006
<sup>233</sup> U inventory	<u>0.356</u>	-----	<u>0.321</u>	-----	<u>0.306</u>	-----
Net fuel-cycle cost	1.679	1.623	1.491	1.476	1.412	1.445
D <sub>2</sub> O and coolant inventory at 10% per year	0.185	0.185	0.185	0.185	0.185	0.185
Total	<u>1.864</u>	<u>1.808</u>	<u>1.676</u>	<u>1.661</u>	<u>1.597</u>	<u>1.630</u>

<sup>a</sup>Including <sup>236</sup>U penalty and fissile plutonium credit.

obtained a conversion ratio of 0.80 compared with the 0.89 obtained by B&W. The associated difference in cost is 0.16 mill/kwhr(e). The B&W estimate of fabrication, processing, and shipping for the oxide fuel is \$62.4/kg, while ours is \$101/kg. The resulting fuel-cycle cost difference is 0.31 mill/kwhr(e). For the metal fuel, costs of fabrication and shipping plus processing are estimated to be \$71.0/kg by B&W and 79.3 by us; there is a resulting cost difference of 0.06 mill/kwhr(e). Reasons for the differences in conversion ratios and fabrication costs are discussed in Chapters 4 and 10.

Table 13.3. Fuel-Cycle Costs for B&amp;W HWOCR Fueled with Th-U Metal in Nested-Cylinder Elements

Thermal efficiency: 34.8%

	Case					
	X-1		X-2		X-3	
Core behavior calculation	12-zone point depletion		12-zone point depletion		12-zone point depletion	
Last-cycle data	74th fueling		74th fueling		74 fueling	
Exposure, Mwd/MF	16,940		19,905		22,839	
Fuel lifetime, full-power days	515		606		697	
Fuel enrichment, wt % $^{235}\text{U} + ^{233}\text{U}$	2.079		2.172		2.269	
Fuel handling plant size, MF of U + Th per year for 15,000-Mw(e) capacity	743		632		551	
Fabrication cost, \$/kg of U + Th	49.4		51.4		53.3	
Processing cost, \$/kg of U + Th	20.3		22.8		25.2	
Fuel shipping cost, total \$/kg of U + Th	5.05		5.05		5.05	
Preexposure fuel holdup, days	103		103		103	
Postexposure holdup through processing, days	197		197		197	
Initial fissile inventory, kg	1900		1900		1900	
First core fuel inventory cost, \$	$23.96 \times 10^6$		$23.96 \times 10^6$		$23.96 \times 10^6$	
First core fabrication cost, \$	$4.536 \times 10^6$		$4.857 \times 10^6$		$5.149 \times 10^6$	
Fuel-cycle cost, mills/kwhr(e)	<u>Last Cycle</u>	<u>30 Years</u>	<u>Last Cycle</u>	<u>30 Years</u>	<u>Last Cycle</u>	<u>30 Years</u>
Burnup and losses <sup>b</sup>	0.349	0.347	0.361	0.361	0.373	0.377
Preparation plus fabrication	0.349	0.350	0.309	0.318	0.280	0.288
Processing	0.140	0.151	0.134	0.138	0.128	0.133
Shipping	0.035	0.036	0.030	0.031	0.026	0.027
$^{235}\text{U}$ and $^{232}\text{Th}$ inventory <sup>a</sup>	0.029	0.434	0.027	0.435	0.027	0.433
Interest on fabrication	0.048	0.082	0.047	0.079	0.047	0.079
Interest on processing and shipping	-0.010	-0.010	-0.011	-0.008	-0.012	-0.008
$^{233}\text{U}$ inventory	<u>0.440</u>	-----	<u>0.420</u>	-----	<u>0.407</u>	-----
Net fuel-cycle cost	1.380	1.390	1.317	1.354	1.276	1.329
D <sub>2</sub> O and coolant inventory at 10% per year	0.181	0.181	0.181	0.181	0.181	0.181
Total	1.561	1.571	1.498	1.535	1.457	1.510

<sup>a</sup>Including  $^{236}\text{U}$  penalty and fissile plutonium credit.

Our calculations of fuel-cycle costs for two earlier B&W core designs<sup>2</sup> are summarized in Table 13.4. The earlier designs had lower specific power, more massive (and hence cheaper) fuel elements, and higher conversion ratios. It can be seen that fuel-cycle cost is slightly lower at equal burnup for both of the earlier designs than for the current ones. The lowest net fuel-cycle cost we obtained for any of the thorium-cycle HWOCR's considered here is the 1.12 mills/kwhr(e) in the case of the earlier B&W thorium oxide design. In comparison with the current B&W thorium oxide design, the lower fuel-cycle cost of the earlier design is only partially offset by 0.1 mill/kwhr(e) greater interest on the

Table 13.4. Fuel-Cycle Costs Calculated for a Late-in-Life Cycle of an Early B&amp;W HWOCR-Th

Thermal efficiency: 34.8%

Case	A-2	B-2
Fuel elements	ThO <sub>2</sub> -UO <sub>2</sub> fueled pin clusters	Th-U metal fueled nested cylinders
Exposure, Mwd/T	18,200	16,800
Feed enrichment, wt %	1.67	1.65
Conversion ratio	0.88	0.90
Specific power, kw/kg of fissile material	30	18.4
Unit costs, \$/kg		
Fabrication	28.6	31.1
Processing	24.3	21.0
Shipping	6.9	5.1
Out-of-pile time, days	294	300
In-pile time, days	866	1214
Initial fissile inventory, kg	2369	3070
Fuel-cycle cost, mills/kwhr(e)		
Burnup	0.19	0.22
Preparation plus fabrication	0.22	0.21
Processing	0.16	0.15
Shipping	0.04	0.04
Inventory, total	0.49	0.68
Fabrication interest	0.03	0.05
Processing interest	<u>-0.01</u>	<u>-0.02</u>
Net fuel-cycle cost	1.12	1.33
D <sub>2</sub> O and coolant inventory at 10% per year	0.29	0.21
Total	<u>1.41</u>	<u>1.54</u>

larger coolant inventory plus 0.17 mill/kwhr(e) greater charges on the capital cost of the core (see Chapt. 14).

The wide range of fuel-cycle costs that we estimated for the various thorium-cycle designs suggests that more extensive optimization is required before a complete comparison can be made between the thorium- and uranium-cycle HWOCR's. The following tentative conclusions are indicated by the designs studied thus far:

1. A massive fuel element should be used so that the fabrication cost, in terms of \$/kg of thorium, is kept low.
2. If fabrication plus processing costs are in the range of \$100/kg, a much higher burnup than 20,000 Mwd/MT is desirable.

3. The lattice dimensions and spatial arrangement must be such as to give high conversion ratios, since the performance of recycled  $^{233}\text{U}$  fuel is very sensitive to neutron economy.

4. It is important to minimize  $\text{D}_2\text{O}$  inventory cost. Consideration should be given to reducing the lattice pitch as far as possible and to using some other material for the reflector region.

5. The conversion ratio could be improved if some means could be devised to separate "burned" fissile fuel from the fissile fuel bred during the exposure cycle.

### 13.6 Summary of Effects of Variations in Ground Rules

A near-optimum example of the fuel-cycle cost breakdown for each of the reference HWOGR designs is presented in Table 13.5, based on a thermal efficiency of 34.8%. Also shown are effects of variations in certain economic factors as calculated from the base case without reoptimization. Table 13.6 gives results for corresponding cases based on a thermal efficiency of 33.0%. The effect of thermal efficiency on net fuel-cycle cost is given in Fig. 13.2.

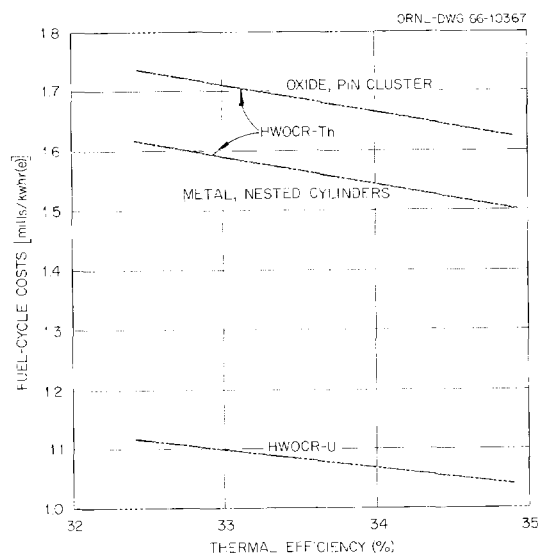


Fig. 13.2. Total Fuel-Cycle Costs of HWOGR Systems as a Function of Thermal Efficiency.

Table 13.5. Summary of Fuel-Cycle Costs and Effects of Variations in Certain Economic Parameters

Thermal efficiency: 34.8%

	AI-CE Uranium- Fueled Design	B&W ThO <sub>2</sub> -UO <sub>2</sub> Fueled Design	B&W Th-U Fueled Design
Case	Q-3	W-3	X-3
Final feed enrichment, wt %	1.251	2.620	2.269
Last-cycle exposure, Mwd/MT	16,801	22,883	22,839
Sum of fabrication, processing, and shipping unit costs, \$/kg	58.7	105	83.6
Fuel-cycle cost, mills/kwhr(e) <sup>a</sup>			
Burnup and losses	0.524	0.510	0.377
Preparation plus fabrication	0.244	0.382	0.288
Processing	0.167	0.133	0.133
Shipping	0.020	0.036	0.027
Uranium inventory	0.062	0.312	0.433
Interest on fabrication	0.072	0.078	0.079
Interest on processing	-0.012	-0.006	-0.008
Plutonium credit	-0.252		
Plutonium inventory	0.031		
Subtotal	0.856	1.445	1.329
D <sub>2</sub> O and coolant inventory <sup>b</sup>	0.191	0.195	0.181
Total	1.047	1.630	1.510
Total fuel-cycle cost with uranium ore cost of \$16/lb U <sub>3</sub> O <sub>8</sub> , <sup>c</sup> mills/kwhr(e)	1.33	1.92	1.79
Total fuel-cycle cost with an interest rate of 5% (includes D <sub>2</sub> O at 5%), mills/kwhr(e)	0.88	1.35	1.18

<sup>a</sup>Discounting at 6%; 10% charges on fuel and fabrication; \$12.05/g for <sup>235</sup>U, -\$12.00/g for <sup>236</sup>U, \$18.00/g for <sup>233</sup>U, \$10.00/g for fissile plutonium.

<sup>b</sup>Fixed charge of 10% per year.

<sup>c</sup>\$16.23/g for <sup>235</sup>U, -\$16.23/g for <sup>236</sup>U, \$24.31/g for <sup>233</sup>U, \$13.51/g for fissile plutonium.

Table 13.6. Summary of Fuel-Cycle Costs and Effects of Variations in Certain Economic Parameters

Thermal efficiency: 33.0%

	AI-CE Uranium- Fueled Design	B&W ThO <sub>2</sub> -UO <sub>2</sub> Fueled Design	B&W Th-U Fueled Design
Case	Q-3	W-3	X-3
Final feed enrichment, wt %	1.251	2.620	2.269
Last-cycle exposure, Mwd/MT	16,801	22,883	22,839
Sum of fabrication, processing, and shipping unit costs, \$/kg	57.5	103	81.8
Fuel-cycle cost, mills/kwhr(e) <sup>a</sup>			
Burnup and losses	0.553	0.538	0.398
Preparation plus fabrication	0.254	0.396	0.304
Processing	0.174	0.134	0.135
Shipping	0.021	0.038	0.028
Uranium inventory	0.066	0.330	0.459
Interest on fabrication	0.076	0.084	0.083
Interest on processing	-0.013	-0.006	-0.008
Plutonium credit	-0.266		
Plutonium inventory	0.033		
Subtotal	0.898	1.514	1.399
D <sub>2</sub> O and coolant inventory <sup>b</sup>	0.201	0.195	0.191
Total	1.099	1.709	1.590
Total fuel-cycle cost with uranium ore cost of \$16/lb U <sub>3</sub> O <sub>8</sub> , <sup>c</sup> mills/kwhr(e)	1.40	2.01	1.89
Total fuel-cycle cost with an interest rate of 5% (includes D <sub>2</sub> O at 5%), mills/kwhr(e)	0.93	1.42	1.24

<sup>a</sup>Discounting at 6%; 10% charges on fuel and fabrication; \$12.05/g for <sup>235</sup>U, -\$12.00/g for <sup>236</sup>U, \$18.00/g for <sup>233</sup>U, \$10.00/g for fissile plutonium.

<sup>b</sup>Fixed charge of 10% per year.

<sup>c</sup>\$16.23/g for <sup>235</sup>U, -\$16.23/g for <sup>236</sup>U, \$24.31/g for <sup>233</sup>U, \$13.51/g for fissile plutonium.

References

1. M. W. Rosenthal et al., A Comparative Evaluation of Advanced Converters, USAEC Report ORNL-3686, Oak Ridge National Laboratory, January 1965.
2. Babcock & Wilcox Company, Thorium Fuel Cycle for Heavy Water Moderated Organic Cooled Reactors, Quarterly Technical Report No. 2, April-June 1965, USAEC Report BAW-393-2, October 1965.

## 14. REACTOR PERFORMANCE

Capital costs given in Table 7.6 in Chapter 7, operation and maintenance costs from Chapter 8, and fuel-cycle costs from Fig. 13.2 in Chapter 13 were used to compute power costs. Reference costs were based on a 0.8 plant factor and a fixed charge rate on the reactor plant of 12% per year. The fuel-cycle cost is the average cost over 30 years. As discussed previously, there is uncertainty in the reactor outlet coolant temperature because of uncertainty in the degree of fuel surface fouling by the coolant; this leads to uncertainty in reactor performance. The results for the reference bases are summarized in Table 14.1; fouling conditions associated with a temperature drop of 25 to 50°F across the fuel-surface fouling film at the peak-surface-temperature location were considered. Figure 14.1 illustrates the results given in Table 14.1.

The power costs for public utility financing are given in Table 14.2. No reoptimization of the design was made, even though the cost bases were different; reoptimization would lead to a small reduction in total power cost.

In the above tables, the operation and maintenance costs were based on values used in the advanced converter study, with upward adjustment of personnel costs in accordance with present salary structures. These costs, as shown, are significantly higher than present estimates for large light-water reactors and should not be used out of context. On the same bases, we would estimate that operation and maintenance costs for HWO CR plants would be only about 0.05 mill/kwhr(e) higher than for light-water reactors; this higher value is due to the annual coolant and heavy-water losses and the slightly higher costs of maintaining a plant with two separate fluid systems. If O&M costs in light-water reactor plants are about 0.22 mill/kwhr(e), then we estimate that the HWO CR O&M costs should be about 0.27 mill/kwhr(e), which would lower the HWO CR power costs presented here by about 0.1 mill/kwhr(e).

As shown in Fig. 14.1 the estimated power-production cost for the AI-CE design concept was 3.46 to 3.54 mills/kwhr(e) for reference conditions. This performance can be improved if axial power-peaking factors

Table 14.1. HWOCR Power Costs for Reference Economic Conditions  
Based on Submitted Designs and ORNL Evaluation

Load factor: 0.8  
 Fixed charges on reactor plant: 12% per year  
 Fixed charges on fabrication and processing plants: 22% per year  
 Fixed charges on fuel and fuel element fabrication working capital: 10% per year  
 Value of fissile plutonium: \$10/g  
 Value of highly enriched uranium: \$12/g of  $^{235}\text{U}$   
 Value of natural uranium: \$8/lb of  $\text{U}_3\text{O}_8$   
 Heavy water and coolant charges: 10% per year for inventory, 0.56% per year for  $\text{D}_2\text{O}$  makeup, 160 lb/hr for coolant makeup

Item	AI-CE Uranium-Fueled Design		B&W (Th-U) $\text{O}_2$ -Fueled Design		B&W Th-U Metal-Fueled Design	
	Outlet coolant temperature, °F	700	675	690	660	700
Power production cost, mills/kwhr(e)						
Capital	2.02	2.08	1.96	2.04	1.94	1.99
Operation and maintenance	0.37	0.37	0.37	0.37	0.37	0.37
Fuel cycle (includes $\text{D}_2\text{O}$ and coolant inventory)	1.07	1.09	1.67	1.73	1.54	1.58
Total	3.46	3.54	4.00	4.14	3.85	3.94

Table 14.2. Power Costs for HWOCR Systems with Public Financing  
Based on Submitted Designs and ORNL Evaluation

Fixed charges on reactor plant: 7% per year  
 Fixed charges on fabrication and processing plants: 22% per year  
 Fixed charges on fuel and fuel element fabrication working capital: 5% per year and 4% discount rate  
 Other conditions: see Table 14.1

Item	AI-CE Uranium-Fueled Design		B&W (Th-U) $\text{O}_2$ -Fueled Design		B&W Th-U Metal-Fueled Design	
	Outlet coolant temperature, °F	700	675	690	660	700
Power production cost, mills/kwhr(e)						
Capital	1.14	1.17	1.10	1.15	1.09	1.12
Operation and maintenance	0.37	0.37	0.37	0.37	0.37	0.37
Fuel cycle (includes $\text{D}_2\text{O}$ and coolant inventory)	0.90	0.92	1.39	1.44	1.20	1.23
Total	2.41	2.46	2.86	2.96	2.66	2.72

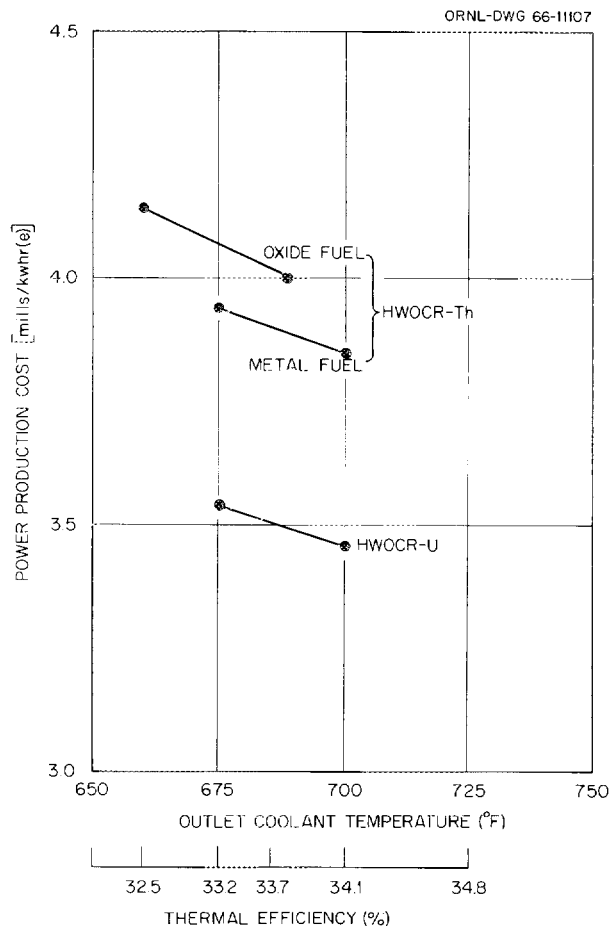


Fig. 14.1. HWOCR Power Production Cost Based on Submitted Designs and ORNL Evaluation (Reference Economic Conditions).

are decreased by use of natural uranium slugs at the ends of fuel assemblies. Decreasing the axial peaking factor would permit the exit coolant temperature to increase; this would lead to an increase in thermal efficiency and a decrease in capital costs. It is estimated that such changes would decrease the power-production cost by about 0.03 mill/kwhr(e).

Of the two B&W concepts, the metal-fueled reactor had the lower power cost; however, the oxide pin design submitted by B&W (and perhaps the metal-ring design) does not appear to represent an optimized system. This is indicated by comparing the results of Tables 13.4 and 13.5. Table 13.5 gives fuel-cycle costs based on the submitted B&W design, while Table 13.4 gives corresponding results from an initial B&W design study.

The oxide-fueled reactor of the first design had significantly lower fuel-cycle costs than others studied. A rough estimate of the capital cost differences between the present oxide-fueled reactor with 335 process tubes and the initial oxide-fueled system having 804 process tubes gives a difference of \$7 million in direct capital costs in favor of the 335-tube design. Applying an overall indirect cost factor of 41%, the capital cost difference between the 804 and 335 process-tube reactors corresponds to 0.17 mill/kwhr(e). Even with this additional cost and the increased D<sub>2</sub>O inventory (included in the fuel-cycle costs of Table 13.4), the 804 process-tube reactor has the lower power production cost and also a higher conversion ratio (by about 0.1). Thus it appears that the power production cost can be lowered and the conversion ratio can be increased by changes in the core design of the thorium-oxide-pin-fueled reactor design submitted, and the same may be true for the thorium-metal-fueled system.

Even if credit is taken for improved HWOCR-Th core designs, it appears unlikely that the power production cost will be as low as that for the HWOCR-U system under the ground rules and bases used in this evaluation. For example, if we assume that the power peaking factors in the thorium system are reduced by use of local thorium absorber (containing no fissile material initially) at the ends of the fuel elements, it is estimated that the maximum reactor outlet-coolant temperature for the B&W design could be about 710°F for the metal-fueled system and about 720°F for the oxide-fueled case — there is much greater potential for reducing the axial power-peaking factor in the oxide-fueled concept relative to the cases evaluated. Taking credit for the above without any penalties results in decreased capital costs and higher thermal efficiencies. Under these circumstances it is estimated that the power production cost for these reactor designs would be in the range 3.7 to 3.8 mills/kwhr(e). If, in addition, we take credit for an increased conversion ratio of about 0.1 (which is about the difference in conversion ratio between the initial B&W designs and the designs submitted) and consider minimal associated penalties, the power production cost from the HWOCR-Th systems is in the range of 3.6 to 3.7 mills/kwhr(e), which

is still higher than the 3.5-mill/kwhr(e) power cost of the HWOOCR-U system. At the same time, it appears that an HWOOCR-U reactor system can be changed to thorium fueling without requiring significant core design changes if associated changes in control and safety problems are not significant. Use of thorium fuels would increase the conversion ratio, but it would also increase the fissile inventory requirement. Because of this, reasonable increases in the price of natural uranium would increase the power production cost in a thorium-fueled HWOOCR about the same as in a uranium-fueled HWOOCR, as indicated in Tables 13.5 and 13.6, which give fuel-cycle costs based on uranium prices of \$8 and \$16 per pound of  $U_3O_8$ .

These power production costs for reference economic conditions can be compared with those obtained in the advanced converter study<sup>1</sup> if appropriate consideration is given to changes in design and in evaluation bases. Of particular interest are the PWR power production costs, which in the advanced converter study were estimated to be about 4.3 mills/kwhr(e). Since the time of that study there have been design changes and reductions in capital costs that were achieved principally through reduced control rod costs, reduced pressure vessel costs, and reduced pump, piping, and heat exchanger costs. The reduction in control rod costs has come about by the use of chemical shim; the reduction in pump, piping, and heat exchanger costs is a result of the use of fewer loops, along with larger equipment; and the reduction in the number of pressure vessel penetrations resulting from the two foregoing developments has reduced pressure vessel cost. There have also been associated reductions in control equipment cost. These changes are estimated to reduce the capital charges from 2.3 to 2.1 mills/kwhr(e) based on a 0.8 load factor and a fixed charge rate of 12% per year.

In addition, the improved bases used in the present study for evaluating fuel preparation, fabrication, and processing costs lower the PWR fuel-cycle cost by about 0.1 mill/kwhr(e); also, increasing the plutonium price from \$7 per gram of fissile material used in the advanced converter study to \$10 per gram of fissile material used here decreases the PWR power cost an additional 0.1 mill/kwhr(e). At the same time, the operation and maintenance costs were considered to be 0.30 mill/kwhr(e) in

the advanced converter evaluation, while the corresponding value used here was 0.34 mill/kwhr(e). The net effect of these changes reduces the PWR power production cost from 4.30 mills/kwhr(e) to about 3.93 mills/kwhr(e) based on present design information and HWOOCR cost bases.

In order to compare HWOOCR power costs with those of other reactor types studied in the advanced converter evaluation, factors similar to those considered above need to be included, and these have not been evaluated in detail. However, some pertinent comments can be made for the HTGR and the PWR reactors studied previously. Relative to the HWR reactors (D<sub>2</sub>O cooled), the primary difference between the results obtained in the advanced converter study and those obtained here are associated with the higher thermal efficiency of HWOOCR systems and the reduced heavy-water inventories. For the HTGR, changing the fuel recycle bases to those used here reduces the fuel-cycle costs about 0.1 mill/kwhr(e); the corresponding change in operation and maintenance costs is an increase of 0.02 mill/kwhr(e). The resulting HTGR power production cost based on the results of the advanced converter study modified directly in accordance with HWOOCR cost bases is about 3.5 to 3.6 mills/kwhr(e) at a conversion ratio in the range of 0.80 to 0.85.

The HWOOCR designs studied here included on-power refueling, and this feature might permit such systems to have very high load factors. Operation at a 0.9 load factor instead of 0.8 would reduce capital inventory and capital charges to the extent that the power costs given in Table 14.1 would be reduced by 0.25 to 0.30 mill/kwhr(e).

The fissile material inventory and consumption requirements influence fuel utilization as well as economic performance. Table 14.3 gives these requirements for the submitted HWOOCR design conditions. The values in Table 14.3 are based on our evaluation results in terms of the specific fissile material inventory, the annual net fissile material consumption, the 30-year net fissile material consumption, and the average conversion ratio over the plant life. The fissile material consumption takes into consideration that the uranium discarded at the end of the uranium cycle contains some <sup>235</sup>U that is not economically available. The results obtained indicate that while the specific inventory is significant with

regard to fuel-cycle costs, fuel consumption is the overriding term over the 30-year life of these reactors relative to fissile material requirements of a given reactor. However, specific inventory becomes significant if the installed electrical capacity associated with a given reactor type is rising rapidly. Estimates of uranium ore requirements for HWOOCR's in an expanding industry are listed in Table 14.4.

Table 14.3. Fuel Requirements of HWOOCR Concepts  
Based on 34% Thermal Efficiency

	AI-CE Uranium Cycle	B&W Thorium Cycle	
		Oxide Fuel	Metal Fuel
Fissile material requirements, kg of $^{235}\text{U}$ per Mw(e)			
Specific fissile inventory <sup>a</sup>	1.15	1.95	2.55
Annual net fissile feed <sup>b</sup>	0.47	0.32	0.25
30-year net fissile feed <sup>b</sup>	14.1	9.7	7.5
Average conversion ratio	0.70	0.74	0.80

<sup>a</sup>Includes out-of-core inventory associated with entire fuel cycle. Core loading of uranium reactor is about 1.0 kg of  $^{235}\text{U}$  per Mw(e), while for the thorium reactors it is about 1.9 and 1.3 kg of  $^{235}\text{U}$  per Mw(e) for the metal and oxide fuels, respectively.

<sup>b</sup>Based on 0.8 load factor and credit for bred fuel.

Table 14.4. Uranium Ore Committed in an Expanding Industry  
of HWOOCR's Having 30-Year Life

Year	Assumed Installed Industry Size [kw(e)]			U <sub>3</sub> O <sub>8</sub> Mined and Committed (short tons)	
	Operating	New Plus Replacement	Cumulative Total	HWOOCR-U	HWOOCR-Th <sup>a</sup>
	$\times 10^6$	$\times 10^6$	$\times 10^6$	$\times 10^6$	$\times 10^6$
1980	40	35	40	0.14	0.10
1990	210	170	210	0.71	0.53
2000	730	520	735	2.46	1.82
2010	1500	770	1540	5.08	3.64
2020	2300	800	2510	8.17	5.71

<sup>a</sup>Based on metal-fueled core.

Reference

1. M. W. Rosenthal et al., A Comparative Evaluation of Advanced Converters, USAEC Report ORNL-3686, Oak Ridge National Laboratory, January 1965.

## 15. SUMMARY AND CONCLUSIONS

An evaluation was made of 1000-Mw(e) HWOCR power plants operating on the uranium or thorium fuel cycle. Power costs and nuclear performance characteristics of the plants were estimated based on engineering evaluations of the reactor cores and plant designs and analyses of performance requirements, design features, capital cost estimates, fuel-cycle performance, and control features.

The reactors were assumed to be in operation in the 1970's and to use technology either developed or considered feasible at the present time. A 30-year reactor plant life was considered. Further assumptions were that:

1. The cost of uranium remains constant over the life of the reactors.
2. The capacities of the fabrication and processing plants are such that they will provide the fuel-cycle needs of identical reactor plants generating a total of 15,000 Mw(e).
3. The power plant, reactor fuel, and fuel fabrication and processing facilities are privately owned.
4. The uranium reactors are fueled with slightly enriched uranium, and the bred plutonium is sold without recycle.
5. The thorium reactors are initially fueled with  $^{235}\text{U}$ , and the bred  $^{233}\text{U}$  is recycled.

Reactor core designs were provided by AI-CE for the uranium fuel cycle and by B&W for the thorium fuel cycle; the plant design was provided by AI-CE.

### 15.1 Reactor Systems Studied

HWOCR's have lattice-type cores in which the organic coolant is separate from the heavy-water moderator. In the designs submitted for the systems studied, the coolant leaves the reactor at 750°F. Steam produced at 725°F and 900 psig in the steam cycle leads to an overall system thermal efficiency of about 35%. The nominal plant rating is 1000 Mw(e). The plant features a process-tube reactor with on-power refueling, carbon steel

primary loops, recovery facilities for decomposed organic coolant, and primary heat-transfer-system components located outside the containment.

Santowax OM coolant (primarily a mixture of ortho- and metaterphenyls) is used to transfer heat from the reactor to the primary heat exchangers. During reactor operation, the organic coolant undergoes radiolytic and pyrolytic decompositions. The decomposition products, as well as corrosion products, are continuously removed from the coolant stream in order to maintain the coolant at an acceptable purity level. High boilers are removed by distillation and are converted to usable coolant by catalytic hydrocracking.

The AI-CE core is designed for uranium carbide fuel made from slightly enriched uranium. Also, the fuel feed material is always slightly enriched uranium, with sale of the plutonium obtained at the end of each fuel-exposure cycle. Bidirectional fueling of adjacent fuel channels in the core is accomplished by means of two fueling machines, one at each end of the core. Also, coolant flow is always in the direction of fuel movement. The fuel is clad with a sintered aluminum product (SAP, consisting of aluminum oxide dispersed in a matrix of aluminum) and is located in 492 fuel channels.

The B&W designs include two basic fuel elements. One design has an annular metallic fuel element clad with Zircaloy-4; the other utilizes pin-type clusters containing oxide fuel clad with SAP material. The initial fuel consists of thorium with  $^{235}\text{U}$  added as the fissile material. In subsequent cycles, the bred  $^{233}\text{U}$  is recycled with makeup  $^{235}\text{U}$  added as needed. Bidirectional fueling in adjacent channels is accomplished with one refueling machine operating from one end of the reactor. Coolant flow through the reactor core is unidirectional, however. With the metallic fuel assembly, 299 process tubes are used; with the oxide fuel assembly, 335 process channels are used.

## 15.2 Evaluation of Core Designs

Evaluations were made of the reactor physics and engineering performance of the reactor core designs. In the reactor physics studies, careful attention was given to details of the cell and neutron-spectrum

calculations; two-dimensional criticality calculations were employed in obtaining power-peaking factors and in estimating neutron-leakage effects. Power-peaking factor studies included considerations of the gross radial and axial power distributions, the channel interactions between fresh and depleted fuel, and the local radial and axial power distributions. Fuel-depletion calculations were used in analyzing the fuel-cycle performance of the systems. Temperature coefficients of reactivity were calculated for the fuel, coolant, and moderator, and void coefficients of reactivity were obtained for the coolant.

The engineering evaluations of the reactor cores included studies of the core thermal and hydraulic performance; evaluation of the computational methods and engineering correlations employed by the designers; examination of materials performance, compatibility, and consistency of design criteria with permissible materials conditions; evaluation of organic coolant performance under reactor conditions; and study of control and safety aspects of the reactors.

The fuel-cycle performance of the reactor cores was based on estimates of fuel reactivity lifetime; associated inventory charges; cost estimates for fuel preparation, fabrication, shipping, and processing; and feasible operating conditions, as determined by our evaluation.

#### 15.2.1 Fluid Flow and Heat Transfer Analyses

A critical review was made of the computer codes and input correlations and the data used by the design sponsors in the thermal and hydraulic analyses of the cores. The computer programs appear to be adequate for design studies. The heat transfer correlation employed appears to be optimistic, however. The engineering factors employed by the design sponsors appear to be slightly low and minor adjustments were made.

Relative to the AI-CE design, the pressure-drop correlation employed appears to be adequate. The critical heat-flux correlation employed seems to be conservative relative to tube- and annular-type flow geometry; however, these DNB correlations were derived from experiments with heated tubes or annuli, and they cannot be directly applied for predicting DNB heat fluxes in multirod fuel-bundle geometry. Because of the lack of

pertinent heat flux data and uncertainties in predicting the diphenyl content of the coolant under recycle conditions, we estimate that the minimum DNB ratio should be no less than 4, a condition which was met by the design conditions. Whether subcooled nucleate boiling could occur in the core is dependent upon the biphenyl concentration in the coolant; however, the biphenyl concentration can be controlled by appropriate operation of the distillation column. These statements also apply to the B&W designs.

The maximum average coolant velocity of 30 fps in the AI-CE design appears to be reasonable, but there will be variations from this value. Velocities in some subchannels will be greater than the average maximum, but no conditions are anticipated that influence feasibility. Considerable flexibility exists in specifying the average coolant velocity. Our hydraulic calculations gave reactor pressure drops in good agreement with the AI-CE value and also with the B&W value for the oxide pin-cluster design. For the B&W nested-cylinder design, we estimated a pressure drop of about 190 psi, while B&W obtained about 165 psi. The pressure drop that we obtained is a feasible one; no economic penalty was imposed because of the above difference.

For the different fuel assemblies, the buildup of a smooth fouling film on the fuel surface appears to impose little penalty relative to pressure drop. A more significant effect on pressure drop would be the character of the film; a film with a rough surface could cause a significant increase in pressure but is not anticipated. Also, there appears to be a significant uncertainty in the pressure drop across fuel assembly junctions because of uncertainty in fuel assembly orientations. Flow starving in some of the subchannels could occur due to misalignment of the fuel assemblies, which could lead to excessive surface temperatures. Studies need to be performed to assure that this does not occur.

The heat transfer coefficient used by AI-CE and also B&W for obtaining peak surface temperatures appears to be high by about 15%.\* We believe that the correlation presented by MIT is the proper one to use for

---

\*In recent conversations, AI-CE indicated they included a 5% reduction in heat transfer coefficient in their thermal calculations, in which case our heat transfer coefficient is about 10% lower than their value.

simple flow geometry, which, for the appropriate set of physical property values, predicts a heat transfer coefficient about 5% lower than values used by the design sponsors; in addition, we estimate that flow conditions through the fuel assemblies result in a further 10% decrease in heat transfer coefficient at local positions (because of flow geometry) and in some flow channels next to the process-tube wall (because of nonconcentric alignment of the fuel assembly in the process tubes). Thus, our evaluation was based on use of the MIT correlation, with the correlation coefficient reduced by 10%.

The adequacy of the machine programs depends on the accuracy with which the input data can be formulated. These data include the fluid-mixing factor, the power-peaking factors, and the engineering factors, as well as the heat transfer coefficient discussed above. At present there is insufficient information available on the mixing factor that corresponds to HWOCR conditions, and the factor used represents an extrapolation of existing experimental data. Also, the relationship between mixing and cross-flow coefficients may be specific to a particular design. At the same time, values employed by the sponsors for the different designs are considered to be feasible. The values specified for the engineering factors appear, in general, to be realistic; however, the factors for mechanical effects and gross flow maldistribution appeared optimistic and were increased by about 20% in our evaluation studies.

### 15.2.2 Power-Peaking Factors

Our calculated values were in reasonable agreement with the AI-CE power-peaking values, except for the gross radial power peak, for which we calculated a value of 1.39 compared with 1.17 by AI-CE. However, we found that significant radial power flattening could be obtained by small changes in spatial concentrations of the fuel and that the AI-CE value was a feasible one. This also illustrates that small changes in fuel concentrations, neutron absorptions, and in local neutron leakage can have relatively large effects on the power distribution, and indicates a need for careful spatial reactivity control in order to limit the power peaking factors throughout reactor operation.

Relative to the thorium core designs, our calculations predict higher axial power-peaking factors and higher fine-radial power-peaking factors than those of B&W; other values were in good agreement. Methods of reducing the axial power-peaking factors appear possible but involve redesign of the fuel assembly and changes in fuel-cycle performance.

### 15.2.3 Organic-Coolant Behavior

Terphenyls appear to be satisfactory organic coolants in that they have relatively low vapor pressures and decomposition rates under proposed temperature conditions. Operation with 10 wt % high boilers in the coolant appears reasonable in conjunction with use of a hydrocracker for recovery of degraded coolant. However, experience is needed relative to practical operating conditions in a catalytic hydrocracker for recovery of coolant from high boilers. Under the proposed operating conditions, and based on results of bench-scale experiments with hydrocracking, we estimate that the diphenyl content of the coolant will be significantly higher than that specified by the design sponsors (12% instead of 2%); at the same time, the diphenyl content can be controlled by appropriate operation of the distillation column. The primary disadvantages of increasing the diphenyl content are associated with the higher coolant vapor pressure and decomposition rate.

Studies of thermal and radiolytic stability of the coolant under operating conditions indicate that the decomposition rate increases with temperature, with a marked increase in decomposition rate as the temperature is increased above about 750°F in a reactor radiation field. The decomposition rate affects the coolant makeup costs and may have an influence on fouling-film formation.

The formation of a fouling film on surfaces of fuel elements is a complex phenomenon that is not completely understood; however, the purity of the coolant is a significant variable, with fouling decreasing with increasing coolant purity. Fouling is also related to coolant decomposition and the velocity of coolant flow past the fuel surface. Based on present information, film formation appears to be lowered by excluding contaminants from the coolant and by maintaining a high coolant velocity.

Nonetheless, film formation occurs in systems approximating HWOCR conditions, even with high-purity coolant and high flow conditions, and cannot be neglected. We estimate that under HWOCR conditions, the temperature drop across the fouling film will be 25 to 50°F at positions of maximum fuel surface temperature.

Corrosion in HWOCR systems is very low and does not appear to be a problem, except for the possibility that corrosion products may play a role in the formation of fouling films. Under design flow conditions, the volume of coolant at fuel surface temperatures is small, so the gross radiation degradation rate of the coolant is not markedly affected by the fuel surface temperature per se. At the same time, the damage to the coolant increases markedly with increasing temperature under reactor conditions, and the maximum coolant temperatures occur in the laminar sub-layer of the coolant where the fluid velocity is low. Although the kinetics of film-formation processes have not been established, it is judged that both the above conditions are conducive to film formation, and that until detailed studies have been made clarifying the relations between coolant purity, flow conditions, radiation damage, temperature, and fouling-film formation, the maximum coolant temperature should not exceed 850°F.

The degradation rate of the coolant is dependent upon the bulk coolant temperatures, which in turn are limited by maximum fuel surface temperatures, permissible local coolant temperatures, and economic considerations. Based on the reactor design submitted and our evaluation criteria, we estimate that the bulk coolant outlet temperature will not be above about 700°F; for this condition, we estimate the pyroradiolytic degradation rate of the coolant to be about 1430 lb/hr and the pyrolytic decomposition rate to be about 70 lb/hr, giving a total terphenyl degradation rate of 1500 lb/hr, the value used in our evaluation.

#### 15.2.4 Temperature Conditions

In evaluating maximum fuel surface temperatures, power-peaking factors calculated by ORNL were used that tended to be higher than those specified by the design sponsors. Also, we employed values for the heat

transfer coefficient and the engineering factors that were slightly different from those used by AI-CE and B&W, and use of these values tended to increase maximum surface temperatures above those specified by the design sponsors. On these bases, we estimate a maximum fuel-surface temperature for the AI-CE design conditions of 878°F, if no fouling film is present; this value was obtained with a basic radial power-peaking factor of 1.17, which appears achievable. For a fouling film on the surface of the fuel elements and a 25 to 50°F temperature drop across the film at the position of maximum fuel surface temperature, a maximum surface temperature of 903 to 928°F results for the AI-CE design conditions.

In order to achieve a maximum surface temperature not in excess of 850°F for the AI-CE design conditions with a 25°F temperature drop across the coolant fouling film at the position of peak surface temperature, the coolant outlet temperature would have to be lowered about 70°F to 680°F. The corresponding decrease in coolant outlet temperature for a 50°F temperature drop across the fouling film would be about 100°F, or an outlet temperature of 650°F. At the same time, it is possible to alter the reactor design conditions so that the coolant outlet temperature can be increased at less economic penalty than that associated with operating the present design at an outlet temperature in the 650 to 680°F range. To account for reoptimization of design conditions, it is estimated that the equivalent coolant outlet temperature to be associated with the present AI-CE design is 675 to 700°F for a fouling-film temperature drop of 25 to 50°F at the position of maximum fuel surface temperature. The above coolant outlet temperature range was used in evaluating the AI-CE design concept; use of this temperature range can be considered equivalent to increasing the fuel cladding thickness so that a maximum SAP surface temperature of about 870°F is permissible, with the decrease in nuclear performance associated with such a design change accounted for by decreasing the coolant outlet temperature about 7°F.

For the B&W oxide pin-cluster design conditions with no fuel surface fouling present, we estimate a maximum fuel surface temperature of about 884°F for fuel assemblies that move in the same direction as the coolant flow; the maximum surface temperature was about 892°F for assemblies

moving opposite to coolant flow. Including a fouling film with a 25 to 50°F temperature drop across it at the position of peak surface temperature would result in a surface temperature value of 917 to 942°F for the oxide pin-cluster design.

For the annular metal element design of B&W and with no fouling film present, we estimate a maximum fuel surface temperature of about 864°F for fuel moving in the same direction as the coolant and about 879°F for fuel moving opposite to coolant flow. Including a fouling film with the characteristics discussed above at the position of peak surface temperature would result in a maximum fuel surface temperature of 904 to 929°F.

If bidirectional coolant flow were employed in the B&W designs, a condition we consider to be feasible, the maximum fuel surface temperature would decrease about 8°F in the oxide-fuel design and about 15°F in the metal-fuel design. In addition, if the SAP cladding thickness of the oxide fuel were increased to permit a maximum surface temperature of 870°F, it is estimated that the effective coolant outlet temperature for the present design would be in the 660 to 690°F range for a 25 to 50°F temperature drop across a fouling film. For the metal-fuel design, it does not appear feasible to increase the maximum fuel-cladding temperature above 850°F because of hydriding effects. However, use of bidirectional coolant flow permits the outlet coolant to be in the 675 to 700°F range (based on a 25 to 50°F drop across a fouling film at positions of maximum surface temperatures). Thus, in evaluating the B&W core designs, the effective coolant outlet temperature was considered to be 660 to 690°F for the oxide pin-cluster design and 675 to 700°F for the metal-cylinder design.

The maximum permissible temperature of the SAP cladding is a function of the strength, creep, and elongation properties of the SAP under reactor conditions. A value of 850°F appears to be reasonable for the maximum permissible temperature for the specified design. This value could be increased slightly if the cladding thickness were increased. In the present design it may be permissible to have cladding temperatures in excess of 850°F for limited periods of time, but this first needs to be established experimentally.

The limitation on fuel center-line temperature is influenced by fuel growth as a function of temperature, reactor exposure, and fission-product behavior under reactor conditions. For the carbide fuel, and based on present information concerning fuel growth, we judge that the maximum fuel temperature should not exceed 2200°F for the proposed operating conditions. We found that the maximum center-line temperature did not exceed the 2200°F value. For the oxide and metal fuels, we also found that the fuel center-line temperatures did not exceed permissible values.

#### 15.2.5 Materials Evaluations

Of particular concern in these reactors are the mechanical properties of SAP. This material has been developed relatively recently, and the specifications and design stresses associated with proper reactor design have not been completely developed. The low ductility of SAP at low strain rates may be a serious limitation, and it appears probable that SAP components in the HWOCR must be designed on the basis of a maximum strain of about 0.5%. The SAP design criteria applied by AI-CE in the present study appear feasible based on available data; however, extensive testing is still needed in order to adequately specify the nuclear code design criteria that need to be satisfied for reactor application of SAP materials. In the B&W oxide pin-cluster core design, the thickness of the process tube should be increased by about 25% to reduce stresses to values consistent with AI-CE values. The Zircaloy calandria tube designs appear satisfactory, with tube stresses well within design limits for that material.

Material compatibility studies indicate that UC and SAP do not react under proposed operating conditions, and we concur that SAP and hyperstoichiometric UC will be suitable for use in the HWOCR environment. Also, both thorium and uranium appear compatible with SAP under the HWOCR operating conditions. Limited data suggest that Zircaloy-4 and thorium metal are compatible under HWOCR conditions for the planned fuel exposures. Reactions between various fuel and cladding components can occur, but available data indicate that such reactions will not proceed to the point where cladding failures occur.

No compatibility problems are anticipated with regard to the organic coolant and SAP materials. Relative to the thorium-metal fuel design, hydriding of Zircaloy-4 by the coolant can take place, particularly in cladding exposed to high temperatures. Hydriding of Zircaloy reduces ductility and can cause severe embrittlement. Protection from hydriding appears possible by the deposition of protective films.

Fuel element performance evaluations were conducted to identify areas that might restrict operating conditions. Of principal concern were fission-gas release and fuel swelling and the ability of the fuel cladding to maintain its integrity. For all fuels, proposed operating conditions are relatively severe, and extensive testing is required to determine actual performance under HWO CR conditions.

The UC fuel element appears to have a satisfactory design and to be suitable for HWO CR application based on present information and feasibility conditions. It should be capable of operating at proposed heat ratings and temperatures. Achievement of desired burnup will be critically dependent on fuel swelling at operating conditions; also, cracking and chipping of fuel could cause excessive local stresses in the SAP cladding. The strict limitations on gap thickness between the fuel and the cladding imply rigid control of dimensional variations of both the UC fuel and the inside diameter of the SAP cladding; we consider such control feasible. Present data on radiation damage to UC fuel indicates that a 2% volumetric growth per 10,000 Mwd/T exposure is reasonable to expect at center-line temperatures of about 2000°F; however, there is significant scatter in the data, and the value could be 3%, which would limit maximum fuel exposure to about 16,000 Mwd/T for the AI-CE design.

The thorium-based fuel elements also appear to have satisfactory designs and to be suitable for HWO CR application based on present information and feasibility conditions. Although thorium fuels themselves have been exposed satisfactorily to high-burnup conditions, experiments must be performed to demonstrate that the effects of compaction and of burnup in SAP-clad vibration-compacted fuel permit such cladding to be used. Reactor exposure of the oxide fuel appears limited by the buildup of fission-product-gas pressure. Relative to the thorium-based metal fuel

elements, exposure experience is limited. Fuel swelling of 3% volume increase per atomic per cent burnup appears feasible, but needs further verification. Temperatures and thermal gradients in the metal appear to be acceptable, but tests need to be performed to determine whether allowances made for distortion in the closely spaced annuli between cylinders are adequate.

#### 15.2.6 Safety and Control Considerations

The use of organic coolant with its relatively high neutron-absorption cross section makes the coolant temperature and void coefficients of reactivity positive in these heavy-water-moderated systems, so an increase in power can cause the reactivity of the system to increase. For the equilibrium core, our calculations indicate a coolant temperature coefficient of about  $4 \times 10^{-5} \Delta k_e / ^\circ F$  for the AI-CE uranium design. Reactivity coefficients calculated for the B&W thorium-based cores also indicated that such cores will have significant positive coefficients of reactivity associated with the temperature and void fraction of the organic coolant. During initial operations, the thorium cores appear to have a more positive coolant temperature coefficient than does the uranium core. Under equilibrium conditions, the reverse tends to be true. The reactivity coefficient calculations, while internally consistent, are not necessarily accurate to more than  $\pm 50\%$ , and experimental measurements are required to adequately evaluate HWOCR reactor safety requirements.

The positive coolant temperature coefficient imposes stringent demands on the operational requirements of the control systems; also, the design of the containment system is dependent on the reliability of the safety systems. The safety and control systems indicated in the design report appear deficient in the areas of reliability and performance; however, we believe that these deficiencies can be corrected and satisfactory systems can be devised for the HWOCR. We suggest that the safety systems be split into two separate and independent shutdown systems. Each shutdown system should have sufficiently fast response and sufficient reactivity control to give protection. Further analyses will be required to establish the precise rod-response times, but based on our evaluation the

specified insertion speed of the shutdown rods appears too slow. The total reactivity control of 4% presently available in the 84 shutdown rods appears sufficient but should be divided equally between two independent shutdown systems that have no common-mode failures.

The rod control system for normal power regulation of the reactor should be made more reliable by use of several controllers that minimize the effects of failure of a controller or failure of input signals to a controller. In addition, both the amount and rate of reactivity addition available for power-distribution control should be increased to provide continued control of the reactor following possible reactivity perturbations during operation. It appears desirable to increase the reactivity worth of the vertical control rods used for spatial power distribution control from 0.1% to 0.3%  $\Delta k_e$ . Also, it appears necessary that fuel loading and control rod positioning be computer controlled in order to adequately consider the effects of interplay between variables. It appears feasible to incorporate the above features through relatively minor design changes.

Information on plant safeguards was not available in sufficient detail for detailed evaluation of the adequacy of the safeguards provided; also, no analyses of reactor incidents were provided. We consider that use of double isolation valves on all main coolant lines penetrating the reactor building makes it feasible to locate the steam generators outside the reactor building. However, plant safeguard requirements are dependent on the conditions associated with the maximum credible accident, which has not been estimated or investigated. Reactor cell construction of reinforced concrete with a steel liner appears feasible and desirable; however, it appears advantageous to suppress any cell pressure buildup by use of vapor-condensation systems.

#### 15.2.7 Fuel-Cycle Conditions

In calculating fuel-cycle costs, unit costs were estimated for fuel preparation, fabrication, shipping, and processing. For evaluation conditions, the estimated costs were

	Costs (\$/kg)		
	UC Fuel	Thorium Oxide- Based Fuel	Thorium-Metal- Based Fuel
Fuel preparation	3.6	6.1	9.1
Fuel fabrication	29	65	44
Fuel shipping	2.5	5.3	3.6
Spent fuel processing	23	26	25

These costs were based on recycle of bred fuel in the thorium fuel cycle, while the uranium fuel cycle consisted of fueling with slightly enriched uranium, with sale of bred plutonium.

Unit cost estimates used by the design sponsors were in general agreement with our estimates. However, the B&W fabrication cost estimates were slightly lower due to consideration of an integrated processing and fabrication plant and due to lower cost estimates for certain fabrication operations.

The fuel-cycle unit cost estimates were used in conjunction with reactor physics calculations to obtain fuel-cycle performance and to optimize fuel-cycle conditions under the reference ground rules. Relative to the physics calculations, our calculational methods and those of AI-CE were similar, and similar results were obtained. The B&W calculations we examined gave results different from ours relative to fuel-depletion concentrations and resonance-escape-probability values; also, values used for the  $^{233}\text{U}$  cross sections were more optimistic than our values. As a result, our conversion ratios tended to be lower and our fuel-cycle costs higher than corresponding B&W values.

### 15.3 Evaluation of Plant Designs

In reviewing the equipment requirements for the HWOCR plants, our general conclusion was that the components described for the conceptual design were feasible to build with present-day manufacturing technology or would require at most a moderate extension of present technology. The large pumps, heat exchangers, and valves of the primary heat transfer system will require special design consideration and performance testing, but the fabrication of these components is within the capability of

present-day manufacturers. The mechanical design of the refueling machines appears to be feasible as described. However, the reliability of the refueling machines must be established through repeated tests of prototype machines under simulated design conditions. Also, emergency conditions that may arise from possible malfunctioning of the machine during a refueling operation must be evaluated and provisions made in the design for coping with these conditions.

The AI-CE core design specifies bidirectional fueling with fueling from both ends of the reactor. The B&W concepts specify bidirectional refueling with fueling from one end; this condition requires about twice as many strokes for fuel movement during a complete fuel change as does the AI-CE procedure. For all concepts, refueling operations take place during reactor operation, a favorable situation relative to attaining high load factors. Also, reactor downtime due to forced outages of heat transfer and steam-cycle equipment should be low, since the equipment is accessible and the radioactivity of the coolant is very low under normal operation. These features, combined with the on-power refueling schemes, can lead to load factors significantly higher than the 80% assumed in this evaluation. However, the durability of SAP tubes must be demonstrated before downtime for process-tube replacement can be discounted as a factor in plant availability. Also, the buildup of xenon poisoning after reactor shutdown will require an off-stream time of about 40 hr before the xenon level will have decayed sufficiently to permit subsequent startup with proposed control systems.

There is a significant economic incentive for minimizing moderator inventory, and as a result the calandria tubes and process tubes are compactly arranged. Equipment, procedures, and methods need to be developed for remote replacement of calandria and process tubes. Access for replacement or maintenance of vessel components will be extremely limited. Alternate designs or some modifications of the present design that facilitate replacement operations should be considered. Also, provisions should be made for inspection and replacement of the heavy-water spray nozzles of the emergency cooling system.

Electrical systems, service systems, site, and structures appear to be adequate for the systems described. Also, auxiliary equipment for the moderator and coolant purification systems can be built as specified. The estimated heavy-water loss rate of about 0.6% per year appears to be feasible. However, more information is needed on the quantities of heavy water which need to be upgraded in quality in order to maintain the specified heavy-water purity.

There is only sparse information available on the operation of a catalytic hydrocracker unit for recovery of degraded coolants, and pilot plant data will be required before detailed evaluation of such a unit in HWOCR systems can be performed. In particular, the biphenyl content of recycled coolant for specified conditions is not known adequately. Based on present information, it appears that the design of the hydrocracker unit is satisfactory.

The turbine plant design data presented by AI-CE have been checked and evaluated. We are in general agreement with the reference design values. Development of the large tandem-compound turbine-generator unit will be required, but such development is in keeping with the current industrial trend in this area. Relative to steam conditions, however, we estimate that the reactor-outlet coolant temperature will not be above 700°F and still meet other specified criteria; with a coolant outlet temperature of 700°F, we estimate that the steam-generator heat transfer area would be increased above the specified value and that steam would be generated at 675°F to give an overall plant thermal efficiency of 34.1%.

The containment scheme, which requires isolation valves between the reactor located inside the containment building and primary heat-transfer system components located outside the containment building, appears feasible for a plant located at the hypothetical Middletown site. Loss of coolant and other possible accidents will have to be evaluated in detail to determine whether the design pressure and integrity of the vessel are adequate and whether sufficient plant safeguards have been provided.

#### 15.4 Performance Evaluation

The power production costs associated with the reactor designs were evaluated, based on our performance estimates and the reference ground rules, which considered a 0.8 plant factor, a capital charge rate of 12% per year, and a fuel-cycle cost averaged over a 30-year plant life. For the AI-CE design concept with uranium carbide fuel, we estimate power costs of 3.46 to 3.54 mills/kwhr(e), the range being associated with uncertainty in fuel surface fouling by the coolant. The corresponding fuel conversion ratio was 0.70 averaged over the fuel cycle, and the specific fuel inventory for the fuel cycle was about 1.1 kg fissile per electrical megawatt. Use of natural uranium fuel in the ends of fuel assemblies would decrease axial power-peaking factors, and such use could reduce power-production costs about 0.03 mill/kwhr(e). Also, if load factors of 90% were achieved, a feasible condition with the proposed on-line refueling scheme and encouraged by the low incremental thermal-energy generation cost of about 7.8 cents per million Btu associated with going from zero to full power production, power costs would be further reduced by about 0.25 mill/kwhr(e).

The power-production costs for the two B&W thorium-based reactor designs were estimated to be 3.85 to 3.94 mills/kwhr(e) for the nested-cylinder metal-fueled concept and 4.00 to 4.14 mills/kwhr(e) for the pin-cluster oxide-fueled concept; the ranges correspond to uncertainty in fuel-surface fouling by the coolant. For the metal-fueled design, the associated average conversion ratio was 0.80, while the specific fuel inventory for the fuel cycle was about 2.55 kg fissile/Mw(e); the oxide-fueled concept had an average conversion ratio of 0.74 and a specific inventory of 1.95 kg fissile/Mw(e). By changing the core designs of the thorium-based reactors, it appears that the power-production costs can be lowered, with corresponding increases in the conversion ratio and also in the specific inventory of fissile fuel. Taking credit for possible performance improvements led to estimated power costs only 0.1 to 0.2 mill/kwhr(e) higher than those obtained for the corresponding HWO-CR-U system under the reference ground rules and bases used in this evaluation. Also, it appears that an HWO-CR-U reactor system can be changed to thorium

fueling without requiring significant core design changes if associated changes in control and safety problems are not significant. These power-production costs can be compared with the value of 3.93 mills/kwhr(e) estimated for pressurized-water reactors (PWR) relative to the reference ground rules and cost bases used in this study. The power-production costs based on publicly owned HWO CR plants having a capital charge rate of 7% per year were estimated to be 2.41 to 2.46 mills/kwhr(e) for the AI-CE design concept, 2.66 to 2.72 mills/kwhr(e) for the B&W metal-fueled reactor, and 2.86 to 2.96 mills/kwhr(e) for the B&W oxide-fueled reactor.

These results were based on what we consider feasible operating conditions and our estimates for capital costs, operating and maintenance costs, and fuel-cycle costs. In obtaining capital costs, we separated the various AI-CE specified costs by breaking them down into the AEC categories of cost accounts. We initially considered the AI-CE design and operating conditions, for which case the cost adjustments we made in the various accounts tended to offset each other to give total direct plant construction costs in good agreement with those presented by AI-CE. These capital costs were then adjusted in accordance with changes in design and operating conditions we considered necessary and reasonable for feasible design and operating conditions to give our final capital cost estimates. On these bases, our estimated capital costs for the AI-CE concept varied from \$118 to \$121/kw(e) for investor-owned plants and from \$114 to \$117/kw(e) for publicly owned plants.

The capital costs for the B&W thorium-based reactor concepts were obtained by estimating the cost differentials associated with variations in design and operation with the uranium-based reactor plant as the reference case. The direct capital cost of the B&W metal-fueled reactor plant was estimated to be \$3.9 million lower than that of the reference uranium-fueled reactor concept, while the direct capital cost of the B&W oxide-fueled concept was about \$3.2 million lower than that of the reference plant. Taking into consideration changes in design and operation that we considered necessary and reasonable for feasible conditions, our estimated capital costs for the B&W metal-fueled reactor concept varied from \$113 to \$116/kw(e) for investor-owned plants, and from \$109 to

\$112/kw(e) for publicly owned plants; the corresponding estimates for the B&W oxide-fueled concept were \$114 to \$119/kw(e) and \$110 to \$115/kw(e).

Operation and maintenance costs were estimated to be about 0.37 mill/kwhr(e) for the different HWO CR concepts being considered. Included in this figure are heavy-water-makeup and organic-coolant-makeup costs, which total about 0.03 mill/kwhr(e).

Fuel-cycle costs were calculated with the present-value discounting technique to obtain 30-year lifetime-average fuel costs. Under reference conditions, we estimated fuel-cycle costs corresponding to the range of power costs given above. The values obtained, including heavy-water and coolant inventories totaling about 0.2 mill/kwhr(e), were 1.07 to 1.09 mills/kwhr(e) for the AI-CE concept with fuel attaining an average exposure of about 17,000 Mwd/T of heavy metal; 1.67 to 1.73 mills/kwhr(e) for the B&W oxide-fueled concept with fuel attaining an average exposure of about 23,000 Mwd/T; and 1.54 to 1.58 mills/kwhr(e) for the B&W metal-fueled concept with fuel attaining an average exposure of about 23,000 Mwd/T [decreasing the average exposure of the metal fuel to 17,000 Mwd/T would increase fuel-cycle costs about 0.06 mill/kwhr(e)].

Under public ownership, the corresponding fuel-cycle costs, including heavy water and organic coolant inventory charges totaling about 0.1 mill/kwhr(e), were estimated to be 0.90 to 0.92 mill/kwhr(e) for the AI-CE concept, 1.39 to 1.44 mills/kwhr(e) for the B&W oxide-fueled concept, and 1.20 to 1.23 mills/kwhr(e) for the B&W metal-fueled concept.

## 15.5 Engineering Development Requirements

The evaluation was based on conditions considered feasible with present-day technology; thus, the performance indicated has not been demonstrated in all respects but appears attainable through engineering research and development. Work areas that need emphasis in developing and demonstrating practicable HWO CR systems are discussed below.

### 15.5.1 Process-Tube and Cladding Material

The HWO CR concept that uses SAP material requires that the material have satisfactory metallurgical and mechanical properties for application

as process tube and cladding. Since SAP is a relatively new material, there is still need for fabrication procedures to be firmly established; also, specifications and information on permissible design stresses for SAP need to be developed more completely based on results of extensive material testing under simulated HWO CR operating conditions. Under long-term high-temperature load conditions, SAP material exhibits low strain capability, and the low ductility of SAP at low strain rates and its influence on reactor design criteria need to be studied thoroughly. Present experimental stress-rupture data require inordinate extrapolation for accurate prediction of the permissible design stress associated with a 30-year process-tube life. Also, the effects of transient stresses and transient local conditions on the mechanical properties and associated permissible design criteria of SAP fuel-cladding material should be studied to determine how transient and local conditions influence permissible design criteria.

In addition to the present SAP development program, it appears desirable that a backup effort be supported in which zirconium-based alloys are developed for HWO CR use. The ability to use such materials for process-tube and fuel-cladding application is dependent upon control of metal hydriding and associated material embrittlement. Studies to date in this area are limited and need to be expanded and conducted under HWO CR-simulated conditions to determine whether zirconium-based alloys, through treatments or modifications, are practicable for HWO CR application.

#### 15.5.2 Organic Coolant

The most important need with respect to the organic coolant is for a better understanding of the factors and mechanisms that influence the formation and suppression of fouling films on fuel-element and other heat-transfer surfaces under HWO CR conditions. Also, the fouling characteristics of the organic coolant under economic HWO CR operating conditions need to be precisely determined. This requires intensive in-pile loop testing under measured and controlled conditions and involves measurement of fluid flow and heat transfer conditions, coolant physical properties

and composition, coolant impurities and their concentrations and chemical and physical forms, and extensive posttest examinations of films.

#### 15.5.3 Control and Safety

Detailed studies need to be made of the control and safety requirements of these large reactors with positive temperature coefficients of reactivity. The reactivity coefficients need to be evaluated more thoroughly and experimental measurements obtained. The maximum credible accident needs to be estimated and factored into the design of the control and/or containment system. The influence of xenon oscillations and control rod movement on reactor stability, spatial power-peaking factors, and reactor control requirements needs specific study.

#### 15.5.4 Thermal and Hydraulic Studies

Detailed measurements of fluid flow conditions, temperature distributions, effective heat transfer coefficients, and the influence of fuel assembly orientation and location on these variables need to be made in full-scale mockups representing HWOCR core-design conditions. These include experimental measurements of fluid mixing in flow channels containing spirally finned elements; effects of fuel-element swelling on flow distribution; determination of core pressure drop and fluid flow distribution as a function of fuel assembly orientations and possible eccentric positioning of fuel assemblies in the process tube; and measurement of the effect of fuel assembly end-plate design on pressure drops, flow distributions, and associated local heat-transfer coefficients.

#### 15.5.5 Fuel-Element Performance

The ability of fuel elements to withstand the maximum exposures planned under HWOCR conditions without failure needs to be further demonstrated with consideration given to the influence of the fine-axial and fine-radial power-peaking factors on maximum fuel exposure. For the uranium carbide fuel, present uncertainties relative to fuel growth and fission-gas release as a function of fuel exposure, temperature, and temperature distribution need to be reduced. Also, cladding integrity under conditions of thermal fuel cycling needs further investigation.

For the thoria-based fuel element and the planned fuel exposures, additional testing is required to demonstrate that vibration compaction is a practical operation when SAP cladding is employed. Also, more information is needed concerning the permissible fuel exposure as determined by fission-product-gas pressure buildup under HWOOCR conditions.

The thorium-metal-based fuel element requires extensive testing to verify its practical application under HWOOCR conditions. Additional experimental results are needed relative to fuel growth and distortion as a function of exposure, temperature, and temperature distribution; and the influence of fuel growth and distortion on coolant flow distribution in the closely spaced annuli between the metal cylinders needs to be better known. Also, the influence of hydrogen pickup by zirconium on permissible fuel-element exposure and on coolant-flow distribution needs to be evaluated experimentally.

#### 15.5.6 Components

Extensive component development work is required to attain the technological status required for building and operating economic HWOOCR power plants. Development of reliable and adequate control and safety systems is needed, along with life testing of these systems. The on-power refueling machines, the large pumps, heat exchangers, and valves of the primary heat transfer system will require performance testing. Also, the catalytic hydrocracker for recovery of degraded organic coolant requires development.

Remote on-power refueling is a major consideration for the HWOOCR concept. The required high reliability of the refueling machines must be demonstrated through repeated tests of prototype machines under simulated HWOOCR conditions. Procedures need to be developed for repair and/or removal of refueling machines under all possible conditions of malfunction. Also, methods need to be developed and tested for remote replacement of calandria and process tubes.



APPENDICES



Appendix A

## BASIS FOR FIXED CHARGES ON NUCLEAR PLANTS

The annual fixed charge applicable to depreciating capital investment was taken as 12% of the investment in a privately owned utility plant.

The following breakdown was used:

Return on money invested	6.0 %
30-year depreciation	1.25
Interim replacements	0.35
Federal income taxes	1.80
Other taxes	2.40
Insurance (excluding liability)	0.20
	<hr/>
	12.00%

The bases for the individual charges are discussed in the following paragraphs.

1. Return on Money Invested. The cost of money reflects the downward trend in bond interest since 1960. It is equivalent to financing the plant with one-third equity capital returning 9% after taxes and two-thirds debt capital drawing 4.5% interest.

2. Depreciation. The 30-year depreciation allowance is calculated by the sinking-fund method.

3. Interim Replacements. The sinking-fund depreciation allowance does not include replacing capital items that have a shorter life span than 30 years. The 0.35% figure follows FPC practice for evaluating coal-fired plants.

4. Federal Income Taxes. The figure of 1.8% for federal income taxes is based on the assumption that the "sum-of-the-year's-digits" method of tax deferrals would be allowed. Under such conditions, the percentage of federal income taxes paid on the initial investment the nth year after startup is  $0.92 + 0.085n$ . The sinking-fund method of normalizing this to a constant return per year then results in the 1.8% per year charge.

5. Other taxes. State and local taxes are taken as 2.4%, as recommended by the FPC.

6. Insurance. A figure of 0.2% is allowed for property damage insurance following conventional plant practice. This does not include costs of third-party liability insurance.

For publicly owned plants, the annual fixed charge was taken as 7% of capital investment. The breakdown was taken as:

Return on money invested	4.00%
30-year depreciation	1.75
Interim replacements	0.35
Local taxes plus insurance	0.90
	<hr/>
	7.00%

Appendix B

## COMPUTER CODES USED IN HWOCR EVALUATION

A prominent design feature of the pin-type fuel assemblies proposed both by AI-CE and by B&W is that advantage is taken of the mixing between fluid flowing in the various subchannels between the pins to reduce the temperature rise in both the coolant and cladding in the hottest subchannel. Careful analysis of the effect of mixing is a rather involved process and has been handled in previous large reactor designs in only a general manner. To facilitate the analysis of this effect of mixing, copies of two computer codes were obtained from Combustion Engineering, Inc., at Windsor, Connecticut, and adapted for our computer, the IBM 7090.

These two codes, which will be referred to as the U-3 code and the THEME 1 code, differ in two essential principles. One difference is the general purpose for which the code was written, and the other is the representation of mixing in the code. Code U-3 was written to describe in detail the temperatures in the coolant and at the cladding surface in a multichanneled flow assembly. THEME 1, on the other hand, was written to represent only generally the entire assembly and the hot subchannel in detail. Therefore U-3 is most useful in evaluating a particular design, and THEME 1 is most useful for studying the effect of varying design parameters. (These two programs are described in detail in Refs. 1 and 2.)

Code U-3 approximates the effect of mixing by assuming that the cross flow between subchannels is proportional to the average linear velocity in the assembly. An energy balance on an increment of length then incorporates the net effect of adding and subtracting coolant at different temperatures from adjacent subchannels. THEME 1 treats mixing through the use of the mixing factor based on the temperature changes with and without mixing. The mixing factor is defined, and once its value is known, the temperature rise in the subchannel with mixing can be calculated.

The U-3 Code

The U-3 code was developed by Oldaker<sup>3</sup> at Chalk River. It was originally written in APEX IV and was later translated into a form of FORTRAN for the IBM-7070 at Windsor, Connecticut, by personnel at Combustion Engineering. In the translation, several modifications were made in the code; the two most significant changes were the following: (1) the original code represented the axial flux distribution as a chopped cosine, while the modification entered the axial flux distribution at a selected number of points and linearly interpolated between these points, and (2) the original code was written for wire-wrapped elements where the intersubchannel flow was directed in a fairly predictable manner and proportionality constants were assigned to the relative flow between elements, while the modified code considered spiral fins directing flow in opposing directions between elements, and the estimation of the relative intersubchannel flow was more gross.

The hydraulic calculations have already been mentioned in the main body of this report. All calculations in this section of the code are made with fluid properties based on an average coolant temperature in the pressure tube that is the sum of the entering temperature and one-half an estimated temperature rise (both input values). No iteration is made to check the validity of this entered temperature rise based on subsequent thermal calculations.

The friction factor correlation is one established by Colebrook:<sup>4</sup>

$$\frac{1}{\sqrt{f}} = -2 \log_{10} \left( \frac{e/D}{3.7} + \frac{2.51}{R \sqrt{f}} \right), \quad (1)$$

where

f = friction factor,

e = pipe roughness,

D = equivalent channel diameter,

R = Reynolds number in the channel.

The pressure drop is related to the friction factor by the following equation:

$$\Delta p = \left( \frac{fL}{D} + K \right) \rho \frac{V^2}{2g} , \quad (2)$$

where

$\Delta p$  = the pressure drop,

$L$  = subchannel length,

$K$  = number of velocity heads lost through entrance and exit to subchannel,

$\rho$  = fluid density,

$V$  = fluid velocity,

$g$  = conversion constant,

and the other terms are as previously defined.

Equation (1) has the disadvantage that it cannot be solved explicitly for the friction factor  $f$  and therefore must be solved by trial and error. In addition,  $f$  is dependent upon the Reynolds number, which is in turn dependent on the velocity. Since the velocity is the result sought, another trial-and-error loop is involved. The procedure in the code is given below:

1. A first trial value is assumed for the velocity.
2. The Reynolds number is calculated for this velocity.
3. A first trial value is assumed for  $f$ .
4. Equation (1) is solved for  $f$  with the first trial value in the right side.
5. The calculated value of  $f$  is compared with the first trial value and if the ratio of the two terms differs by more than 0.001 from unity, the trial value is set equal to the calculated value and step 4 is repeated; repetition is continued until the convergence criterion is satisfied.
6. The velocity in the subchannel is calculated by using the calculated value for  $f$  and an estimate for the pressure drop across the subchannel (an input value) in a rearrangement of Eq. (2).
7. The calculated velocity is compared with the assumed value from step 1 and if the ratio of the two terms differs by more than 0.001 from unity, the assumed value is replaced with the calculated value and the calculation is returned to step 2; repetition is continued in this larger loop until the convergence criterion is satisfied.

8. The mass flow through the subchannel is found by multiplying the resultant velocity by the flow area of the subchannel and the density of the coolant.

9. All the above steps are performed successively for each of the subchannels in the pressure tube (or the segment of it under consideration).

10. The mass flow through each subchannel is summed, and the sum is compared with the total flow through the pressure tube (or segment), which is an input value. If the ratio of the two values does not agree with unity within 0.0001, the estimate of the pressure drop through the subchannel (which is the same as for the pressure tube) is readjusted in direct proportion to the ratio of the calculated mass flow and the prescribed mass flow, and the program is returned to step 1. When the convergence criterion on the flow rate is fulfilled, calculation proceeds to the thermal portion of the program, and the mass flow rates through each subchannel are retained.

Although these calculations consume relatively little machine time, it appears that they could be expedited by (1) using the Moody<sup>5</sup> approximation of the Colebrook correlation and (2) saving the final results from one loop to be used as the first trial values in successive iterations of the same loop. These first trial values could then be reset between cases.

The representation of mixing in the code can be explained by first considering the change in temperature of the coolant over an incremental (or unit) length without mixing:

$$dt_u = \frac{W}{MC_p} , \quad (3)$$

where

$dt_u$  = temperature change without mixing,

$W$  = heat input from the surrounding elements in that length,

$M$  = mass flow rate in the subchannel,

$C_p$  = heat capacity of the coolant.

When mixing is considered, the three masses,  $m_2$ ,  $m_3$ , and  $m_4$ , coming in from the three adjacent subchannels are balanced by the same mass,  $m_1$ ,

leaving the subchannel for which the calculation is being made at its average temperature,  $t_1$ . If  $t_2$ ,  $t_3$ , and  $t_4$  represent the average temperatures in the respective adjacent subchannels, the following heat balance for the subchannel may be written:

$$m_1 C_p dt_m = W + m_2 C_p t_2 + m_3 C_p t_3 + m_4 C_p t_4 - m_1 C_p t_1 \quad , \quad (4)$$

where  $dt_m$  is the temperature change with mixing and the rest of the terms are as defined in the previous text. Also,

$$m_1 = m_2 + m_3 + m_4 = M \quad (5)$$

in order for constant coolant flow to be maintained in the subchannel.

Rearranging Eq. (4) leads to the following expression:

$$dt_m = \frac{W}{M C_p} + \frac{m_2}{M} t_2 + \frac{m_3}{M} t_3 + \frac{m_4}{M} t_4 - \frac{m_1}{M} t_1 \quad (6)$$

or

$$dt_m = dt_u + t_c \quad , \quad (7)$$

where  $t_c$  is the temperature correction due to mixing. In the code, the intersubchannel flow rates,  $m$ , are taken as the product of the mixing constant, AMIXC, and the average velocity, VAV, which is determined in the hydraulic section of the code. The cross flow, which is the product of AMIXC and VAV, is symbolized in the code as CROSS and has the units of mass per unit length per unit time. For a given length, ANCR, the cross flow is the product of CROSS and ANCR. Note that this product is equal to  $m_2$ ,  $m_3$ , and  $m_4$  and that  $m_1 = M$  is equal to three times this product. Combining the symbols of Eq. (6) and the program symbols defined above, we have

$$t_c = \frac{(CROSS)(ANCR)}{M} (t_2 + t_3 + t_4 - 3t_1) \quad . \quad (8)$$

In the original version of the program, whose validity was verified by comparing calculated results with experimental results for wire-wrapped elements, there were additional factors symbolized as FLO2, FLO3, and FLO4 that were used as multipliers of the temperatures given in Eq. (8). These were proportionality constants that specified the amount of flow

from each of the neighboring subchannels, and they were varied depending upon the relative geometry of the assembly. In the modification made by Combustion Engineering these factors were assumed to be either 1.0 or 0.5, depending upon whether the intersubchannel connection was the junction of two opposing spiral fins or the junction of a spiral fin with a wall or straight fin. The selection of these values, particularly in the presence of a straight fin, appears to have no supporting experimental evidence.

The calculation of  $W$ , the heat input per unit length, is the only remaining major factor to be discussed. For the hot pressure tube, the average linear heat-generation rate for the entire reactor is multiplied by the basic radial flux factor and the flux tilt. Within the pressure tube the elements are divided into zones of constant local rod radial flux factor. This local rod radial factor is a function of axial position, as has already been discussed in the report, but a "judicious" average is entered to represent the pressure tube over its entire length. We now have average heat-generation rates for each zone, and the only remaining factor to be used is the peak gross axial flux factor. Multiplication by this factor gives the maximum flux in the pressure tube in each zone.

In the original version of the code, the axial power variation was assumed to be represented by a chopped cosine curve. Since the axial flux pattern for the AI-CE design could not be represented by such a curve, this feature was removed, and both the normalized axial flux and the normalized integral axial flux were entered at selected axial positions. Linear interpolation between the entered points was made. Coolant temperature calculations were made over the selected increment of length, ANCR, and interpolation was made between the selected flux points above and below the summed values of ANCR. If the difference in axial distance between two selected points at which axial flux factors were entered was less than ANCR, the intervening factors were skipped in the calculation, but their influence on the normalized flux integral was considered.

The calculation and printout of cladding temperatures were made at selected intervals equal to or greater (usually greater) than ANCR. At

these intervals, it was a simple matter to evaluate the coolant properties at the exit temperature for the increment and then to evaluate the film heat transfer coefficient and the cladding surface temperature. The correlation used to predict the film heat transfer coefficient has already been discussed in this report.

#### THEME 1 Code

The second program, called THEME 1, was originated by Jesick<sup>6</sup> and programmed by R. Zielinski at Combustion Engineering, Inc., for the HWOGR program. As has been previously indicated, THEME 1 examines principally the hot subchannel and can be used to make parametric studies for reactor design. It has four options from which one may be chosen. The options are (1) a pressure-tube orificing-factor search based on a maximum allowable surface temperature and a stated reactor temperature change, (2) a pressure-tube average-velocity search on the same basis, (3) a reactor temperature-change search based on a maximum allowable surface temperature and a stated average velocity in the pressure tube, and (4) a calculation of the pressure-tube velocity and the cladding surface temperatures for a stated number of pressure tubes. In the first three options, the number of pressure tubes is varied to meet the given reactor power output under the stated conditions. It is obvious that the first three options are most valuable for reactor design, while the last option is most valuable for evaluating a given design.

The major variable in this calculation, at least for the first three options listed above, is the number of pressure tubes. For all options, except the last, a first trial value near 1000 is assumed and iterations are made to approach the maximum allowable surface temperature. For the first two options, as soon as the reactor power and the temperature change of the coolant in passing through the reactor have been specified, the total flow rate can be calculated. Then, based on the assumed number of tubes, the flow through each tube and the conditions in each tube can be calculated. In the third option, the specified maximum velocity and the assumed number of pressure tubes defines the total coolant flow through the reactor, and the same calculations can be made.

Several factors must be established for the input to THEME 1, since we wish to represent all the pins that may not be the same size (diameter). It is necessary, therefore, to define an "effective" number of pins (which may differ from the actual number) and a "heat transfer area correction factor" that accounts for the fact that the larger pins have to "work" harder than the smaller pins. In these calculations, one pin size is selected as the "basic" pin; this is usually the one occurring in the largest number. The effective number of pins is found by adding to the number of basic pins the number of other sized pins multiplied by the ratio of the heat transfer area per unit length of this pin to the same quantity for the basic pin.

The heat transfer area correction factor, FHT, is found from the following relationship:

$$FHT = \frac{N_b A_b^c / A_T^c}{N_b A_b^t / A_T^t}, \quad (9)$$

where

$N_b$  = number of basic pins,

$A_b^c$  = cross-sectional area of the fuel in the basic pins,

$A_T^c$  = same quantity for the entire assembly,

$A_b^t$  = heat transfer area of the basic pins,

$A_T^t$  = total heat transfer area in an assembly.

Next, a factor of 1.04 is built into the code (not an input number) to account for possible flow maldistribution between pressure tubes. This factor cannot be entered into U-3 except by decreasing the prescribed flow rate per pressure tube. This application in U-3 will give the correct temperatures as a result of a decrease in flow, but it also gives a corresponding underestimation of the pressure drop through the tube. The factor is applied in THEME 1 after the calculation of the pressure drop through the pressure tube.

Another factor that is entered into the code is an orificing factor. This is defined as the ratio of the flow through the pressure tube to the

flow through an average pressure tube. The orificing factor is entered in U-3 by multiplying the total coolant flow divided by the number of pressure tubes by the orificing factor to get the prescribed flow rate through the hot pressure tube.

Although provisions are made to enter certain engineering factors in THEME 1, the factors given in Table II-1, page II-7, Volume II of AI-CE-Memo-6 (Ref. 7) cannot be used directly. In the first place, these factors contain the 1.04 factor to account for flow maldistribution between pressure tubes that is already included in THEME 1. In the second, the factors included in  $F(\Delta T_f)$  to account for mechanical effects (1.10) and for rod and bundle location and bowing (1.02) are also included in  $F(Q/A)$ , and inclusion of the second factor automatically includes this portion of the former factor. The remaining portion of  $F(\Delta T_f)$  consists of a 1.05 factor to represent the uncertainty in predicting the local heat transfer coefficient. This factor is entered by multiplying the heat transfer coefficient by 0.952. However, this factor was taken as unity in the AI-CE calculations.

A flux tilt factor is entered in THEME 1 to account for the distortion of the flux pattern due to the use of control rods. This is the same factor as that considered in calculating the peak zone fluxes entered in U-3.

The same friction factor correlation is used in THEME 1 as in U-3 [see Eq. (1)]. The entire pressure tube, however, is represented as its hydraulic equivalent (total flow area and equivalent hydraulic diameter); after the pressure drop has been calculated for it, the same pressure drop is applied to the hot subchannel (with its flow area and equivalent hydraulic diameter), and the flow through the tube is calculated. Equation (1) must still be evaluated by trial and error, but this is the only loop involved in this calculation.

The basic radial flux factor is entered into THEME 1, and it is used in much the same manner as in U-3 to calculate the heat-generation rate in the hottest pressure tube. It is only necessary to enter the local rod radial factors for those elements surrounding the hot subchannel, since this is the only subchannel for which the thermal calculations are performed. Again, as in U-3, the gross normalized axial flux distribution

is entered at selected axial positions to provide the axial gross peak-to-average flux ratio.

From these factors the heat input to the hot channel is calculated as a function of axial position. Two heat fluxes are calculated; one includes the factor representing the engineering factor on the coolant temperature and the other includes the engineering factor on the flux. The first is used to calculate the heat input to the coolant, and the second is used to calculate the temperature drop across the film. The same heat transfer correlation as used in U-3 is used in THEME 1. Temperature calculations are made only at the selected points at which the axial flux factors are entered.

Mixing is treated in THEME 1 through the use of the mixing factor defined in Volume II of AI-CE-Memo-6 (Ref. 7). It is

$$M = \frac{\Delta T_{HC} - \Delta T_{HC}^M}{\Delta T_{HC} - \Delta T_A} , \quad (10)$$

where

- M = mixing fraction,
- $\Delta T_{HC}$  = temperature rise in hot subchannel without mixing,
- $\Delta T_{HC}^M$  = temperature rise in hot subchannel with mixing,
- $\Delta T_A$  = overall temperature rise in the fuel assembly over the same length.

It is possible to calculate all quantities except  $\Delta T_{HC}^M$ , but if the mixing fraction is known, this quantity can be determined from the preceding relationship.

An additional facility, not contained in U-3, is that THEME 1 calculates a critical heat flux from an empirical relationship, which is discussed in this report and in Appendix D. From this value and the maximum flux in the hot channel, the critical flux ratio (or DNB ratio) is calculated as a function of axial position.

After each calculation, the maximum surface temperature for the hot subchannel is retained and compared with the maximum allowable surface temperature. If they do not agree within 1°F, the number of assumed

tubes (for all options except the last) is adjusted and the calculation is repeated. After the maximum surface temperature has been satisfied, or after the first calculation for the last option, the stored temperatures and other vital data are printed.

#### References

1. J. P. Sanders, The Modified U-3 Code: A Thermal-Hydraulic Code for Axial Flow with Mixing in Fuel Bundles, USAEC Report ORNL-4016, Oak Ridge National Laboratory (to be issued).
2. J. P. Sanders, ORNL Version of THEME 1 Code: A Thermal-Hydraulic Code for Analysis of the Hot Channel in a Fuel Bundle, USAEC Report ORNL-4015, Oak Ridge National Laboratory (to be issued).
3. I. E. Oldaker, Sheath Temperatures - A G-20 Computer Program for Fuel Bundles, Canadian Report AECL-2269, May 1965.
4. C. F. Colebrook, Turbulent Flow in Pipes with Particular Reference to the Transition Region Between Smooth and Rough Pipe Laws, Proc. Inst. Civil Eng., 11: 133 (1939).
5. L. F. Moody, An Approximate Formula for Pipe Friction Factors, Mechanical Eng., 69: 1005-1006 (December 1947).
6. J. F. Jesick, THEME Computer Programs, Letter to W. S. Flinn, Combustion Engineering, Inc.
7. Combustion Engineering, Inc., and Atomics International, Heavy Water Organic Cooled Reactor - 1000 Mwe Nuclear Power Plant Conceptual Design, USAEC Report AI-CE-Memo-6, Vol. II, Oct. 1, 1965.

Appendix CREVIEW OF ORGANIC COOLANT HEAT TRANSFER CORRELATIONS  
AND PHYSICAL PROPERTIES

The Organic Reactor Heat Transfer Manual,<sup>1</sup> issued December 1, 1962, is a collection of data, methods, and relationships considered most reliable (at the time of publication) for the thermal design and analysis of organic-cooled reactors. Based on some earlier heat transfer studies with Santowax R,<sup>2,3</sup> Santowax OM,<sup>3</sup> and diphenyl,<sup>3,4</sup> the manual recommends the Dittus-Boelter correlation

$$\text{Nu} = 0.0243 \text{Re}^{0.8} \text{Pr}^{0.4} , \quad (1)$$

for heating of irradiated and unirradiated polyphenyl mixtures flowing turbulently in heated smooth tubes and annuli, with the physical properties being evaluated at the bulk fluid temperature. The result obtained with the correlation was shown (Fig. IV-1 of Ref. 1) to be below the mean of the reported data.<sup>2-4</sup> This correlation was used by both AI-CE and B&W in estimating the thermal performance of their HWOCR reference reactor designs.

Heat transfer coefficients have been measured<sup>5,6</sup> over the Reynolds number range 10,000 to 50,000 in annular channels with longitudinal fins, which are similar to PNPf fuel assemblies. The data, after correction for fin efficiency, agree with the Dittus-Boelter correlation as modified by McAdams, that is,

$$\text{Nu} = 0.023 \text{Re}^{0.8} \text{Pr}^{0.4} , \quad (2)$$

in which the physical properties are evaluated at the bulk temperature. The maximum deviation was reported<sup>5</sup> as 10%.

The Organic Reactor Heat Transfer Manual<sup>1</sup> points out that coefficients lower than those given by Eq. (2) are to be expected if a coolant channel with longitudinal fins has an open flow area such that the mean velocity between the fins is less than the mean velocity in the entire flow channel. This type of geometry exists in the individual subchannels formed within the finned fuel rod assemblies proposed for the reference

reactor designs. Studies<sup>7</sup> of triangular and square coolant passages have shown that velocities, shear stresses, and heat transfer near the corners are lower than average values and that friction factors and average Nusselt numbers are lower than in a tube. Additional references for consideration in noncircular geometries and fuel rod assemblies are given in a comprehensive review (which contains a bibliography with 98 entries) by Pinchera.<sup>8</sup>

In his June 1962 review,<sup>8</sup> Pinchera examined the experimental heat transfer data for organics and, noting the uncertainties in physical properties, recommended Eq. (2) for general use. A more recent correlation, developed in the ORGEL program for Santowax OM2 + HB and reported<sup>9</sup> at the 1964 Geneva Conference, is

$$\text{Nu} = 0.00835 \text{Re}^{0.9} \text{Pr}^{0.4} \quad . \quad (3)$$

The same correlation (except that the exponent on the Reynolds number was 0.902) was presented also at that time by Boxall<sup>10</sup> and his co-workers in the Canadian organic reactor program. The ORGEL data, shown in Fig. 5.1 of this report (Fig. 2 of Ref. 9), are mostly for Reynolds numbers in the range  $9 \times 10^4$  to  $3 \times 10^5$ , with a few data points in the range  $3 \times 10^4$  to  $9 \times 10^4$ . It is reported that 95% of the data points fall within a scatter band of  $\pm 6\%$  of the given equation when physical properties derived from their program and evaluated at the mean coolant temperature are used.

The most recent progress report<sup>11</sup> on the MIT organic in-pile loop program summarizes all the MIT heat transfer data and appears to be the best source for determining basic heat transfer coefficients. (A topical report<sup>12</sup> on the MIT experience has been issued, but as yet we have been unable to obtain a copy.) The test results (466 data points) are shown in Fig. C.1 (Fig. 5.1 of Ref. 11). They fall, generally, in a scatter band of  $\pm 10\%$  around values given by Eq. (2), where the physical properties are evaluated at the bulk temperature. The physical properties used<sup>13</sup> were derived from measurements reported earlier.<sup>14</sup> Most of the data are for Reynolds numbers in the range  $10^4$  to  $10^5$ , which is somewhat lower than the range covered by the ORGEL data.

An earlier correlation, based on the MIT test results available up to that time, was reported<sup>14</sup> as

$$\text{Nu} = 0.0079 \text{Re}^{0.9} \text{Pr}^{0.4} (\pm 10\%) \quad . \quad (4)$$

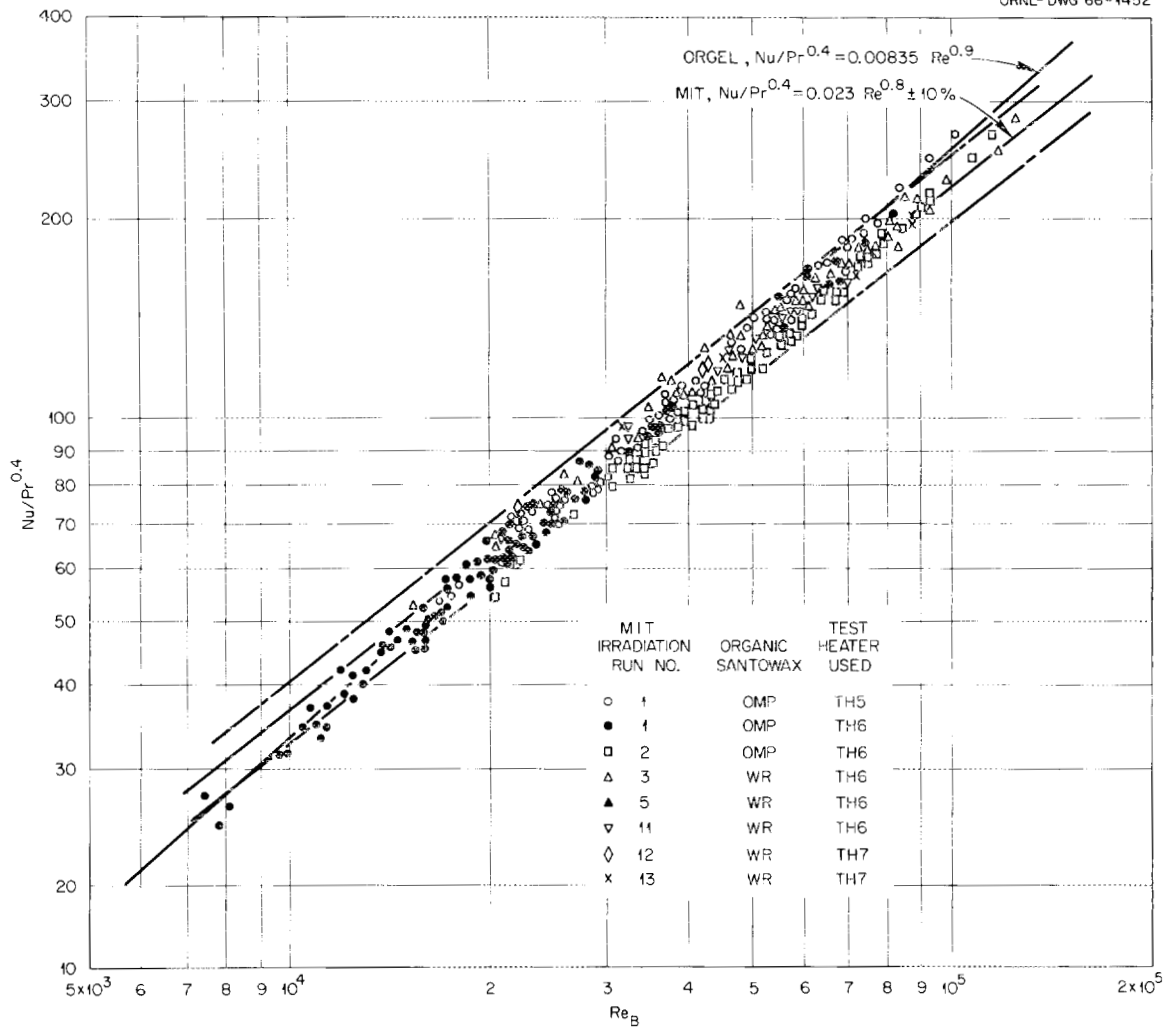


Fig. C.1. Heat Transfer Data for MIT-Irradiated Organic Coolant.

This expression, except for a 5% lower coefficient, is the same as the ORGEL and Canadian correlations.

For comparison with these data we reevaluated the Santowax OM (ratio O:M = 2:1) experimental heat transfer data reported earlier<sup>3,15</sup> with the physical properties presented in the AI-CE reference design memo.<sup>16</sup> The reevaluated data points are shown in Fig. 5.1 superimposed on the data extracted from the ORGEL paper.<sup>9</sup> The reevaluated data from Ref. 3, which are for Santowax OM without high boilers, fall generally below the ORGEL correlation but appear to correlate rather well with the MIT correlation, Eq. (2). The reevaluated data from Ref. 15, which are for Santowax OM

with 2.5 to 18% HB, appear to correlate rather well with the ORGEL correlation.

Figure 5.1 shows the MIT correlation superimposed on the ORGEL data, and Fig. C.1 shows the ORGEL correlation superimposed on the MIT data. As noted in the latter figure the two correlations agree rather well for Reynolds numbers in the range  $10^4$  to  $10^5$ . Also, for all practical purposes the Canadian correlation is the same as the ORGEL correlation.

It is to be noted that the ORGEL and MIT data were derived from annular and tubular heated sections, respectively, and not from multi-element heated sections. We have found references<sup>17,18</sup> to Canadian organic heat transfer experiments in simulated fuel rod bundles. However, we have as yet been unable to obtain these references for study. It is clear though that any adverse effects on heat transfer coefficients due to geometry and flow factors needs to be included in evaluating temperatures.

Coolant physical properties are intimately related to the heat transfer correlations through the dimensionless moduli. We have investigated the effect of temperature and high-boiler content on heat transfer coefficients in some detail for various physical property tabulations. Physical properties used in the AI-CE and B&W reference reactor designs were reported in Ref. 16 without noting the source of the information.\* Equations for computing physical properties as a function of temperature and high-boiler content were reported in the ORGEL paper.<sup>9</sup> (The numerical values of the coefficients in these equations were inadvertently omitted from the English-translation preprint distributed at Geneva. However, we have recently obtained<sup>20</sup> the constants for use in comparing the data.) These are based on extensive measurements made with Santowax OM2 plus OMRE high boilers. The physical properties obtained from the MIT organic in-pile loop program have been reported in detail.<sup>14</sup>

---

\*Since completion of our evaluation, AI-CE has published a review of organic coolant physical properties.<sup>19</sup> The review covers a wider range of coolants than is of interest in this evaluation, but in general there appears to be agreement in the data reported<sup>19</sup> and the data we report, as it should be, since both studies relied on the U.S., the Canadian, and the Euratom programs as sources for the data.

Physical properties from these three sources are summarized in Table C.1. The Prandtl numbers, calculated from the data, are also tabulated for comparison. These data are shown graphically in Figs. C.2 through C.6. In general the differences in the data are not large, except for the Prandtl number. The large differences occur as the temperature is decreased and the high-boiler content is increased. The MIT and ORGEL data generally agree closely with each other and fall below the AI-CE data. Figure C.3, which shows the thermal conductivity data, seems to

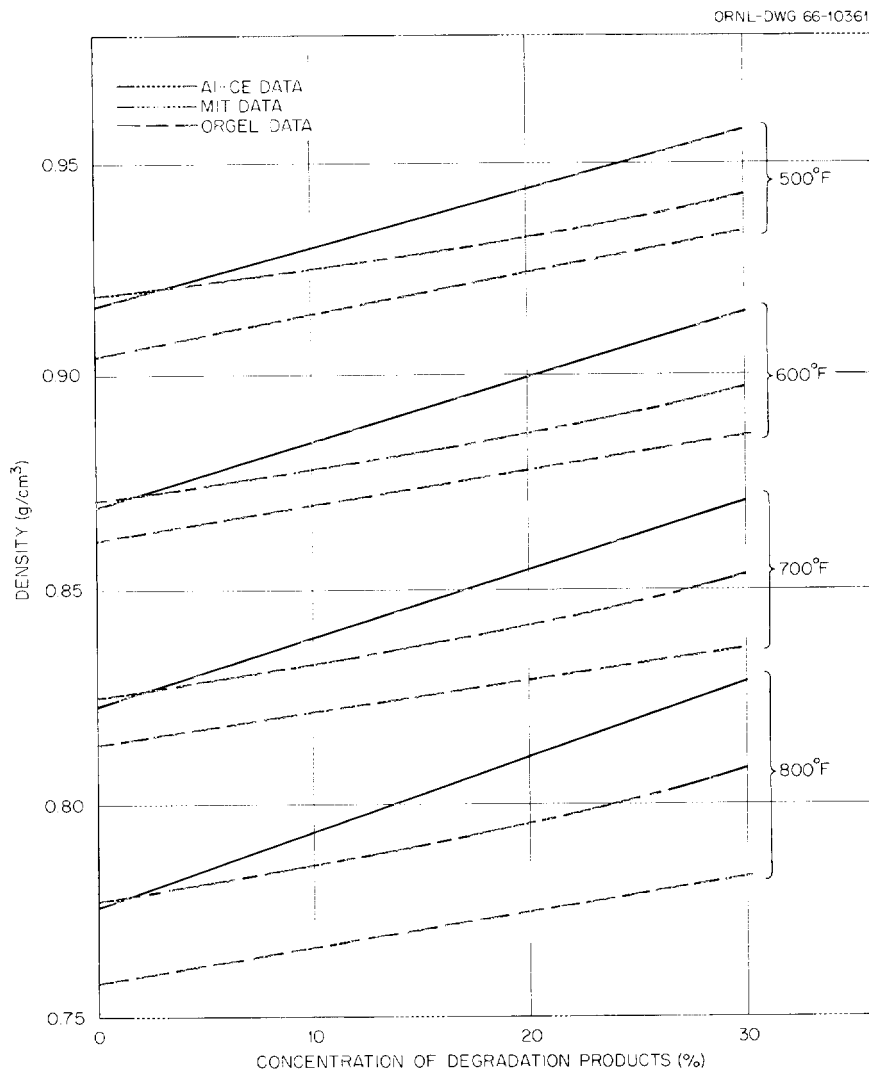


Fig. C.2. Coolant Density Versus High-Boiler Content and Temperature.

Table C.1. Organic Coolant Physical Properties Used by Various Groups

Physical Property	High-Boiler Content (%)	Physical Property Value											
		At 500°F			At 600°F			At 700°F			At 800°F		
		AI-CE	MIT	ORGEL	AI-CE	MIT	ORGEL	AI-CE	MIT	ORGEL	AI-CE	MIT	ORGEL
Density, g/cm <sup>3</sup>	0	0.917	0.919	0.904	0.870	0.871	0.860	0.824	0.825	0.811	0.776	0.777	0.757
	10	0.930	0.925	0.914	0.855	0.878	0.870	0.839	0.833	0.821	0.794	0.786	0.767
	20	0.944	0.933	0.925	0.900	0.887	0.878	0.855	0.842	0.829	0.810	0.796	0.775
	30	0.958	0.942	0.932	0.915	0.897	0.886	0.871	0.854	0.836	0.829	0.808	0.782
Thermal conductivity, Btu/hr·ft.°F	0	690	688	675	660	644	642	620	602	608	590	562	574
	10	710	708	688	680	667	657	650	630	629	610	591	597
	20	730	729	700	700	691	673	670	657	645	640	620	618
	30	750	750	713	720	715	689	690	685	664	670	650	640
Viscosity, centipoise	0	0.54	0.56	0.52	0.37	0.37	0.36	0.26	0.27	0.26	0.20	0.21	0.20
	10	0.66	0.61	0.58	0.43	0.41	0.40	0.30	0.30	0.29	0.23	0.23	0.23
	20	0.79	0.69	0.67	0.51	0.47	0.45	0.35	0.34	0.33	0.26	0.26	0.25
	30	0.98	0.82	0.77	0.63	0.55	0.51	0.43	0.40	0.37	0.31	0.30	0.28
Specific heat, Btu/lb.°F	0 to 30	0.534	0.527	0.526	0.566	0.555	0.557	0.599	0.583	0.589	0.631	0.610	0.620
Prandtl number	0	10.11	10.39	9.81	7.679	7.717	7.474	6.079	6.328	6.072	5.176	5.516	5.202
	10	12.01	11.03	10.80	8.661	8.316	8.124	6.690	6.718	6.615	5.758	5.795	5.655
	20	13.98	12.07	12.22	9.979	9.135	9.033	7.572	7.301	7.293	6.203	6.186	6.167
	30	16.89	13.96	13.76	11.985	10.332	10.036	9.034	8.239	7.964	7.065	6.813	6.658

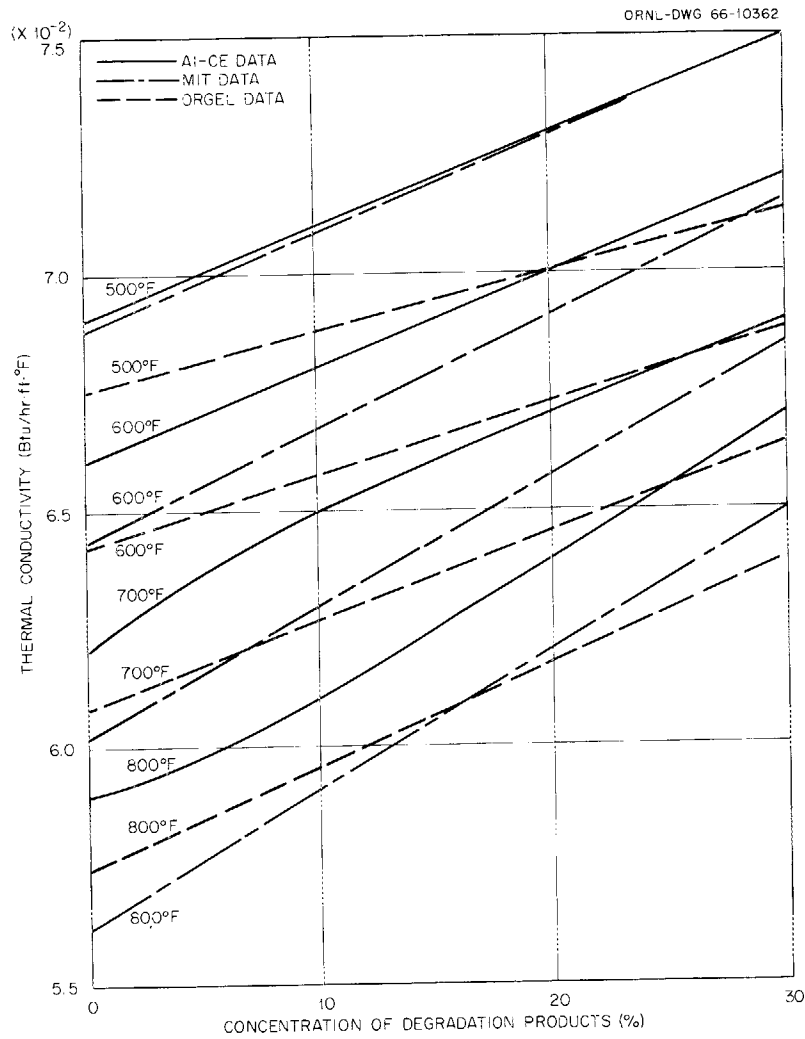


Fig. C.3. Coolant Thermal Conductivity Versus High-Boiler Content and Temperature.

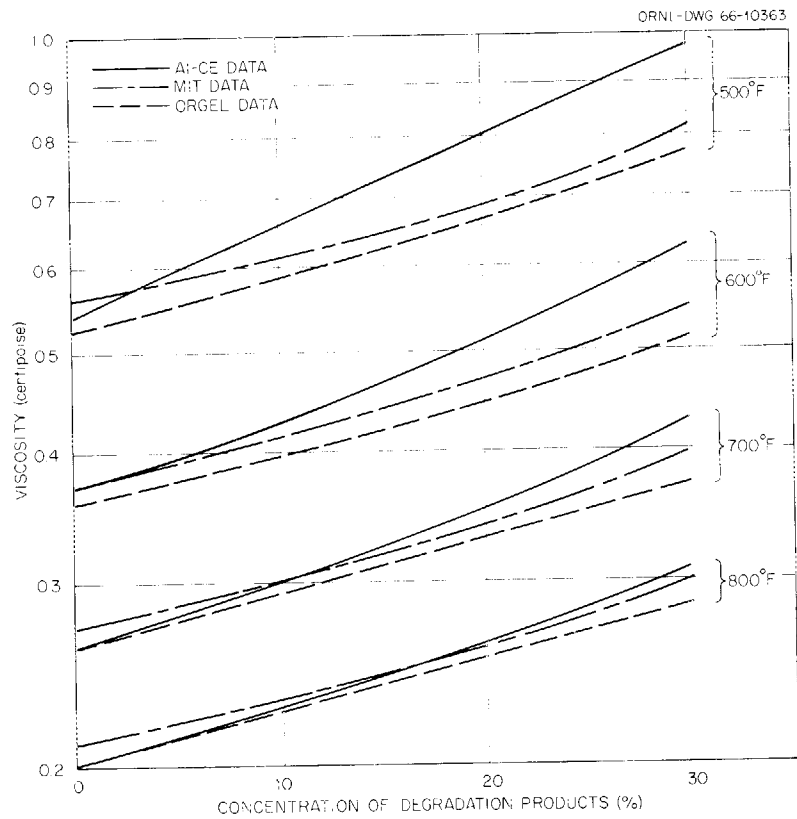


Fig. C.4. Coolant Viscosity Versus High-Boiler Content and Temperature.

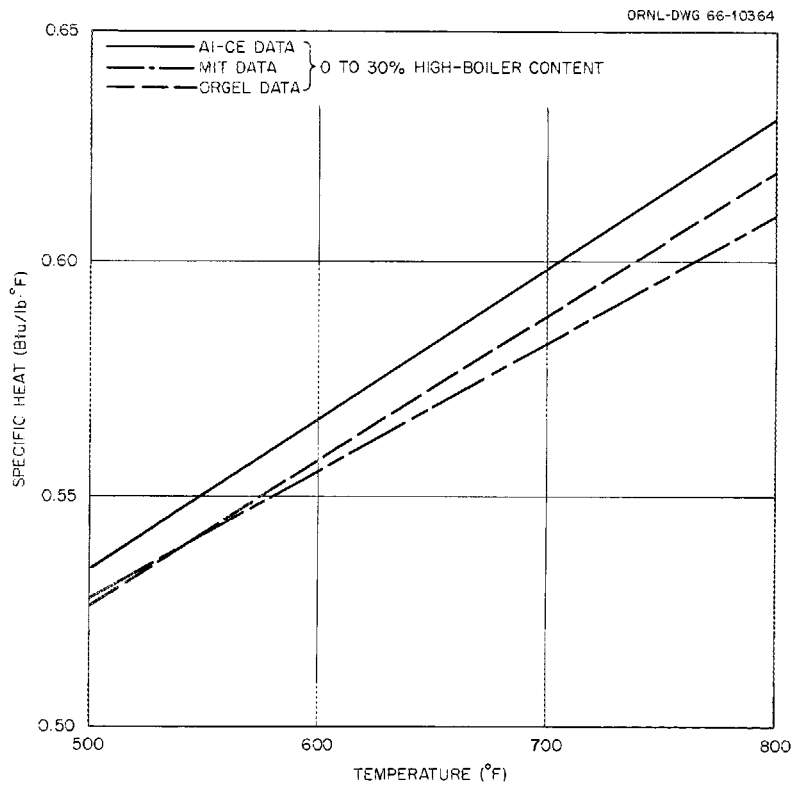


Fig. C.5. Coolant Specific Heat Versus High-Boiler Content and Temperature.

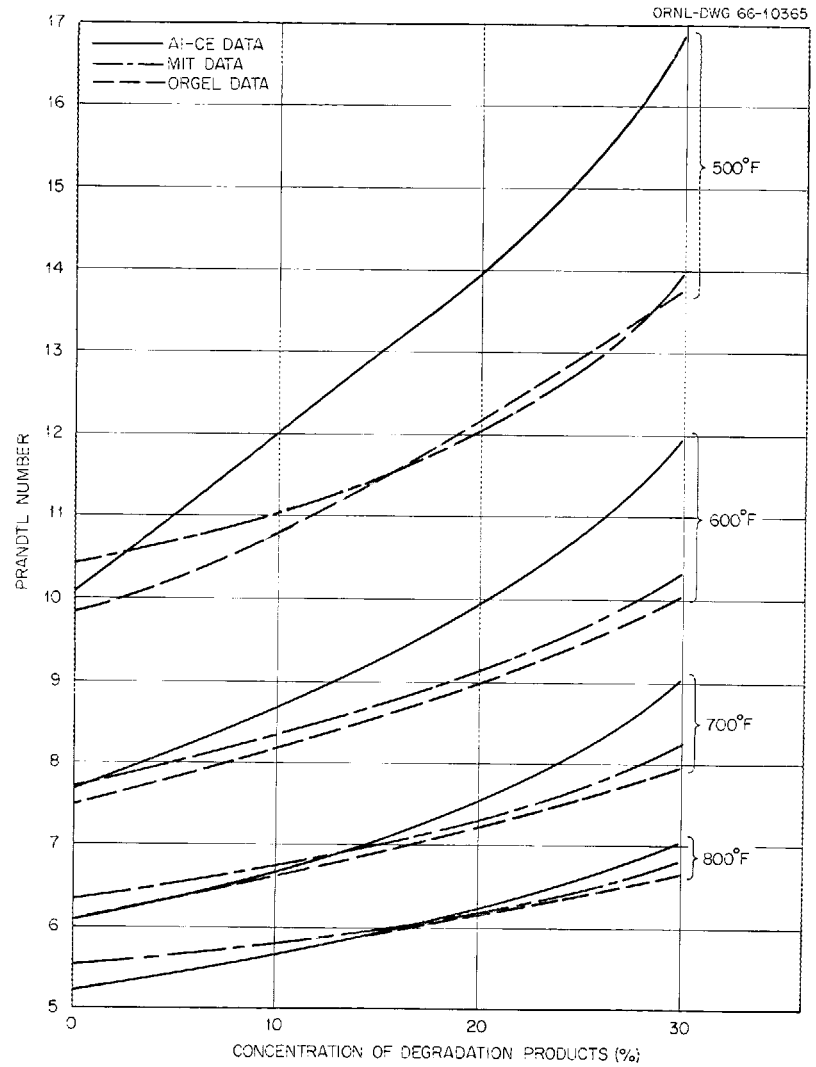


Fig. C.6. Prandtl Number Versus High-Boiler Content and Temperature.

point out a definite need to obtain additional data, as also recommended in the MIT program.<sup>14</sup>

The effect of physical properties on the heat transfer coefficient is shown by Fig. C.7, where we plotted the normalized heat transfer coefficient as a function of temperature and high-boiler content. We defined the normalization factor,  $h_o$ , to be the heat transfer coefficient obtained from Eq. (2) at 650°F and 0% high-boiler content. Thus the plot shows

$$\frac{h}{h_o} = \frac{k}{k_o} \left( \frac{\rho}{\rho_o} \frac{\mu_o}{\mu} \right)^{0.8} \left( \frac{Pr}{Pr_o} \right)^{0.4} \quad (5)$$

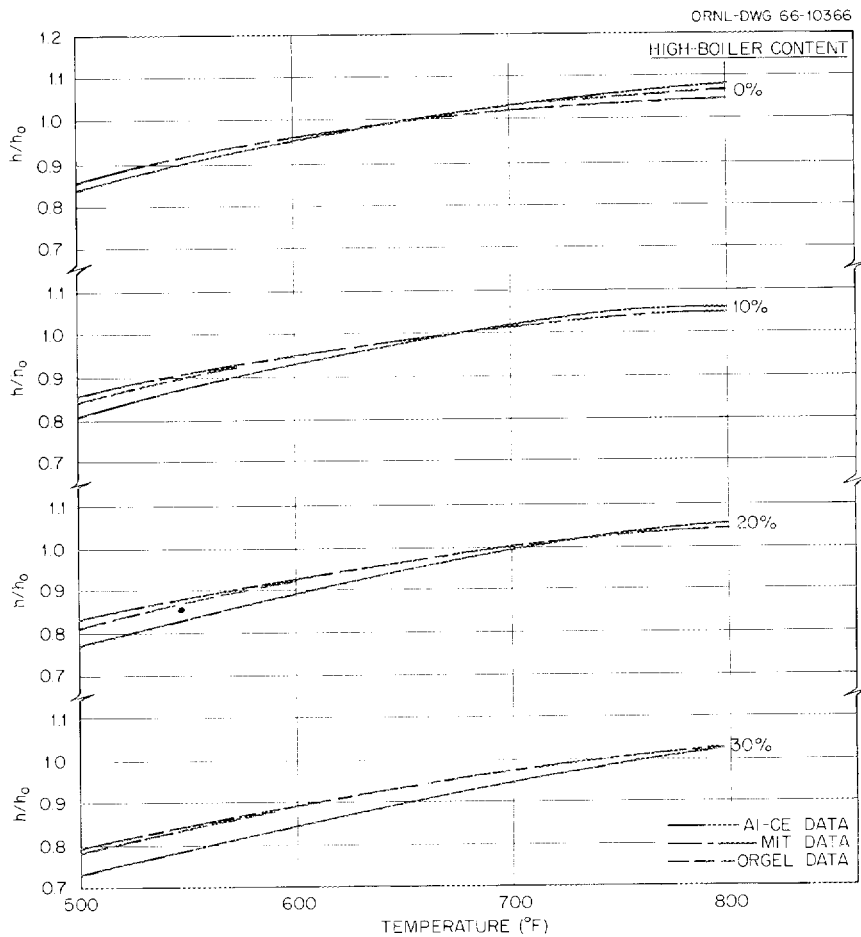


Fig. C.7. Heat Transfer Variation with High-Boiler Content and Temperature.

Several conclusions can be drawn from Fig. C.7:

1. The variations in heat transfer coefficient with temperature and high-boiler content are in fair agreement for the three sets of data.

2. The use of the AI-CE physical properties results in more variation of heat transfer coefficient with temperature than does use of the MIT or ORGEL data. However, at operating conditions of 10% high-boiler content, no significant difference in the overall coefficient can be attributed to differences in physical property variation with temperature associated with the three sets of data.

3. No significant difference in heat transfer coefficient was found when using the physical properties given by MIT or ORGEL; however, for high-boiler contents above about 10%, the physical properties used by AI-CE tend to give low values for the average heat transfer coefficient.

4. Excluding the effect associated with velocity along the length of a coolant tube, the heat transfer coefficient for 10% high-boiler content varies about  $\pm 8\%$  from the average for a bulk mean temperature rise from 600 to 800°F.

We conclude from our evaluation of heat transfer correlations that the correlation used in the reference design studies is too optimistic, for two reasons: (1) extensive experimental data do not support the correlation, and (2) the effects of geometry are such that the coefficients are lower than those obtained from correlations based on data for smooth tubes and annuli. Discounting the effects of geometry for the moment, we believe the correlation derived from the MIT organic in-pile loop program is the best of those examined, since the MIT data are extensive and were obtained from a dynamic system in which the radiolytic high boilers were in-bred rather than added from an external supply. At the same time, the variation of the AI-CE heat transfer coefficient with high-boiler content appears conservative. This implies that the high-boiler content of the reference reactor might be increased slightly above 10% with some advantage.

As mentioned we have not examined the Canadian data obtained from fuel rod bundles,<sup>17,18</sup> but other information<sup>1,7</sup> indicates lower coefficients in noncircular coolant passages. Therefore we believe the coefficients computed from correlations based on smooth-tube and annuli data

should be reduced by about 10% to account for the effects of noncircular geometry and of decreased velocity between the fuel-pin fins. In the absence of experimental data on prototype fuel bundles, we recommend that the heat transfer coefficients in the reference reactors be based on the relationship

$$\text{Nu} = 0.0207 \text{Re}^{0.8} \text{Pr}^{0.4} \quad (6)$$

The 10% reduction in coefficient indicated in Eq. (6) from what would be calculated from the MIT recommendation of Eq. (2) is attributed to geometry effects and not to the lower bound of the correlation.

The MIT and ORGEL physical property data are in close agreement and are presumably based on more recent and more extensive data than the AI-CE values. These observations, in addition to the fact that the MIT data were obtained from a system in which the radiolytic high boilers were in-bred, indicate use of the MIT physical property data.

There is a clear need for measurements of heat transfer coefficients associated with finned fuel bundles in order to determine the actual reduction factor to be applied to the smooth-tube and annuli data. Also, further refinement in the coolant thermal conductivity data appears desirable.

#### References

1. Atomics International, Organic Heat Transfer Manual, USAEC Report NAA-SR-Memo 7343, Dec. 1, 1962.
2. C. Grove-Palmer and H. Pass, An Investigation of the Heat Transfer and Burnout Properties of a Proposed Organic Reactor Coolant, British Report AERE-R3111, February 1960.
3. M. Silberberg and D. A. Huber, Forced Convection Heat Transfer Characteristics of Polyphenyl Reactor Coolants, USAEC Report NAA-SR-2796, Atomics International, Jan. 15, 1959.
4. J. P. Stone et al., Heat Transfer Studies on Some Stable Organic Fluids in a Forced-Convection Loop, Report NRP-5675, Massachusetts Institute of Technology, Oct. 26, 1961.

5. Atomics International, Annual Technical Progress Report, Fiscal Year 1961, USAEC Report NAA-SR-6370, pp. III-D-17 to -20.
6. S. Sudar and C. R. Davidson, Heat Transfer from a Longitudinal Finned Surface to Organic Coolant, Trans. Am. Nucl. Soc., 4(1): 9 (1961).
7. R. G. Deissler and M. F. Taylor, Analysis of Turbulent Flow and Heat Transfer in Noncircular Passages, Report NASA TR R-31, 1959.
8. G. C. Pinchera, Heat Transfer by Means of Organic Coolants, Energia Nucleare, 10(6): 319-335 (1963). An English translation by J. Saxon is available as TRG Information Series 449(W), 1965.
9. F. Lanza, R. Ricque, and J. Villeneuve, Heat Transfer by Organic Liquids, Third United Nations International Conference on the Peaceful Uses of Atomic Energy, Geneva, 1964, A/Conf. 28/P/93.
10. D. G. Boxall et al., Development of Fuel and Coolant Tubes for a Reactor Cooled by Organic Liquid, Third United Nations International Conference on the Peaceful Uses of Atomic Energy, Geneva, 1964, A/Conf. 28/P/23.
11. D. T. Morgen et al., In-Pile Loop Studies of Organic Coolant Materials, Progress Report for January 1-September 30, 1965, USAEC Report MIT-334-33, Massachusetts Institute of Technology, Nov. 1, 1965.
12. A. H. Swan and E. A. Mason, Friction Factor and Heat Transfer Correlation for Irradiated Organic Coolants, USAEC Report MIT-334-23, Massachusetts Institute of Technology, September 1965.
13. W. N. Bley, Massachusetts Institute of Technology, personal communication to R. H. Chapman, Oak Ridge National Laboratory, Jan. 26, 1966.
14. C. D. Sawyer and E. A. Mason, The Effects of Reactor Irradiation on Santowax OMP at 610°F and 750°F, USAEC Report MITNE-39, Massachusetts Institute of Technology (also USAEC Report IDO-11107), September 1963.
15. W. N. Bley, An In-Pile Loop Study of the Performance of Polyphenyl Reactor Coolants, USAEC Report NAA-SR-2470, Atomics International, Sept. 15, 1958.
16. Combustion Engineering, Inc., and Atomics International, Heavy Water Organic Cooled Reactor - 1000 Mwe Nuclear Power Plant Conceptual Design, USAEC Report AI-CE-Memo-6, Vol. II, Oct. 1, 1965.

17. J. T. Rogers and T. M. Chapman, The Effect of Element Spacing on Local Heat Transfer Coefficients in Rod Bundles in an Organic Coolant, Report R63CAP49, Canadian General Electric Co., Ltd., July 1963.
18. J. T. Rogers, T. M. Chapman, and G. M. Barns, Local Heat Transfer Coefficients in Simulated Reactor Fuel Bundles, Paper presented at EIC Regional Conference on Heat Transfer at Kingston, Ontario, May 1964.
19. H. Mandel, Physical Properties of Some Polyphenyl Coolants, USAEC Report AI-CE-15, Combustion Engineering, Inc., and Atomics International, Apr. 15, 1966.
20. J. C. Lený, Euratom, personal communications to R. H. Chapman, Oak Ridge National Laboratory, Jan. 10 and Feb. 1, 1966.

Appendix D

## REVIEW OF CRITICAL HEAT FLUX CORRELATIONS

The departure from nucleate boiling (DNB) in multicomponent coolant mixtures is not so easily nor so accurately predicted as it is for single-component systems, such as water. It is, perhaps, fortuitous that the critical heat flux of an organic mixture is generally greater than a linear interpretation of the values for the pure components would indicate.<sup>1</sup> Also, as indicated in Fig. D.1, it has been shown that higher critical heat fluxes result from the addition of high boilers (pyrolytic and radiolytic products) and byphenyl to a mixture of terphenyls.<sup>2</sup> These are important points, since organic reactor coolants inherently contain these additional species.

An attempt to produce a generalized correlation of burnout data was made by Griffiths.<sup>3</sup> This correlation, although quite complex and requiring extensive knowledge of the coolant physical and thermodynamic properties, can be used to predict upper and lower bounds of the critical heat flux for organic coolants. Because of a lack of detailed coolant data and the complex nature of the Griffiths correlation, empirical relations of the following type have been used to estimate the critical heat flux in organic-cooled systems:

$$(Q/A)_{\text{crit}} = A + B \Delta T_{\text{SC}} V^n, \quad (1)$$

where

$(Q/A)_{\text{crit}}$  = critical heat flux, Btu/hr·ft<sup>2</sup>,

$\Delta T_{\text{SC}}$  = amount of subcooling, °F,

$V$  = coolant velocity, fps,

$A, B, n$  = empirical constants evaluated for each coolant.

(Subcooling as defined here is the saturation temperature minus the bulk fluid temperature.) Core and Sato<sup>4</sup> were able to correlate some early data on Santowax R and diphenyl with simple relations of the above type. However, they were unable to correlate their data for a polyphenyl mixture

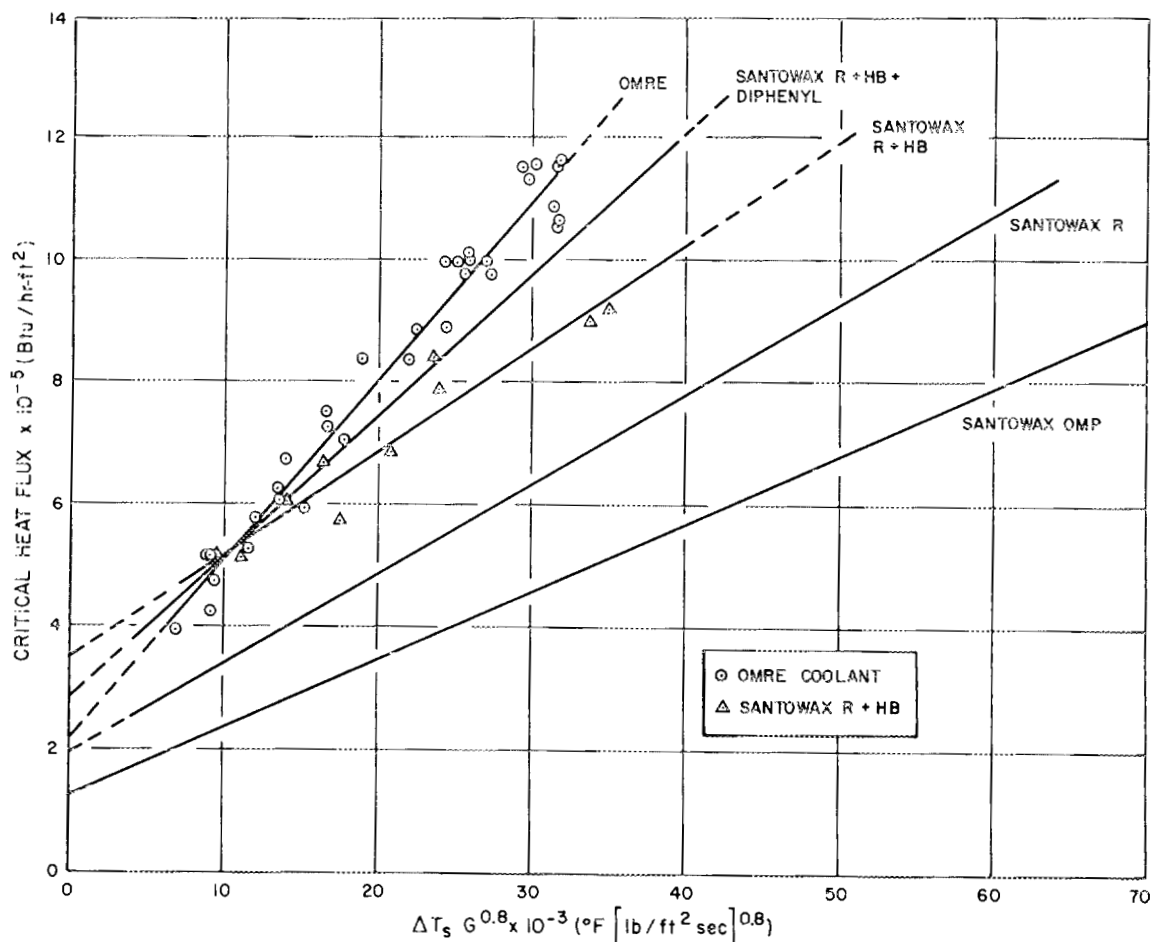


Fig. D.1. Critical Heat Flux of Some Polyphenyl Coolants. (From Ref. 2)

(approximate composition: 15 wt % diphenyl, 58 wt % O-terphenyl, 24 wt % M-terphenyl, and 3 wt % P-terphenyl) by such a simple relationship. Some British experimenters<sup>5</sup> were able to correlate their Santowax R data within the limits of the Core and Sato expression for Santowax R, but their data were slightly above the upper limit given by the Griffiths correlation. In some later experiments Core and Sato<sup>6</sup> were able to correlate some Santowax OMP (composition: 0.4 wt % diphenyl, 12.6 wt % O-terphenyl, 58.6 wt % M-terphenyl, and 27.9 wt % P-terphenyl) data by the simple equation

$$\left(\frac{Q}{A}\right)_{\text{crit}} = 100,000 + 407 \Delta T_{\text{SC}} v^{2/3} \quad (2)$$

Lurie and Robinson<sup>7</sup> investigated OMRE-II coolant and Santowax R with various additives and were able to correlate their results with the previous data<sup>4-6</sup> with an expression of the type

$$(Q/A)_{\text{crit}} = A + B \Delta T_{\text{SC}} G^n, \quad (3)$$

where  $G$  is the mass velocity in  $\text{lb}/\text{sec}\cdot\text{ft}^2$  and the other symbols are as previously defined. For Santowax OMP they obtained the relationship

$$(Q/A)_{\text{crit}} = 129,000 + 11 \Delta T_{\text{SC}} G^{0.8}. \quad (4)$$

Figure D.1 (from Ref. 2) gives the data of Lurie and Robinson, which indicate that the presence of high boilers and diphenyl in the terphenyl coolants is beneficial from a critical heat flux viewpoint for the same degree of subcooling and the same mass flow rate. However, as pointed out by Rogers and Barns,<sup>8</sup> the data of Lurie and Robinson on OMRE Core II coolant are not consistent with this conclusion. The OMRE II coolant, which contains only 14% radiolytic high boilers, gave, in general, significantly higher DNB heat fluxes than the virgin Santowax R coolant containing 35% total high boilers (27% OMRE radiolytic, 8% pyrolytic). This observation is also apparent in Fig. D.1. Since there were no other significant differences in the two coolants, Rogers and Barns<sup>8</sup> suggest that the simple definition of high boilers used to date may not be adequate for correlation of DNB heat fluxes as a function of high-boiler content. They further suggest that classifying the high boilers by weight percentage in various molecular weight groups might permit correlation of the data as a function of high-boiler content and molecular weight. Such a proposal might give greater confidence in results obtained from out-of-pile experiments.

Van Meel<sup>9</sup> investigated a number of polyphenyl coolants of interest to the ORGEL program. The effects of dissolved water and nitrogen (anticipated as a pressurizing gas) were included in the experimental studies. High boilers were apparently not included in the studies reported; however, mention was made that the experimental program was continuing and further results would be forthcoming. Van Meel's correlation for pure

OM2 (ORGEL coolant), when converted to the units used here, is

$$(Q/A)_{crit} = 256,800 + 142.24G + 18.31 \Delta T_{SC} G^{3/4} \quad (5)$$

From Eq. (5), it is noted that Van Meel found a velocity effect as the amount of subcooling tended to zero, which is contrary to the previously mentioned correlations. It is also noted that none of the above correlations include a pressure effect other than that inherent in  $\Delta T_{SC}$ .

Boxall et al.<sup>10</sup> of the Canadian organic coolant program presented an "asymptotic" correlation at the 1964 Geneva Conference for Santowax OM plus 30% OMRE high boilers as

$$(Q/A)_{crit} = 311,700 + 557 \Delta T_{SC} V^{2/3} \quad (6)$$

for flow in annuli with  $L/D_e > 60$  (same units as above). Figure D.2 (from Ref. 10) indicates rather good agreement with the Lurie and Robinson

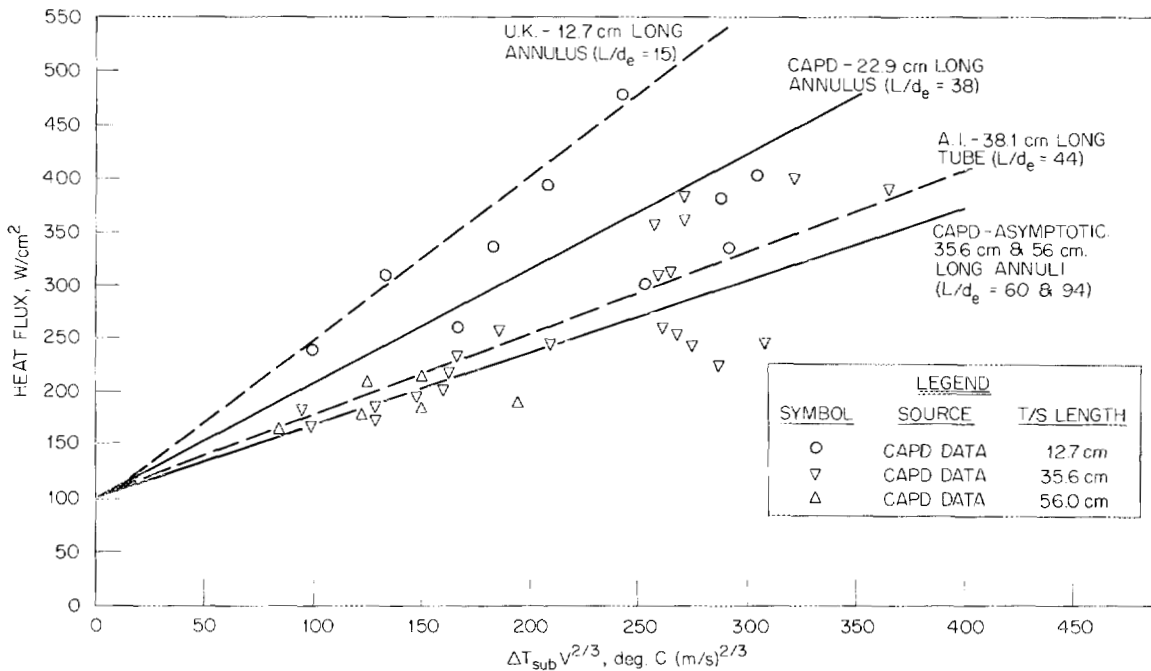


Fig. D.2. DNB Heat Fluxes for a Terphenyl Mixture with 30% High Boilers. (From Ref. 10)

data<sup>7</sup> for Santowax R with 35% total high boilers. The figure also indicates a length effect. This correlation is based on the work of Rogers and Barns,<sup>8</sup> which was published more recently and is discussed below.

In reporting their work, Rogers and Barns<sup>8</sup> attempted to find correlations of the types reported by earlier investigators<sup>6-9</sup> without too much success. The results of their experiments with Santowax OM plus 30% OMRE high boilers heated in annuli with  $L/D_e > 60$  were best correlated by the expression

$$(Q/A)_{\text{crit}} = 395,100 + (944.4 + 7.565p)(G \times 10^{-6}) \Delta h_{\text{SC}} \quad (7)$$

where

$$(Q/A)_{\text{crit}} = \text{DNB heat flux, Btu/hr}\cdot\text{ft}^2,$$

$$p = \text{pressure, psia,}$$

$$G = \text{mass flow rate, lb/hr}\cdot\text{ft}^2,$$

$$\Delta h_{\text{SC}} = \text{subcooled enthalpy difference, Btu/lb.}$$

This equation is valid for pressures of 50 to 240 psia, a bulk temperature of 700°F, coolant velocities of 5 to 32 fps, and  $L/D_e \geq 60$ .

Several significant points are to be noted about Eq. (7):

1. A very definite pressure effect was detected, contrary to the results of the earlier investigators.
2. An entrance length effect was detected that essentially disappears at  $L/D_e \approx 60$ .
3. The data for Santowax R plus 35% total high boilers of Lurie and Robinson<sup>7</sup> correlate reasonably well with this expression.
4. The measured DNB heat fluxes for Santowax OM plus 30% OMRE high boilers are significantly higher than the data of Core and Sato<sup>6</sup> for Santowax OMP.

5. The correlation presented by Boxall et al.,<sup>10</sup> Eq. (6), was apparently revised upward. The intercept was increased about 27%, a pressure effect was added, and the velocity effect became more significant.

All the previously discussed correlations were derived from experiments with heated tubes or annuli. Rogers and Barns<sup>8</sup> point out that it is meaningless to apply Eq. (7) in an attempt to predict DNB failure heat

fluxes for multielement fuel bundle designs, even when subchannel conditions are used to evaluate the parameter  $G \Delta h_{SC}$ . Application of the equation in this manner would probably lead to unsafe designs, they argue. These comments also seem appropriate to the other correlations, since they were derived from similar heated sections.

Boxall et al.<sup>10</sup> and Rogers and Barns<sup>8</sup> make reference to experiments<sup>11</sup> performed to measure DNB heat fluxes in two-element test sections, which simulate a portion of a multielement fuel bundle. In their reference to these experiments, Rogers and Barns say it is shown<sup>11</sup> that the failure mechanism in multielement fuel bundles may be due to coke-out, as well as true DNB. The term "coke-out" is used to characterize the rapid formation and deposition of pyrolytic decomposition products in a relatively hot stagnant region and the consequent rapid growth of the deposited layers, which cause overheating and eventually failure of the heating element. Occurrence of coke-out is not only a function of surface temperature but results from the interaction of surface temperature and nonuniform flow velocity. Observed failures have been at surface temperatures above 650°C. Boxall et al.<sup>10</sup> report that coke-out failure heat fluxes do not correlate with subchannel  $\Delta T_{SC}^{2/3}$ ; however, failures have occurred with fluxes about 25% below DNB values for similar conditions.

It is also reported<sup>8</sup> that true localized DNB failures occurred under certain circumstances in the two-element test section. Observed occurrences were located in a gap region between the elements and on the downstream side of helical spaces. It is noted that the coolant velocity and subcooling in these regions will in general be significantly lower than the average values in the adjacent subchannel. These comments also seem appropriate to the longitudinally spiraled finned surfaces proposed for the HWOCR fuel rods.

In the description of the AI-CE reference reactor design,<sup>12</sup> it is reported that Eq. (4), as recommended in the Organic Heat Transfer Manual,<sup>13</sup> was used to estimate the DNB heat flux. However, the THEME 1 computer program used by AI-CE to evaluate the hot-channel thermal performance has Eq. (2) programmed. Since the two correlations are for the same data, we conclude that approximately the same DNB heat flux will result from either

correlation. B&W also used Eq. (2) to estimate the DNB heat flux in their reference reactor designs.<sup>14</sup>

Our conclusion based on this limited review is that the correlations derived from the Canadian organic coolant program,<sup>8</sup> Eqs. (6) and (7) above, are probably the most reliable; they certainly are for annuli of  $L/D_e > 60$ . We have been unable to locate in the literature a correlation derived from tests of multielement sections. Rogers and Barns advise against the use of Eq. (7) to predict DNB heat fluxes in multielement fuel bundles, and we agree it cannot be used without qualifications (neither can the other correlations). Thus, in using any of the correlations, a reasonable safety factor should be applied in the form of a DNB ratio. The design bases<sup>12</sup> specified a minimum DNB ratio of 2.0; it would appear that this should be increased and should be about 4 when using Eq. (6). Also, it should be pointed out, as discussed in Section 5.5 of this report, that the amount of subcooling is dependent upon the equilibrium concentration of biphenyl.

It is recommended that additional research be initiated to investigate DNB correlations in multielement rod bundles of the type proposed in the HWO CR reference designs. The effects of higher concentrations of biphenyl on coolant vapor pressure should be investigated in order to permit more precise determination of the subcooling available for retardation of localized boiling.

#### References

1. G. C. Pinchera, Heat Transfer by Means of Organic Coolants, Energia Nucleare, 10(6): 319-335 (1963). An English translation of this article is presented by J. Saxon in TRG Information Series 449(W), 1965.
2. Atomics International, Annual Technical Progress Report, AEC Unclassified Programs, Fiscal Year 1962, USAEC Report NAA-SR-7400, Nov. 15, 1962.
3. P. Griffiths, The Correlation of Nucleate Boiling Burnout Data, ASME paper 57-HT-21 presented at ASME-AIChE Heat Transfer Conference, University Park, Pa., August 1957.

4. T. C. Core and K. Sato, Determination of Burnout Limits of Polyphenyl Coolants, USAEC Report IDO-28007, Aerojet-General Corporation, Feb. 14, 1958.
5. C. Grove-Palmer and H. Pass, An Investigation of the Heat Transfer and Burnout Properties of a Proposed Organic Reactor Coolant, British Report AERE-R311, February 1960.
6. T. C. Core and K. Sato, Determination of Burnout Limits of Santowax OMP, USAEC Report AGC-1672, Aerojet-General Corporation, Sept. 15, 1959.
7. H. Lurie and J. M. Robinson, Critical Heat Flux of Some Polyphenyl Coolants, USAEC Report NAA-SR-Memo 7524, Atomics International, Sept. 28, 1962.
8. J. T. Rogers and G. M. Barns, DNB Fluxes in an Annular Test Section for a Terphenyl Coolant Containing 30 Per Cent High Boilers, Report R63CAP67, Canadian General Electric Company, Ltd., June 1965.
9. D. A. van Meel, Burnout in Subcooled Forced Convection Boiling of Polyphenyls, Third United Nations International Conference on the Peaceful Uses of Atomic Energy, Geneva, 1964, A/Conf. 28/P/590.
10. D. G. Boxall et al., Development of Fuel and Coolant Tubes for a Reactor Cooled by Organic Liquid, Third United Nations International Conference on the Peaceful Uses of Atomic Energy, Geneva, 1964, A/Conf. 28/P/23.
11. J. T. Rogers, Heat Transfer Failure Mechanisms in Simulated Organic Cooled Fuel Bundles, Report R64CAP10, Canadian General Electric Company, Ltd., May 1965.
12. Combustion Engineering, Inc., and Atomics International, Heavy Water Organic Cooled Reactor - 1000 Mwe Nuclear Power Plant Preliminary Conceptual Design, USAEC Report AI-CE-Memo-6, Vol. II, Oct. 1, 1965.
13. Atomics International, Organic Heat Transfer Manual, USAEC Report NAA-SR-Memo 7343, Dec. 1, 1962.
14. Babcock & Wilcox Company, 1000 Mwe Thorium HWOCR Preliminary Conceptual Design Data for ORNL Evaluation, Nov. 15, 1965.

Appendix E

## REVIEW OF ENGINEERING HOT-CHANNEL FACTORS

A review was made of the engineering hot-channel factors used in the reference reactor designs to determine their adequacy. As the number of pressure-tube reactors in existence is rather small, the literature on hot-channel factors for this type of reactor is quite limited. It is necessary to know how these factors are defined and the manner in which they are applied before one can make meaningful comparisons with the values reported, especially those reported for open-lattice grid-type cores. In particular, it is reported<sup>1</sup> that in the Canadian program extensive irradiation and out-of-pile tests on heat transfer, together with mixing flow tests and reliable estimates of neutron power distributions, are preferred to the hot-spot-factor approach. A comprehensive statistical approach, consisting of a Monte Carlo computer program for evaluating the thermal-hydraulic performance for input fabrication tolerances, has been developed for the ORGEL program.<sup>2</sup> Although this computer program is complex, it appears to provide the necessary data for detailed design studies. Its use for preliminary designs is probably not warranted.

Flow maldistribution is used to describe the variation of coolant flow in the process tubes from that specified. A value of 1.04 was selected for this factor to indicate that the flow in a pressure tube may differ by as much as  $\pm 4\%$  from the design value. Some CVTR measurements<sup>3</sup> show that for the 36-pressure-tube CVTR, the maximum flow deviation was 3.4% at startup. A large hydraulic model of a pressurized-water reactor indicated a 5% maximum deviation at the inlet.<sup>3</sup> For the large number of pressure tubes with their attendant "pigtailed" and orifices in the reference reactor designs, it appears that a factor of at least 1.05 is appropriate.

The effects of fabrication tolerances on fuel diameter, density, enrichment, and eccentricity should be of a statistical nature and can be evaluated accordingly,<sup>4</sup> provided sufficient data are available. The values used in the reference design appear optimistic; however, we have

no extensive experience relative to the case at hand and, therefore, have no real basis for taking exception to the values used.

The values for rod and bundle dislocation and bowing also appear optimistic. It has been assumed in the reference design that the rod bundle will be located concentrically within the pressure tube and will thus uniformly maintain a 30-mil radial clearance between the bundle and the pressure-tube liner. It seems most likely that the bundles will be located eccentrically and that flow distribution will consequently be considerably different from that assumed. The effect of eccentric positioning can be evaluated with the U-3 code as it was for the Canadian pressure-tube reactor designs.<sup>1</sup> Extensive calculations, which we have not undertaken, are likely to be required to establish the proper value of this subfactor.

In summary, no large changes from the AI-CE values were considered for the engineering factors. While in general they appear to be realistic, there is little experimental data that can be used in judging the accuracy. Extensive experimental studies will be required to determine the proper values.

#### References

1. A. D. Iane et al., The Thermal and Hydraulic Characteristics of Power Reactor Fuel Bundle Designs, Can. J. Chem. Engr., October 1963, pp. 226-234.
2. FIAT Sezione Energia Nucleare, Statistical Methods for Hot Channel and Hot Spot Calculation, Final Report No. 1, EURAEC-910, Oct. 30, 1963.
3. R. D. Sandberg and A. A. Bishop, Analysis of CVTR Post-Construction Thermal and Hydraulic Data, USAEC Report CVNA-221, Carolinas-Virginia Nuclear Power Associates, May 1965.
4. Harold Chelemer and Long Sun Tong, Engineering Hot-Channel Factors for Open-Lattice Cores, Nucleonics, 20(9): 68-73 (September 1962).

Appendix F

## ANALOG COMPUTER STUDY OF HWOCR CONTROL DYNAMICS

Analog Model

The HWOCR has, in general, a positive power coefficient of reactivity, and therefore perturbations in flux level will tend to grow with time. In this situation it is important to examine the adequacy of the control system with regard to the prevention of positive or negative excursions. An adequate control system must prevent a perturbation from producing or forcing a plant shutdown and should minimize the disturbance seen by the load. In order to study control system requirements, an analog simulation of the HWOCR was performed as outlined below. During these investigations, the mathematical model and parameter values employed were revised in accordance with developed information. The results given in this report are based on the final calculations made with the model described below and the parameter values given in Tables F.1, F.2, and F.3. Figure F.1 is a graphical representation of the analog model used in these control studies.\*

Reactor Kinetics Model

The cylindrical core of the HWOCR is about 22 ft in diameter and 18 ft long. These large dimensions make kinetic spatial effects potentially important, and the positive coolant temperature coefficient will emphasize local temperature variations. In an attempt to include such effects, the reactor was divided into five axial sections. The separation was made axially because that is the direction of coolant flow and the gradient in fuel burnup. Radial flux tilts may be of concern in the overall control problem but are probably of less importance under fast transient conditions. The number of sections was limited to five by the size of the analog installation.

---

\*Copies of the associated analog computer diagram can be obtained from R.S. Stone, Instrumentation and Controls Division, Oak Ridge National Laboratory, P.O. Box X, Oak Ridge, Tennessee 37830.

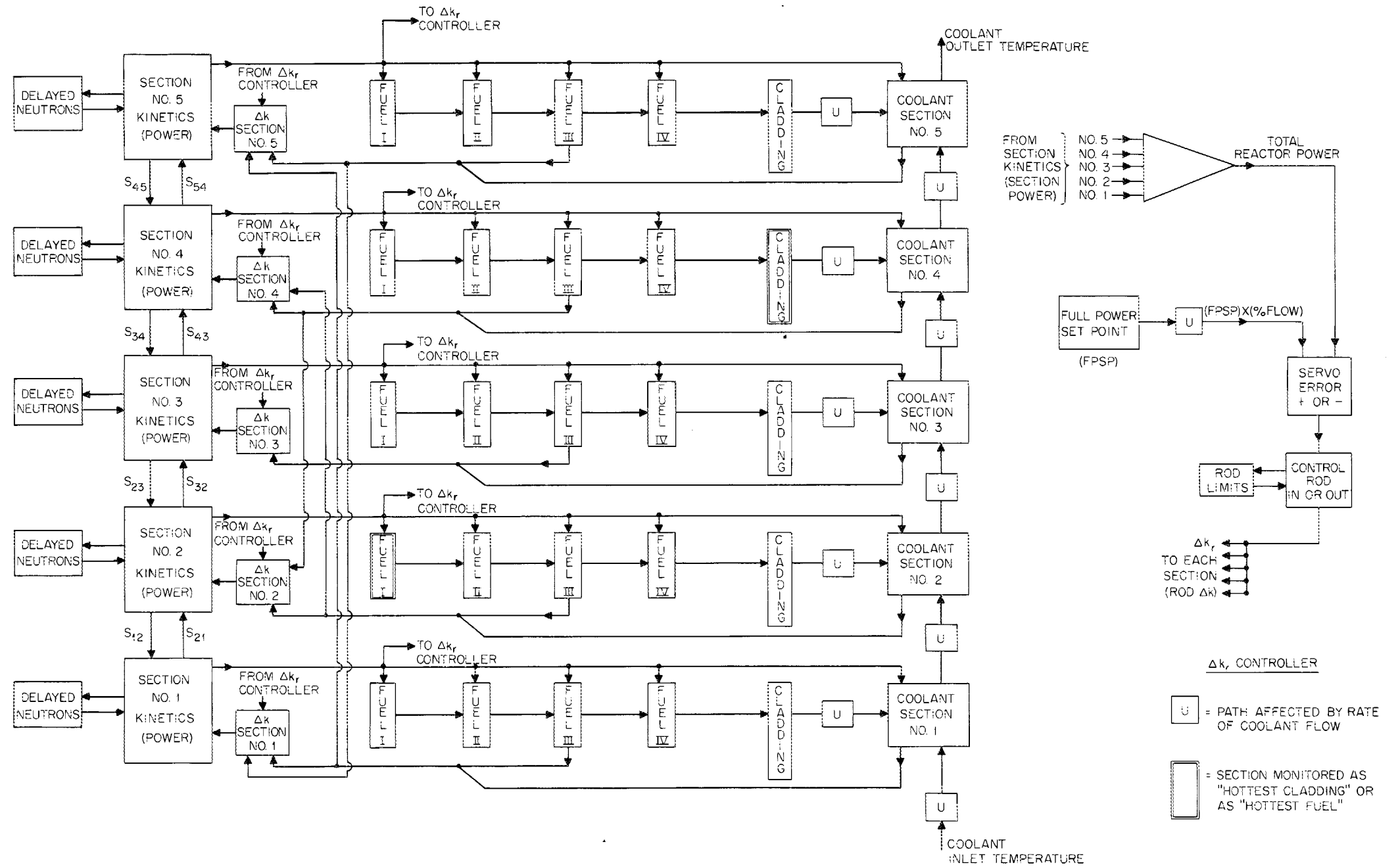


Fig. F.1. Block Diagram of HWOCR Simulation.

In the simulation employed, each of the five axial sections of the core can be considered to be a subcritical assembly, with a source consisting of leakage neutrons from the adjoining sections. For a purely thermal reactor, the flux balance equation for the pth section is

$$\frac{1}{V} \dot{\phi}_p = (1 - \beta) v \Sigma_f \phi_p - \Sigma_a \phi_p + S_p + \sum_i \lambda_i C_{ip} \quad , \quad (1)$$

where  $S_p$  is the leakage source, taken to be

$$S_p \cong \frac{D}{V_p} \sum_q \frac{\phi_q - \phi_p}{z_{qp}} A_{qp} \quad , \quad (2)$$

where q refers to a section adjacent to p,  $z_{qp}$  is the distance between q and p, and  $A_{qp}$  is the cross-sectional area for neutron transfer between q and p. All the terms are defined in Table F.3 at the end of this appendix. Substituting Eq. (2) into (1) and gathering terms in  $\phi_p$  gives

$$\begin{aligned} \frac{1}{V} \dot{\phi}_p = & \left[ (1 - \beta) v \Sigma_f - \Sigma_a - \frac{D}{V_p} \sum_q \frac{A_{qp}}{z_{qp}} \right] \phi_p \\ & + \frac{D}{V_p} \sum_q \frac{A_{qp}}{z_{qp}} \phi_q + \sum_i \lambda_i C_{ip} \quad . \quad (3) \end{aligned}$$

At this point, it is useful to define

$$k_p = \frac{v \Sigma_f}{\Sigma_a \left( 1 + \frac{D}{\Sigma_a V_p} \sum_q \frac{A_{qp}}{z_{qp}} \right)}$$

and

$$l_p = \frac{1}{v \Sigma_a \left( 1 + \frac{D}{\Sigma_a V_p} \sum_q \frac{A_{qp}}{z_{qp}} \right)} \quad .$$

It should be understood that this is a one-dimensional model. If radial leakage exists, it can be considered to contribute to the net values of  $k_p$  and  $l_p$ .

Multiplying Eq. (3) by

$$\frac{1}{\Sigma_a \left( 1 + \frac{D}{\Sigma_a V_p} \sum_q \frac{A_{qp}}{z_{qp}} \right)}$$

and substituting  $k_p$  and  $l_p$  as defined above gives

$$l_p \dot{\phi}_p = (1 - \beta) k_p \phi_p - \phi_p + l_p v \frac{D}{V_p} \sum_q \frac{A_{qp}}{z_{qp}} \phi_q + l_p v \sum_i \lambda_i C_{ip} \quad (4)$$

In the above,  $l_p$  and  $k_p$  are defined as though the ends of the individual sections were bare. This gives an expression in  $\phi_q$  that can be taken as a "source" term accounting for neutrons diffusing in from adjacent sections.

In a large reactor such as the HWOCR, leakage should be relatively unimportant in determining  $l$ , so it is assumed that the  $l_p$ 's are the same as the  $l$  for the whole reactor, or 570  $\mu$ sec. The  $k_p$ 's are those necessary for criticality and flux distribution in the reactor as a whole. In the cross-leakage source expression, the geometric term  $A_{qp}/V_p z_{qp}$  is the same for each pair of sections. The distance between sections,  $z_{qp}$ , is about 105 cm. The quantity  $A_{qp}/V_p$  can be considered to be the reciprocal of the length of the pth section, so

$$\frac{A_{qp}}{V_p z_{qp}} = \frac{1}{105^2} = \frac{1}{1.1 \times 10^4 \text{ cm}^2} \quad .$$

The materials term is

$$l_p v D \cong \frac{D}{\Sigma_a + \frac{2D}{z_{qp}^2}} = 203 \text{ cm} \times 0.9777 \text{ cm} = 198 \text{ cm}^2 \quad .$$

The whole leakage expression thus becomes

$$l \frac{vD}{P} \frac{A_{qp}}{V_p z_{qp}} \phi_q = \frac{198\phi_q}{1.1 \times 10^4} = 0.0180\phi_q ,$$

and Eq. (4), written in terms of reactor power, becomes

$$\dot{P}_p = (1 - \beta)k_p P_p - P_p + 0.0180 (P_{p-1} + P_{p+1}) + l \sum_i \lambda_i X_{ip} . \quad (5)$$

The supplementary equation involving the delayed neutrons is

$$l \dot{X}_{ip} = \beta_i k_p P_p - l \lambda_i X_{ip} . \quad (6)$$

In Eqs. (5) and (6)

$$X_i = C_i \sum_f \epsilon V$$

and is related to  $C_i$  as  $P$  is related to  $\phi$ .

At design point,

$$\dot{P}_p = \dot{X}_{ip} = 0$$

and

$$\beta k_p P_p = l \sum_i \lambda_i X_{ip} ,$$

so

$$(k_p[0] - 1) P_p + 0.0180 (P_{p-1} + P_{p+1}) = 0 ,$$

or

$$\Delta k_p[0] = k_p[0] - 1 = 0.0180 \frac{P_{p-1} + P_{p+1}}{P_p} . \quad (7)$$

From Fig. II-9 of Ref. 1, the relative power ratios in the five sections from inlet to outlet are about 0.7 : 1.3 : 1.3 : 1.1 : 0.6.

If the  $\Delta k$ 's are calculated for the five individual sections of the core with Eq. (7) and the relative power levels from Fig. II-9, a value of about -3% is obtained for each section. Individual values are listed in Table F.3.

Two delayed-neutron groups were used, with the number being dictated by the available analog equipment. In order to emphasize the faster groups, the normal delayed groups 1 and 2 were placed in one lumped group, and normal groups 3 through 6 in the other. In each lumped group

$$\beta_n = \sum \beta_i$$

and

$$\lambda_n = \frac{\sum \lambda_i \beta_i}{\beta_n},$$

with the summation carried out for the normal delayed groups involved in each case. The values obtained are listed in Table F.3. Arguments may be advanced for more or for different groups, but for the transients investigated the exact delayed-neutron time constants are relatively non-critical

#### Heat Transfer Model

Heat transfer through an average fuel pin is simulated by breaking the pin into four equal-thickness radial shells and writing equations for the heat conduction between these shells. Making the shells of equal thickness means that those on the outside have larger volumes but tends to equalize the thermal time constants. The fineness of this four-shell model allows a close representation of the temperature profile, as typified by Fig. II-7 of Ref. 1. Heat transfer equations for the fuel give expressions of the form

$$\begin{aligned} \dot{T}_{fi} = & \frac{u_{fi}}{C_p \rho_f} + \frac{\frac{K_f A_{i-}}{\Delta x_i}}{C_p \rho_f V_i} [T_{f(i-1)} - T_{fi}] \\ & - \frac{\frac{K_f A_{i+}}{\Delta x_i}}{C_p \rho_f V_i} [T_{fi} - T_{f(i+1)}]. \end{aligned} \quad (8)$$

All terms are identified and evaluated in Table F.3, and coefficients for each shell are given below in the section entitled "Temperature Relations."

The following heat balance equation was developed that relates cladding temperature to fuel and coolant temperatures:

$$h_w A_{cw} (T_c - T_w)_p = \frac{\left(\frac{KA}{\Delta x}\right)_{Hp} \left(\frac{KA}{\Delta x}\right)_f}{\left(\frac{KA}{\Delta x}\right)_{Hp} + \left(\frac{KA}{\Delta x}\right)_f} (T_{fIV} - T_c)_p \quad (9)$$

Because equilibrium fuel has undergone a higher degree of burnup in section 2 than in section 1 of the reactor, and in section 3 than in section 2, the heat transfer coefficient for the gas gap between fuel and cladding varies from section to section. The calculated heat transfer coefficients used were obtained from Combustion Engineering,<sup>2</sup> and the resulting factors for Eq. (9) are listed in Table F.3. These coefficients for heat transfer from fuel to cladding are extremely important values; when the power level is raised, they determine the relative temperature increases in the fuel and coolant and hence help set the net power coefficient of reactivity. Results of the present simulation might be changed drastically if experimental results showed appreciable changes in values of heat transfer coefficients.

Data supplied by Coppersmith<sup>2</sup> were manipulated to yield a design-point value of 0.556 Btu/sec·ft<sup>2</sup>·°F for the film coefficient  $h_w$  for heat transfer from the fuel cladding to the coolant. A report<sup>3</sup> by Atomic International indicates that this coefficient varies as the 0.8 power of the Reynolds number. For the present simulation, the temperature dependence of the relation was neglected, but the 0.8-power variation with flow was retained. A reasonably good approximation for including the exponential expression  $U_w^{0.8}$  was obtained by setting

$$h_w = \left( 0.072 + 0.484 \frac{U_w}{U_w[0]} \right) \quad (10)$$

A quantity useful in analyzing the thermal behavior of the coolant is  $\Delta T_{wp}$ , the temperature increase experienced by a given differential volume of the coolant in passing through section p. In the steady-state condition,  $\Delta T_{wp}$  has the same numerical value as the difference between

the inlet and exit temperatures. The coolant exit temperature for the section is  $T_{wpe}$ , which makes the inlet temperature  $T_{w(p-1)e}$ . The following equation relates these temperatures:

$$T_{wpe} t = T_{w(p-1)e} (t - \tau_{wp}) + \Delta T_{wp} . \quad (11)$$

The mean temperature  $T_{wp}$  of the coolant in the section is approximately the temperature found at a point halfway through the section. Thus

$$T_{wp} t \cong T_{w(p-1)e} \left( t - \frac{1}{2} \tau_{wp} \right) + \frac{1}{2} \Delta T_{wp} . \quad (12)$$

The transport delay per section is small (0.134 sec at design point), and little error is introduced by neglecting the half-section lags. Then,

$$T_{wp} t \cong T_{w(p-1)e} t + \frac{1}{2} \Delta T_{wp} . \quad (13)$$

The transport delay was simulated by the following first-order approximation:

$$T_{w(p-1)e} (t - \tau_{wp}) \cong T_{w(p-1)e} t \left( 1 - e^{-t/\tau_{wp}} \right) . \quad (14)$$

A heat balance yields the equation for the rate of change of the mean temperature of the coolant in the section:

$$\begin{aligned} \dot{T}_{wp} &= \frac{P_{wp} + h_w A_c (T_c - T_w)_p}{(C_p \rho V)_w} - \frac{T_{wpe} - T_{w(p-1)e}}{\tau_{wp}} \\ &= 0.00184 P_p + 6.342 h_w (T_c - T_w) \\ &\quad - 7.47 \frac{U_w}{U_w [o]} (T_{wpe} - T_{w(p-1)e}) . \end{aligned} \quad (15)$$

The rate of change of the quantity  $\Delta T_{wp}$  is approximately twice the rate of change of the mean temperature of the coolant in the section for relatively slow variations in the inlet temperature. The relationship

$$\dot{\Delta T}_{wp} = 2\dot{T}_{wp} \quad (16)$$

was used in calculating  $\Delta T_{wp}$  in the model. Substitution of Eqs. (11) and (16) into Eq. (15) gives

$$\begin{aligned} \frac{\dot{\Delta T}_{wp}}{2} = & 0.00184 P_p + 6.342 h_w (T_c - T_w)_p \\ & - 7.47 \frac{U_w}{U_w[o]} \left[ \Delta T_{wp} + T_{w(p-1)} e^{-(t - \tau_{wp})} - T_{w(p-1)} e^{-t} \right]. \end{aligned} \quad (17)$$

The constants used above are listed in Table F.3, and design-point temperatures are given in the section below entitled "Temperature Relations."

Although the analog model provided coolant transport delays and heat transfer relations associated with fluid flow external to the reactor core, this feature was not used in the calculations. In most simulator runs, the inlet temperature was held constant at 595°F, although in a few cases the inlet temperature was step increased by a small amount during the run.

#### Temperature Coefficients

The temperature of only one radial fuel shell in each section was used in computing the effect of fuel temperature changes on reactivity. In order to assign the fuel temperature coefficient in proportion to relative volume, fuel shell I (the innermost shell) should be assigned 1/16 of the coefficient; shell II, 3/16; shell III, 5/16; and shell IV, 7/16. Analog equipment restrictions dictated a simpler arrangement, so the entire fuel temperature coefficient was assigned to shell III. The error inherent in this arrangement does not appear to be significant, even in the transient case.

Temperature variations in one section of the reactor model in some cases produce a reactivity variation in another section as well. Since

the direction of coolant flow alternates from one process tube to the next, the outlet section of the fuel assembly is located in a region of the reactor that is equally influenced by inlet and outlet process tubes. For this reason, the reactivity effects due to temperature changes in the fuel and coolant in section 5 were applied both to section 5 and section 1, and vice versa. The same was true for sections 2 and 4. Temperature changes in section 3 affect reactivity only in section 3.

Fuel and coolant temperature coefficients vary from section to section because of the axial gradient in fuel burnup. The numerical values used in the simulation were derived from temperature coefficients supplied by Coppersmith<sup>2</sup> of Combustion Engineering. His values, however, were for a point reactor model and hence represented the proper temperature coefficients only when applied to the reactor as a whole. In the ORNL model, a temperature change in section 3 was assumed to affect reactor kinetics by altering only the reactivity in section 3; reactivity changes in sections 1 or 5 affected both sections 1 and 5; and changes in sections 2 or 4 affected both sections 2 and 4, as explained above. In essence, the values of the temperature coefficients for the ORNL model were determined by balancing a small reactivity increase applied to one section or pair of sections against a smaller reactivity decrease applied to all sections. The ratio of these equivalent reactivities then served as a multiplier for the point reactor temperature coefficient. The temperature coefficients used are listed in Table F.1.

### Reactivity Control

Reactivity variations produced by control rod motion were applied uniformly to all five sections of the core. The control scheme had zero dead band and corresponded to use of an on-off constant-speed servo which goes positive or negative depending upon the sign of the error signal. The error signal compared nuclear power with demand, and demand was proportional to coolant flow. At 100% flow, demand was for 100% power, and any loss of flow depressed the power set point.

Table F.1. Temperature Coefficients of Reactivity

Temperature Coefficient	Value When Applied to Whole Reactor; from Ref. 2 ( $\Delta k_e / ^\circ\text{F}$ )	Value When Applied Only to Sections Directly Affected; Empirically Determined ( $\Delta k_e / ^\circ\text{F}$ )	Sections Directly Affected
	$\times 10^{-5}$	$\times 10^{-5}$	
$\alpha_{f1}$	-0.101	-0.842	1, 5
$\alpha_{f2}$	-0.146	-0.265	2, 4
$\alpha_{f3}$	-0.135	-0.563	3
$\alpha_{f4}$	-0.088	-0.160	2, 4
$\alpha_{f5}$	+0.001	+0.008	1, 5
$\alpha_{w1}$	-0.038	-0.32	1, 5
$\alpha_{w2}$	+0.71	+1.29	2, 4
$\alpha_{w3}$	+1.282	+5.342	3
$\alpha_{w4}$	+1.462	+2.658	2, 4
$\alpha_{w5}$	+0.776	+6.47	1, 5

### Temperature Relations

#### Derivation of Equations and Evaluation of Coefficients

When physical and geometrical constants for the four fuel shells are substituted into Eq. (8), the time rate of change of the temperatures in  $^\circ\text{F}/\text{sec}$  can be expressed as follows:

$$\dot{T}_{fIp} = 0.2364P_p + 5.40T_{fIIp} - 5.40T_{fIp} \quad , \quad (8a)$$

$$\dot{T}_{fIIp} = 0.2364P_p + 1.80T_{fIp} + 3.60T_{fIIIp} - 5.40T_{fIIp} \quad , \quad (8b)$$

$$\dot{T}_{fIIIp} = 0.2364P_p + 2.16T_{fIIp} + 3.24T_{fIVp} - 5.40T_{fIIIp} \quad , \quad (8c)$$

$$\dot{T}_{fIVp} = 0.2364P_p + 2.314(T_{fIII} - T_{fIV})_p - 5.786(T_{fIV} - T_{fs})_p \quad . \quad (8d)$$

In each section of the fuel, the rate of heat transfer from shell IV to the surface in Btu/sec can be expressed as

$$Q_p = \frac{K_f A_{IVp}}{\Delta x_{IVp}} (T_{fIV} - T_{fs})_p = 0.1701 L_p (T_{fIV} - T_{fs})_p .$$

The quantity  $Q_p$  is also the rate of heat transfer from the surface of the fuel to the cladding and can be expressed as

$$Q_p = (hA)_{Hp} (T_{fs} - T_c)_p .$$

When the heat capacity of the cladding is neglected, the quantity  $Q_p$  is also the rate of heat transfer from the cladding to the coolant and can be further expressed as

$$\begin{aligned} Q_p &= h_w A_c (T_c - T_w)_p \\ &= h_w [A_c(\text{wall}) + A_c(\text{fins})] (T_c - T_w)_p \\ &= h_w (0.1364 L_p + 0.1360 L_p) (T_c - T_w)_p \\ &= 0.2724 h_w L_p (T_c - T_w)_p . \end{aligned}$$

By equating these expressions in  $Q_p$ ,  $T_{fs}$  can be obtained in terms of  $T_{fIV}$  and  $T_c$  so that

$$T_{fIVp} = 0.2364 P_p + 2.314 (T_{fIII} - T_{fIV})_p - \frac{5.786 (T_{fIV} - T_c)_p}{1 + 0.1701 \frac{L_p}{(hA)_{Hp}}} . \quad (8d')$$

The values of  $(hA)_{Hp}/L_p$  for the five core sections are listed in Table F.3. By further manipulation of the heat flow equations,  $T_c$  can be related to  $T_{fIV}$  and  $T_w$  by the expression

$$6.342 H_w (T_c - T_w)_p = \frac{3.960 (T_{fIV} - T_c)_p}{1 + 0.1701 \frac{L_p}{(hA)_{Hp}}} . \quad (18)$$

This form of the equation is chosen to simplify the analog circuit by making the coefficient of the  $(T_c - T_w)$  term identical to that in Eq. (17).

### Design-Point Values

By setting time derivatives equal to zero and substituting design-point power into Eq. (8), the design-point temperature differences between each pair of fuel shells and between fuel shell IV and the cladding can be calculated. Equation (18) then gives  $(T_c - T_w)_p$ , and by following the same procedure with Eq. (15) as was employed with Eq. (8), the temperature rise  $[T_{wpe} - T_{w(p-1)e}]$  can be obtained. The desired design-point outlet temperature is 750°F, and with this number and the calculated temperature differences as a starting point, the whole set of design-point temperatures can be obtained. Their values are given in Table F.2.

The procedure described above yields an inlet temperature of 597.9°F instead of the design temperature of 595°F. This discrepancy is probably due to neglect of the variation of coolant heat capacity with temperature and could be removed by changing coolant capacity from section to section. The error is less than 2% of the total temperature rise in the coolant and was neglected.

Table F.2. Design-Point Temperatures

	Axial Section				
	5 (outlet)	4	3	2	1
Temperatures, °F					
$T_{wpe}$	750	731.5	697.6	658.5	619.4
$T_{w(p-1)e}$	731.5	697.6	658.5	619.4	597.9
$T_{wp}$	740.8	714.6	678.0	638.9	608.7
$T_{cp}$	779.7	785.9	762.3	723.2	654.1
$T_{fIVp}$	943.4	1158.3	1287.9	1337.2	1014.2
$T_{fIIIp}$	992.1	1247.6	1393.5	1442.8	1071.1
$T_{fIIp}$	1024.6	1307.1	1463.9	1513.2	1109.0
$T_{fIp}$	1040.8	1336.9	1499.1	1548.4	1128.0

Table F.3. Glossary of Terms and Parameter Values

Terms	Definitions	Values
A	Area	For radial heat transfer through the fuel the surface area is $2\pi \times L$ . For flow the coolant cross-sectional area is $22.3 \text{ ft}^2$ . For axial neutron transfer, $\frac{A_{3D}}{V_p} = \frac{1}{z} = \frac{1}{105 \text{ cm}}$
C	Atomic density of delayed neutron precursors	
$C_p$	Heat capacity	$C_{pf} \approx 0.063 \text{ Btu/lb}\cdot^\circ\text{F}$ $C_{pw} \approx 0.59 \text{ Btu/lb}\cdot^\circ\text{F}$
D	Diffusion constant	Overall D for HWOCR = $0.977 \text{ cm}$ (from Ref. 2)
h	Heat transfer coefficient	$h_w$ for coolant film taken to be $\left( 0.372 + 0.484 \frac{U_w}{U_w[0]} \right)$ $= 0.556 \text{ Btu/sec}\cdot\text{ft}^2\cdot^\circ\text{F}$ at design point
$(hA)_{HP}/L_p$	These values are for heat transfer per foot of pin. They may be transformed to Ref. 2 values per section of pin (from which they were obtained) by multiplying them by $3.46 \text{ ft}$ .	$(hA)_{H1}/L_1 = 0.02153 \text{ Btu/sec}\cdot^\circ\text{F}\cdot\text{ft}$ $(hA)_{H2}/L_2 = 0.02370 \text{ Btu/sec}\cdot^\circ\text{F}\cdot\text{ft}$ $(hA)_{H3}/L_3 = 0.02835 \text{ Btu/sec}\cdot^\circ\text{F}\cdot\text{ft}$ $(hA)_{H4}/L_4 = 0.03497 \text{ Btu/sec}\cdot^\circ\text{F}\cdot\text{ft}$ $(hA)_{H5}/L_5 = 0.04566 \text{ Btu/sec}\cdot^\circ\text{F}\cdot\text{ft}$
K	Thermal conductivity	$K_f = 13 \text{ Btu/hr}\cdot\text{ft}\cdot^\circ\text{F}$ $= 3.6 \times 10^{-3} \text{ Btu/sec}\cdot\text{ft}\cdot^\circ\text{F}$
$k_p$	Nuclear multiplication of section p; $\Delta k_p = k_p - 1$	Design point values for individual sections (numbered from inlet end): $\Delta k_1[0] = -3.35\%$ $\Delta k_2[0] = -2.77\%$ $\Delta k_3[0] = -3.33\%$ $\Delta k_4[0] = -3.11\%$ $\Delta k_5[0] = -3.29\%$ $k \text{ overall } [0] = 1.000$
L	Fuel pin length	Core length is $17.3 \text{ ft}$ overall or $3.46 \text{ ft}$ per section. Effective fuel pin length is core length multiplied by the number of pins and is $2.81 \times 10^5 \text{ ft}$ or $5.62 \times 10^4 \text{ ft}$ per section.
l	Prompt neutron lifetime	$5.70 \times 10^{-6} \text{ sec}$
P	Nuclear power	$P_1[0] = 433 \text{ Mw}$ $P_w[0] = 680 \text{ Mw}$ $P_2[0] = 804 \text{ Mw}$ $P_5[0] = 371 \text{ Mw}$ $P_3[0] = 804 \text{ Mw}$ $P_T[0] = 3093 \text{ Mw}$
Q	Rate of heat transfer	
$S_p$	Neutron source due to leakage from adjacent sections	
T	Temperature	
t	Time	
$U_w$	Coolant speed through the core	$U_w[0] = 30 \text{ ft/sec}$

Table F.3 (continued)

Terms	Definitions	Values
u	Power density	$u_F[0] = 13.4P_P \text{ Btu/sec}\cdot\text{ft}^3$ $u_W[0] = 0.00165P \text{ Btu/sec}\cdot\text{ft}^3$
V	Volume	$V_{fi}$ = volume of a particular fuel shell $= \pi(x_+^2 - x_-^2)L$ $V_{wP}$ = volume of coolant in one section $= 77.2 \text{ ft}^3$
v	Neutron speed	Effective v for HWCCR = $3.56 \times 10^5 \text{ cm/sec}$ .
$X_i$	$C_i \Sigma_i$ , eV, "potential power" stored in neutron precursors of group i	$\Sigma_i$ , eV is the multiplier used to convert kinetic equations in $\phi$ to equations in P.
x	Radial distance from center of fuel pin	$\Delta x$ between fuel shells = 0.005 ft $\Delta x$ across helium gap = 2.5 mils $= 2.1 \times 10^{-4} \text{ ft}$
$z_{qp}$	Axial center-to-center distance between fuel sections	$z_{qp} = 105 \text{ cm} = 3.46 \text{ ft}$
$\alpha_p$	Temperature coefficient of reactivity = $\frac{\partial k}{\partial T_p}$	Individual values are shown in Table F.1.
$\beta$	Fraction of fission neutrons delayed	$\beta_1 = 0.00073$ $\beta_2 = 0.00417$ Total $\beta = 0.0049$
$\epsilon$	Energy released per fission	
$\lambda$	Delayed-neutron decay constant	$\lambda_1 = 1.90 \text{ sec}^{-1}$ $\lambda_2 = 0.179 \text{ sec}^{-1}$
$\nu$	Neutron yield per fission	
$\rho$	Mass density	$\rho_F$ = density of fuel $= 13.6 \text{ g/cc} = 849 \text{ lb/ft}^3$ $\rho_W$ = density of coolant $\approx 0.86 \text{ g/cc} = 53 \text{ lb/ft}^3$
$\Sigma_a$	Absorption cross section	Average $\Sigma_a \approx 4.74 \times 10^{-3} \text{ cm}^{-1}$
$\Sigma_f$	Fission cross section	Average $\nu \Sigma_f \approx 4.89 \times 10^{-3} \text{ cm}^{-1}$
$\tau$	Coolant transport time	Steady state coolant transit time through one section = $\tau_{wP}[0] = 0.134 \text{ sec}$
$\phi$	Neutron flux	
[o]		Identifies a design-point condition

Subscripts

c	Cladding on the fuel
e	Identifies the down-stream boundary of coolant in a section of process tube
f	Fuel
H	Helium gas gap between fuel and cladding
i	Used to number delayed-neutron groups and also heat transfer shells in the fuel
n	Identifies a delayed-neutron group obtained by lumping several normal groups
p	Used to specify axial sections of the core, except that as a subscript for C, p indicates heat capacity at constant pressure
q	Axial sections adjacent to p

Table F.3 (continued)

Terms	Definitions	Values
r	Refers to nuclear multiplication change due to control rod motion	
s	Surface of the fuel	
w	Organic coolant (wax)	
I, II, III, IV	Identify fuel shells, starting at the center	
1, 2, 3, 4	Identify core sections, starting at the inlet end	

$T_{f(i-1)}$      $T_{fi}$      $T_{f(i+1)}$   
 $A_{i-}$      $A_{i+}$   
 $\Delta x_i$      $\Delta x_i$   
toward center    toward cladding

Symbols identifying temperatures, surface areas, and distances in heat transfer equations of fuel pins. Radial shell  $i$  is typical, with adjacent shells  $(i-1)$  and  $(i+1)$  being toward the center and toward the outside of the pin, respectively. Areas  $A_{i-}$  and  $A_{i+}$  are the surface areas through which the heat flows from shell  $(i-1)$  to shell  $i$  and from shell  $i$  to shell  $(i+1)$ . Distance  $\Delta x_i$  is the distance involved in the heat transfer from one shell to an adjacent shell. All shells have equal thickness.

Cross Section of Typical Radial Shells of Fuel Pin

### References

1. Combustion Engineering, Inc., and Atomics International, Heavy Water Organic Cooled Reactor - 1000 Mwe Nuclear Power Plant Preliminary Conceptual Design, USAEC Report AI-CE-Memo-6, Vol. II, Oct. 1, 1965.
2. W. C. Coppersmith, Combustion Engineering, Inc., personal communication with R. S. Stone, Oak Ridge National Laboratory.
3. Atomics International, Organic Reactor Heat Transfer Manual, USAEC Report NAA-SR-Memo-7343, Sect. IV, Dec. 1, 1962.

## Appendix G

COMPARISON OF ADVANCED CONVERTER FUEL-PROCESSING  
COSTS ON DIFFERENT BASES

In the advanced converter evaluation,<sup>1</sup> spent-fuel processing costs were estimated for six reactor concepts under general ground rules essentially the same as for the present HWOCR evaluation; that is, single-purpose processing plants were specified to exactly match the amount and type of fuel for a 15,000-Mw(e) industry based on each concept. A summary of these estimates at throughput rates corresponding to burnups near the economic optimum is given in Table G.1. At the reference 22% per year fixed-charge rate (FCR) on capital, the estimated processing costs in \$/kg varied from 18.7 to 97.6; in mill/kwhr(e) the cost range was fairly narrow, from 0.191 to 0.230. In the present HWOCR evaluation we have estimated fuel-processing costs on two bases, one being exactly the same as for the advanced converter evaluation, and the other a revised basis that is felt to be more realistic. For comparison, we also have reestimated processing costs for the six previously evaluated reactors on the HWOCR revised basis; the results are shown in Table G.2.

For comparison between uranium-fueled reactors or between thorium-fueled reactors, either the old or the new estimates will give the same cost ranking; however, for comparing uranium-fueled reactors with thorium-fueled reactors or for comparing these estimated future costs with present-day processing charges by Nuclear Fuel Services (NFS), we believe that the new estimates are preferable. The new estimates are 72 to 81% of the old ones for the uranium fuels, and 59 to 65% for the thorium fuels, as indicated in Table G.2. The reasons for the differences are explained in Chapter 11.

For comparative evaluation purposes, HWOCR fuel fabrication costs were estimated for equilibrium cores on the bases used in the advanced converter study<sup>1</sup> (fuel preparation costs were included in fabrication costs). These estimates are listed in Table G.3 for the AI-CE fuel element. Estimates for the B&W oxide fuel element are given in Table G.4. Similar estimates could not be made for the thorium metal fuel because

there were no metal-fueled cores considered in the advanced converter study.

Table G.1. Summary of Spent-Fuel Processing Cost Estimates for Previous Advanced Converter Evaluation.

Basis: Single-purpose plants serving 15 reactors of a given concept, 1000 Mw(e) each; 0.8 reactor load factor; burnup approximately equal to the estimated economic optimum<sup>a</sup>

	PWR	SSCR	HWR-U	HWR-Th	HFGR <sup>b</sup>	SGR
Reference material burnup, Mwd/T	21,248	29,580	12,540	23,000	48,500	16,750
Thermal efficiency, %	31.1	31.2	26.8	26.1	44.4	43.6
Throughput rates, MT/yr						
Uranium	645	34.9	1280	24.5	7.14	587
Thorium		426		688	189	
Plutonium	4.11		5.93			3.42
Fission products	14.1	14.0	16.3	16.7	10.0	10.0
Reference material	663	475	1300	730	206	600
Batches processed per year	19.2	6.91	57.1	73.0	54.0	48.7
Processing days per year	156	255	155	155	155	155
Turn-around days per year	154	55	155	155	155	155
Total revenue days per year	310	310	310	310	310	310
Processing rates						
Reference material, MT/day	4.23	1.86	8.40	4.71	1.37	3.87
Fissile material, kg/day	44.7	75.8	38.3	83.3	102	73.5
Total capital investment, \$	$58.5 \times 10^6$	$59.3 \times 10^6$	$65.8 \times 10^6$	$67.5 \times 10^6$	$57.9 \times 10^6$	$59.0 \times 10^6$
Operating cost, \$/yr	$5.37 \times 10^6$	$5.47 \times 10^6$	$6.33 \times 10^6$	$6.55 \times 10^6$	$5.30 \times 10^6$	$5.45 \times 10^6$
Ultimate waste disposal charge, \$/yr	$2.52 \times 10^6$	$2.51 \times 10^6$	$2.75 \times 10^6$	$2.79 \times 10^6$	$2.05 \times 10^6$	$2.05 \times 10^6$
Unit costs at 15% per year FCR, <sup>c</sup> \$/kg	25.2	35.6	14.6	26.7	77.7 <sup>d</sup>	27.3
Unit costs at 15% per year FCR, <sup>c</sup> mill/kwhr(e)	0.159	0.161	0.181	0.185	0.152	0.156
Unit costs at 22% per year FCR, <sup>c</sup> \$/kg	31.4	44.2	18.2	33.2	97.6 <sup>d</sup>	34.2
Unit costs at 22% per year, mill/kwhr(e)	0.198	0.200	0.224	0.230	0.191	0.195

<sup>a</sup>See Ref. 1 for details.

<sup>b</sup>HFGR case based on separate processing of the thorium and uranium particles.

<sup>c</sup>Fixed charge rate.

<sup>d</sup>Average cost per kilogram of reference material (thorium plus uranium charged to reactor).

## G.3

Table G.2. Revised Spent-Fuel Processing Cost Estimates for Advanced Converter Reactors

Basis: Single-purpose plants serving 15 reactors of a given concept, 1000 Mw(e) each; 0.8 reactor load factor; burnup approximately equal to the estimated economic optimum<sup>a</sup>

	PWR	SSCR	HWR-U	HWR-Th	HTGR <sup>b</sup>	SGR
Reference material burnup, Mwd/MT	21,248	29,580	12,540	23,000	48,500	16,750
Thermal efficiency, %	31.1	31.2	26.8	26.1	44.4	43.6
Throughput rate, MT/yr	663	475	1300	730	206	600
Processing days per year	260	260	260	260	260	260
Processing rate, MT/day	2.55	1.83	5.00	2.81	1.00 <sup>c</sup>	2.31
Total capital investment, \$	40.0 × 10 <sup>6</sup>	34.4 × 10 <sup>6</sup>	52.2 × 10 <sup>6</sup>	40.0 × 10 <sup>6</sup>	31.0 × 10 <sup>6</sup>	41.3 × 10 <sup>6</sup>
Operating cost, \$/yr	4.00 × 10 <sup>6</sup>	3.44 × 10 <sup>6</sup>	5.22 × 10 <sup>6</sup>	4.00 × 10 <sup>6</sup>	3.10 × 10 <sup>6</sup>	4.13 × 10 <sup>6</sup>
Total waste disposal charge, \$/yr	2.15 × 10 <sup>6</sup>	2.36 × 10 <sup>6</sup>	2.35 × 10 <sup>6</sup>	2.63 × 10 <sup>6</sup>	1.91 × 10 <sup>6</sup>	1.93 × 10 <sup>6</sup>
Unit costs at 15% per year FCR <sup>d</sup>						
\$/kg	18.3	23.1	11.8	17.3	46.9 <sup>e</sup>	20.4
Mill/kwhr(e)	0.116	0.104	0.147	0.120	0.092	0.117
Cost expressed as per cent of corresponding cost in Table G.1	72.6	64.9	81.2	64.8	60.4	74.7
Unit costs at 22% per year FCR <sup>d</sup>						
\$/kg	22.5	28.1	14.7	21.1	57.4 <sup>e</sup>	25.3
Mill/kwhr(e)	0.142	0.127	0.181	0.147	0.113	0.144
Cost expressed as per cent of corresponding cost in Table G.1	71.7	63.6	80.8	63.6	58.8	74.0

<sup>a</sup>See Ref. 1 for details.

<sup>b</sup>HTGR case based on separate processing of the thorium and uranium particles.

<sup>c</sup>Processing rate for thorium particles. The rate for the enriched uranium particles is much lower.

<sup>d</sup>Fixed charge rate.

<sup>e</sup>Average cost per kilogram of reference material (thorium plus uranium charged to reactor).

Table G.3. Estimated Cost of Fuel Element Fabrication  
for AI-CE HWOCR Equilibrium Core Calculated on  
Advanced Converter Study Bases

Production Rate (kg/day)	Operating Expense (\$/kg of metal)	Capital Charges <sup>a</sup> (\$/kg of metal)	Hardware Costs (\$/kg of metal)	Fuel Preparation (\$/kg of metal)	Total Costs (\$/kg of metal)
2000	16.48	9.92	6.57	7.72	40.68
2500	15.15	9.31	6.52	6.86	37.84
3000	14.18	8.85	6.49	6.23	35.74
3475 <sup>b</sup>	13.46	8.50	6.46	5.76	34.17
4000	12.82	8.17	6.43	5.35	32.77
5000	11.89	7.69	6.39	4.75	30.72

<sup>a</sup>Capital charge rate of 22% per year.

<sup>b</sup>Reference case.

Table G.4. Estimated Cost of Fuel Element Fabrication  
for B&W HWOCR Thorium-Oxide Core Calculated on  
Advanced Converter Study Bases

Production Rate (kg/day)	Operating Expense (\$/kg of metal)	Capital Charges <sup>a</sup> (\$/kg of metal)	Hardware Costs (\$/kg of metal)	Fuel Preparation (\$/kg of metal)	Total Costs (\$/kg of metal)
1500	22.11	25.19	25.38	4.84	77.51
2000	20.09	23.02	24.41	4.09	71.61
2590 <sup>b</sup>	18.58	21.31	23.62	3.52	67.02
3000	17.81	20.42	23.19	3.23	64.66
4000	16.92	18.87	22.42	2.74	60.95

<sup>a</sup>Capital charge rate of 22% per year.

<sup>b</sup>Reference case.

#### Reference

1. M. W. Rosenthal et al., A Comparative Evaluation of Advanced Converters, USAEC Report ORNL-3686, Oak Ridge National Laboratory, January 1965.

Internal Distribution

- |                         |  |
|-------------------------|--|
| 1. R. E. Adams          | 91. T. L. McLean                       |
| 2. G. M. Adamson        | 92. H. G. MacPherson                   |
| 3. T. D. Anderson       | 93. R. E. MacPherson                   |
| 4. E. D. Arnold         | 94. F. C. Maienschein                  |
| 5. W. P. Barthold       | 95. J. G. Merkle                       |
| 6. S. E. Beall, Jr.     | 96. M. L. Myers                        |
| 7. R. J. Beaver         | 97. L. C. Oakes                        |
| 8. L. L. Bennett        | 98. H. G. O'Brien                      |
| 9. H. Beutler           | 99. A. R. Olsen                        |
| 10. J. O. Blomeke       | 100. R. C. Olson                       |
| 11. O. W. Burke         | 101. A. M. Perry                       |
| 12. R. S. Carlsmith     | 102. J. T. Roberts                     |
| 13. C. E. Center (K-25) | 103. R. C. Robertson                   |
| 14. R. H. Chapman       | 104. M. W. Rosenthal                   |
| 15. R. D. Cheverton     | 105. D. P. Roux                        |
| 16. C. J. Claffey       | 106. R. Salmon                         |
| 17. C. W. Collins       | 107. J. P. Sanders                     |
| 18. G. L. Copeland      | 108. A. W. Savolainen                  |
| 19. F. L. Culler        | 109. J. L. Scott                       |
| 20. J. L. English       | 110. M. J. Skinner                     |
| 21. E. P. Epler         | 111. I. Spiewak                        |
| 22. T. B. Fowler        | 112. W. G. Stockdale                   |
| 23. R. D. Frey          | 113. R. S. Stone                       |
| 24. E. H. Gift          | 114. J. R. Tallackson                  |
| 25. D. G. Harman        | 115. D. B. Trauger                     |
| 26. F. E. Harrington    | 116. J. T. Venard                      |
| 27. V. O. Haynes        | 117. D. R. Vondy                       |
| 28. H. W. Hoffman       | 118. C. S. Walker                      |
| 29. R. S. Holcomb       | 119. T. N. Washburn                    |
| 30. R. W. Horton        | 120. D. B. Wehmeyer                    |
| 31. W. H. Jordan        | 121. A. M. Weinberg                    |
| 32. Lincoln Jung        | 122. F. G. Welfare                     |
| 33-82. P. R. Kasten     | 123. R. P. Wichner                     |
| 83. R. B. Korsmeyer     | 124. L. V. Wilson                      |
| 84. C. E. Larson (K-25) | 125. F. R. Winslow                     |
| 85. D. B. Lloyd         | 126. L. B. Yeatts, Jr.                 |
| 86. A. L. Lotts         | 127. F. C. Zapp                        |
| 87. M. I. Lundin        | 128-130. Central Research Library      |
| 88. H. F. McDuffie      | 131-132. Document Reference Section    |
| 89. C. J. McHargue      | 133-263. Laboratory Records Department |
| 90. H. A. McLain        | 264. Laboratory Records, R.C.          |

External Distribution

- 265. R. A. Charpie, UCC, New York, N.Y.
- 266-269. F. C. DiLuzio, U.S. Department of the Interior, Washington, D.C.
- 270. H. L. Falkenberry, TVA, Chattanooga, Tenn.
- 271. A. A. Giambusso, AEC, Washington
- 272. R. E. Hoskins, TVA, Chattanooga, Tenn.
- 273. Lenton Long, Battelle-Northwest Pacific Laboratory
- 274. E. A. Mason, Massachusetts Institute of Technology
- 275. S. R. Sapirie, AEC, ORO
- 276. M. Shaw, AEC, Washington
- 277. W. L. Smalley, AEC, ORO
- 278. J. A. Swartout, UCC, New York, N.Y.
- 279-280. Reactor Division, AEC, ORO
- 281. Division of Research and Development, AEC, ORO
- 282-553. Given distribution as shown in TID-4500 under Reactor Technology category (25 copies - CFSTI)